

HETEROGENEOUS REACTIONS OF TROPOSPHERIC TRACE-GASES ON SOLID MODEL AEROSOL SURFACE: A LABORATORY STUDY

THÈSE N° 2746 (2003)

PRÉSENTÉE À LA FACULTÉ ENVIRONNEMENT NATUREL, ARCHITECTURAL ET CONSTRUIT

SECTION DES SCIENCES ET INGÉNIERIE DE L'ENVIRONNEMENT

ÉCOLE POLYTECHNIQUE FÉDÉRALE DE LAUSANNE

POUR L'OBTENTION DU GRADE DE DOCTEUR ÈS SCIENCES

PAR

Christian SANTSCHI

physicien diplômé EPF
de nationalité suisse et originaire de Sigriswil (BE)

acceptée sur proposition du jury:

Dr M. Rossi, directeur de thèse
Prof. C. Comninellis, rapporteur
Dr J. Crowley, rapporteur
Dr J. Staehelin, rapporteur
Prof. H. van den Bergh, rapporteur

Lausanne, EPFL
2003

Abstract

The first part of this laboratory study deals with heterogeneous reactions of bromine- and chlorine-containing species relevant to the atmosphere with solid model alkali salt substrates. The second part of this work treats the heterogeneous interaction of acidic compounds with various mineral dust substrates. The aim of this study is to investigate the role of adsorbed water, $\text{H}_2\text{O}(\text{a})$ and the influence of defect surface sites on the reactions. Furthermore, reaction mechanisms are proposed for the different interactions. Steady state and pulsed valve uptake experiments have been performed in a low-pressure flow reactor. In order to characterise the solid samples images have been taken using a scanning electron microscope (SEM). Furthermore, a few scans using a photoacoustic cell coupled to a FTIR spectrometer have been performed.

First, the interaction of gaseous Cl_2 , HCl , BrCl , Br_2 , Cl_2O and HOCl with solid KBr and furthermore, the reaction of Cl_2O and HOCl on solid NaCl have been investigated. The reaction products of the reactions of Cl_2 , Cl_2O and HOCl with KBr have been Br_2 and BrCl . The reaction of Cl_2O with KBr leads to slow additional formation of HOCl , BrOCl and Cl_2 , and the reaction of HOCl with KBr leads to slow formation of HOBr , Cl_2O , Br_2O and BrOCl . The reaction of Cl_2O on solid NaCl leads to formation of Cl_2 but also a slow formation of HOCl has been observed which is attributed to the reaction with adsorbed $\text{H}_2\text{O}(\text{a})$. The interaction of HOCl with NaCl was immeasurably slow under our conditions.

In order to measure the amount of adsorbed $\text{H}_2\text{O}(\text{a})$ desorption experiments have been carried out and a calibration curve has been obtained. While performing desorption experiments on ground KBr grains and thin KBr films sprayed on a gold-coated substrate desorption of HOBr has been observed which we attributed to the presence of surface adsorbed molecular bromine. Using the SEM we found that pumping and heating the substrate lead to a better-ordered surface. The exposure of the salt sample to an excess of chlorine or bromine leads also to a recrystallisation of the surface.

Furthermore, all reactions on alkali salt samples have shown that adsorbed halogen species are retained on the surface. These adsorbed species play a crucial role for the reactions of halogens with alkali salt. In the case of HOCl on KBr we explain the autocatalytic behaviour of the reaction by the presence of adsorbed halogen species, particularly Br_2 . In the Cl_2/KBr

system a regeneration of the surface has been observed which we explain with desorption of adsorbed intermediates, but also by crystallisation of KCl that may lead to a recycling of reactive sites. In contrast to Cl_2/KBr no regeneration of the substrate towards formation of gaseous bromine-containing species has been observed in the HOCl/KBr system. We explain this with the fact that KOH thermodynamically does not tend to crystallise in the presence of H_2O as does the alkali halide.

In the second part the reactions of CO_2 , SO_2 , HCl and HNO_3 on various CaCO_3 substrates such as roughened and polished marble and low- and high-ordered precipitated CaCO_3 have been carried out. Additionally, a few HNO_3 uptake experiments have been performed on dust substrates such as Saharan Dust, Kaolinite and Arizona Road Dust. On these substrates a fast uptake of HNO_3 but no reaction products have been observed.

In the case of SO_2 and HCl interacting with precipitated CaCO_3 the observed reaction product has been CO_2 . Whereas HNO_3 uptake experiments on precipitated CaCO_3 additionally lead to a slow formation of H_2O . HCl uptake experiments on polished marble plates have not led to formation of any reaction product. However, HNO_3 uptake experiments on polished and roughened marble led to formation of H_2O but not of CO_2 . We explain these observations with the dependence of the rate of surface chemistry on the morphology of the sample.

The HCl and HNO_3 uptake experiments on precipitated CaCO_3 have shown a delay in the formation of CO_2 whereas it is immediately released after the exposure of the CaCO_3 sample to SO_2 . Furthermore, an uptake of CO_2 has been observed on precipitated CaCO_3 . All uptake experiments on CaCO_3 have shown saturation due to a limited number of reactive sites.

In order to explain these results we have speculated the existence of an intermediate species $\text{Ca}(\text{OH})(\text{HCO}_3)$. This intermediate may be formed by exposure of the CaCO_3 sample to ambient H_2O and CO_2 . Acidic compounds such as HCl and HNO_3 react rapidly with the basic OH part of the intermediate and subsequently more slowly with the bicarbonate part of the intermediate. This explains the delay of formation of CO_2 in the reaction of HCl and HNO_3 with CaCO_3 . In contrast to acidic species, SO_2 attacks with preference the bicarbonate part of the intermediate. This leads to an immediate release of CO_2 after exposure of the CaCO_3 sample to SO_2 . The reaction of SO_2 with the OH part of the intermediate leads to loss of SO_2 . The mass balance between loss of SO_2 and yield of CO_2 has shown a deficiency of CO_2 , which may be explained with a slow reaction with the OH part of the intermediate.

Zusammenfassung

Im ersten Teil dieser zweiteiligen Laborstudie wurden heterogene Reaktionen von brom- und chlorhaltigen Gasen, die in der Atmosphäre eine wichtige Rolle spielen, mit Alkali Salz Modelloberflächen untersucht. Weiter wurden im zweiten Teil dieser Arbeit diverse heterogene Reaktionen von sauren Verbindungen mit Mineralstaub untersucht. Der Einfluss von adsorbiertem Wasser $H_2O(a)$ und Fehlstellen auf die Reaktionen wurde im Speziellen untersucht. Zu diesem Zweck führten wir Experimente im stationären Zustand und mit gepulsten Ventilen in einem Niederdruckflussreaktor durch. Mittels Aufnahmen eines Scanning Electron Microscope (SEM) charakterisierten wir die Oberflächen der festen Proben.

Zuerst wurde die Wechselwirkung von Cl_2 , HCl , $BrCl$, Br_2 , Cl_2O und $HOCl$ mit festen KBr - und die Wechselwirkung zwischen Cl_2O und $HOCl$ mit festen $NaCl$ -Proben untersucht. Die beobachteten Reaktionsprodukte der Reaktion von Cl_2 , Cl_2O und $HOCl$ mit KBr waren Br_2 und $BrCl$. Die Reaktion von Cl_2O mit KBr führte zudem zu einer langsamen Bildung von $HOCl$, $BrOCl$ und Cl_2 und diejenige von $HOCl$ war von einer langsamen Bildung von $HOBr$, Cl_2O , Br_2O , $BrOCl$ und auch Cl_2 begleitet. Cl_2O mit $NaCl$ schliesslich führte zur Bildung von Cl_2 und $HOCl$, wobei die Bildung von $HOCl$ auf die Reaktion mit adsorbiertem Wasser zurückzuführen ist. Die Reaktion von $HOCl$ mit $NaCl$ war unmessbar langsam.

Um die Menge von adsorbiertem Wasser $H_2O(a)$ zu bestimmen, führten wir Desorptionsexperimente durch, die uns Kalibrationskurven für die verschiedenen KBr Proben lieferten. Während des Aufheizens der KBr -Proben wurde die Desorption von $HOBr$ beobachtet. Jedoch nur die zerstoßenen KBr -Körner und die gespritzten dünnen KBr -Filme führten zu einer Bildung von gasförmigem $HOBr$. Diese Beobachtung erklärten wir mit dem Vorhandensein von adsorbiertem molekularem Brom auf diesen Proben. Mittels SEM haben wir gezeigt, dass Pumpen und Aufheizen der KBr -Proben zu einer Rekrystallisation der Oberfläche führt. Eine Rekrystallisation wurde auch beobachtet, wenn die Salz-Probe einer erhöhten Konzentration von elementarem Chlor oder Brom Gas ausgesetzt wurde.

Weiter haben wir gezeigt, dass adsorbierte Halogenverbindungen eine entscheidende Rolle bei heterogenen Reaktionen auf Salzoberflächen spielen. Im $HOCl/KBr$ System wurde das autokatalytische Verhalten des Systems mit der Anwesenheit von adsorbiertem Br_2 erklärt. Im

Cl₂/KBr System wurde im Gegensatz zum HOCl/KBr System eine Regeneration der Oberfläche festgestellt, die wir zum einen mit der Desorption von adsorbierten Molekülen und andererseits mit einer Kristallisation von adsorbierten Reaktionsprodukten, den Alkalihalogeniden erklärten. Da thermodynamisch gesehen KOH in der Anwesenheit von Wasser nicht zur Kristallisation neigt, findet im HOCl/KBr System, einmal gesättigt, keine Regeneration der Oberfläche statt.

Im zweiten Teil der Arbeit wurden die Reaktionen von CO₂, SO₂, HCl und HNO₃ mit verschiedenen Mineralstaub Oberflächen, wie aufgerauhtem und poliertem Marmor und ausgefälltem CaCO₃ mit unterschiedlicher Anzahl von Fehlstellen untersucht. Zusätzlich wurden einige HNO₃ Experimente auf Sahara Staub, Kaolinit und Arizona Road Dust durchgeführt. Auf diesen Substraten wurden eine schnelle Aufnahme von HNO₃, aber keine Reaktionsprodukte beobachtet.

Im Falle der Reaktionen von SO₂, HCl und HNO₃ mit ausgefälltem CaCO₃ wurde CO₂ als Reaktionsprodukt beobachtet. Die Aufnahme von HNO₃ führte zu einer zusätzlichen Bildung von H₂O. HCl Aufnahmeexperimente auf Marmor-Proben führten zu keinem gasförmigen Reaktionsprodukt. Wir erklärten diese Beobachtungen mit der Abhängigkeit der Oberflächenchemie von der Oberflächenbeschaffenheit der Probe.

Die Aufnahmeexperimente der sauren Verbindungen HCl und HNO₃ auf ausgefälltem CaCO₃ führten zu einer verzögerten Bildung von CO₂, wohingegen die Bildung von CO₂ durch die Aufnahme von SO₂ sofort nach Reaktionsbeginn einsetzte. Schliesslich wurde eine Aufnahme von CO₂ auf ausgefälltem CaCO₃ beobachtet. Alle ausgeführten Experimente zeigten eine Sättigung der Reaktionsoberfläche.

Um diese Resultate erklären zu können, führten wir das adsorbierte Zwischenprodukt Ca(OH)(HCO₃) ein. Dieses Zwischenprodukt kann in Anwesenheit von H₂O und CO₂, das sich in der Atmosphäre befindet, gebildet werden. Die sauren Verbindungen wie HCl und HNO₃ reagieren schnell mit dem OH-Teil und langsam mit dem Bicarbonat des Zwischenprodukts. Das erklärt die Verzögerung bei der Bildung von gasförmigen CO₂ bei der Reaktion von sauren Verbindungen mit CaCO₃. Im Gegensatz zu den sauren Verbindungen reagiert SO₂ schnell mit dem Bicarbonat und langsam mit dem OH-Teil des Zwischenprodukts. Das führt zu einer sofortigen Freisetzung von CO₂ nach dem Reaktionsstart. Die Reaktion mit dem OH-Teil resultiert in einem Verlust von SO₂. Die Massenbilanz zwischen SO₂ und CO₂ zeigt ein zu grosses Verschwinden von SO₂, was man mit der langsamen Reaktion von SO₂ mit dem OH-Teil des Zwischenprodukts erklären kann.

Table of Contents

1. Introduction	1
1.1. Earth's atmosphere	1
1.2. Tropospheric and Stratospheric Ozone, Oxidation Capacity	5
1.3. Halogen Species in the Atmosphere	7
1.4. Atmospheric Particles	10
1.4.1. Sea-salt Particles	12
1.4.2. Mineral Dust	14
1.5. Acid Rain	16
1.6. Motivation for the Present Work	19
1.7. References	23
2. Experimental Section	31
2.1. Knudsen Flow Reactor	31
2.1.1. Description of the Apparatus	34
2.1.2. The Measurement Principles	36
2.2. Calibrations	40

2.2.1.	Calibration of HOCl	41
2.2.2.	Calibration of H ₂ O	42
2.3.	The High Temperature Support	43
2.4.	Data Acquisition	44
2.5.	References	47
3.	Preparation of Halogen and Alkali Salt Samples	48
3.1.	Gaseous Samples	48
3.1.1.	Preparation of HCl	49
3.1.2.	Preparation of BrCl	50
3.1.3.	Preparation of Cl ₂ O	50
3.1.4.	Preparation of HOCl	51
3.2.	Solid Samples	51
3.2.1.	Grain Samples	52
3.2.2.	Ground Grains Samples	54
3.2.3.	Thin Salt Films Deposited on a Pyrex Substrate	54
3.2.4.	Thin KBr Salt Films on a Gold-Plated Substrate	55
3.3.	References	56
4.	Reactions of Chlorine and Bromine Compounds on Alkali Salt Surfaces ...	58
4.1.	H ₂ O on Different KBr Substrates	58
4.1.1.	Introduction	58
4.1.2.	Results and Discussion	60
4.1.3.	Conclusions	78

4.2.	Uptake Experiments of HCl on KBr	80
4.2.1.	Introduction	80
4.2.2.	Results	81
4.3.	Uptake Experiments of Cl ₂ on KBr	82
4.3.1.	Introduction	82
4.3.2.	Results and Discussion	83
4.3.3.	Conclusions	100
4.3.4.	Tables	102
4.4.	The Role of Adsorbed Molecular Bromine Br ₂ on KBr and KCl	104
4.4.1.	Introduction	104
4.4.2.	Results and Discussion	105
4.4.3.	Conclusions	110
4.5.	Uptake Experiments of BrCl on KBr	111
4.5.1.	Introduction	111
4.5.2.	Results	111
4.6.	Uptake Experiments of Cl ₂ O on KBr	113
4.6.1.	Introduction	113
4.6.2.	Results and Discussion	113
4.6.3.	Conclusions	122
4.6.4.	Tables	124
4.7.	Uptake Experiments of HOCl on KBr	126
4.7.1.	Introduction	126
4.7.2.	Results and Discussion	128
	A) Surface Activation	129
	B) Role of Adsorbed Water	136
	C) Surface Defects	148
	D) Mechanism and Autocatalytic Behaviour	152

4.7.3.	Conclusions	153
4.7.4.	Tables	155
4.8.	Uptake Experiments of Cl ₂ O on NaCl	163
4.8.1.	Introduction	163
4.8.2.	Results and Discussion	163
4.8.3.	Conclusions	170
4.8.4.	Tables	171
4.9.	Uptake Experiments of HOCl on NaCl	173
4.9.1.	Introduction	173
4.9.2.	Results	173
4.9.3.	Tables	175
4.10.	General Discussion	176
4.11.	References	179
5.	Preparation of Mineral Dust and Acidic Samples	187
5.1.	Gaseous Samples	187
5.1.1.	Preparation of HNO ₃	187
5.2.	Solid Samples	188
5.2.1.	Precipitated CaCO ₃	188
5.2.2.	Roughened and Polished Marble	189
5.2.3.	Various Mineral Dusts	190
5.3.	References	191
6.	Reactions of Acidic Compounds on Mineral Dust	192
6.1.	H ₂ O on CaCO ₃	192
6.1.1	Introduction	194

6.1.2	Results	194
6.2.	Uptake Experiments of CO ₂ on CaCO ₃	197
6.2.1.	Introduction	197
6.2.2.	Results and Discussion	197
6.2.3.	Conclusions	204
6.2.4.	Tables	205
6.3.	Uptake Experiments of SO ₂ on CaCO ₃	206
6.2.1.	Introduction	206
6.2.2.	Results and Discussion	206
6.2.3.	Conclusions	218
6.2.4.	Tables	219
6.4.	Uptake Experiment of HNO ₃ on CaCO ₃	220
6.4.1.	Introduction	220
6.4.2.	Results and Discussion	220
6.4.3.	Conclusions	231
6.4.4.	Tables	233
6.5.	Uptake Experiment of HCl on CaCO ₃	234
6.5.1.	Introduction	234
6.5.2.	Results and Discussion	234
6.5.3.	Conclusions	241
6.5.4.	Tables	243
6.6	Uptake Experiments of HNO ₃ on Various Mineral Dusts	244
6.7.	General Discussion	245
6.8.	References	247
7.	Outlook	248

Appendix

A	BET Surfaces of Various Mineral Dusts	252
B	Adsorbed H ₂ O on Various Mineral Dusts	253
	Curriculum Vitae	255

Chapter 1

1. Introduction

1.1. The Atmosphere of the Earth

Of the 9 planets of our solar system the following, namely Venus, Earth, Mars, Jupiter, Saturn, Uranus and Neptune own a substantial atmosphere. However it is supposed that Earth, alone amongst those planets, supports life in the form we know it.

On Earth the absolutely necessary conditions, namely the presence of liquid water, the persistence of liquid water and the existence of a magnetic field are satisfied.

The distance between sun and earth (149,6 million km (6, 5)) as well as the size of our planet and the presence and composition of our atmosphere enabled the development of life on earth. It seems that our atmosphere (Greek: atmos = vapour and sphaira = ball) is essential for the support of life as we know it. The composition of our atmosphere is determined by biological processes acting in harmony with physical and chemical changes. The main components of Earth's atmosphere are listed in table 1.1.1.

Chapter 1

Table 1.1.1: Main constituents of the atmosphere of the Earth and lifetimes τ of the main components (3). The total mass m of the atmosphere is estimated to be $m = 5.2 \cdot 10^{18}$ kg. The lifetime τ is defined as $\tau = \frac{M}{F}$ where M is denoted as the amount of the chemical species and F the rate of removal and destruction (3, 5).

gas	formula	% _v	lifetime
Nitrogen	N ₂	78.08	1.6*10 ⁷ a
Oxygen	O ₂	20.94	3-10*10 ³ a
Argon	Ar	0.934	
Carbon Dioxide	CO ₂	0.035	3-4a
Neon	Ne	0.0018	
Helium	He	0.00052	10 ⁶ a
Methane	CH ₄	0.00017	9a
Ozone	O ₃	0.000001-0.000004	~100d

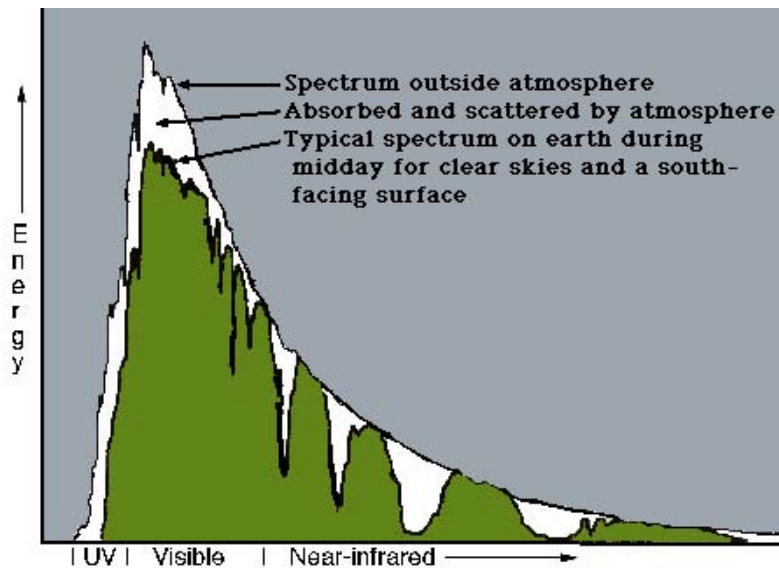


Figure 1.1.1: Change of the spectral distribution of solar radiation penetrating through the atmosphere.

An important role of the atmosphere of the earth is the protection of life against solar radiation particularly, against high-energy ultraviolet radiation (UVR). A Harmful consequence of UVR at the terrestrial surface is an enhancement of genetic damages on the cellular level. UVR is subdivided into UV-C ($\lambda < 280$ nm), UV-B ($280\text{nm} < \lambda < 320\text{nm}$) and UV-A ($320\text{nm} < \lambda < 350\text{nm}$) (7). UV-C and UV-B are almost totally absorbed by the

Chapter 1

atmosphere. Figure 1.1.1 shows the spectral distribution of solar radiation including absorbance by the atmosphere.

The absorbance of solar radiation by the atmosphere leads to warming of the earth. The equivalent black body temperature of the earth T_E would be -18°C , using equation 1.1.1a and the Stefan-Boltzmann law (equation 1.1.b):

$$(\pi R^2)(1-\alpha)S = 4\pi R^2\sigma T^4 \quad (4) \quad \text{(equation 1.1.1a)}$$

R : 6000km (Earth radius)

α : 0.3 (4) (Albedo)

T : temperature

$$S = \sigma T_E^4 \quad \text{(equation 1.1.1b)}$$

σ : $5.67 * 10^{-8} \text{ Wm}^{-2}\text{K}^{-4}$

(Stefan-Boltzmann constant)

S : 1370 Wm^{-2} (7)

(irradiance of the sun)

Roughly 20% of the incoming solar radiation is absorbed by the atmosphere, 31% is backscattered to space and 49% is absorbed by the surface of the earth (3). The absorption of solar radiation by some atmospheric constituents can lead to photochemical reactions, which play a crucial role in atmospheric chemistry.

The absorbance of outgoing longwave infrared (terrestrial or thermal) radiation ($\lambda > 750\text{nm}$ (7)) by the atmosphere contributes to its warming. This warming is known as greenhouse effect. The most important absorbing greenhouse gases are listed in table 1.1.2.

Based on its vertical temperature structure the atmosphere is divided into different regions. Figure 1.1.2 shows a temperature-altitude profile of the atmosphere. The two lowest regions are named the troposphere- and the stratosphere (Greek: tropos = turning, Latin: stratos = layer). Rather strong vertical mixing characterises the troposphere. In this region “weather is going on”, air parcels may reach velocities of more than 100km h^{-1} in the updrafts of large thunderstorms. The troposphere extends from the surface of the Earth up to the tropopause, which is at 10 to 15km altitude depending on latitude and season. The lower 2 km of the troposphere is referred to as the planetary boundary layer (PBL) where most of the emissions are occurring owing to human activity.

Chapter 1

Table 1.1.2: Concentrations and lifetime of the most important greenhouse gases (1).

^{a)} : mixing ratio in the unpolluted troposphere

^{b)} : maximum mixing ratio in the stratosphere at 25-30km altitude

gas	formula	concentration	lifetime
Carbon Dioxide	CO ₂	350ppm	3-4a
Methane	CH ₄	1.7ppm	9-15a
Nitrous Oxide	N ₂ O	310ppb	120a
chlorofluorocarbon	CFC	100ppt-1ppb	> 100a
Ozone	O ₃	10-40ppb ^{a)} 10ppm ^{b)}	~100d
Water	H ₂ O		10d

In contrast the structure of the stratosphere is rather stratified due to a temperature inversion at the tropopause which means that the vertical mixing is very small compared to the troposphere.

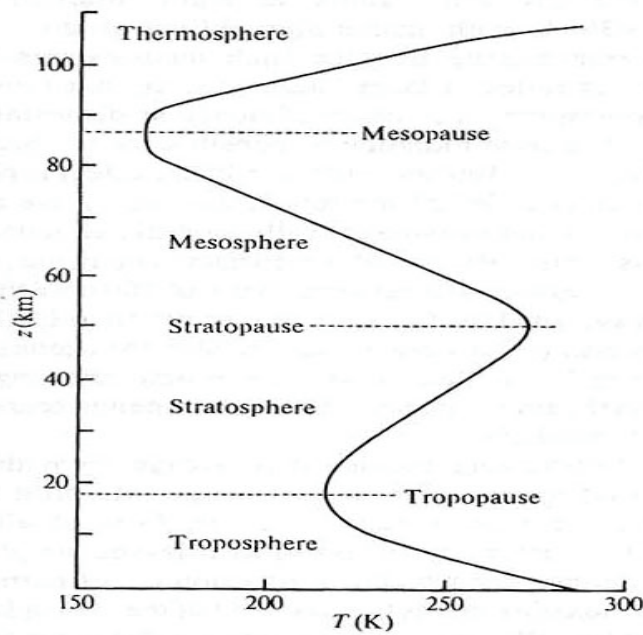


Figure 1.1.2: Temperature-altitude profile of the atmosphere of the earth. The curve shown represents the atmospheric structure at 40°N in June (4, 5).

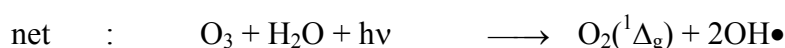
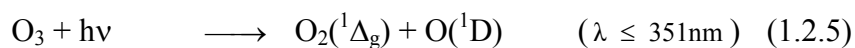
1.2. Tropospheric- and Stratospheric Ozone, Oxidation Capacity

Ozone O_3 (Greek: ozein = to smell), discovered in 1839 by Christian Friedrich Schoenbein (8), is a natural constituent of the atmosphere and occurs both in the stratosphere and the troposphere corresponding to 90% and 10% of the total atmospheric loading, respectively. In the stratosphere, ozone forms a protective layer shielding the Earth from harmful ultraviolet radiation. It is formed by the reaction cycle 1.2.1-4 (3):



Reaction cycle (1.2.1-4) was proposed by Chapman 1930 who gave it its name.

First, tropospheric ozone plays a controlling role in the oxidation capacity of the troposphere and is itself an oxidant. O_3 is the major precursor for all known oxidising agents in the troposphere, most notably for the hydroxyl radical OH.



Second, ozone is a major pollutant in the troposphere. O_3 may be toxic to living tissue and damaging to some organic materials, which leads to an important impact on human health, such as nasal and throat irritation at low concentration or an impairment of mechanical lung function at higher concentration. Third, O_3 is an effective greenhouse gas. Its concentration and lifetime are listed in table 1.1.2.

Natural tropospheric ozone originates partly from the transport of stratospheric ozone to the troposphere. Furthermore it may be generated by the interaction of O_2 with natural NO_x (Reactions 1.2.7 and 1.2.8) which originates from lightning and biogenic processes.

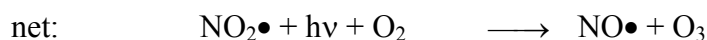
Chapter 1

Since the early 19th century of the industrialisation in Europe and America the consumption of easily available fossil fuels has dramatically increased and with it as a consequence also the concentrations of volatile organic compounds (VOC) and nitrogen oxides ($\text{NO}_x = \text{NO} + \text{NO}_2$). The main source of anthropogenic NO_x is high temperature combustion. In table 1.2.1 typical mixing ratios of NO_x are listed. Sources of methane, CH_4 , as an example of a VOC are enteric fermentation in animals, emissions from wet land areas, termites and natural gas leakage. O_3 can be formed by the simultaneous presence of VOC's, NO_x and photons.

Table 1.2.1: Typical Boundary Layer NO_x Mixing Ratios
(2)

Region	NO_x [ppb]
Urban-suburban	10-1000
Rural	0.2-10
Remote tropical forest	0.02-0.08
Remote marine	0.02-0.04

The formation of tropospheric ozone may be explained as follows:



The VOC may react in the following way:



Reactions 1.2.9-11 regenerate the lost NO_2 and the OH -radical is generated in reactions 1.2.5 and 1.2.6. A closed cycle in NO_x for the formation of O_3 is thereby constituted.

A sink for O₃ is:



Also NO reacts quickly with ozone and contributes to the loss of O₃. For an efficient O₃ formation the relative ratios between VOC's and NO_x is important.

The most important oxidants in the troposphere are O₃, HO₂, H₂O₂ and OH. They essentially determine the oxidation capacity of the atmosphere and are therefore involved in many chemical reactions.

The hydroxyl radical OH is the major oxidising chemical species in the troposphere. The concentration of this short-lived (~1s) free radical is very difficult to measure and may vary dramatically even on a local scale (9).

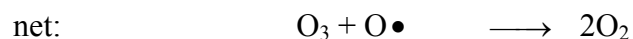
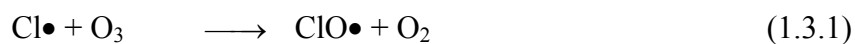
Furthermore data from field measurements and laboratory studies suggest that atomic halogens are important free radicals which contribute to the oxidation potential of the troposphere (10).

1.3. Halogen Species in the Atmosphere

Studies on the decay of organics in marine air masses and sudden destruction of O₃ in the lower arctic troposphere (11-13) suggested the effects of halogen (Greek: hals = salt, genesis = formation) atom chemistry (14, 15). Halogen compounds containing chlorine, bromine, iodine and fluorine atoms have been observed in the atmosphere. Halogen atoms are strong oxidising species. As an example the oxidation rate of common gaseous compounds by chlorine atoms is approximately 100 times faster than the analogous oxidation rate involving OH radical.

Chapter 1

CFC's are long-lived halogen containing compounds that are stable under tropospheric conditions, and which eventually find their way to the stratosphere. Once in the stratosphere they absorb UV-radiation ($190 < \lambda < 220\text{nm}$), photodissociate and release atomic chlorine which is of serious consequence for the protecting ozone-layer owing to the following reactions:

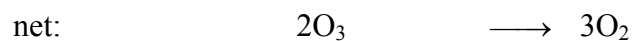
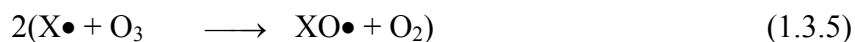


Reactions 1.3.1 and 1.3.2 represent another ozone loss cycle analogous to reactions 1.2.12 and 1.2.13.

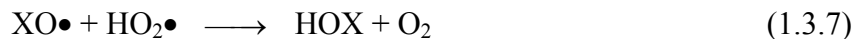
Field measurements have shown a strong anticorrelation of halogen species and O_3 concentration (16). Halogen compounds are involved in the control of the tropospheric O_3 budget. Photodissociable bromine and chlorine species such as Cl_2 , Br_2 , BrCl , HOCl , HOBr and others play an important role in this chemistry. Those species may release atomic Br or Cl in the presence of light, that is upon photodissociation:



Once X is present in atomic form it may induce catalytic cycles for destruction of O_3 , similar to reactions in the stratosphere



other important reactions leading to the generation of chlorine or bromine atoms are (2):



or

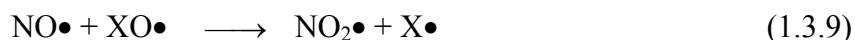


Table 1.3.1: Concentrations and lifetimes of the most important halogen species present in the troposphere (4, 5).

gas	formula	concentration	lifetime	source	
				natural	anthropogenic
methyl chloride	CH ₃ Cl	530ppt	1.5a	90%	10%
methyl bromide	CH ₃ Br	9-10ppt	0.7a	50%	50%
chloroform	CHCl ₃	6-13ppt	0.55a		
bromoform	CHBr ₃	0.2-0.3ppt	20d		

Natural species carrying halogens are halogenated organics such as methyl halides CH₃X or polyhalogenated species CHX₃, where X = Br, Cl, I (17, 2). Important sources are biomass burning, wood mold and biological activity in seawater. Methyl chloride is the major natural source of atmospheric chlorine (3). Natural methyl bromide appears to emanate mainly from the oceans, man-made CH₃Br sources are agricultural fumigation activities and emissions from leaded gasoline. Concentrations and lifetimes are listed in Table 1.3.1.

High chlorine concentrations measured in coastal air masses (18, 19) suggest the existence of other halogen sources than mentioned above. Furthermore, a deficit of chlorine in marine aerosols compared to seawater has been found. This so-called chlorine deficit confirms the suggestion of marine aerosols as a chlorine source (2). Marine aerosols are an inexhaustible reservoir of halogen atoms. Bounded halogen atoms may be released into the atmosphere by heterogeneous chemical reactions (3).

1.4. Atmospheric Particles

Aerosols are present to a large extent in the atmosphere. Generally, their average values near the earth surface are $\sim 10^3$ particle cm^{-3} over the oceans, $\sim 10^4$ particle cm^{-3} over rural land areas, and 10^5 particle cm^{-3} or higher in polluted air (3). They may be emitted directly as particles (primary aerosol) or formed in the atmosphere by gas-to-particle conversion processes (secondary aerosol). Important natural aerosol sources are volcanic activity, soil erosion and aerosol formation from sea spray (20). The global input of aerosol of anthropogenic origin is about 20% of the total amount of released aerosols (by mass). Main sources of aerosols are road dust, wind erosion of tilled land, fuel combustion and emissions by industrial processes (3). Removal processes are sedimentation, rain- and washout, Brownian diffusion, and coagulation depending on the particle size. Figure 1.4.1 indicates the principal formation and removal processes as a function of the particle diameter.

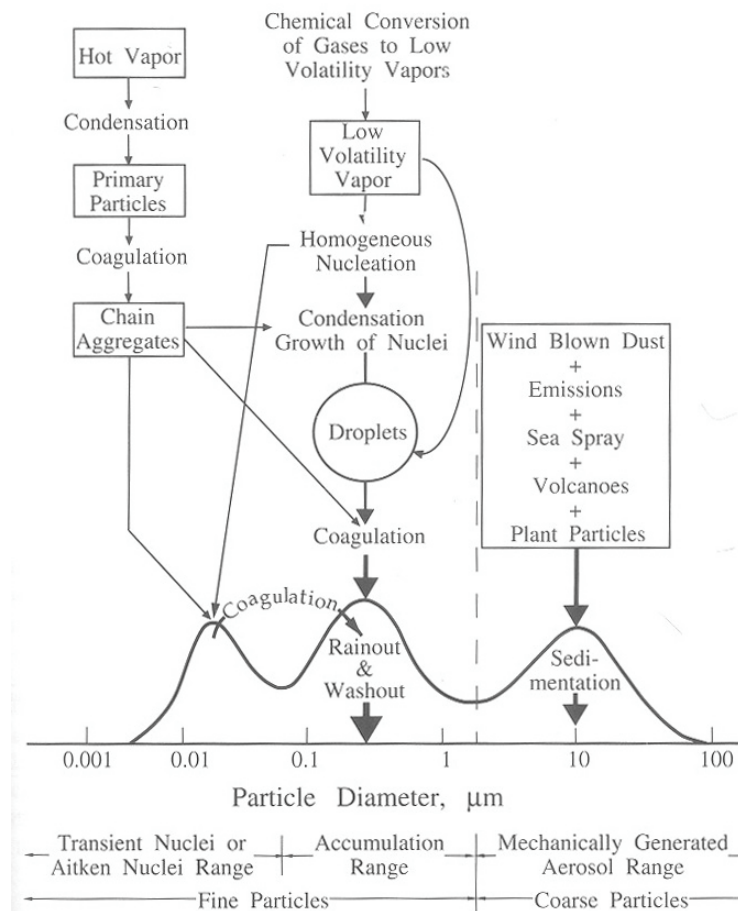


Figure 1.4.1: Idealised scheme of the distribution of particle surface area of an atmospheric aerosol. Principal modes, sources and particle formation and removal mechanism are indicated (2, 5).

Chapter 1

Tropospheric particles include the following:

- Sea-salt particles
- Sulfate aerosols
- Aqueous salt aerosols
- Soot
- Dust

Their size ranges from a few nanometers (nm) to tens of micrometers (μm). Their residence-time and with that the transport range of aerosols is mainly determined by their size. The travel distance of fine particles (Figure 1.4.1) ranges between hundreds and thousands of km. For coarse particles the transport range is smaller than tens of km.

Figure 1.4.2 shows an estimate of the aerosol residence-time as a function of its diameter (3).

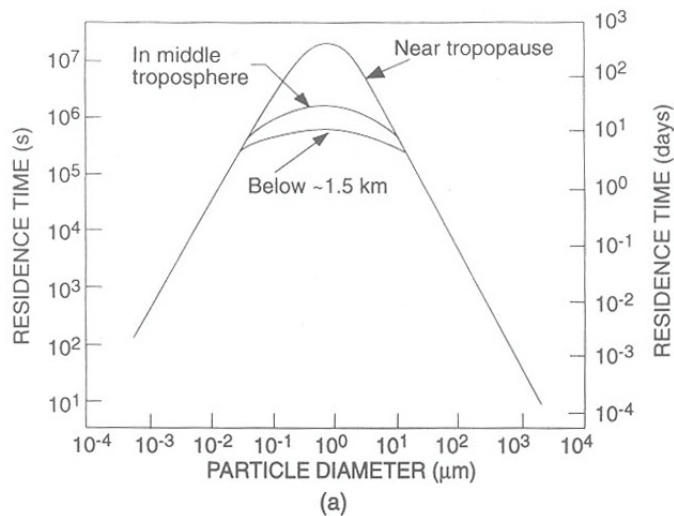


Figure 1.4.2: Estimates of the residence time of atmospheric aerosol as a function of its diameter (3).

The nomenclature of the distribution of the diameter d (21, 2) is as follow:

$d < 2.5\mu\text{m}$	fine mode	$0.1 - 1\mu\text{m}$: accumulation mode
		$0.01-0.1\mu\text{m}$: Aitken mode
		$0.01-0.001\mu\text{m}$: nucleation mode
$d > 2.5\mu\text{m}$	coarse mode		

Small particles with $d < 10$ nm have a small residence time τ . The major removal mechanism is diffusion to cloud particles and Brownian coagulation whereas aerosols with $d > 20\mu\text{m}$ have a small residence time τ as well but their removal mechanism is mainly sedimentation, impacting onto surfaces and precipitation scavenging.

Particles smaller than $1\mu\text{m}$ diameter have atmospheric concentrations in the range of tens to tenths of particles cm^{-3} , those exceeding $1\mu\text{m}$ diameter typically exhibit concentrations less than 10 particles cm^{-3} (21).

There is evidence of a significant climate forcing due to anthropogenic aerosols. Anthropogenic aerosols cause a loss of solar irradiation relative to preindustrial time (direct forcing) and enhance the population of cloud condensation nuclei (CCN) which leads to an enhanced cloud formation (indirect forcing) (22).

Furthermore, a relationship between mortality and the concentration of fine particles $\text{PM}_{2.5}$, as well as with particle sulfate is seen (23). $\text{PM}_{2.5}$ and PM_{10} are particles smaller than 2.5 and $10\mu\text{m}$, respectively. The human body may take in aerosols through the respiratory system by inhalation, and subsequent deposition and take them up by absorption into the blood stream (24).

The presence of aerosols also has a strong influence on atmospheric chemistry. Heterogeneous chemical processes may influence the oxidation potential of atmosphere for example heterogeneous reactions of NO_y with sea salt particles leading to a release of gaseous halogen species.

1.4.1. Sea-Salt Particles

The oceans are the most important source of sea-salt aerosol on the order of approximately $1000\text{-}5000$ Tg y^{-1} , including giant particles that are not transported very far (3). Typical sea-salt aerosol concentrations in the marine boundary layer (MBL) are on the order of 5 to 30 particles cm^{-3} (2) but they have also been measured 900 km inland from coastal areas (25).

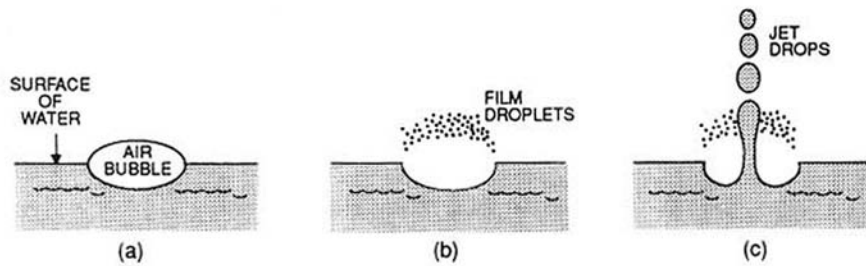


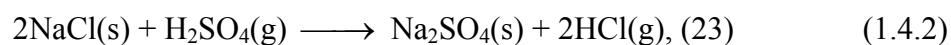
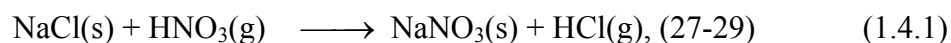
Figure 1.4.3: Schematic diagrams (2) to illustrate the manner in which film droplets and jet drops are produced when air bubble bursts at the surface of water. The time between a) and b) is ~ 2 ms. The size of the jet drops are $\sim 15\%$ of the diameter of the air bubble. The film droplets are ~ 5 to $30\mu\text{m}$ diameter before evaporation (3, 5).

The major mechanism for ejecting material into the air is bubble bursting (26). Figure 1.4.3 shows a schematic diagram of the manner in which salt-water droplets burst into air (3). A fraction of the droplets thrown out of the water into the air for about 15cm, evaporate, and form sea-salt particles with diameter $d > 2\mu\text{m}$ in this way (case c)). Much smaller aerosols are formed when the upper portion of the air bubble bursts at the water surface (case b)). Some droplets originate from evaporated foam and windblown spray but generally the drops are too large in order to reside for long time in the air. Sea-salt particles consist mainly of sodium (Na) and chlorine (Cl). Their main components are listed in table 1.4.1.

Table 1.4.1: Composition of sea-salt ignoring atmospheric conversion (2)

Species	Percent by weight
Cl	55.04
Na	33.61
SO_4^{2-}	7.68
Mg	3.69
Ca	1.16
K	1.1
Br	0.19
C	$3.5 \cdot 10^{-3}$ - $8.7 \cdot 10^{-3}$
Al	$4.6 \cdot 10^{-4}$ - $5.5 \cdot 10^{-3}$
Ba	$1.4 \cdot 10^{-4}$
I	$1.4 \cdot 10^{-4}$

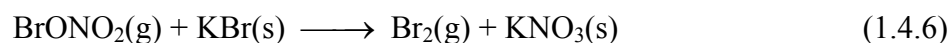
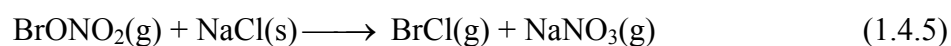
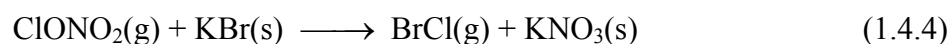
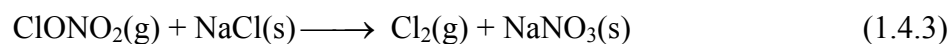
Considering the composition of sea-salt particles one may suggest that they may be an important source of tropospheric halogen. It has been found that halogen compounds may evolve in the presence of strong acids. The most important representatives of this type of reaction are the reaction of nitric acid HNO_3 and sulfuric acid H_2SO_4 with NaCl.



With the release of hydrochloric acid HCl chlorine is removed from the aerosol which leads to a deficit in chlorine in the aerosol.

HCl does not absorb photons above 290nm (23). However, photodissociable species such as X_2 and HOX (X = Br, Cl) or BrCl are of particular interest with respect to depletion of O_3 (reaction 1.3.3-1.3.6).

Such reactions are (30):



The formation of BrONO_2 and ClONO_2 is known to occur in the atmosphere via the reaction of XO with NO_2 (30), where X = Br, Cl.

The release of photodissociable halogen species by sea-salt aerosols is sufficient to induce a catalytic cycle for ozone O_3 destruction as described above.

1.4.2. Mineral Dust

An important category of atmospheric particles is mineral dust. The suspension of solid particles produced by mechanical disintegration of material such as crushing, grinding and blasting (2) is a general definition of atmospheric dust. The diameter d_p exceeds $1\mu\text{m}$. The most important elemental constituents of mineral dust are silicon Si, aluminium Al, calcium Ca, iron Fe, and magnesium Mg. Usually, the elements found in aerosols occur in the form of stable oxides for example SiO_2 , Fe_2O_3 , Fe_3O_4 , Al_2O_3 , carbonates such as CaCO_3 or sulphates such as CaSO_4 . Their exact chemical form is in general uncertain (2).

Chapter 1

The principal source regions of mineral aerosols are arid areas, which cover about one third of the land surface of the earth. Further sources are volcanic eruptions and some open sources such as quarrying. Unpaved roads are also an important source for mineral dust in North America (31). The estimated global source strength approaches to approximately 2000 Tg yr^{-1} and is highly variable in space and time (32, 33).



Figure 1.4.3: Dust-event over Lausanne (Switzerland) in April 2002.

Mineral dust may be transported over thousands of kilometres (34). So each year several hundred million tons of African dust are transported over the Atlantic to the Caribbean, Central America, and South America (35, 36). Storms and warm air updrafts can lift dust as high as 5000 m above the African desert, and then out across the Atlantic. Saharan Dust has also been observed over Central Europe.

As an example for observed Saharan Dust over Central Europe Figure 1.4.3 shows Saharan Dust collected during a dust-event over Lausanne (Switzerland) in April 2002. The corresponding backward trajectories of the air parcels calculated for Lausanne are shown in Figure 1.4.4. During the dust event on the 8th of April 2002 the backward trajectories show clearly the incoming air masses arriving from the south, whereas after the dust event the 9th of April 2002 the incoming air masses originate from the east or north-east.

On a global scale the highest concentration of man-made aerosols occur above the continents of North America and Europe and locally in the former Soviet Union and on the coasts of China and Japan (20).

The presence of mineral dust in the troposphere plays an important role in environmental acidification as well (37, 38, 4). Environmental acidification influences the acidity of natural

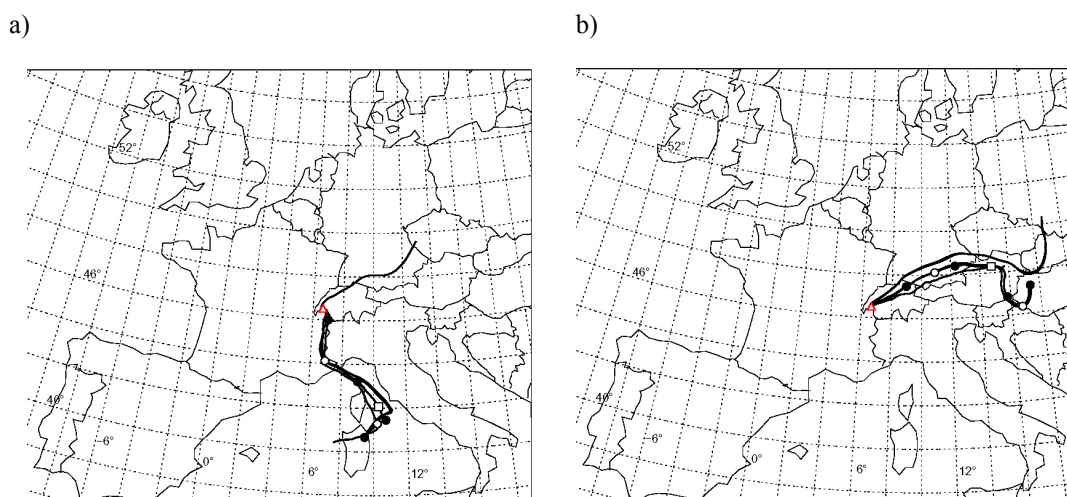


Figure 1.4.4: Backward trajectories of the dust event over Lausanne on the 8th of April 2002. a) shows the trajectories calculated for Lausanne on the 8th of April 2002 06 UTC and b) for Lausanne the on 9th of April 2002 18 UTC, respectively. The trajectories have been calculated by MeteoSwiss and are based of local model forecasts.

precipitation. Experimental studies have shown that mineral dust may be an efficient sink of strong acids such as nitric acid HNO_3 , HCl and H_2SO_4 .

1.5. Acid rain

Natural precipitation is slightly acid, partly due to CO_2 dissolved in the falling droplets (4). Carbonic acid is a weak acid, so that the pH value in saturated water is limited to minimum values of about 5.6. Over the last few decades acid rain with pH values lower than 5.0 has occurred in industrial areas and the acids involved have mostly been ‘strong’ ones, such as sulphuric, nitric and hydrochloric acid. Figure 1.5.1 presents a global pattern of acidity of precipitation.

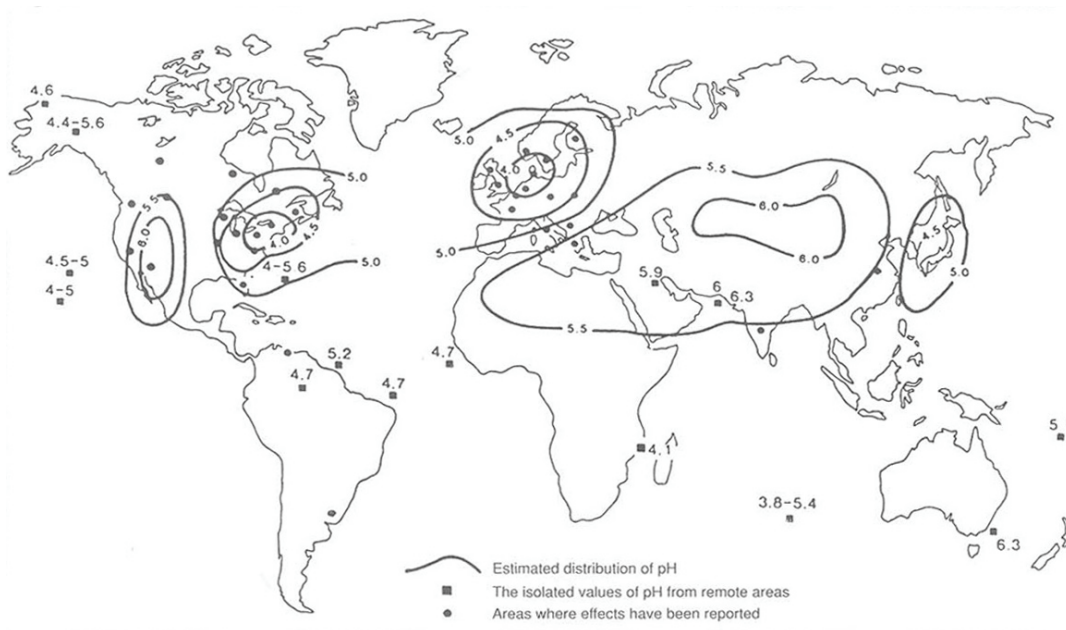


Figure 1.5.1: Map of the global pattern of precipitation acidity (2).

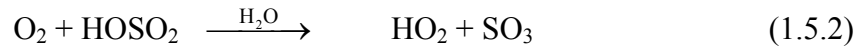
Effects of acid deposition include the following:

1. Acidification of surface water and subsequent damage to aquatic ecosystems: abundant data show a significant correlation between increasing acidity and decreasing fish population (2).
2. Damage of forest and vegetation: Forest decline has been observed in many parts of the world. For example, in 1988 52% and 71% of the forest in Germany and Czechoslovakia, respectively, are affected (39).
3. Damage of materials and structures: Limestone and marble is used in the construction of buildings and monuments. Both rock types are largely composed of calcite (CaCO_3), which is sensitive to acidic deposition (40, 41).

Strong acids such as HNO_3 and H_2SO_4 have their origin in gaseous NO_x and SO_2 , respectively. The main sources of SO_2 are volcanic activity and fuel (coal) combustion whereas NO_x sources are mainly anthropogenic. The concentration of SO_2 ranges from 0.02 to more than 1ppb in the free troposphere of remote areas and polluted continental air, respectively. Atmospheric lifetimes of SO_2 and NO_x and their oxidant products are 1 to 3 days

(2). The concentration of NO_x are given in table 1.2.1. Most of the acidity in the affected rainwater used to be due to H_2SO_4 (4).

The conversion of SO_2 to H_2SO_4 can occur in the gas-phase with the hydroxyl radical and O_2 (4).



In addition, SO_2 can be converted in atmospheric drops with aqueous hydrogen peroxide H_2O_2 (4):



Over the past few years the relative concentration $\frac{\text{NO}_3^-}{\text{SO}_4^-}$ has increased dramatically from 0.2

to 0.7 (4). The change has been brought about both by a reduction of SO_4^- and an increase of NO_3^- .

The formation of HNO_3 includes the following reactions (23):



In developing control strategies to deal with acid deposition it is desired to relate the deposition flux at site j to the strength of the source flux i , the so-called source-receptor relationship. Unfortunately, development of a reliable source-receptor relationship remains a challenging task (2). Figure 1.5.2 shows a conceptual scheme of atmospheric sulphur source-receptor relationship.

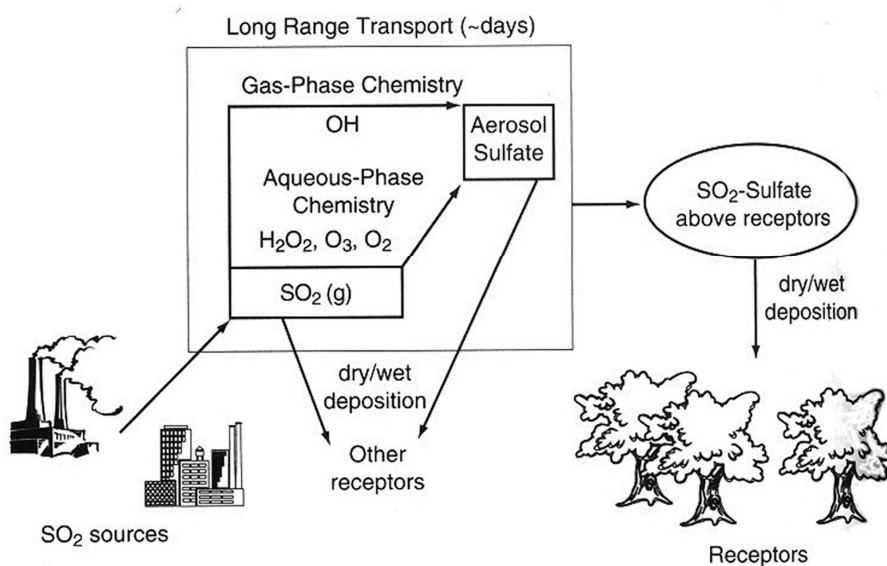


Figure 1.5.2: Conceptual scheme of the atmospheric sulphur source-receptor relationship (2)

1.6. Motivation for the Present Work

Three major axis compose atmospheric science, which are:

- Numerical modelling
- Field measurements
- Laboratory studies

The present work deals with laboratory studies. In order to increase the understanding of atmospheric processes and the reliability of atmospheric models more information about chemical reactions occurring in the atmosphere are needed. Until recently, homogeneous gas-phase reactions have been thought to be the only reactions of any significance in the atmosphere. However, it is now established that heterogeneous reactions on the surface of aerosols play an important role in atmospheric chemistry.

Chapter 1

In this work heterogeneous reactions on different model substrates as surrogates for atmospheric aerosols have been studied in a low-pressure flow reactor with the aim to contribute to a better understanding of the importance of heterogeneous processes on aerosol surfaces.

In the first part reactions of halogen compounds on alkali salts and in the second part reactions of acidic compounds on model mineral dust have been studied. The emphasis has been put on the elucidation of the reaction mechanism, but the kinetics of the reactions has also been considered.

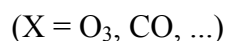
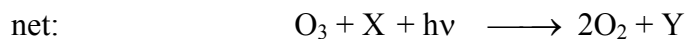
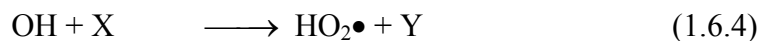
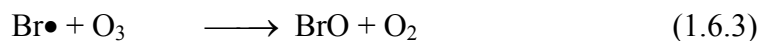
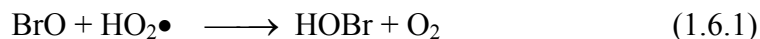
1) Halogen compounds on alkali salts

As already mentioned in section 1.3 halogen radicals such as atomic chlorine and bromine are strong oxidisers and contribute to the tropospheric oxidation potential. Atomic bromine Br and chlorine Cl are mainly produced by photodissociation (reactions 1.3.3 and 1.3.4).

Sea salt constitutes a large reservoir of halogens and there are several possible heterogeneous mechanisms to transform the sea salt halides to reactive halogen species (42). Examples for the release of photodissociable halogens are reactions 1.4.3 –1.4.6. Recent measurements have shown that bromine free radicals are important players in the photochemistry of the lower troposphere (43). Arctic field studies in the spring have shown an anticorrelation between brominated species and a dramatic depletion of ground-level ozone on the time scale of one day, or so (15).

Bromine oxide, BrO, is proposed to be an important agent for tropospheric ozone depletion (44, 12) during which BrO has been measured in concentrations of several ppt (42). Bromine oxide may be involved in catalytic cycle reactions leading to a deletion of ozone.

A possible reaction cycle may be



Those mechanisms involve regeneration of photochemically active bromine. Another possible reaction cycle has been presented in section 1.3, reactions 1.3.5 and 1.3.6. BrO can react with itself regenerating molecular bromine which may photodissociate and complete a reaction cycle that destroys ozone while preserving the bromine radicals. In the Arctic springtime, a “bromine explosion” occurs as the sunlight returns and sharply increases the rate of Br₂ photolysis (43). Model studies have shown that it is almost certain that sea salt is the source of reactive halogen species (42).

The bromine to chlorine ratio in sea salt has been determined as approximately 1: 600 (45), however a substantial segregation of Br⁻ to the surface of NaCl has been observed (46). The enrichment of interfacial bromide may lead to an enhanced release of bromine compounds through heterogeneous reactions on sea salt.

In this work heterogeneous reactions of chlorine compounds on bromine containing alkali salt substrates have been investigated. Such reactions may convert chlorine compounds to photochemically active bromine compounds. As model substrates different sample presentations such as grains, ground grains and thin films of KBr have been used.

As a specific example the reaction of HOCl on KBr has been studied in detail. Hypochlorous acid HOCl is a photochemically active compound. In the presence of photons HOCl decays into active Cl and OH radicals. Both of them contribute to the oxidation capacity of the atmosphere (section 1.2 and 1.3 (47, 48)).



Model studies of the troposphere predict a HOCl concentration of up to 35ppt (49). However, the tropospheric concentration of HOCl has not been confirmed by field measurements until now.

The surface of aerosols is far from being perfect. Surface defects and adsorbed H₂O play a very important role in heterogeneous reactions on these substrates. For a better understanding of the structure and nature of aerosol surfaces the role of adsorbed H₂O and surface defects have been investigated.

2) Acidic Compounds on Mineral Dust

In the troposphere the $R_N = [\text{HNO}_3]/[\text{NO}_x]$ ratio is generally overestimated by a factor of 5-10 in photochemical models in comparison to measurements. Removal processes involving rainout and washout of HNO₃ have been proposed to explain the low R_N measured. However, this suggestion cannot provide a mechanism which maintains the high average NO_x concentration observed (38). Experimental studies have shown, that mineral dust may be efficient sink of strong acids such as nitric acid HNO₃, HCl and H₂SO₄ (37, 50, 51).

A good knowledge of heterogeneous uptake of acidic compounds on mineral dust is urgently needed in order to develop a reliable source-receptor relationship mentioned above.

In this work the uptake of HNO₃, HCl, CO₂ and SO₂ on calcium carbonate CaCO₃ as a surrogate for mineral dust aerosol has been studied. As we have done in the first part on alkali halide substrates the role of adsorbed H₂O has been investigated in detail. Moreover, a few uptake experiments of HNO₃ on Kaolinite, Arizona Road Dust and Saharan Dust have been performed.

1.7. References

- (1) WMO: *IPCC Second Assessment Climat Change 1995*. (1995) pp. 63.
- (2) Seinfeld J. H. and S. N. Pandis: *Atmospheric Chemistry and Physics*. (John Wiley & Sons, 1998).
- (3) Hobbs P. V.: *Introduction to Atmospheric Chemistry*. (Cambridge University Press, 2000) pp. 262.
- (4) Wayne R. P.: *Chemistry of Atmosphere*. (Oxford University Press, 2000) pp. 775.
- (5) Yokouchi Y., Y. Noijiri, L. A. Barrie, D. Toom-Sauntry, T. Machida, Y. Inuzuka, H. Akimoto, H. J. Li, Y. Fujinuma and S. Aoki: *A strong source of methyl chloride to the atmosphere from tropical coastal land*. *Nature*. (2000), vol. 403, pp. 295-298.
- (6) Gerthsen C., H. O. Kneser and H. Vogel: *Physik*. (Springer-Verlag, 1992) pp. 920.
- (7) Häckel H.: *Meteorologie*. (Verlag Eugen Ulmer, 1993) pp. 402.
- (8) IOA: *200th Anniversary of Christian Friedrich Schönbein, the Discoverer of Ozone*. International Ozone Symposium 21 and 22 October 1999. (Basel, 1999) pp. 374.

Chapter 1

- (9) Prinn R. G., J. Huang, R. F. Weiss, D. M. Cunnold, P. J. Fraser, P. G. Simmonds, A. McCulloch, C. Harth, P. Salameh, S. O'Doherty, R. H. J. Wang, L. Porter and B. R. Miller: *Evidence for substantial variations of atmospheric hydroxyl radicals in the past two decades*. Science. (2001), vol. 292, pp. 1882-1888.
- (10) Finlayson-Pitts B. J.: *Chlorine Atoms as a Potential Tropospheric Oxidant in the Marine Boundary-Layer*. Research on Chemical Intermediates. (1993), vol. 19, pp. 235-249.
- (11) Impey G. A., P. B. Shepson, D. R. Hastie, L. A. Barrie and K. G. Anlauf: *Measurements of photolyzable chlorine and bromine during the Polar sunrise experiment 1995*. Journal of Geophysical Research-Atmospheres. (1997), vol. 102, pp. 16005-16010.
- (12) Langendorfer U., E. Lehrer, D. Wagenbach and U. Platt: *Observation of filterable bromine variabilities during Arctic tropospheric ozone depletion events in high (1hour) time resolution*. Journal of Atmospheric Chemistry. (1999), vol. 34, pp. 39-54.
- (13) Platt U.: *Reactive halogen species in the mid-latitude troposphere - Recent discoveries*. Water Air and Soil Pollution. (2000), vol. 123, pp. 229-244.
- (14) Barrie L. A., J. W. Bottenheim, R. C. Schnell, P. J. Crutzen and R. A. Rasmussen: *Ozone Destruction and Photochemical-Reactions at Polar Sunrise in the Lower Arctic Atmosphere*. Nature. (1988), vol. 334, pp. 138-141.

Chapter 1

- (15) Finlayson-Pitts B. J., F. E. Livingston and H. N. Berko: *Ozone Destruction and Bromine Photochemistry at Ground-Level in the Arctic Spring*. *Nature*. (1990), vol. 343, pp. 622-625.
- (16) Platt U. and M. Hausmann: *Spectroscopic Measurement of the Free-Radicals NO₃, BrO, IO, and OH in the Troposphere*. *Research on Chemical Intermediates*. (1994), vol. 20, pp. 557-578.
- (17) Platt U. and G. K. Moortgat: *Heterogeneous and homogeneous chemistry of reactive halogen compounds in the lower troposphere - The papers were presented at the XXIII General Assembly of the European Geophysical Society in Nice, France, 20-24 April 1998*. *Journal of Atmospheric Chemistry*. (1999), vol. 34, pp. 1-8.
- (18) Pszenny A. A. P., W. C. Keene, D. J. Jacob, S. Fan, J. R. Maben, M. P. Zetwo, M. Springeryoung and J. N. Galloway: *Evidence of Inorganic Chlorine Gases Other Than Hydrogen-Chloride in Marine Surface Air*. *Geophysical Research Letters*. (1993), vol. 20, pp. 699-702.
- (19) Spicer C. W., E. G. Chapman, B. J. Finlayson-Pitts, R. A. Plastridge, J. M. Hubbe, J. D. Fast and C. M. Berkowitz: *Unexpectedly high concentrations of molecular chlorine in coastal air*. *Nature*. (1998), vol. 394, pp. 353-356.
- (20) Harrison R. M. and R. V. Grieken: *Atmospheric Particles*. (John Wiley & Sons Ltd., 1998) pp. 610.

Chapter 1

- (21) Raes F., R. Van Dingenen, E. Vignati, J. Wilson, J. P. Putaud, J. H. Seinfeld and P. Adams: *Formation and cycling of aerosols in the global troposphere*. Atmospheric Environment. (2000), vol. 34, pp. 4215-4240.
- (22) Charlson R. J. and J. Heintzenberg: *Aerosol Forcing of Climate*. (John Wiley & Sons Ltd, 1995) pp. 416.
- (23) Finlayson-Pitts B. J.: *Chemistry of the Upper and Lower Atmosphere*. (Academic Press, 2000) pp. 969.
- (24) Salma I., I. Balashazy, W. Hofmann and G. Zaray: *Effect of physical exertion on the deposition of urban aerosols in the human respiratory system*. Journal of Aerosol Science. (2002), vol. 33, pp. 983-997.
- (25) Shaw G. E.: *Aerosol Chemical-Components in Alaska Air Masses .2. Sea Salt and Marine Product*. Journal of Geophysical Research-Atmospheres. (1991), vol. 96, pp. 22369-22372.
- (26) Blanchard D. C. and A. H. Woodcock: *Bubble Formation and Modification in the Sea and Its Meteorological Significance*. Tellus. (1957), vol. 9, pp. 145-158.
- (27) Beichert P. and B. J. Finlayson-Pitts: *Knudsen cell studies of the uptake of gaseous HNO_3 and other oxides of nitrogen on solid NaCl: The role of surface-adsorbed water*. Journal of Physical Chemistry. (1996), vol. 100, pp. 15218-15228.

- (28) Fenter F. F., F. Caloz and M. J. Rossi: *Kinetics of Nitric-Acid Uptake by Salt*. Journal of Physical Chemistry. (1994), vol. 98, pp. 9801-9810.
- (29) Vogt R. and B. J. Finlayson-Pitts: *A Diffuse-Reflectance Infrared Fourier-Transform Spectroscopic (Drifts) Study of the Surface-Reaction of NaCl with Gaseous NO₂ and HNO₃*. Journal of Physical Chemistry. (1994), vol. 98, pp. 3747-3755.
- (30) Aguzzi A. and M. J. Rossi: *The kinetics of the heterogeneous reaction of BrONO₂ with solid alkali halides at ambient temperature. A comparison with the interaction of ClONO₂ on NaCl and KBr*. Physical Chemistry Chemical Physics. (1999), vol. 1, pp. 4337-4346.
- (31) Lee D. S., R. D. Kingdon, J. M. Pacyna, A. F. Bouwman and I. Tegen: *Modelling base cations in Europe - sources, transport and deposition of calcium*. Atmospheric Environment. (1999), vol. 33, pp. 2241-2256.
- (32) Tegen I. and I. Fung: *Modeling of Mineral Dust in the Atmosphere - Sources, Transport, and Optical-Thickness*. Journal of Geophysical Research-Atmospheres. (1994), vol. 99, pp. 22897-22914.
- (33) Zhang Y., Y. Sunwoo, V. Kotamarthi and G. Carmichael: *Photochemical Oxidant Processes in the Presence of Dust: An Evaluation of the Impact of Dust on Particulate Nitrate and Ozone Formation*. Journal of Applied Meteorology. (1994), vol. 33, pp. 813-824.

Chapter 1

- (34) Avila A. and J. Penuelas: *Increasing frequency of Saharan rains over northeastern Spain and its ecological consequences*. Science of the Total Environment. (1999), vol. 228, pp. 153-156.
- (35) Schmidt L. J.: *When the Dust Settles*. (2001).
- (36) Swap R., M. Garstang, S. Greco, R. Talbot and P. Kallberg: *Saharan Dust in the Amazon Basin*. Tellus Series B-Chemical and Physical Meteorology. (1992), vol. 44, pp. 133-149.
- (37) Fenter F. F., F. Caloz and M. J. Rossi: *Experimental-Evidence for the Efficient Dry Deposition of Nitric-Acid on Calcite*. Atmospheric Environment. (1995), vol. 29, pp. 3365-3372.
- (38) Hauglustaine D. A., B. A. Ridley, S. Solomon, P. G. Hess and S. Madronich: *HNO₃/NO_x ratio in the remote troposphere during MLOPEX 2: Evidence for nitric acid reduction on carbonaceous aerosols?* Geophysical Research Letters. (1996), vol. 23, pp. 2609-2612.
- (39) Mader S. S. and G. W. Cox: *Environmental Biology-Acid Rain and Soil Erosion*. (1996/1997).
- (40) Baedecker P. A. and M. M. Reddy: *The Erosion of Carbonate Stone by Acid-Rain - Laboratory and Field Investigations*. Journal of Chemical Education. (1993), vol. 70, pp. 104-108.

Chapter 1

- (41) Graedel T. E.: *Mechanisms for the atmospheric corrosion of carbonate stone*. Journal of the Electrochemical Society. (2000), vol. 147, pp. 1006-1009.
- (42) Barrie L. and U. Platt: *Arctic tropospheric chemistry: an overview*. Tellus Series B-Chemical and Physical Meteorology. (1997), vol. 49, pp. 450-454.
- (43) Wennberg P.: *Atmospheric chemistry - Bromine explosion*. Nature. (1999), vol. 397, pp. 299-301.
- (44) Hausmann M. and U. Platt: *Spectroscopic Measurement of Bromine Oxide and Ozone in the High Arctic During Polar Sunrise Experiment 1992*. Journal of Geophysical Research-Atmospheres. (1994), vol. 99, pp. 25399-25413.
- (45) Weast R. C.: *Handbook of Chemistry and Physics*. (CRC Press, 1986).
- (46) Ghosal S., A. Shbeeb and J. C. Hemminger: *Surface segregation of bromine in bromide doped NaCl: Implications for the seasonal variations in Arctic ozone*. Geophysical Research Letters. (2000), vol. 27, pp. 1879-1882.
- (47) Burkholder J. B.: *Ultraviolet-Absorption Spectrum of HOCl*. Journal of Geophysical Research-Atmospheres. (1993), vol. 98, pp. 2963-2974.
- (48) Molina L. T. and M. J. Molina: *Ultraviolet-Spectrum of HOCl*. Journal of Physical Chemistry. (1978), vol. 82, pp. 2410-2414.

- (49) Vogt R., P. J. Crutzen and R. Sander: *A mechanism for halogen release from sea-salt aerosol in the remote marine boundary layer*. *Nature*. (1996), vol. 383, pp. 327-330.
- (50) Goodman A. L., E. T. Bernard and V. H. Grassian: *Spectroscopic study of nitric acid and water adsorption on oxide particles: Enhanced nitric acid uptake kinetics in the presence of adsorbed water*. *Journal of Physical Chemistry A*. (2001), vol. 105, pp. 6443-6457.
- (51) Hanisch F. and J. N. Crowley: *Heterogeneous reactivity of gaseous nitric acid on Al_2O_3 , $CaCO_3$, and atmospheric dust samples: A Knudsen cell study*. *Journal of Physical Chemistry A*. (2001), vol. 105, pp. 3096-3106.

Chapter 2

2. Experimental Section

2.1. Knudsen Flow Reactor

The Knudsen reactor, developed originally as a VLPP (Very Low Pressure Pyrolysis) more than thirty years ago by Benson et al. (2), is a low-pressure flow reactor operating under molecular flow conditions. The technique has been applied to study the kinetics of chemical reactions of a wide variety of systems. In the pressure regime of P_{tot} less than 1mbar or so, gas-wall interactions are strongly favoured over gas-gas interactions for the geometrical dimensions of our reactor. The Knudsen reactor is thus used here for the study of the heterogeneous interactions of gases with solid substrates.

The measurements are based among others on the idea of a differential observation of the outflow of the reactant of interest in the absence and presence of a solid substrate. Two different types of measurements may be performed.

Chapter 2

1) Steady state experiments:

Figure 2.1 illustrates a typical steady state uptake experiment. A constant flow of molecules F_{in} is injected into the reactor. The outflow F_{out} is measured keeping the sample compartment isolated from the gas in the reactor using a movable plunger. Lifting the plunger enables the interaction of the gas with the solid sample of interest. We compare the outflows actuating the plunger into the upper and lower position, which means that the sample compartment changes from the open to the closed position or vice versa, respectively. This allows to draw conclusions on the kinetics of the interaction between the gaseous reactant and the exposed surface.

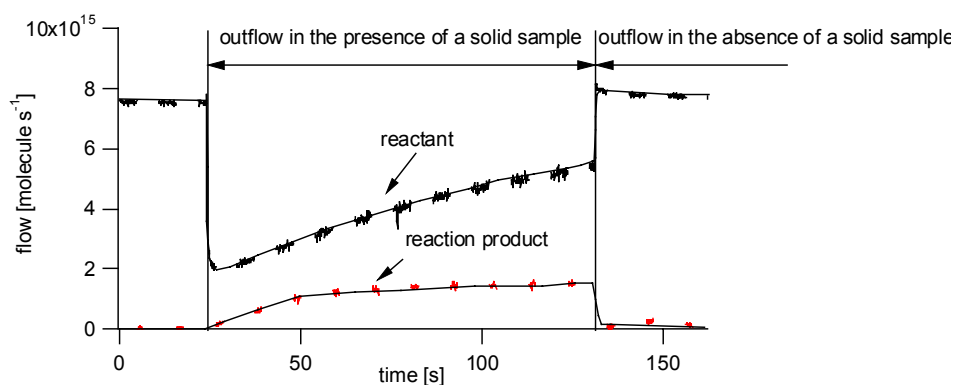


Figure 2.0.1: Outflow F_{out} as a function of time of a typical steady state uptake experiment performed in the 14mm-orifice reactor. The level of the reactant decreases upon lifting the plunger and a reaction product is formed.

Further information is obtained by the analysis of the reaction products. Mass balances, which means a comparison of the number of lost molecules with the number of generated molecules give important information about the reaction mechanism.

2) Pulsed valve experiments:

Figure 2.2 illustrates a typical pulsed valve uptake experiment. A known dose of molecules is introduced into the reactor by opening an electromagnetically controlled valve for a given time, typically on the order of a few milliseconds.

Chapter 2

Similar to steady state experiments differential measurements are carried out by comparing the outflow F_{out} of a reference with the outflow F_{out} of a reactive pulse, which means that pulses performed with the sample compartment open or closed, respectively. The difference in shape and total area of the pulses provide information on the heterogeneous interaction of the gas with the surface of the sample.

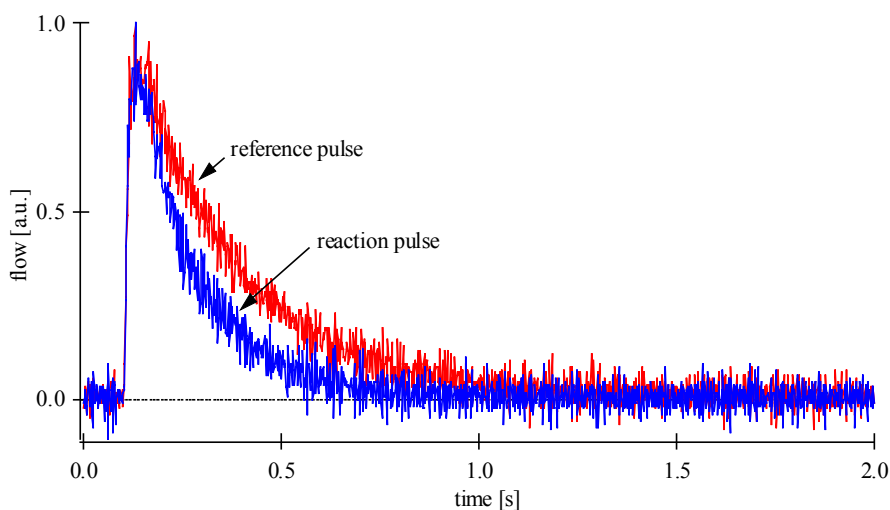


Figure 2.0.2: Outflow as a function of time of a typical pulsed valve uptake experiment. The reference pulse is performed with the closed and the reaction pulsed with the opened sample compartment, respectively.

The advantages of pulsed valve experiments are

- Small doses, of the order of a few percents of a surface monolayer, may be injected which means small surface modification.
- Products can be observed with a high time resolution. This may be useful for understanding the reaction mechanism.
- Mass balances are easy to perform with pulsed valve experiments.

2.1.1. Description of the Apparatus

A detailed description of the apparatus is given by Fenter (3) and Caloz (4). In this section we give a short description of the experimental set-up. Figure 2.1.1 shows a schematic drawing of the low-pressure flow reactor.

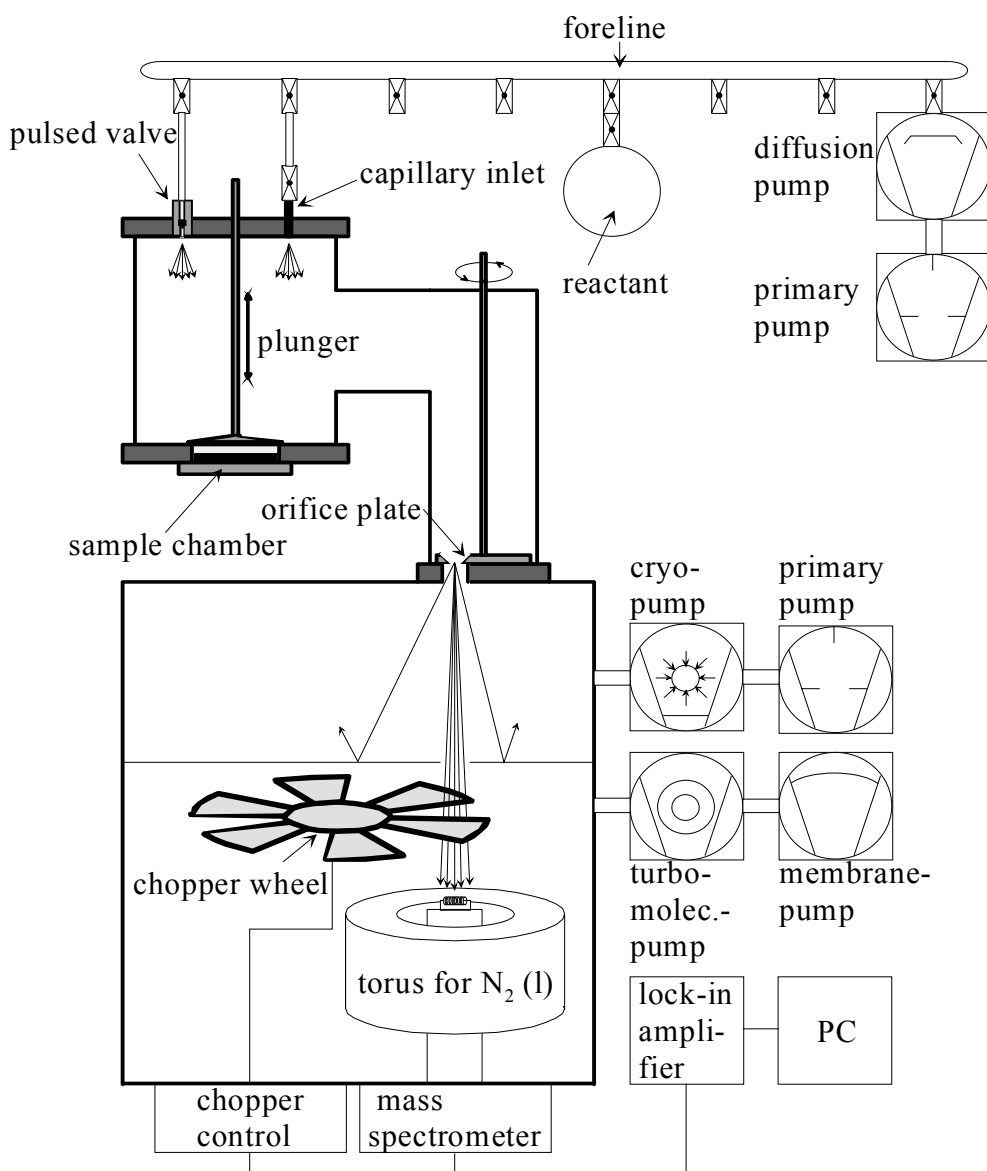


Figure 2.1.1: Schematic drawing of the experimental setup. The Knudsen cell is mounted on a differentially pumped chamber system. The upper chamber is pumped by a cryogenic pump whereas the lower chamber by a turbo molecular pump. The detection of the molecules is performed using a quadrupole mass spectrometer.

Chapter 2

The apparatus consists of a vacuum line from which molecules are introduced into the reactor. The vacuum line is used to store and mix reactants. The reactants are injected into the reactor either continuously via a capillary or in pulses of millisecond duration via a solenoid valve. The pressure in the fore-line is measured by a Baratron pressure gauge (MKS Baratron 122AA-00010AB). The inlet flow is usually in the range 10^{12} to 10^{15} molecule s^{-1} which corresponds to a gas concentration in the reactor on the order of 10^9 to 10^{13} molecule cm^{-3} .

The Knudsen reactor is a chamber of known volume constructed of glass and stainless steel elements and sealed with Viton O-rings. The inner walls of the reactor have been coated with a perfluoropolymer (Teflon, Dupont FEP 120 suspension) in order to minimise surface adsorption and catalytic reactions at the wall surfaces. The applied coating is transparent and thin (about 0.1 mm). The Teflon coating is kept as thin as possible in order to avoid micro pores generated in the Teflon.

The sample support is separated from the reactor volume by a plunger in order to carry out uptake experiments. The volume of the sample compartment is about 1% of the total volume of the cell. This arrangement eliminates the effect of reactant dilution when the sample chamber is connected to the reactor chamber when lifting the isolation plunger, as well as the systematic errors associated with abrupt increase in the non-reactive surface area.

The residence time of the gaseous species in the reactor is determined by the cross-section of the escape orifice. The cross-section of the escape orifice may be controlled by a rotatable orifice plate (see Figure 2.1.1) which allows the use of up to 4 orifices, selected by turning a rod. The plate we used for this work is equipped with 1, 4, 8 and 14mm orifices. This leads to a potential variation of the gas residence time of greater than two orders of magnitude (Section 2.1.2).

Gaseous species are analysed using mass spectrometry (MS). The mass spectrometer (Balzers QMA 421) is mounted in the lower part of the differentially pumped vacuum

Chapter 2

chamber. A differentially pumped arrangement has been chosen in order to increase the quality of the effusing molecular beam formed at the exit orifice of the reactor. The upper and lower chambers are pumped by a cryogenic and turbo molecular pump, respectively. The molecular beam has been modulated by a chopper-wheel leading to a modulation frequency ν of 230Hz. Chopped beam and lock-in amplifier (Stanford Research SRS 830 DSP) allow discrimination between the background signal in the detection chamber and the contribution originating from the reactor. In order to minimise the level of residual molecules in the lower chamber, where the detection takes place, a torus around the head of the spectrometer is installed. The torus is filled with liquid nitrogen and acts as a cryogenic pump and lowers the pressure by about a factor of ten. Residual molecules in the chamber lead to a increased level of noise in the demodulated MS-signal, which is the output of the lock-in amplifier. The use of the torus improves the signal to noise ratio significantly. This is important for water measurements at $m/e = 18$ because of its presence in the detection chamber that is caused by micro leaks of the reactor and chambers.

2.1.2. The Measurement Principle

Under molecular flow conditions, each molecule that enters the reactor may leave the cell through the escape orifice and is lost when it undergoes an interaction in a collision with the surface of the sample. Not every collision of the molecule with the sample surface leads to a chemical reaction or absorption. Knowing the probability γ of the loss of a molecule per collision and the collision frequency the reaction rate may be determined.

The goal of the measurement is the determination of the reaction probability γ . From gas kinetic theory the average gas-wall collision frequency of a molecule per cm^2 of the surface sample, referred to Z_1 , is given by

$$Z_1 = \frac{\bar{c}}{4V} = \sqrt{\frac{8RT}{\pi M}} \frac{1}{4V} \quad (\text{equation 2.1.1})$$
$$[Z_1] = \text{collision cm}^{-2} \text{ s}^{-1}$$

Chapter 2

where R is the ideal gas constant, T the temperature of the reactor in Kelvin, M the molar mass, V the volume of the reactor and \bar{c} the mean velocity of a molecule. The number of collisions per second over the total sample may be calculated using equation 2.1.2.

$$\omega = Z_1 A_s \quad (\text{equation 2.1.2})$$

where A_s is the geometric surface of the sample. Typical values of ω are in the range 50 to 100s^{-1} for the samples we use having an area of 20cm^2 . In this work the geometrical area A_s of the sample holder is used in order to calculate the collision frequency of the sample. The use of geometrical area A_s does not take into account pore diffusion and is a good approximation for a fast reaction system.

For a first order reaction the probability for a molecule to undergo a reaction per unit time may be expressed in the following way:

$$\frac{1}{N} \frac{dN}{dt} = -k_{\text{uni}} \quad (\text{equation 2.1.3})$$

where k_{uni} is the rate constant for a first order reaction. It follows that the reaction probability per collision γ is:

$$\gamma = \frac{k_{\text{uni}}}{\omega} \quad (\text{equation 2.1.4})$$

γ is also known as the uptake coefficient of a reaction, and is a property of the reaction system. This means that it is a parameter which does not depend on the experimental setup.

Chapter 2

Every molecule which “collides” with the orifice is lost. This means that for the orifice we have $\gamma = 1$. Using equation 2.1.4 and 2.1.2 the escape rate constant of a molecule may be written as

$$k_{\text{esc}} = Z_1 A_H = \frac{\bar{c}}{4V} A_H \quad (\text{equation 2.1.5})$$

where A_H is the orifice area. The gas-phase residence time τ of a molecule in the reactor is defined as

$$\tau = \frac{1}{k_{\text{esc}}} \quad (\text{equation 2.1.6})$$

Typical residence times τ are in the range of 0.1 to 0.3s and 10 to 35s corresponding to the 14mm- and 1mm-orifice reactor, respectively. Solving equation 2.1.3 leads to an exponential decay of N . k_{esc} may be experimental determined measuring the decay of the MS-signal after halting the inflow.

The mass spectrometer probes the effusive molecular beam leaving the Knudsen reactor through the escape orifice. It would be desirable to calculate the uptake coefficient γ based on the outflow F_{out} and the k_{esc} . For F_{out} the following relation may be used

$$F_{\text{out}} = k_{\text{esc}} N \quad (\text{equation 2.1.7})$$

For a constant inflow F_{in} we obtain for steady state conditions:

$$\frac{dN}{dt} = F_{\text{in}} - F_{\text{out}} - k_{\text{uni}} N = 0 \quad (\text{equation 2.1.8})$$

Using equation 2.1.7 and 2.1.8 we obtain

Chapter 2

$$k_{\text{uni}} = \left(\frac{F_{\text{in}}}{F_{\text{out}}} - 1 \right) k_{\text{esc}} \quad (\text{equation 2.1.9})$$

Introducing equation 2.1.9 into 2.1.4 equation 2.1.10 results for the uptake coefficient γ :

$$\gamma = \left(\frac{F_{\text{in}}}{F_{\text{out}}} - 1 \right) \frac{k_{\text{esc}}}{\omega} \quad (\text{equation 2.1.10})$$

The outflow is linearly related to the mass spectrometer signal S . Thus, we can write:

$$\gamma = \left(\frac{S_0}{S_R} - 1 \right) \frac{k_{\text{esc}}}{\omega} \quad (\text{equation 2.1.11})$$

where S_0 and S_R are the MS-signals measured with closed and open sample compartment, respectively.

For pulsed valve experiments the following relation may be used in order to calculate the uptake coefficient γ :

$$k_{\text{dec}} = k_{\text{eff}} + k_{\text{esc}} \quad (\text{equation 2.1.12})$$

where k_{dec} is the decay of the MS-signal of the reaction pulse (Figure 2.2). k_{esc} corresponds to the decay of the reference pulse. The uptake coefficient γ based on a pulsed valve experiment may be expressed as follows:

$$\gamma = \frac{k_{\text{dec}} - k_{\text{esc}}}{\omega} \quad (\text{equation 2.1.13})$$

Chapter 2

In order to calculate the uptake coefficient γ some parameter of the reactor should be known. Table 1.2.1 summarises the reactor parameters.

Table 1.2.1: Knudsen cell parameters (1)

Parameter	Value
Reactor volume	1830cm ³
Calculated surface area	1300cm ²
Sample compartment surface area	19.6cm ²
Chopper frequency	235Hz
Orifice-Ø	1, 4, 8 and 14mm

2.2. Calibrations

In order to measure the absolute outflow F_{out} in molecule s^{-1} the MS-signal needs to be calibrated. Based on the ideal gas law (equation 2.2.1) the MS-signal is calibrated in the following manner:

$$pV = nRT \quad (\text{equation 2.2.1})$$

$$\frac{dN}{dt} = \frac{dp}{dt} \underbrace{\frac{RT}{V_c}}_X N_A = F_{\text{in}} \quad (\text{equation 2.2.2})$$

where R is the gas constant, T the temperature in Kelvin, V_c a calibrated Volume and N_A Avogadro's number. Under the assumption that $F_{\text{out}} = F_{\text{in}}$ the calibration factor K results:

$$S K = \frac{dp}{dt} X \quad (\text{equation 2.2.3})$$

where S the mass spectrometer signal is.

Chapter 2

The pressure has been measured using a pressure gauge MKS Baratron 122AA-00010AB and the decay $\frac{dp}{dt}$ in the calibrated volume V_c using a stop-watch. Furthermore, the pressure in the calibration volume V_c may be recorded by the computer-based data acquisition (Section 2.3). The calibration has been carried out on a regular basis in order to take into account possibly changes of the sensitivity of the mass spectrometer.

Knowing the calibration factor K of a given species i its concentration c^i can be calculated using equation 2.2.4:

$$[c^i] = \frac{S^i K^i}{k_{\text{esc}}^i V} \quad (\text{equation 2.2.4})$$

where S , K , k_{esc} and V are the MS-signal, the calibration factor, the escape rate constant and the volume of the reactor, respectively.

Hypochlorous acid, HOCl, and water, H₂O, are two gases that are too unstable or too sticky, respectively, for calibration to take place in the way described above. We have chosen a different technique in order to perform these calibrations.

2.2.1. Calibration of HOCl

Because of the wall-catalysed decomposition of hypochlorous acid by wall collisions it could not be stored in the calibrated glass volume at ambient temperature, hence $\frac{dp}{dt}$ could not be measured in order to carry out a calibration.

Chapter 2

The calibration of HOCl has been performed in the following way using reaction 2.2.1:



An unknown amount of HOCl has been introduced into the reactor where it has been condensed on an ice surface at $T = 160\text{K}$. The unavoidable impurity Cl_2O in HOCl does not condense under the present conditions. The uptake coefficient of reaction (2.2.1) has been measured as $\gamma = 0.25$ at $T = 200\text{K}$ (5). During deposition of HOCl the MS-signal of the loss of HOCl has been monitored. Subsequently, the condensed HOCl has been exposed to a continuous HCl flow while the production of Cl_2 has been monitored. The amount of the resulting Cl_2 has been determined using the known calibration factor K_{Cl_2} of Cl_2 . From reaction (2.2.1) 1 molecule of HOCl(a) lost corresponds to the formation of 1 molecule of $\text{Cl}_2\text{(g)}$ which means that the total amount of measured $\text{Cl}_2\text{(g)}$ corresponds to the total amount of HOCl adsorbed before. The calibration factor K_{HOCl} for HOCl may be calculated using equation 2.2.5:

$$K_{\text{HOCl}} = \frac{N(\text{Cl}_2\text{(g)})}{A(\text{HOCl})} \quad (\text{equation 2.2.5})$$

where $N(\text{Cl}_2\text{(g)})$ corresponds to the total amount of measured Cl_2 and $A(\text{HOCl})$ is the MS-signal for HOCl loss integrated over time.

2.2.2. Calibration of H₂O

Gaseous H_2O has a large surface residence time on the walls of the calibration volume. This leads to an error in the calibration. In order to minimise this error 9 μl of H_2O have been frozen on the low-temperature support at $T = 180\text{K}$ (a detailed description of the low-temperature support may be found in the thesis of Caloz 1997 (1)). Subsequently, the temperature of the support has been slowly increased so that the MS-signal of the desorbing H_2O could be recorded.

Chapter 2

9 μl of H_2O correspond to 0.5 mmol of H_2O or $N = 0.5 \cdot 10^{-3} \cdot N_A$ molecules. The calibration factor $K_{\text{H}_2\text{O}}$ may now be calculated using equation 2.2.6:

$$N = K_{\text{H}_2\text{O}} \int S(t) dt \quad (\text{equation 2.2.6})$$

where N_A is Avogadro's number and $S(t)$ the MS signal of H_2O .

2.3. The High Temperature Support

In order to control the amount of adsorbed water on solid samples they have been heated under vacuum conditions. We have used a support in which samples may be heated in situ up to 750 K inside the low-pressure environment of the reactor.

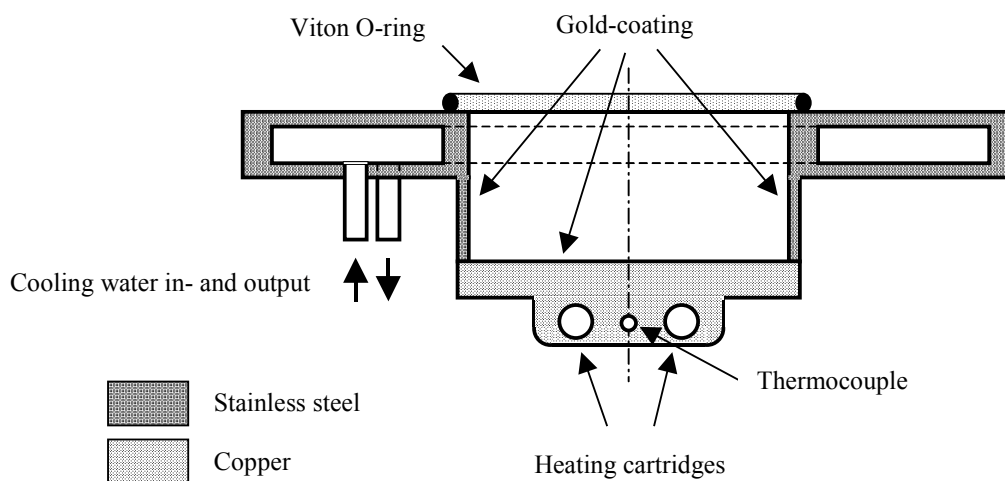


Figure 2.3.1: Schematic drawing of the high temperature support (HTS). The bottom of the support represents the reactive surface. Its diameter d is 5cm corresponding to a reactive surface of 19.6 cm^2 .

The high temperature support (HTS) is heated by two 6 mm cartridges located outside of the reactor cell (Figure 2.3.1). The heated copper dish is thermally insulated from the reactor by a thin-walled stainless steel wall and furthermore cold water is circulated in the base flange in order to prevent any heating of the O-rings.

Chapter 2

The temperature is controlled by variation of the electrical voltage applied to the two 200 W cartridges and measured by a type K thermocouple fastened into the copper block. The internal surface of the support is coated with a thin gold layer of a few μm thickness in order to protect the copper block against chemical corrosion but also to minimise adsorption of gaseous species.

2.4. Data Acquisition

The personal computer (PC) based signal acquisition has been made possible by an acquisition board DAQ 6024E supplied by National Instruments (NI).

The acquisition card contains:

- 16 single-ended or 8 differential analog inputs with a resolution of 12Bits (1 in 4096). The maximal sampling rate is 200kSamples/s, which means that the maximum sample frequency is 12.5kHz for each channel.
- 2 analog outputs with a resolution of 12Bits and a maximum output range of $\pm 10\text{V}$.
- 8 digital in/outputs

The acquisition card is controlled by the graphical programming language LabView supplied by NI which manages the acquisition of 6 analog inputs, the pulse generation for the pulsed valve experiments, monitoring of the signals and writing to the harddisk. Figure 2.3.1 shows a schematic illustration of the acquisition setup.

Chapter 2

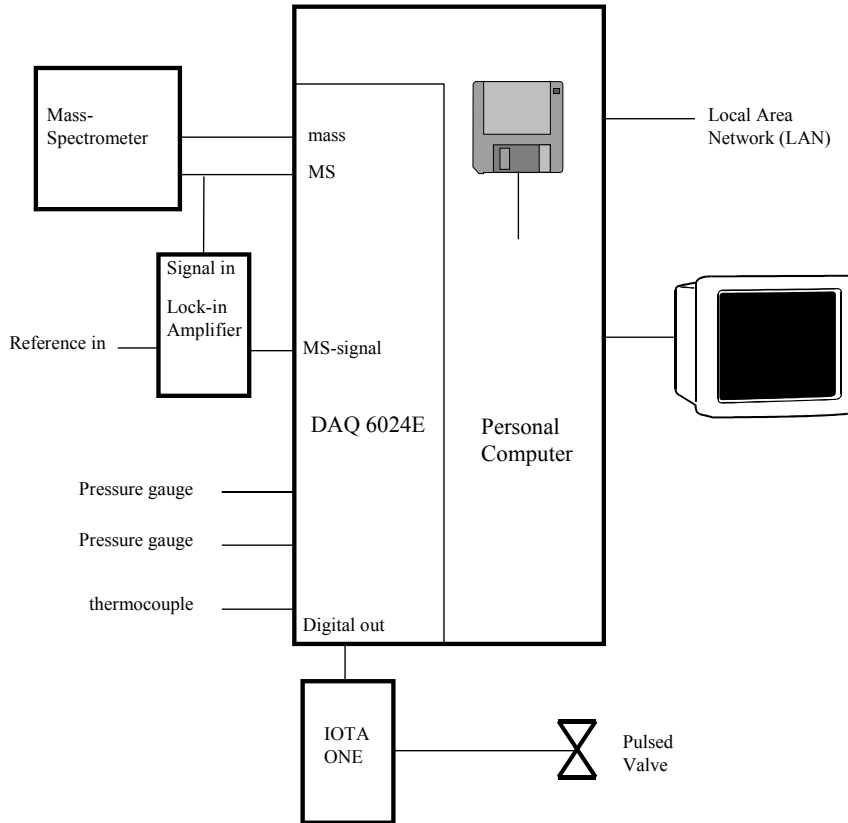


Figure 2.4.1: Schematic illustration of the personal computer based data acquisition.

For steady state experiments the acquisition works in one point mode which means every recorded point is immediately written to the harddisk which allows a long term acquisition. The sample frequency attributed to steady state experiments is 10Hz.

Pulsed valve experiments are recorded in a buffered mode which allows fast acquisition over a short time. The sample frequency for pulsed valve experiments is 1kHz.

Furthermore, the analog inputs are configured as differential inputs in order to reduce electromagnetically induced noise. This is important for small signals such as the ones we record from thermocouples. The used cables are screened against electrically induced noise and twisted pairs are used in order to minimise induced noise. Figure 2.4.2 shows the input configuration of the analog inputs.

Chapter 2

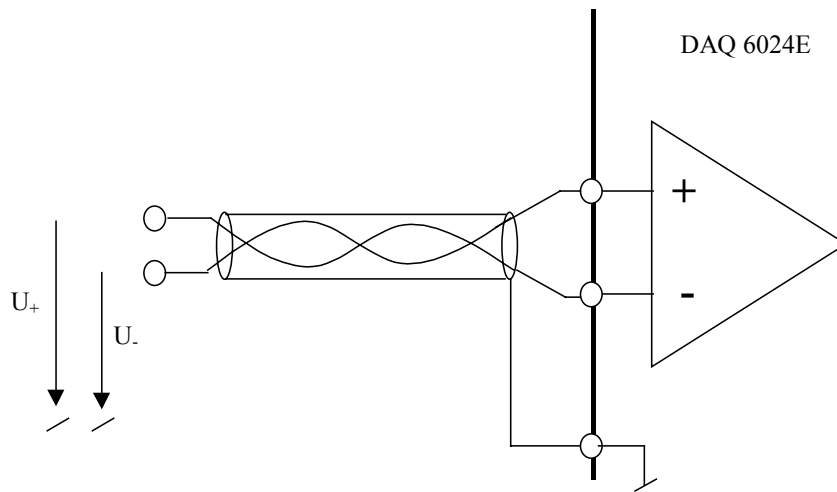


Figure 2.4.2: Configuration of the differential input of the card. The device is connected between U_+ and U_- .

At the + input and the - input of the card we have $U_+ + U_n$ and $U_- + U_n$, respectively. Where U_n means additional noise.

The input signal U_{in} may be written as

$$U_{in} = (U_+ + U_n) - (U_- + U_n) = U_+ - U_- \quad (\text{equation 2.4.1})$$

Induced noise may be considerably reduced using differential inputs.

In order to minimise noise, closed loops of the ground wire should be avoided and only one well defined potential should be used as reference ground GND.

2.5. References

- (1) Caloz F.: *Laboratory Kinetic Studies of Heterogeneous Processes Relevant to the Marine Troposphere*. (EPFL, 1997) pp. 236.
- (2) Benson S. W. and G. N. Spokes: *Very Low-Pressure Pyrolysis .I. Kinetic Studies of Homogeneous Reactions at Molecular Level*. *Journal of the American Chemical Society*. (1967), vol. 89, pp. 2525-2532.
- (3) Fenter F. F., F. Caloz and M. J. Rossi: *Paper II: Simulation of flow conditions in low-pressure flow reactors (Knudsen cells) using a Monte Carlo technique*. *Review of Scientific Instruments*. (1997), vol. 68, pp. 3180-3186.
- (4) Caloz F., F. F. Fenter, K. D. Tabor and M. J. Rossi: *Paper I: Design and construction of a Knudsen-cell reactor for the study of heterogeneous reactions over the temperature range 130-750 K: Performances and limitations*. *Review of Scientific Instruments*. (1997), vol. 68, pp. 3172-3179.
- (5) Oppliger R.: *Kinetics Studies of heterogeneous Reactions of chlorine and bromine Reservoirs relevant to the lower Stratosphere*. Thesis N° 1779. (1998) pp. 161.

Chapter 3

3. Preparation of Halogen and Alkali Salt Samples

3.1. Gaseous Samples

In this chapter we describe the preparation of the solid and gaseous samples we used for the experiments of halogen compounds on alkali salt substrates in chapter 4.

Some samples require to be synthesised in the laboratory because they are not stable at ambient temperature and therefore not commercially available.

The synthesised unstable gaseous products have been stored in a cooling bath kept at $\vartheta = -80^{\circ}\text{C}$. Because some of them are photochemically unstable they have been stored in darkened storage bulbs.

In order to achieve a certain purity of the gaseous samples we purified commercially available gases such as Cl_2 and Br_2 .

Chapter 3

In order to remove residual HCl from Cl₂ we pumped it through sodium hydroxide, NaOH:



Reaction 3.1.1 is a very exothermic. Cl₂ may be monitored at the parent peak $m/e = 70$ (100%) and $m/e = 35$ (33%), where the value in the brackets means the relative intensity compared to the parent peak.

In order to remove residual H₂O from Br₂ that we stored in a glass bulb we pumped it through diphosphorus pentoxide, P₂O₅, before we used it for the syntheses of our samples. Br₂ has been monitored at the base peak $m/e = 160$ (100%) but also at $m/e = 79$ (25%) and $m/e = 81$ (25%) (1).

3.1.1. Preparation of HCl

HCl has been synthesised in the laboratory from the reaction of pure sulfuric acid H₂SO₄ on dry NaCl at room temperature under vacuum conditions (reaction 3.1.2).

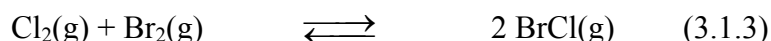


The resulting gaseous HCl has been trapped in a bulb at the temperature of liquid nitrogen. The purity of HCl has been checked in the flow reactor. Any possible impurities such as H₂O and Cl₂ have been below the detection limit of the mass spectrometer.

The base mass spectrometric peak of HCl is at $m/e = 36$ (100%). Furthermore, fragment peaks are at $m/e = 35$ (17%) and $m/e = 38$ (32%) (1).

3.1.2. Preparation of BrCl

Gaseous BrCl is obtained by mixing a small amount of Br₂ in excess Cl₂ at room temperature according to reaction 3.1.3.



Subsequently, the mixture has been distilled at T = 200 K.

The mass spectrometric peaks are at m/e = 116 (100%) and m/e = 114 (114%). Other fragment peaks are at m/e = 35 (28%) and m/e = 79 (25%).

3.1.3. Preparation of Cl₂O

Dichloromonoxide, Cl₂O, has been synthesised by reacting Cl₂ with mercuric oxide, HgO (2) according to reaction 3.1.4:



The reacting mixture of HgO-Cl₂ has been kept at least 24h in a circulating methanol bath at T = 193K in order to complete the reaction. The separation of the excess Cl₂ from Cl₂O has been performed by distillation in a standard vacuum line. The Cl₂ has been pumped off at T = 200K from the mixture of Cl₂O and Cl₂ while Cl₂ and Cl₂O have been monitored at masses 70 and 51, respectively, by mass spectrometry. Cl₂ could almost completely be removed from the sample. The purified Cl₂O has been stored in a methanol cooling bath at T = 190K for long-term storage.

3.1.4. Preparation of HOCl

The hypochlorous acid, HOCl, gas sample has been generated by hydrolysis of Cl₂O according to equation 3.1.5:



Typically, a gaseous sample of Cl₂O has been deposited on frozen H₂O at T = 77K, after which the mixture has been heated up to ambient temperature and again cooled down to T = 200K. The resulting HOCl sample has been distilled in a standard vacuum line at T = 210K in order to remove impurities of Cl₂O and Cl₂ where the HOCl, Cl₂O and Cl₂ flows have continuously been monitored by mass spectrometry. According to the equilibrium constant K = 0.082 (2) for reaction (3.1.5) HOCl always contains a certain amount of Cl₂O. For long-term storage the HOCl reservoir has been kept in a Teflon coated glass bulb at T = 190K. Very little signs of HOCl decomposition have been observed at this temperature.

HOCl has been monitored at m/e = 52. The contribution of HOCl to the MS-signal at m/e = 51 is less than 5% of the parent ion at m/e = 52 (3).

3.2. Solid Samples

Commercially available KBr and NaCl (Fluka AG) have been used for the experiments with gaseous halogen species described in section 4. The purity of KBr and NaCl is better than 99.5% (value given by supplier). The NaCl and KBr samples have been prepared in the same way, therefore if no specification is given in the following sections the procedure applies to both NaCl and KBr.

In this section we describe the preparation of grains, ground grains, thin films sprayed on Pyrex and gold-coated substrates, respectively.

3.2.1. Grain Samples

In this work commercially available salt is called grains. The diameter d of the KBr and NaCl grains has been determined by optical microscopy to be on the order of 150 μm and 400 μm , respectively. The ratio between the apparent density of crystalline KBr to KBr grains has been measured as $\frac{\rho_g}{\rho_c} = 0.47$ from the weight of KBr grains filled into a known volume V resulting in an apparent density $\rho_g = 1.3 \text{ g cm}^{-3}$ compared to $\rho_c = 2.75 \text{ g cm}^{-3}$ of crystalline KBr (4). For NaCl we calculated $\frac{\rho_g}{\rho_c} = 0.65$ with $\rho_g = 1.4 \text{ g cm}^{-3}$ and $\rho_c = 2.17 \text{ g cm}^{-3}$ (5). The weight measurements have been performed using a balance Mettler Toledo model PR5002 DeltaRange.

The total surface A_S of the KBr and NaCl grains has been estimated to be on the order of $145 \cdot 10^{-4} \text{ m}^2 \text{ g}^{-1}$ and $69 \cdot 10^{-4} \text{ m}^2 \text{ g}^{-1}$, respectively calculated from the apparent density and the average size of the grains knowing that salt is a non-porous material (6). The surface A_S has been calculated by a cubic approximation:

$$m_g = d^3 \rho_c \quad (\text{equation 3.2.1})$$

where m_g means the mass of one particle. The total number of particles n_g per cm^3 may be expressed as follows:

$$n_g = \frac{\rho_g}{m_g} \quad (\text{equation 3.2.2})$$

$$A_V = 6d^2 n_g = 6 \frac{\rho_g}{\rho_c d} \quad (\text{equation 3.2.3})$$

Chapter 3

where A_V is the surface area per cm^3 . Thus the surface per gram is:

$$A_S = \frac{A_V}{\rho_g} = 6 \frac{1}{\rho_c d} \quad (\text{equation 3.2.4})$$

A_S means the total sample surface per gram. A spherical approximation results also in equation 3.2.4.

The BET surface of KBr of comparable particle size (125 –200 μm) results in $440 \cdot 10^{-4} \text{ m}^2 \text{ g}^{-1}$ (7). The BET surface is slightly higher than the surface we estimated. This may be due to the inaccurate determination of the particle size and the cubic approximation (Figure 5.1.1).

The surface number density n_S of the salt sample which means the number of ion-pairs cm^{-2} has been approximated as follows (8):

$$n_S = \sqrt[3]{\frac{\rho_c}{M_A} N_A} \quad (\text{equation 3.2.5})$$

where ρ_c is the density of the crystalline salt, M_A the molecular weight and N_A Avogadro's number.

This leads to a ion-pair surface density of $n_S = 5.8 \cdot 10^{14}$ molecule cm^{-2} with $\rho_c = 2.75 \text{ g cm}^{-3}$ (4) and $M_A = 119 \text{ g mol}^{-1}$ (9) and $n_S = 7.9 \cdot 10^{14}$ molecule cm^{-2} with $\rho_c = 2.17 \text{ g cm}^{-3}$ (5) and $M_A = 58.4 \text{ g mol}^{-1}$ (9) for KBr and NaCl, respectively.

We may calculate the total number of molecule on the surface per g using equations 3.2.4 and 3.2.5. The total number of superficial ion-pairs results in $N = 8.4 \cdot 10^{16}$ molecule g^{-1} and $5.4 \cdot 10^{16}$ molecule g^{-1} for KBr and NaCl, respectively.

Chapter 3

N is defined as follows:

$$N = n_s A_s \quad (\text{equation 3.2.6})$$

3.2.2. Ground Grains Samples

Commercially available salt grains have been crushed by hand using a pestle and mortar. The particle size has been determined by optical microscopy to be on the order of $10\mu\text{m}$. The ratio between the density of KBr crystalline and KBr ground grains $\delta_{\text{gg}} = 1.5\text{g cm}^{-3}$ has been calculated as $\delta_c/\delta_{\text{gg}} = 0.55$. The density of ground KBr ρ_{gg} has been determined in the same way as the density of KBr grains ρ_g .

The total surface density A_s of ground grains has been estimated using equation 3.2.4 and results to be on the order of $0.22\text{ m}^2\text{ g}^{-1}$.

For KBr ground grains we may calculate the total number of molecule per g using equations 3.2.4, 3.2.5 and 3.2.6. The total number of superficial ion-pairs results in $N = 1.3 \cdot 10^{18}\text{ molecule g}^{-1}$.

3.2.3. Thin Salt Films Deposited on a Pyrex Substrate

Commercially available salt grains have been dissolved in pure methanol (Fluka AG, purity $\geq 99.8\%$). The saturated methanol salt solution has been sprayed onto a Pyrex glass plate of 19.6 cm^2 cross section heated up to $T = 500\text{K}$. The spray has been dispensed using an atomizer type ESBE from Thayer & Chandler together with gaseous nitrogen N_2 . The solvent immediately evaporates over the hot Pyrex plate and the salt forms a coherent film across the substrate of the Pyrex support. The sample has been slowly cooled down to ambient conditions. The homogeneity of the salt coverage has been checked by means of scanning electron microscopy (SEM). Figure 4.4.1 shows a SEM-image of a thin KBr film sprayed on a Pyrex substrate.

Chapter 3

A typical mass m of a salt film is of the order of 5 to 10mg which corresponds to a typical thickness between 1 and 2 μ m. The weight measurements have been performed using a balance provided by Mettler Toledo model AE 240. The thickness h has been calculated using the density of crystalline KBr ρ_c and the geometrical cross section A_S of the Pyrex support.

$$h = \frac{m}{\rho_c A_S} \quad (\text{equation 3.2.7})$$

Films prepared using H₂O-methanol-salt solutions have also been used for uptake experiments. Solutions that contain more than 10%_v of H₂O have not resulted in homogeneous salt film coverage. While spraying the H₂O-methanol-salt solution across the hot Pyrex substrate small particles of KBr have been formed and blown away by the jet of the atomizer as the KBr particles did not adhere to the Pyrex plate.

3.2.4. Thin KBr Salt Films on a Gold-Plated Substrate

Thin salt films deposited on a gold-plated support have been prepared in the same way as those on the Pyrex substrate. The high temperature support described in Section 2.3 has been used as the gold-coated support. In contrast to the thin KBr films sprayed on a Pyrex substrate the temperature T of the gold-plated substrate was set at $T = 350\text{K}$ and the N₂ flow had to be reduced considerably for better adhesion of the salt-methanol solution. A SEM-image (Figure 4.1.1) displays the homogeneity of the thin salt film prepared as described. In order to perform SEM-imaging a sample on gold-coated plat has been prepared under identical condition.

3.3. References

- (1) Caloz F.: *Laboratory Kinetic Studies of Heterogeneous Processes Relevant to the Marine Troposphere*. (EPFL, 1997) pp. 236.
- (2) Knauth H. D., H. Alberti and H. Clausen: *Equilibrium-Constant of the Gas Reaction $Cl_2O + H_2O = 2HOCl$ and the Ultraviolet-Spectrum of $HOCl$* . *Journal of Physical Chemistry*. (1979), vol. 83, pp. 1604-1612.
- (3) Oppliger R.: *Kinetics Studies of heterogeneous Reactions of chlorine and bromine Reservoirs relevant to the lower Stratosphere*. Thesis N° 1779. (1998) pp. 161.
- (4) Weast R. C.: *Handbook of Chemistry and Physics*. (CRC Press, 1986).
- (5) Kuchling H.: *Taschenbuch der Physik*. (Verlag Harry Deutsch, 1986) pp. 678.
- (6) Keyser L. F., S. B. Moore and M. T. Leu: *Surface-Reaction and Pore Diffusion in Flow-Tube Reactors*. *Journal of Physical Chemistry*. (1991), vol. 95, pp. 5496-5502.
- (7) Walter H. U.: *Adsorption of Water on Powders of NaCl-Type Alkaline Halide Crystals*. *Zeitschrift Fur Physikalische Chemie-Frankfurt*. (1971), vol. 75, pp. 287-298.

Chapter 3

- (8) Gutzwiller L.: *Heterogeneous kinetics of some atmospherically relevant reactions. Experiments and modeling*. Thesis N^o 1527. (Ecole Polytechnique Fédérale de Lausanne (EPFL), 1996) pp. 167.

- (9) NIST-Chemistry-WEBBook: *NIST Chemistry WEBBook*.
<http://webbook.nist.gov/chemistry/>

Chapter 4

4. Reactions of Chlorine and Bromine Compounds on Alkali Salt Surfaces

4.1. H₂O on Different KBr Substrates

4.1.1. Introduction

On planet earth water is present in the solid, liquid and gaseous phase, consequently, it is an ubiquitous atmospheric constituent. H₂O is a potent greenhouse gas whose concentration is highly variable in the troposphere owing to its short life-time (Table 1.1.2.). The total mass of atmospheric H₂O has been estimated to be on the order of $1.3 \cdot 10^{16}$ kg (1).

Chapter 4

Water is necessary not only for many biological processes but also plays an important role in the atmosphere. Together with O_3 and photons H_2O is involved in the formation of hydroxyl radicals (Reaction 1.2.5 and 1.2.6). OH is the main oxidant in the troposphere.

Adsorbed water on solid substrates may influence the chemical and physical behaviour of the heterogeneous processes taking place on the interface of the substrates. The adsorption of H_2O on crystalline $NaCl$ has been thoroughly studied because OH groups may be formed in the presence of adsorbed H_2O where H_2O may adsorb through hydrogen-bonds (2, 3). Furthermore, it has been found that hydration of surface ions weakens ionic bond strengths (4), which may considerably change the chemical behaviour of salt surfaces. The adsorption of water is strongly correlated to the defect structure of the surface (5). Specifically, it has been shown by atomic force microscopy that water primarily adsorbs at step edges (4).

However, surfaces of solid alkali salt aerosols are as a rule not perfect crystalline surfaces because they contain various types of defect sites which are generally not well known.

For heterogeneous reactions on salt particles surface adsorbed water $H_2O(a)$ plays a crucial role. This has been shown for reactions such as HNO_3 on $NaCl$ (6-8) where surface adsorbed $H_2O(a)$ enhances the mobility of interfacial ions to the point of crystallisation. Nevertheless, it has been found that dissociation of $H_2O(a)$ on $NaCl$ surfaces leading to $NaOH$ and HCl rather is a rare event (9).

Heterogeneous reactions of halogen compounds on salt substrates performed in a low pressure Knudsen reactor have shown that both the reaction kinetics as well as the yield of the reaction are controlled by the amount of surface-adsorbed $H_2O(a)$ (Section 4.7). Desorption experiments involving adsorbed water have been performed in a low pressure Knudsen reactor in order to estimate the number of adsorbed $H_2O(a)$ molecules on different KBr substrates such as grains, ground grains and thin films sprayed on a gold-coated copper substrate. The preparation of the samples is described in chapter 3. The obtained calibration curves have been used to estimate the amount of $H_2O(a)$ for other uptake experiments on salt surfaces. In order to reduce the adsorbed $H_2O(a)$ the samples have been either pumped or heated under vacuum. In order to minimise the amount of

Chapter 4

adsorbed $\text{H}_2\text{O}(\text{a})$ thin KBr and NaCl films sprayed on a gold-coated copper substrate have been used.

Furthermore, some structural aspects of the substrate are pointed out within the scope of our experimental set-up.

4.1.2. Results and Discussion

In order to survey the morphology and of the substrates for structural surface change induced by pumping and heating the sample the thin KBr films sprayed on a gold-coated copper substrate have been examined by Scanning Electron Microscopy (SEM).

In order to compare the samples treated in different ways as described below a thin film of KBr has been exposed for four days to ambient conditions as a reference sample, whereas a similar substrate prepared in the same way has been pumped for four days in the 14mm-orifice reactor. The SEM-images obtained have shown an irreversible recrystallisation of the pumped substrate proving that the spray-coated KBr film is metastable. Dai (4) observed using Atomic Force Microscopy (AFM) that by lowering the humidity over a NaCl surface relatively well-ordered surface structure may be obtained. Figure 4.1.1 shows a thin KBr film sprayed on a gold-coated substrate exposed for 4 days to ambient conditions. The KBr sample in figure 4.1.2 has been pumped in the 14mm-orifice reactor for 4 days. An irreversible change has been observed. This means that the conversion of a sprayed KBr surface to a more crystalline surface is occurring due to pumping of the surface, whereas a later exposure of the same sample to ambient conditions during 5 days conversely did not lead to disorder of the surface. Similar experiments using thin KBr films sprayed on a Pyrex substrate have also shown a recrystallisation upon pumping of the surface of the substrate.

The fact that pumping of the KBr sample at ambient temperature induces a substantial change of surface structure confirms the presence of an ionic transport-mechanism due to the existence of mobile ions supported by adsorbed $\text{H}_2\text{O}(\text{a})$.

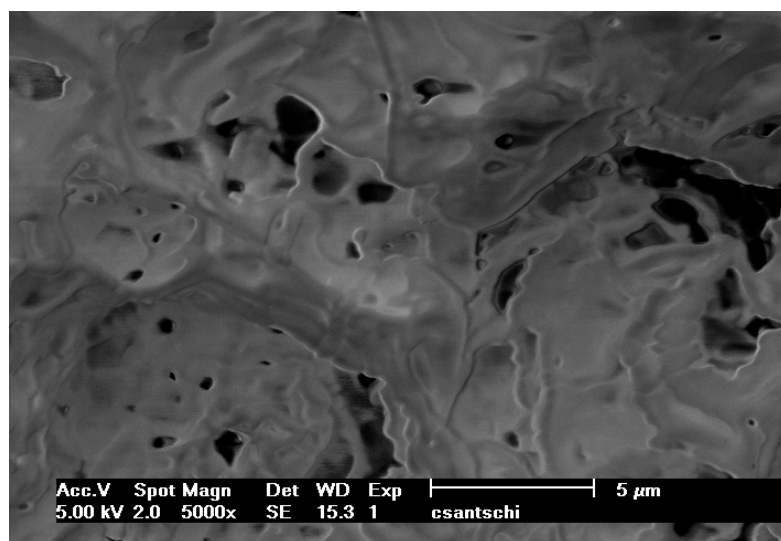


Figure 4.1.1: SEM-image of a thin KBr film sprayed on a gold-coated copper substrate. The sample has been exposed for four days to atmospheric conditions.

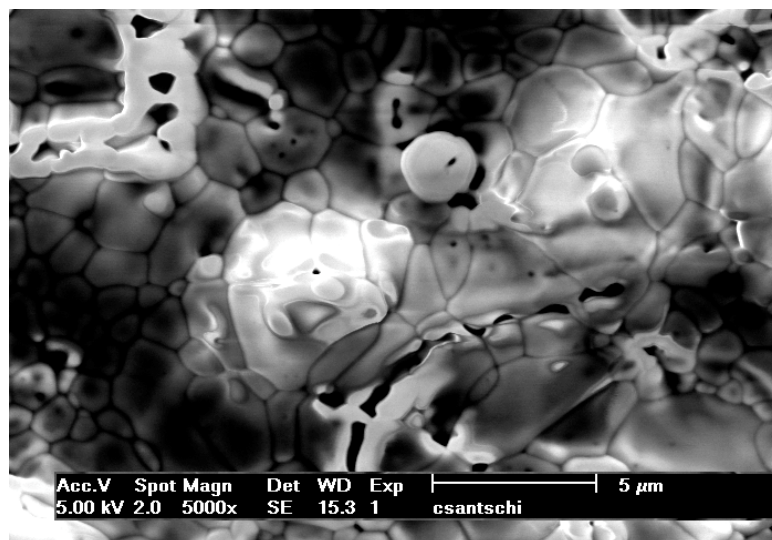


Figure 4.1.2: SEM-image of a thin KBr film sprayed on a gold-coated copper substrate. The sample has been pumped in the 14mm-orifice reactor for four days.

Furthermore, when a thin KBr film sprayed on a gold-coated copper substrate has been heated to $T = 620$ K in the 14mm-orifice reactor SEM-images show a crystallisation of the surface subsequent to heating. Unfortunately we currently are not equipped to record SEM-images in situ. In order to record SEM-images we were obliged to transport the

Chapter 4

samples from our reactor to the microscope. This implies an exposure of the sample to ambient conditions, in particular to several Torr of H₂O vapour.

A SEM-image of a heated thin film of KBr sprayed on a gold-coated copper substrate is displayed in figure 4.1.3.

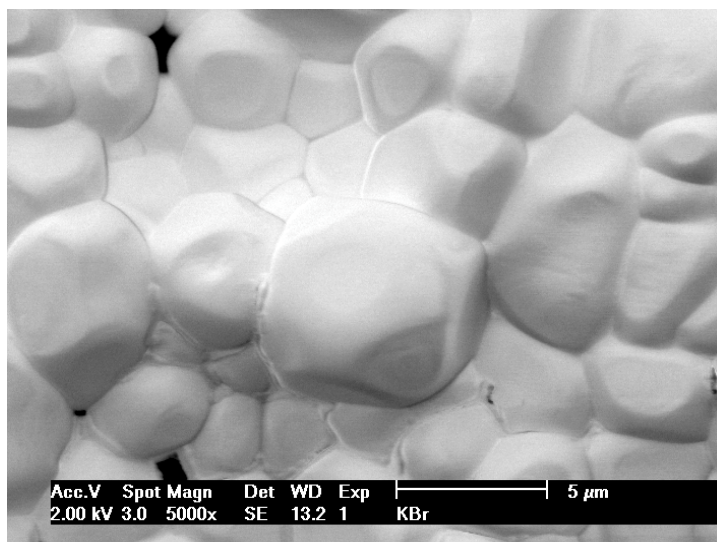
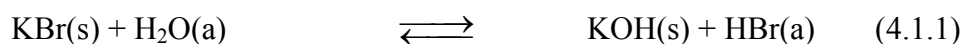


Figure 4.1.3: SEM-image of a thin KBr film sprayed on a gold-coated copper substrate. The sample has been heated to $T = 620\text{K}$.

In analogy to NaCl, we conclude that even at temperatures much lower than the melting point $T_m(\text{KBr}) = 1007\text{ K}$, a structural change of the KBr sample towards a crystalline structure sets in at typically $T = 620\text{ K}$ (Figures 4.1.1 and 4.1.3). NaCl bulk diffusion appeared to commence above $T = 537\text{K}$ according to Harrison et al (10, 11). Heating of the sample under vacuum may lead to a shift of the equilibrium 4.1.1 towards the left-hand side owing to desorption of H₂O(a).

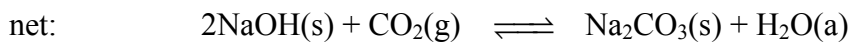
In the context of surface adsorbed H₂O(a) and its relation to the presence of mobile surface-ions we were interested in the question of the existence of basic sites. Basic sites are expected to be formed by the hydrolysis reaction 4.1.1 of KBr on defect sites of the bulk material.



Chapter 4

However, HBr and KOH are not necessarily completely dissolved as they also may form ion-pairs. Monte Carlo simulations predict the formation of ion-pairs for concentrated water solutions of NaCl and LiCl which are thought to be intermediates in many chemical reactions (12).

In order to check the surface for basic OH-sites, KBr grains have been exposed to CO₂. An uptake of CO₂ on the KBr grains may be a indicator for surface OH-sites in analogy to the reaction of carbon dioxide CO₂ with NaOH (3) (Reactions 4.1.2 and 4.1.3).



It is assumed that CO₂ interacts with OH-sites formed on the KBr surface. It is not known whether or not CO₂ reacts with NaCl (3). Therefore, we assume that CO₂ does not directly interact with KBr and that only a reaction with OH-sites occurs in analogy to reaction 4.1.2 and 4.1.3:

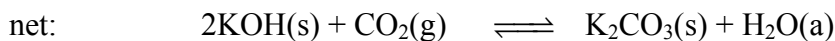
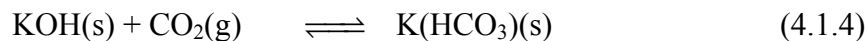


Figure 4.1.4 illustrates an uptake experiment performed in the 1mm-orifice reactor, where an initial uptake coefficient $\gamma_{\text{ini}} = 1.1 \cdot 10^{-4}$ has been measured. The solubility of CO₂ amounts to 1.5 g in 1 l of H₂O(l) at T = 293 K and P = 10⁵ Pa (13), which means that CO₂ is soluble in H₂O(l) to a very small extent. The total loss of CO₂ is measured to be 7*10¹⁴ molecule g⁻¹. The dimension of the KBr grains has been determined by optical microscopy to be on the order of d = 150µm (Section 3.2.1). Using the estimated surface area A_S of the grains we arrive at A_S = 145*10⁻⁴ m² g⁻¹ with a cubic approximation of the

Chapter 4

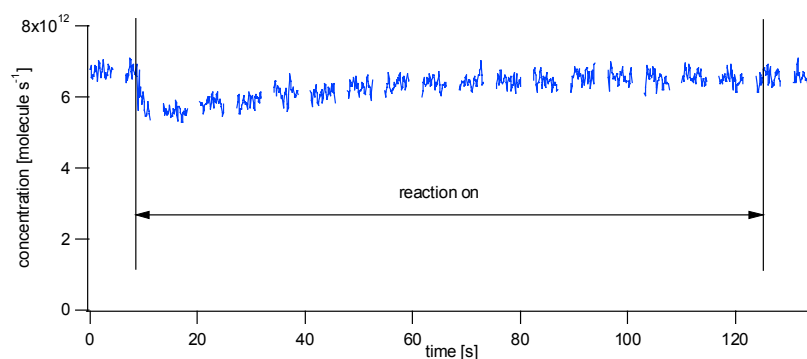


Figure 4.1.4: Uptake experiment of CO₂ on 5g of KBr grains. The experiment has been carried out in the 1mm-orifice reactor and CO₂ monitored at m/e = 44.

KBr grains (Section 3.2.1). Therefore, an approximate loss of $1 \cdot 10^{12}$ molecule cm⁻² of CO₂ has been observed. The surface density of KBr has been estimated using equation 3.2.5 (14) (Section 3.2.1):

$$n_s = \sqrt[3/2]{\frac{\rho_v \cdot N_A}{M}} \quad (\text{equation 3.2.5})$$

where the surface number density n_s is given in molecule cm⁻², the volume density ρ_v in g cm⁻³ and M corresponds to the molecular weight of KBr.

Applying equation 3.2.5 leads to $n_s(\text{KBr}) = 5.8 \cdot 10^{14}$ molecule cm⁻² which has to be compared to the loss of $1 \cdot 10^{12}$ molecule cm⁻² of CO₂.

We conclude therefore that the surface of KBr grains surface contains basic sites which may react with CO₂ corresponding to less than 1% of the total surface.

In order to estimate the amount of the residual H₂O(a) adsorbed on the different KBr samples for the following uptake experiments of halogen compounds the H₂O(a) has been desorbed by heating the salt samples. In order to obtain a calibration curve for adsorbed H₂O(a) the KBr samples have been pumped for a given time prior to H₂O desorption. Subsequently, the remaining adsorbed water has been desorbed at T = 620 K. A few single point measurements have been carried out in order to estimate the amount of adsorbed H₂O(a). Figure 4.1.5 displays the MS-signals of a typical desorption curve. The amount of H₂O desorbing from samples has been measured using mass-spectrometry at

Chapter 4

$m/e = 18$ and the obtained values have been plotted as a function of pumping time. Figure 4.1.6 shows the amount of adsorbed $\text{H}_2\text{O(a)}$ from a thin KBr film sprayed on a gold-coated substrate as a function of pumping time t_p . Figure 4.1.7 and 4.1.8 show a calibration curve of $\text{H}_2\text{O(a)}$ adsorbed on KBr grains and ground grains, respectively.

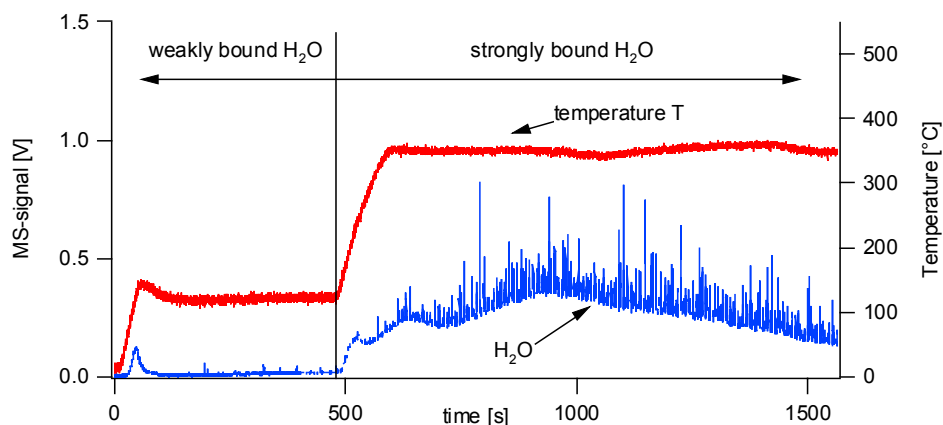


Figure 4.1.5: Desorption experiment carried out on KBr grains in the 14mm-orifice reactor. H_2O has been monitored at $m/e = 18$. The weakly- and strongly-bound H_2O has been desorbed at $T = 400$ K and $T = 620$ K, respectively.

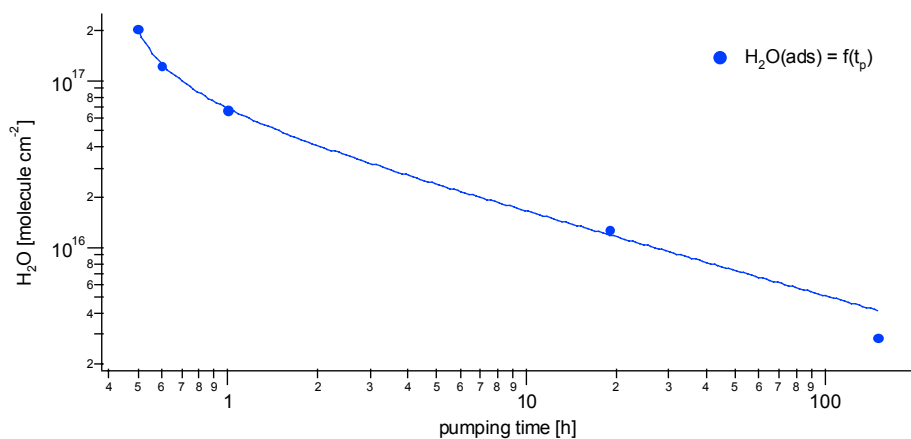


Figure 4.1.6: Quantity of $\text{H}_2\text{O(a)}$ adsorbed on thin KBr films sprayed on a gold-coated copper substrate. The sample has been pumped for a certain time t_p within the Knudsen flow reactor before the residual $\text{H}_2\text{O(a)}$ has been desorbed by heating the sample to $T = 620$ K.

Chapter 4

After pumping the sample for a given time t_p the KBr substrates have previously been heated to $T = 400$ K in order to desorb weakly-bound $\text{H}_2\text{O}(\text{a})$. After the MS-signal of H_2O has decreased to the background level, the temperature T was raised to $T = 620$ K in order to determine the amount of strongly-bound $\text{H}_2\text{O}(\text{a})$ (Figure 4.1.5).

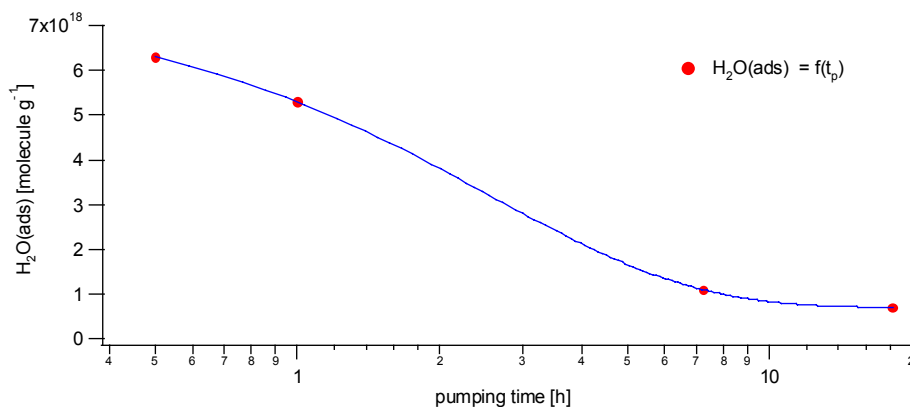


Figure 4.1.7: Quantity of $\text{H}_2\text{O}(\text{a})$ on KBr grains as function of pumping time t_p . The sample has been pumped for a given time t_p within the Knudsen flow reactor before the residual $\text{H}_2\text{O}(\text{a})$ has been desorbed by heating the sample to $T = 620\text{K}$.

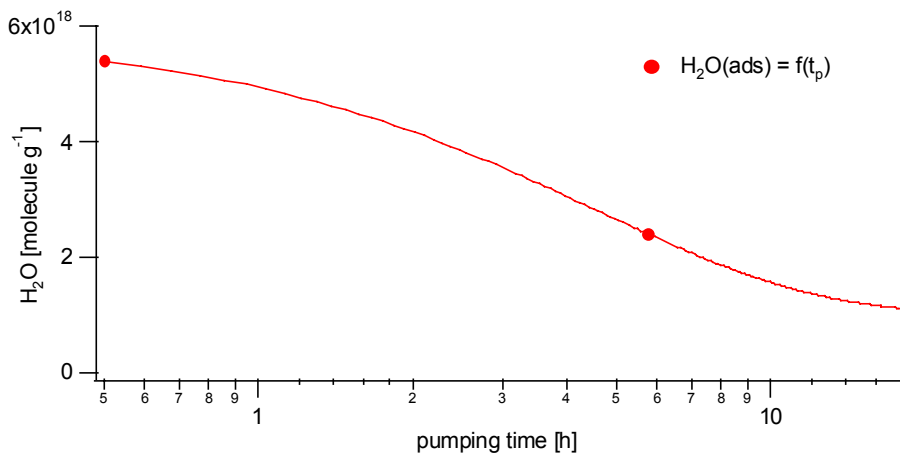


Figure 4.1.8: Quantity of $\text{H}_2\text{O}(\text{a})$ on ground KBr grains as function of pumping time t_p . The sample has been pumped for a given time t_p within the Knudsen flow reactor before the residual $\text{H}_2\text{O}(\text{a})$ has been desorbed by heating to $T = 620\text{K}$.

Chapter 4

For KBr grains we calculated the density of adsorbed $\text{H}_2\text{O}(\text{a})$. Using the estimated surface $A_S = 145 \text{ cm}^2 \text{ g}^{-1}$ (Section 3.2.1) and the amount of adsorbed $\text{H}_2\text{O}(\text{a})$ from figure 4.1.7 we obtain approximately $\rho_{(\text{H}_2\text{O})} = 3 \cdot 10^{16} \text{ molecule cm}^{-2}$ after a pumping time t_p of one hour. For NaCl it has been calculated that least six molecule of H_2O are necessary in order to dissolve a NaCl molecule (15). When we compare the H_2O surface density with one for KBr, $n_s(\text{KBr}) = 5.8 \cdot 10^{14} \text{ molecule cm}^{-2}$, we approximately obtain 15 molecules of H_2O per molecule of KBr. In analogy to NaCl this may lead to the suggestion that the KBr on the surface exists in form of both dissolved and ion-pair KBr.

Desorption experiments on thin KBr films sprayed on a Pyrex substrate have shown that the amount of $\text{H}_2\text{O}(\text{a})$ adsorbed on a bare Pyrex-plate is many times higher than the one on the KBr substrate. This makes the determination of the amount of adsorbed $\text{H}_2\text{O}(\text{a})$ on a thin KBr film sprayed onto a Pyrex substrate virtually impossible.

Using the corresponding surface areas A_S (Section 3.2) the amount of $\text{H}_2\text{O}(\text{a})$ for KBr grains, ground grains and thin KBr films sprayed on a gold-coated substrate are $3 \cdot 10^{16} \text{ molecule cm}^{-2}$, $2.5 \cdot 10^{15} \text{ molecule cm}^{-2}$ and $3 \cdot 10^{16} \text{ molecule cm}^{-2}$ after one hour of pumping time, respectively.

While we heated the KBr grains and ground grains as well as the thin film sprayed on a gold-coated copper substrate we have additionally monitored HBr at $m/e = 82$ in order to search for residual HBr generated by equilibrium (4.1.1). In order to complete our data HOBr has also been monitored at $m/e = 96$. HBr has only been observed in small amounts whereas desorption of unexpected HOBr has been observed on KBr ground grains and thin KBr films sprayed on a gold-coated copper substrate (Figure 4.1.9). In contrast to the above mentioned samples no desorption of HOBr has been observed on KBr grains.

Desorption of HOBr has only been observed for a sample that has been heated for the first time at a temperature above $T = 470 \text{ K}$ so it is a unique event for each KBr sample. Furthermore, the desorption rate of H_2O is increasing simultaneously with the rate of release of HOBr as displayed in figure 4.1.9. Therefore, bulk KBr does not decompose at

Chapter 4

$T = 620\text{K}$ (16), whereas specific surface sites obviously lead to a release of HOBr and HBr associated to the presence of $\text{H}_2\text{O(a)}$.

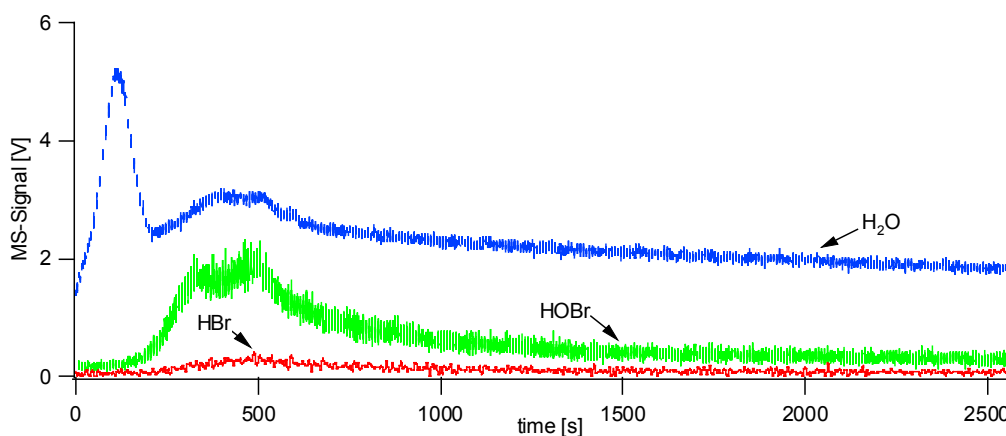


Figure 4.1.9: MS-signal of H_2O , HOBr and HBr desorbing from a thin film of KBr sprayed on a gold-coated copper substrate carried out in the 14mm-orifice reactor at temperature $T = 620\text{K}$. The signal of H_2O has been recorded at 10 times smaller sensitivity compared to HBr and HOBr.

The quantity of released HBr has been on the order of 10% of the released HOBr. A release of Br_2 has not been observed on any surface heated to $T = 620\text{K}$. Therefore, the mass balance between HBr and HOBr according to reaction 4.1.6 is not satisfied.

The formation of HOBr has to be accompanied with a change of the oxidation-state of Br. Together with reaction 4.1.6 the present result leads us to the suggestion of adsorbed molecular Br-Br which decays while the sample is heated to $T = 620\text{K}$ in the presence of $\text{H}_2\text{O(a)}$ leading to HOBr and HBr.



Where Q represents thermal energy and Br-Br suggests a hydrated ion-pair ($\text{Br}^+ \cdot \text{Br}^-$).

Chapter 4

The presence of Br-Br may be an indicator for a formation of an F-center. By grinding the KBr grains an anion may be pulled out of the crystal matrix leaving a vacancy where an electron may be trapped (17).



The deficient mass balance of HBr may be explained by the neutralisation reaction 4.1.8:



At ambient temperature the equilibrium 4.1.6 is placed on the left side, nevertheless, thermal energy shifts it to the right-hand side in view of the endothermic nature of the reaction.

According to reaction 4.1.6 we presume that molecular bromine on the surface exists as Br-Br pairs or KBr_3 which is also a stable bromine compound. Moreover, reaction 4.1.8 supports the assumption of basic surface sites existing as K-OH.

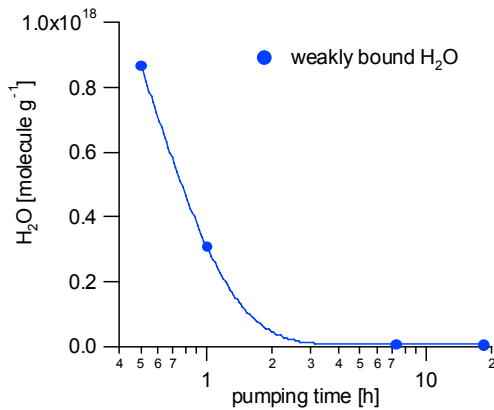
Desorption experiments performed on KBr grains at $T = 620\text{K}$ have not shown desorption of either HOBr or HBr. This means that mechanical treatment of the grains by grinding or the rapid evaporation of the solvent of salt solutions not only leads to surface-defects which may be steps, corners, edges and vacancies but also may lead to the formation of surface-adsorbed molecular bromine possibly in form of Br-Br pairs.

During thermal desorption of $\text{H}_2\text{O(a)}$ we distinguished between weakly- and strongly-bound $\text{H}_2\text{O(a)}$ by applying different desorption temperatures T as indicated in figure 4.1.5. As already defined above weakly- and strongly-bound $\text{H}_2\text{O(a)}$ refers to the quantity of adsorbed $\text{H}_2\text{O(a)}$, which desorbed at $T \leq 400\text{ K}$ and $T \geq 400\text{ K}$, respectively. Figure 4.1.10 shows a graph of weakly- and strongly-bound $\text{H}_2\text{O(a)}$ on KBr grains as a function of pumping-time t_p during which period the sample was pumped at ambient temperature. After approximately 3 hours of pumping the amount of weakly-bound $\text{H}_2\text{O(a)}$ drops towards zero, whereas strongly-bound $\text{H}_2\text{O(a)}$ persists even after 10 hours of pumping.

Chapter 4

The ratio $r = \frac{\text{H}_2\text{O}(\text{weakly-bound})}{\text{H}_2\text{O}(\text{strongly-bound})}$ decreases from $r = \frac{1}{10}$ at 0.5h to $r = \frac{1}{90}$ at 18h pumping time.

a)



b)

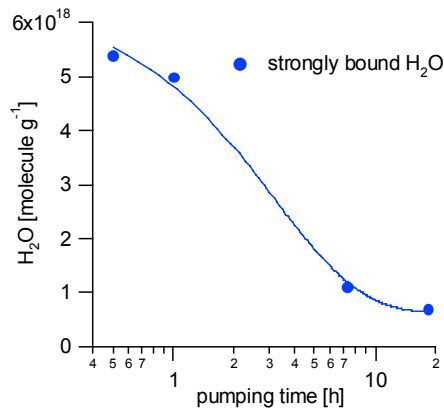


Figure 4.1.10: a) shows the amount of weakly-bound H₂O on KBr grains as a function of pumping time. The H₂O has been desorbed at temperature T = 400K. b) shows the amount of residual strongly-bound H₂O on KBr grains. It has been desorbed at T = 620K.

In order to investigate the adsorption of H₂O on thin KBr films sprayed on a gold-coated substrate we applied the basic idea of a dope and probe experiment which involved the following steps:

1. Conditioning the sample in the reactor cell by heating it to T = 620K in order to desorb residual H₂O(a), that is the sum of weakly- and strongly-bound H₂O(a).
2. Adsorption of H₂O in the reactor cell at ambient temperature at a known partial pressure of H₂O.
3. Desorption of H₂O(a) by heating the sample to T = 620K.
4. Plotting the measured amount of desorbing H₂O as a function of the partial pressure of H₂O.

Chapter 4

The basic intent of this experiment has been to desorb the maximum of adsorbed $\text{H}_2\text{O}(\text{a})$ in order to use this dry substrate as a reference surface onto which we intended to adsorb H_2O at a given H_2O vapour pressure. After recording SEM-images of the heated spray-coated KBr sample we noticed that the heating of the KBr sample to $T = 620 \text{ K}$ leads to a substantial change of the sample surface as displayed in 4.1.3. The heat-treated sample obviously has different surface properties compared to the sample of interest. Nevertheless, we present here a short description of the work we have performed.

Reference pulsed valve and steady-state experiments on the bare gold-coated sample holder have not shown any interaction of H_2O with the sample holder.

In order to measure the minimal exposure time t_e for reaching steady-state the experiments have been performed at different exposure times t_e to a constant pressure of H_2O vapour. A thin KBr film sprayed on a gold-coated copper substrate has been prepared according to point 1 described above. Subsequently, steps 2-4 as described above have been carried out for different exposure times t_e at a constant H_2O concentration $c(\text{H}_2\text{O}) = 8 \cdot 10^{12} \text{ molecule cm}^{-3}$ in the 4mm-orifice reactor. Figure 4.1.11 shows a plot of $\text{H}_2\text{O}(\text{a})$ as a function of exposition time t_e . The adsorption experiments on such surfaces have shown that steady-state is reached within a time-scale of 15 minutes at the above H_2O concentration.

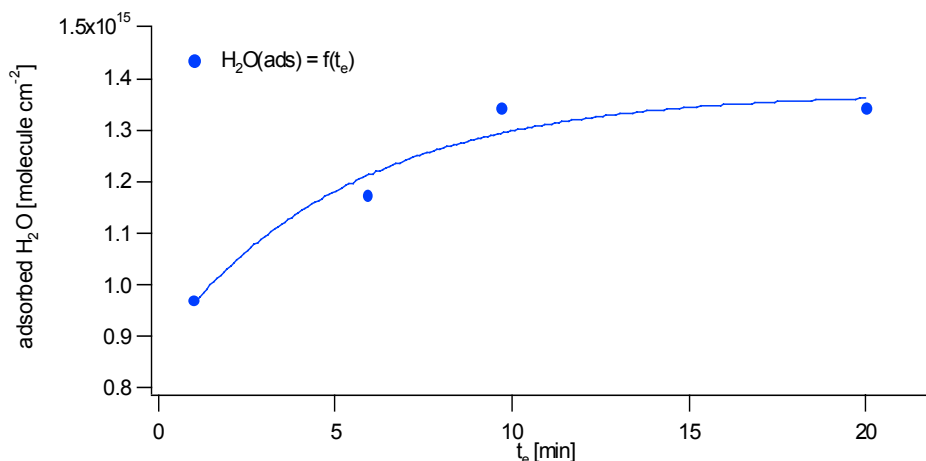


Figure 4.1.11: H_2O dope and probe experiment carried out on a thin KBr film sprayed on a gold-coated copper substrate in the 4mm-orifice reactor. The amount of adsorbed H_2O is plotted as a function of the exposure time t_e to H_2O vapour.

Chapter 4

In order to investigate the dependence of $H_2O(a)$ of such a sample on the H_2O partial pressure steps 1-4 described above have been carried out at different concentrations of water vapour in the range of $5 \cdot 10^{11}$ to $5 \cdot 10^{13}$ molecule cm^{-3} .

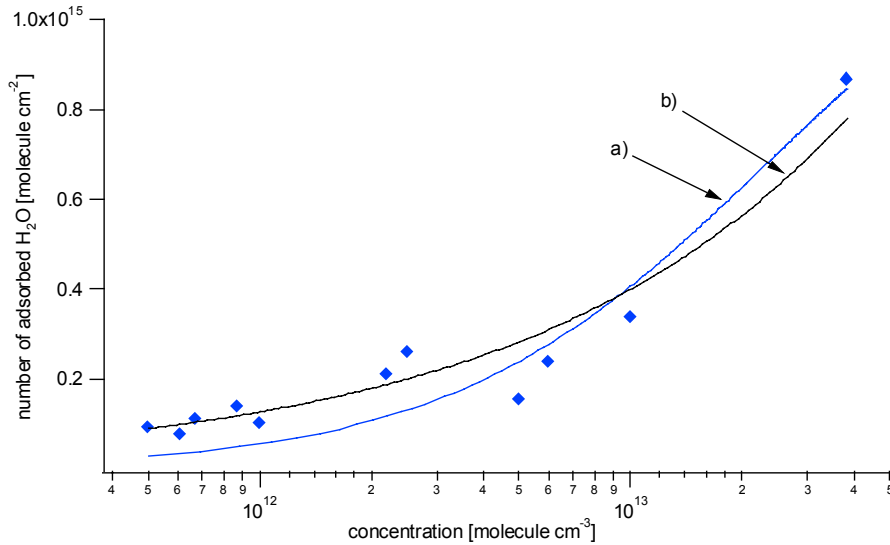


Figure 4.1.12: Weakly-bound H_2O adsorbed on a sprayed KBr film deposited on a gold coated copper substrate. Before carrying out the experiment the sample had been heated to $T = 620K$. Figure 4.1.3 shows the corresponding SEM image of such a sample. Curve a) shows a data-fit according to an adsorption-desorption model: $H_2O(a) = \frac{S_0kc}{1+kc}$ and b) using linear adsorption and

quadratic desorption (equation 4.1.9): $H_2O(a) = \frac{S_0}{2} \left(\left(\sqrt{(qc)^2 - 4qc} \right) - qc \right)$

For weakly-bound $H_2O(a)$ we found that within the present measurement range the amount of adsorbed $H_2O(a)$ does not depend on the pumping time prior to the conditioning. In order to propose a mechanism for the adsorption of H_2O on such surfaces the amount of adsorbed $H_2O(a)$ as a function of the concentration $c(H_2O)$ has been fitted (Figure 4.1.12). We have compared different fits of a modified Langmuir-Hinshelwood type adsorption-desorption model using a least-squares criteria χ^2 , which is defined in the following way:

Chapter 4

$$\chi^2 = \sum \left(\frac{y - y_i}{\sigma_i} \right)^2 \quad (\text{equation 4.1.1})$$

where y and y_i corresponds to the calculated and the experimental value of point i , respectively. The standard deviation for the point i is denoted by σ_i .

The models are based on the comparison of the surface coverage θ as a function of the concentration. The surface coverage θ is defined as:

$$\theta = \frac{S}{S_0} \quad (\text{equation 4.1.2})$$

where S_0 and S are the total and the number of occupied reactive surface sites, respectively.

The condition of steady-state allows to equate the rate of change of the surface coverage θ due to adsorption and desorption. We may apply the steady-state condition (equation 4.1.3) as we have shown above that the system is in steady-state after 15 minutes, or so.

$$\dot{\theta} = 0 \quad (\text{equation 4.1.3})$$

The first model is a linear adsorption and desorption model which is briefly explained as follows:

For adsorption the rate of change in surface coverage θ is

$$\dot{\theta} = k_1 S_0 c (1 - \theta) \quad (\text{equation 4.1.4})$$

where c is the concentration of H_2O .

Chapter 4

For the desorption rate we may write

$$\dot{\theta} = k_2 S_0 \theta \quad (\text{equation 4.1.5})$$

Equating equations 4.1.4 and 4.1.5 results in the Langmuir equation (18):

$$\theta = \frac{kc}{1+kc}, \quad \text{with } k = \frac{k_1}{k_2} \quad (\text{equation 4.1.6})$$

Introducing equation 4.1.6 into equation 4.1.2 leads to equation 4.1.7 for the amount of adsorbed $\text{H}_2\text{O(a)}$ which is numerically equal to the number of occupied reactive surface sites.

$$S = \frac{S_0 kc}{1+kc} \quad (\text{equation 4.1.7})$$

Curve a) in figure 4.1.12 shows a fit to the data according to equation 4.1.7.

The second model is based on a linear adsorption and quadratic desorption. For adsorption we use equation 4.1.4, whereas for desorption we put:

$$\dot{\theta} = k_2 S_0^2 \theta^2 \quad (\text{equation 4.1.8})$$

When we apply steady-state condition (equation 4.1.3) and use the definition of the surface coverage (equation 4.1.2) we obtain for the number of adsorbed $\text{H}_2\text{O(a)}$:

$$S = \frac{S_0}{2} \left(\left(\sqrt{(qc)^2 - 4qc} \right) - qc \right), \quad \text{with } q = \frac{k_1}{k_2 S_0} \quad (\text{equation 4.1.9})$$

Curve b) in figure 4.1.12 shows a fit of the data according to equation 4.1.9.

Chapter 4

A third fit has been performed using a model for adsorption with dissociation (18). For adsorption we have used:

$$\dot{\theta} = k_1 c S_0^2 (1-\theta)^2 \quad (\text{equation 4.1.10})$$

For desorption equation 4.1.8 has been used. Using steady-state condition (equation 4.1.3) and the definition of the surface coverage (equation 4.1.2) we obtained for the amount of adsorbed $\text{H}_2\text{O}(\text{a})$:

$$S = S_0 \frac{\sqrt{qc}}{1+\sqrt{qc}}, \text{ with } q = \frac{k_1}{k_2 S_0} \quad (\text{equation 4.1.11})$$

The comparison of the models in a least-squares sense, actually the comparison of χ^2 , is favourable for the models described by equations 4.1.9 and 4.1.11. Therefore we are unable to distinguish between linear adsorption and quadratic dependence of the rate of desorption and adsorption with dissociation comparing χ^2 .

It has been shown by Fourier transform infrared spectroscopy (FTIR) that water dissociation on NaCl surfaces is a rare event (9). In analogy to NaCl surfaces we assume that dissociation is a rare event on KBr surfaces and therefore favour the model implying the quadratic dependence of the rate of desorption. It may be explained schematically as displayed in figure 4.1.13.

A H_2O molecule adsorbs onto a free active adsorption site on the KBr surface and migrates towards other adsorbed $\text{H}_2\text{O}(\text{a})$ before it desorbs into the gas-phase. This mechanism corresponds to the formation of H_2O clusters on the surface, which has been proposed by Wassermann and Dai (19, 5) in molecular dynamics calculations and Monte Carlo simulations, respectively, as well as Foster (20) using infrared spectroscopy. This also indicates that the binding energy of $\text{H}_2\text{O}(\text{a})$ towards the KBr surface is stronger than with fellow water molecules within an adsorbed water cluster.

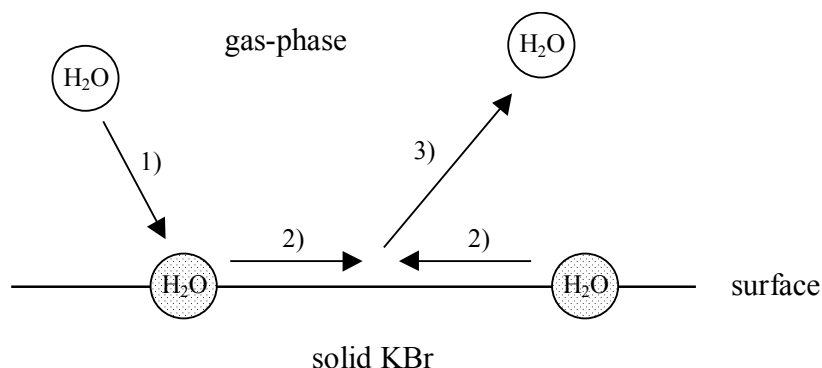


Figure 4.1.13: Schematic illustration of adsorption of H₂O on a thin film of KBr sprayed on a gold-coated substrate. 1) a H₂O molecule adsorbs on the KBr surface and migrates and towards another adsorbed molecule 2). After colliding with another adsorbed H₂O one of them desorbs into the gas-phase.

The data fitting using the second model resulted in a value for the total amount of reactive sites of $S_0 = 1.3 \cdot 10^{17}$ molecule cm⁻² and $q = 9.3 \cdot 10^{-19}$ cm³ molecule⁻¹.

In contrast to weakly-bound H₂O(a), a dependence of the amount of strongly-bound H₂O(a) on the pumping time t_p prior to step one of the dope and probe experiment has been found. Two samples prepared under identical conditions, one pumped for two hours, the other for approximately 20h have been exposed to the same pressure of H₂O(g) for the same length of time. On the sample pumped for 20h an amount of approximately 20 times less adsorbed H₂O(a) has been measured as displayed in figure 4.1.14.

On KBr grains we have seen that desorption of strongly-bound H₂O(a) by pumping the substrate is a rather slow process (Figure 4.1.10). This may suggest that the recrystallisation of the surface due to pumping (Figure 4.1.2) is also a slow process at ambient temperature. Furthermore, we may suggest that a sample pumped for a shorter time contains more sites where H₂O(g) adsorption leads to strongly-bound H₂O(a). We conclude therefore that recrystallisation due to heating as we have observed (Figure 4.1.3) may also be a slow process in the absence of H₂O(a).

Chapter 4

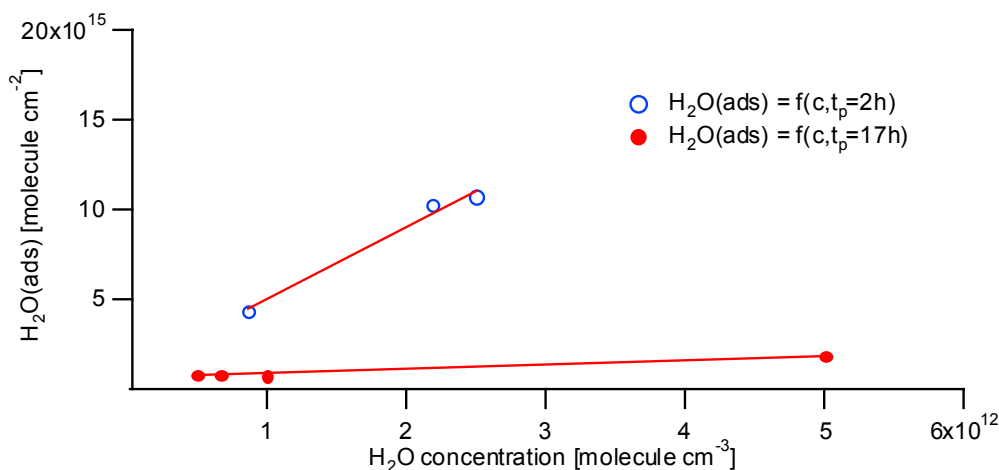


Figure 4.1.14: Strongly bound H₂O adsorbed on KBr film sprayed on gold coated copper substrate. Before carrying out the experiment the sample has been heated to $T = 620$ K. Figure 4.1.3 shows a SEM image of a sample heated to $T = 620$ K. Different amounts of adsorbed H₂O have been found on a sample pumped for two and for 17h before conditioning, respectively. The exposure time t_c has been 15 minutes.

In order to compare KBr substrates prepared in different ways FTIR-spectra have been recorded using a photo-acoustic-cell. Figure 4.1.15 shows a spectrum of a freshly ground sample and a ground sample exposed for 3 days to ambient conditions.

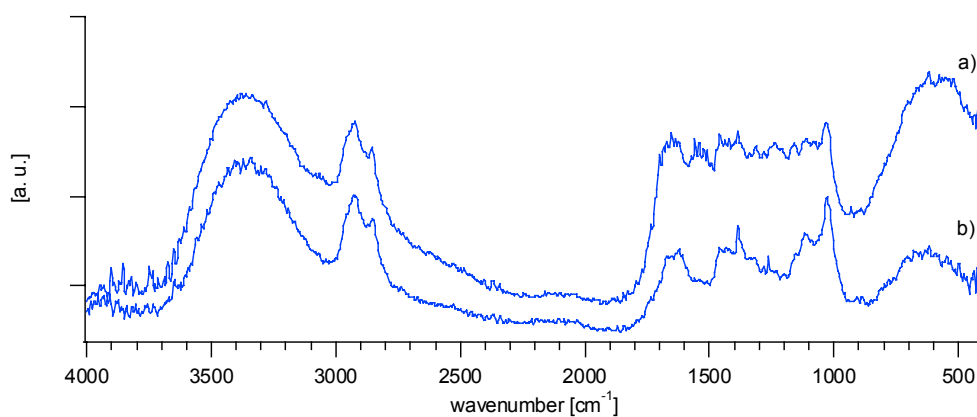


Figure 4.1.15: FTIR spectrum of ground KBr grains. The spectrum has been taken in a photo-acoustic-cell. Spectrum a) originates from a freshly ground sample, whereas b) belongs to a sample exposed for 3 days to ambient conditions.

The ratio between the broad peak centred at 600cm^{-1} and the one centred at 3350cm^{-1} is higher on the freshly prepared sample. This means that a freshly ground sample is not stable under ambient conditions. The broad peak at 3350cm^{-1} may be attributed to liquid $\text{H}_2\text{O}(\text{l})$ (21). The peaks between 1500cm^{-1} and 1700cm^{-1} are attributed to gaseous $\text{H}_2\text{O}(\text{g})$ (22). The decrease of the peak centred at 600cm^{-1} due to an exposure of the sample to ambient conditions shows that a sample of ground grains is metastable and may be therefore chemically more active.

4.1.3. Conclusions

We found by means of SEM-imaging that thin KBr films sprayed on a gold-coated copper support undergo a substantial change towards a higher degree of crystallinity due to removal of adsorbed $\text{H}_2\text{O}(\text{a})$ by pumping. This confirms the presence of mobile ions on the KBr surface whose abundance is controlled by the amount of adsorbed $\text{H}_2\text{O}(\text{a})$.

Furthermore, we also observed a change of the surface structure due to heating of the KBr sample under vacuum conditions to a temperature $T = 620\text{K}$ on the basis of SEM-images. This temperature is well below the melting point of KBr and the change is irreversible even under atmospheric conditions. Ionic diffusion processes apparently set in well below the melting point of KBr.

While performing desorption experiments on KBr grains and ground grains as well as on thin films of KBr sprayed on a gold-coated copper substrate we obtained calibration curves for the amount of adsorbed $\text{H}_2\text{O}(\text{a})$ as a function of pumping time prior to desorption. These curves are used for the experiments of halogen species on KBr substrates in order to estimate the amount of adsorbed $\text{H}_2\text{O}(\text{a})$ remaining on the substrate. For thin KBr films sprayed on a Pyrex substrate no calibration curve has been obtained because the amount of adsorbed $\text{H}_2\text{O}(\text{a})$ on the bare Pyrex plate exceeds the amount of adsorbed $\text{H}_2\text{O}(\text{a})$ on the KBr film by a multiple.

Chapter 4

While heating the samples in vacuum the desorption of HBr, HOBr and Br₂ has been monitored. The formation of HOBr and small amounts of HBr has been observed on KBr ground grains and thin KBr films sprayed on a gold-coated copper substrate, but not on KBr grains. The formation of gaseous Br₂ has not been observed on any KBr sample. Grinding and rapid evaporation of the solvent of the salt solution may lead to a change in the oxidation-state of bromine and consequently to a possible formation of surface adsorbed Br-Br pairs.

On thin KBr films sprayed on a gold-coated copper substrate, which has been conditioned by heating to $T = 620$ K before performing the dope and probe experiment we have found that weakly-bound H₂O(a) rather follows a quadratic than a linear desorption law which is consistent with the formation of H₂O(a) clusters on the surface. For strongly-bound H₂O(a) we observed that its amount depends on the pumping time prior to the conditioning due to crystallisation of the sample by pumping.

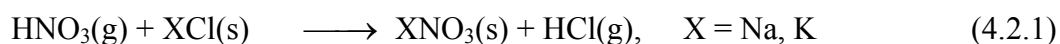
The presence of surface-adsorbed basic sites or surface hydroxyl groups has been shown by the interaction of the surface with carbon dioxide CO₂. We estimated the amount of basic sites to be less than 1% of the total amount of surface sites.

In addition, we found using a photo-acoustic cell that the surface of ground KBr is not stable at ambient conditions.

4.2. Uptake Experiments of HCl on KBr

4.2.1. Introduction

Concentrations of 100-300ppt of HCl are commonly measured in remote oceanic regions (23). Near urban areas the concentration may increase up to about 3000ppt. In urban areas the principal sources are coal combustion by power plants and incineration of municipal waste. In coastal regions the volatilisation from sea-salt particles is considered the major source of HCl. This volatilisation is a function of the deposition of strong acids such as HNO₃ on marine aerosols (Reaction 4.2.1 (24)).



Furthermore, HCl may be generated by hydrogen abstraction from hydrocarbons (Reaction 4.2.2).



HCl is not photochemically active under tropospheric conditions because it does not photolyse at $\lambda > 290\text{nm}$ (25), whereas it contributes to atmospheric acidity.

Small amounts of HCl are present as a contamination in gas samples of Cl₂O and HOCl. The HCl impurity is in the range of 2-5%. This provided the motivation to complete the study of the participating reactants so that a few uptake experiments of HCl on solid KBr salt particles have been performed using a low-pressure flow reactor. The synthesis of HCl is described in section 3.1.1.

4.2.2. Results

A mass spectrometric scan in the absence and the presence of a KBr sample has been performed. Neither on KBr grains nor on a thin KBr film sprayed on a Pyrex substrate reaction products have been identified. However, uptake experiments in the 14 mm-orifice reactor show a sharp initial uptake on fresh KBr grains and a fresh thin KBr film sprayed on a Pyrex substrate. The uptake coefficient amounts to $\gamma_{\text{ini}} = 3.6 \cdot 10^{-2}$ and $\gamma_{\text{ini}} = 6.9 \cdot 10^{-2}$ on a thin KBr film sprayed on a Pyrex substrate and KBr grains, respectively. After 30s or so, the samples are saturated in both cases. Figure 4.2.1 shows an HCl uptake experiment carried out on KBr grains in the 14mm-orifice reactor.

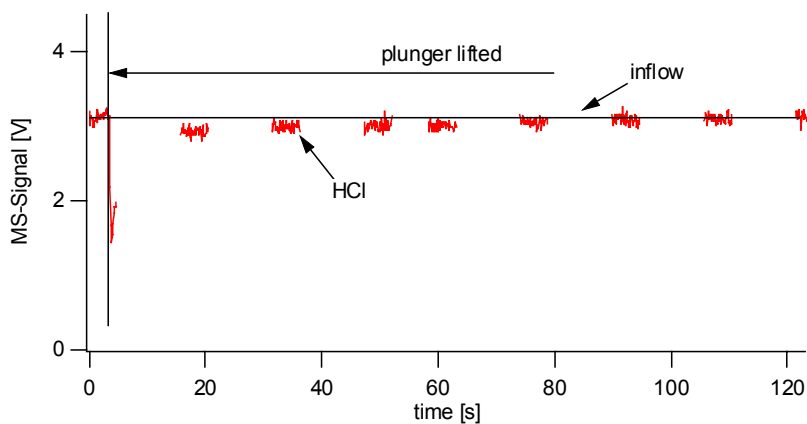


Figure 4.2.1: MS-Signal of a HCl uptake experiment on KBr grains carried out in the 14mm-orifice reactor. HCl has been monitored at $m/e = 36$.

4.3. Uptake Experiments of Cl₂ on KBr

4.3.1. Introduction

Molecular chlorine has been observed in unexpected high concentrations in coastal air masses (26). Laboratory investigations (27) and model studies (28) have suggested that reactive chlorine species may contribute significantly to the oxidative capacity of the lower marine troposphere. The measured Cl₂ mixing ratio lies between 10 and 150ppt. Cl₂ not only is a photochemically active halogen species but it may as well contribute to bromine activation (29, 30) by heterogeneous reaction with bromine containing salt aerosols. Reactions of Cl₂ on bromine containing salt aerosols are expected to be an important Cl₂ sink and source for Br₂ in the marine boundary layer. In order to investigate this aspect we studied the heterogeneous reaction of Cl₂ on different KBr substrates.

Furthermore, Cl₂ is present as an inevitable impurity in the gas sample of Cl₂O and HOCl. Moreover, it has been detected as a reaction product in the heterogeneous reaction of HOCl on solid KBr (Section 4.7). There is strong evidence that surface-adsorbed Cl₂ plays a decisive role in this reaction. Uptake experiments of HOCl on KBr carried out in the flow reactor have shown that salt surface contamination by adsorbed bromine and chlorine species on the surface plays a crucial role in the reaction kinetics of the interaction of HOCl on solid KBr (Section 4.7).

It is well known that surface adsorbed water H₂O(a), plays an important role in heterogeneous reactions on salt surfaces (6, 7, 31, 32). The influence of the amount of adsorbed H₂O(a) on the reaction kinetics has been investigated in this work by varying the pumping time and heating of the KBr sample. In order to estimate the amount of adsorbed H₂O(a) calibration curves obtained by desorption experiments carried out on different KBr samples (grains, ground grains and thin films sprayed on a gold-coated copper substrate, for further details see section 4.1 H₂O on KBr) have been used. The

Chapter 4

remaining quantity of $\text{H}_2\text{O}(\text{a})$ at a given experimental condition has been measured in quantitative thermal desorption experiments.

In order to investigate the interaction of Cl_2 with KBr at steady-state and in the pulsed valve mode uptake experiments on KBr have been performed in a low-pressure flow reactor. The reaction has been investigated in terms of reaction products and kinetics.

The preparation of the gaseous and solid samples has been performed following the procedures described in chapter 3.

4.3.2. Results and Discussion

In order to investigate the products of the reaction of Cl_2 with solid KBr a mass-spectrometric scan of the effluent of the reactor at a steady-state flow rate of Cl_2 in the absence and the presence of KBr grains has been performed. The MS-scan of the Cl_2 sample with the plunger in the lower position disclosed a slight impurity of HCl. A comparison shown in figure 4.3.1 shows both formation of Br_2 monitored at $m/e = 79, 81$ and $158, 160, 162$ and slow production of HBr as measured at $m/e = 80$ and 82 .

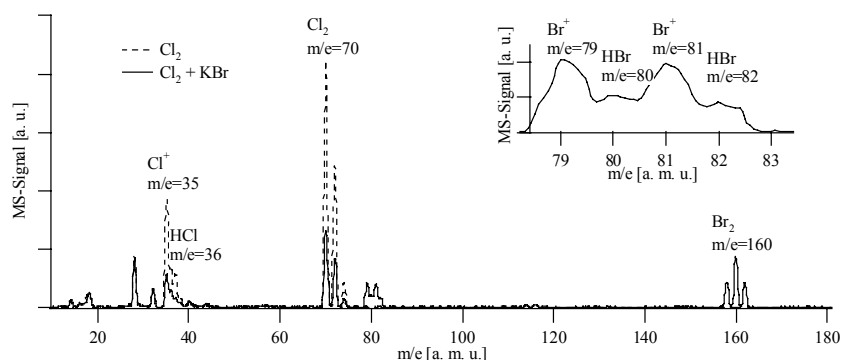


Figure 4.3.1: Mass-spectrometric scan of the Cl_2 sample and the reaction of Cl_2 with KBr grains. The MS-scans have been carried out in the 4mm-orifice reactor.

Chapter 4

The experimental conditions and main results corresponding to the following experiments for steady-state and pulsed valve experiments are summarised in tables 4.3.1 and 4.3.2, respectively, which are attached at the end of this section.

On a fresh sample of KBr grains exposed to Cl_2 the main observed reaction product has been Br_2 . Traces of BrCl and HBr have also been detected. In order to separate the different reactions the number of moles of lost HCl present as an impurity in Cl_2 has been compared with the number of moles of HBr formed. A one to one correspondence according to the overall reaction 4.3.1 has been found, which suggests that no additional HBr is formed in the reaction with Cl_2 and that the formed HBr stems from the reaction with the impurity of HCl after reacting according to the following reaction:



For the following experiments we therefore assume that the formation of HBr originates from the reaction of HCl with KBr so that we do not mention the formation of HBr any more.

On a virgin KBr sample the only observed reaction product at the start of the experiment has been Br_2 and small amounts of HOCl . Figure 4.3.2 shows a typical uptake experiment

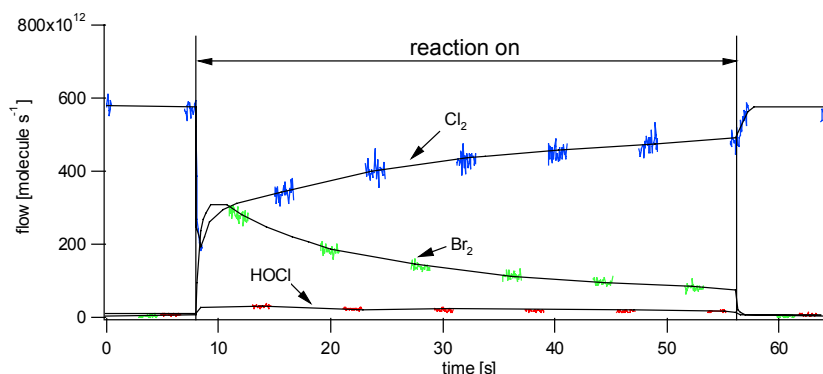


Figure 4.3.2: Calibrated data of a typical uptake experiment of Cl_2 on KBr . Cl_2 , Br_2 and HOCl have been monitored at $m/e = 70$, $m/e = 160$ and $m/e = 52$, respectively.

Chapter 4

of Cl_2 on KBr grains performed in the 14mm-orifice reactor (Table 4.3.1, experiment 1). The rate of formation of Br_2 is decreasing with time simultaneously to the decrease of the uptake of Cl_2 .

The formation of HOCl displayed in figure 4.3.2 may be explained by the hydrolysis reaction 4.3.2 of Cl_2 with surface adsorbed $\text{H}_2\text{O}(\text{a})$:

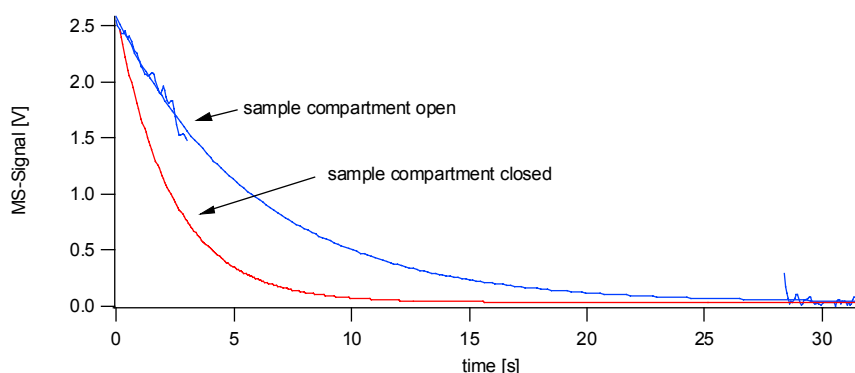


Figure 4.3.3: Stopped-flow experiment carried out in the 4mm-orifice reactor. After reaching steady-state the inflow of Cl_2 has been halted. The experiment has been performed in the absence and the presence of KBr grains. Cl_2 has been monitored at $m/e = 70$.

In the empty reactor the decay of the MS-signal attributed to Cl_2 obeys an exponential law (Chapter 2, Section 2.1.2) which has been experimentally confirmed. The gas-phase residence time of Cl_2 in the empty 4mm-orifice reactor has been determined to be $\tau_{\text{Cl}_2, 4\text{mm}} = 2.4\text{s}$. The presence of a KBr grain sample increases τ to a value of $\tau_{\text{Cl}_2, 4\text{mm}} = 5.9\text{s}$, (Table 4.3.1, Experiment 2). Figure 4.3.3 shows the raw MS-signals of the signal decay in the absence and the presence of KBr grains. The increased Cl_2 residence time τ or decreased effective effusion constant k confirms the presence of surface adsorbed chlorine which is desorbing upon halting the Cl_2 flow according to equilibrium (4.3.3). It represents a virtual source of Cl_2 as long as the supply lasts. A possible explanation may be the large Cl_2 solubility of 14,6g in 1l of $\text{H}_2\text{O}(\text{l})$ (33).

Chapter 4



Furthermore, consecutive uptake experiments on the same KBr grain sample have been carried out. The delay between the first and the second experiment has been chosen to be 10 minutes, or so. The comparison of the rates of uptake on a virgin sample and one which already has been exposed to Cl_2 exhibits a smaller initial rate of uptake on an already exposed sample. This agrees well with the proposed equilibrium (4.3.3) when the second and further exposure is inhibited by partial saturation of the free adsorption sites S for Cl_2 . Nevertheless, the initial rate of uptake of the second uptake experiment has been faster than the rate of uptake at the end of the first uptake experiment. This means, first, in the absence of Cl_2 the number of free S gradually increases, and, second, that even after several minutes reactive sites remain occupied. Thus, a partial regeneration of the surface takes place.

In order to investigate the time dependent regeneration of the surface adsorption rate of Cl_2 on solid KBr the following uptake experiments of Cl_2 on thin KBr films which were sprayed on a gold-coated copper substrate have been performed. The experimental conditions are listed in table 4.3.1, experiment 4. First, the KBr film had been exposed to Cl_2 in the 4mm-orifice reactor until steady state had been reached. Once steady state had been reached the plunger had been lowered and the sample compartment kept closed for a certain time, thus the sample compartment is isolated from the gas flow. This time we call regeneration-time t_r . After waiting for $t = t_r$ the plunger had been lifted again and the Cl_2 uptake monitored. The initial uptake is displayed as a function of t_r in figure 4.3.4 which shows the regeneration of the uptake rate of the sample as a function of time between two successive experiments. Regeneration means that a rearrangement of the mobile ions must occur on the sample surface leading to the liberation of occupied surface sites.

The regeneration may be due to crystallisation of KCl. Crystallised KCl is thermodynamically more stable than KBr, $\Delta H_f^0 = -436.74 \frac{\text{kJ}}{\text{mol}}$ and $\Delta H_f^0 = -393,8 \frac{\text{kJ}}{\text{mol}}$,

Chapter 4

respectively (34). So, we propose that KCl formed on the surface may crystallise and free up occupied sites.

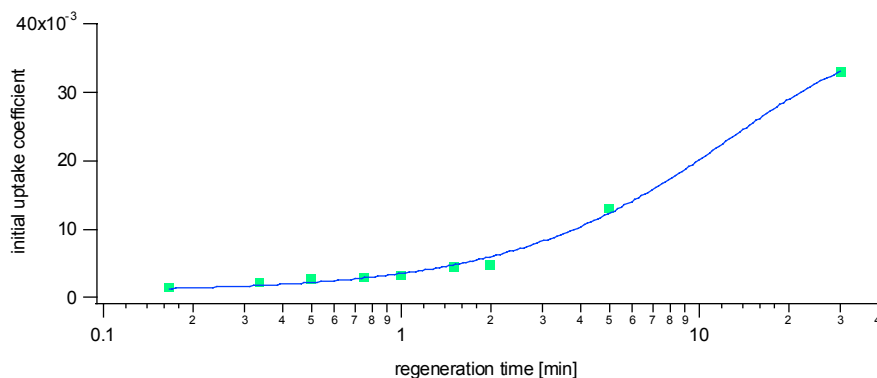


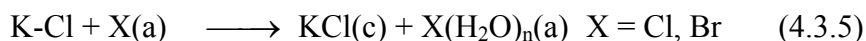
Figure 4.3.4: Repetitive uptake experiment of Cl₂ on thin KBr film sprayed on a gold-coated copper substrate carried out in the 4mm-orifice reactor. After reaching steady-state the sample compartment has been isolated from the Cl₂ flow. After the regeneration time t_r , the sample had again been exposed to Cl₂.



The hyphen means hydrated KCl.

The crystallisation we propose is in analogy to the HNO₃/NaCl and N₂O₅/NaCl systems which have been studied by Finlayson-Pitts (6, 31, 35). They observed a reorganisation of the NaCl surface leading to the formation of NaNO₃ crystals.

Furthermore, molecular dynamics simulations of concentrated aqueous NaCl solutions suggest that adsorbed halogen species tend to form clusters (36) with H₂O(a), which may lead to a deficiency of H₂O(a) on the surface, resulting in a dehydration of K-Cl. This means that adsorbed halogen species withdraw H₂O(a) from the mobile K-Cl and may thus enhance a crystallisation process. An analogous situation is shown in the exposure of KBr to gaseous Br₂ to be discussed below (Section 4.4).



Chapter 4

Where K-Cl means hydrated KCl ($\text{KCl}(\text{H}_2\text{O})_m$). In contrast, KBr substrates that have been exposed to HOCl have not regenerated under the same conditions. This situation will be discussed in more detail in section 4.7.

In order to investigate the observed surface-contamination by adsorbed Cl_2 we have performed pulsed valve experiments (Table 4.3.2). Figure 4.3.5 shows the MS-signal of a typical pulsed-valve experiment of Cl_2 on a thin KBr film sprayed on a Pyrex substrate performed in the 14mm-orifice reactor.

Subsequent identical Cl_2 pulses have been injected into the reactor. Because the Balzers mass spectrometer QMS-410 allows to monitor only one mass at a time we have alternately recorded the MS-signal of Cl_2 and Br_2 at $m/e = 70$ and $m/e = 160$, respectively. For one pair of pulses the ratio between the yield of Br_2 and the loss of Cl_2

($R = \frac{\text{Br}_2}{\text{Cl}_2}$) has been determined and displayed as a function of the sum over all injected molecules.

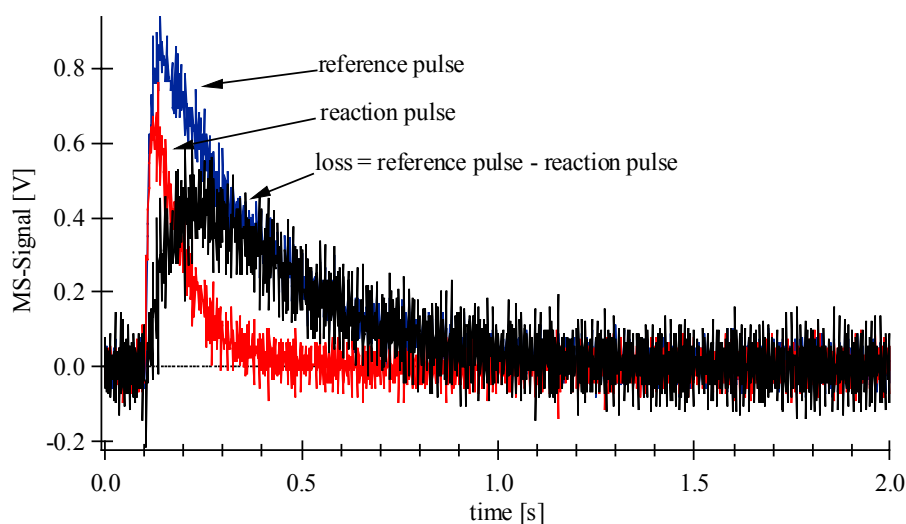


Figure 4.3.5: Typical pulsed valve uptake experiment of Cl_2 on a thin film of KBr sprayed on a Pyrex support. The experiment has been carried out in the 14mm-orifice reactor. Cl_2 has been monitored at $m/e = 70$. The opening-time for Cl_2 dosing was $t_a = 1\text{ms}$. The injection dose amounted to $1.8 \cdot 10^{13}$ molecule pulse $^{-1}$.

Chapter 4

$$\text{Total injected dose} = K \sum A_p \quad (\text{equation 4.3.1})$$

where K and A_p mean the calibration factor of the MS-signal and the integrated area of the MS-signal of one pulse, respectively. K is given in $\frac{\text{molecule}}{V_s}$ and A_p in V_s .

The pulsed valve experiments have shown an increase of the ratio R with increasing number of pulses or equivalently with the total amount of the injected Cl_2 , which may be a further indicator for surface-contamination by halogen species. Figure 4.3.6 shows R as a function of the total injected dose. Knudsen cell uptake experiments of Cl_2 on NaCl and KCl carried out by Mochida (37) led to an uptake of Cl_2 but no products were observed which confirms the suggestion of surface-adsorbed halogen. Galwey (38) has shown evidence of halogen retention on KBr surfaces. They believe that reactant KBr dissolved in condensed halogens retained at the reaction interface interacts with chlorine to form polyhalide intermediates. We suggest that these intermediates may be present on a contaminated surface leading to an enhanced formation of Br_2 which explains the increase of R .

In order to study the mechanism responsible for the retention of halogens this experiment has been carried out with different amounts of adsorbed water $\text{H}_2\text{O}(\text{a})$. The thin film of KBr sprayed on a Pyrex substrate had been pumped for different durations ranging from 15 minutes to 40h. The amount of $\text{H}_2\text{O}(\text{a})$ on the KBr substrate sprayed on the Pyrex substrate could not be estimated by the desorption experiments we have performed on the other samples (Section 4.1.2) because the amount of $\text{H}_2\text{O}(\text{a})$ on bare Pyrex and the KBr film sprayed on the Pyrex support were of the same order of magnitude. In order to indicate the amount of $\text{H}_2\text{O}(\text{a})$ we give the pumping time t_p for this kind of substrate. The ratio R on the sample pumped for 40h is slightly smaller than on the briefly pumped sample (Figure 4.3.6).

Chapter 4

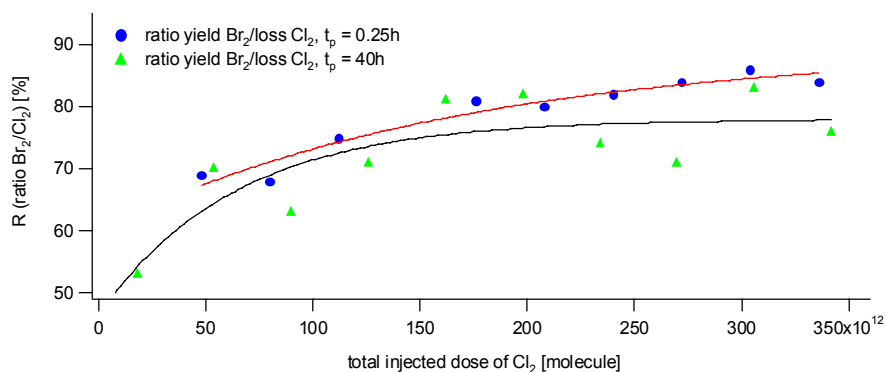


Figure 4.3.6: Pulsed valve experiment in the 14mm-orifice reactor carried out on a thin film of KBr sprayed on a Pyrex substrate. The samples had been pumped for 0.25h and 40h. The injection dose amounts to $1.8 \cdot 10^{13}$ molecule pulse⁻¹, the yield of Br₂ is only slightly smaller for a KBr sample pumped for 40h compared to 0.25h.

In order to investigate the influence of H₂O(a) on the contaminated substrate an already contaminated KBr film has been exposed for 5 minutes to ambient conditions. This occurred at a temperature of 20°C and a relative humidity of 30% corresponding to approximately 6 Torr of H₂O(g). After exposing the thin film to ambient conditions we have pumped the sample for 10 minutes before carrying out the Cl₂ uptake experiments. Pumping for ten minutes is necessary in order to be in the pressure range of the mass spectrometer. In contrast to the behaviour of the virgin sample R decreases as a function of the total injected dose of Cl₂ for the intermittently exposed sample, which is displayed in figure 4.3.7 a and b. The surface-contamination persists even at ambient conditions on the time scale of our experiment.

When we compare the corresponding uptake coefficients γ we come to the conclusion that the exposure of the sample to ambient conditions does not dramatically change the kinetics of the reaction, whereas prior pumping leads to a decrease of the uptake coefficient, probably due to a modification of the surface structure as we have shown in section 4.1.2, figures 4.1.1 and 4.1.2.

Chapter 4

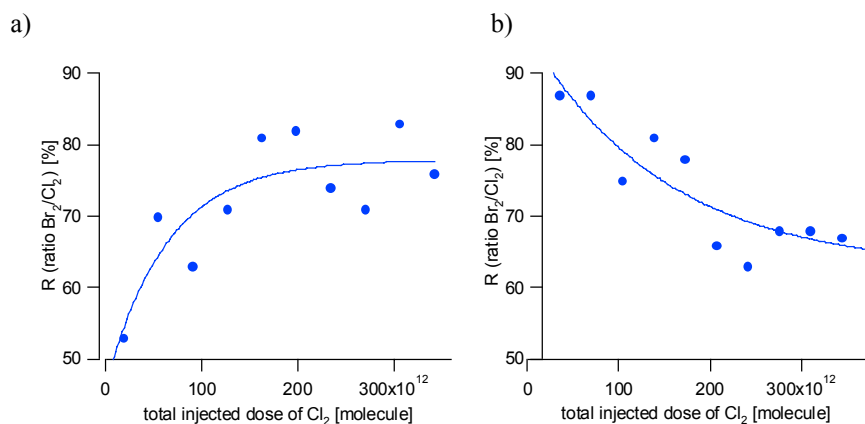


Figure 4.3.7: Pulsed valve experiment of Cl_2 on a thin KBr film sprayed on a Pyrex substrate performed in the 14mm-orifice reactor. a) shows the ratio $R = \frac{\text{Br}_2}{\text{Cl}_2}$ of an experiment carried out on a fresh and b) on the same contaminated sample exposed to approximately 6 Torr of H_2O .

Figure 4.3.8 shows the initial uptake coefficient γ_{ini} of the reactions measured on

- a fresh sample pumped for 15 minutes,
- a fresh sample pumped for 40h,
- the same sample as above pumped for 40h, but briefly exposed to ambient air prior to Cl_2 uptake.

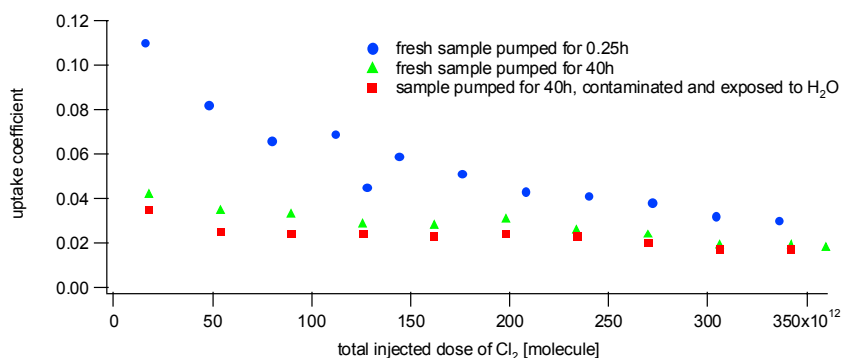


Figure 4.3.8: Uptake coefficients resulting from pulsed valve experiments of Cl_2 on thin films of KBr sprayed on a Pyrex substrate carried out in the 14mm-orifice reactor.

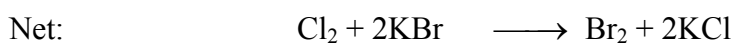
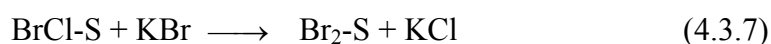
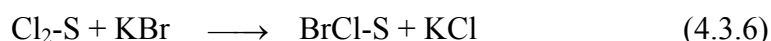
Chapter 4

The fact that the uptake coefficient does not significantly change whereas the yield of Br₂ increases after an exposure to H₂O(g) may lead to the conclusion that

- 1) the presence of H₂O(a) enhances the conversion of surface adsorbed chlorine to surface-adsorbed bromine or polyhalide species,
- 2) bromine species are not removed from the surface under ambient conditions,
- 3) the adsorbed bromine species may be displaced by chlorine adsorbing on the surface.

1) and 2) explain the yield of Br₂ of almost 100% of the lost Cl₂ and 3) may explain that the uptake coefficient remains almost unchanged after an exposure of the KBr sample to ambient conditions, which means that a “bromine site” is kinetically almost equivalent to a “free site”.

This may be explained by the following reaction scheme:



On a contaminated sample the adsorbed species Br₂-S are already present leading to an enhanced value of R upon Cl₂ heterogeneous interaction (Figure 4.3.7):

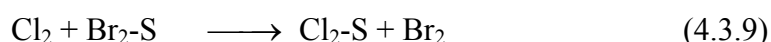


Figure 4.3.9 shows an illustration of the reaction mechanism given above. On a fresh KBr sample the interfacial reservoir is filled up by adsorption of Cl₂ at the surface followed by reaction with reactive KBr-sites to form adsorbed BrCl, which interacts with a second

KBr-site to form adsorbed molecular bromine (situation a)). The increasing amount of adsorbed molecular bromine is displaced by adsorbed Cl_2 and released to the gas-phase as Br_2 (situation c)). In the absence of gaseous Cl_2 the reaction on the surface continues and leads to an accumulation of molecular bromine by reactions 4.3.4 and 4.3.5 (situation b)). The accumulation of molecular bromine explains that the ratio R increases on a contaminated sample. The displacement of bromine by chlorine explains therefore that the uptake coefficient does not dramatically change on a contaminated sample. As we mentioned above, this means that an empty site and a site occupied by molecular bromine have a similar effect on the uptake rate of chlorine.

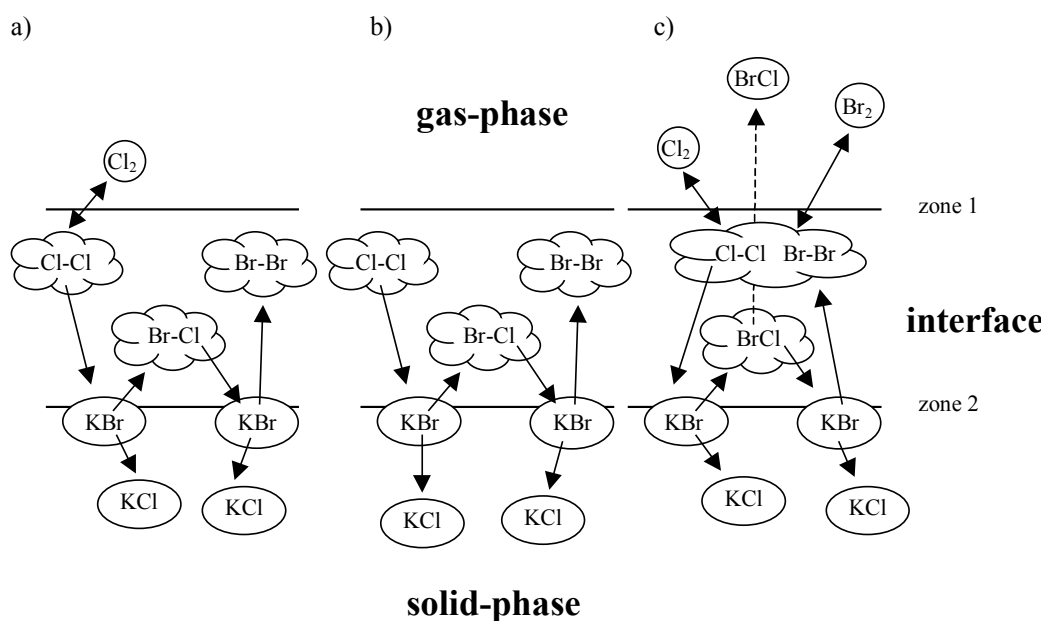


Figure 4.3.9: Schematic illustration of the reaction of Cl_2 on KBr. Situation a) illustrates the reaction on a fresh, situation b) in the absence of Cl_2 and situation c) on a contaminated sample. The adsorbed hydrated intermediate species are indicated by clouds.

The observed rate of formation of BrCl sets in after a delay and increases with time whereas the rate of production of Br_2 decreases with time as it is shown in figure 4.3.10. The experimental details of the experiment of figure 4.3.10 are listed in table 4.3.1, experiment 1c. BrCl as an intermediate product had already been observed in the reaction of Cl_2 on NaBr (39). It may be explained by the surface coverage of KCl from previous

Chapter 4

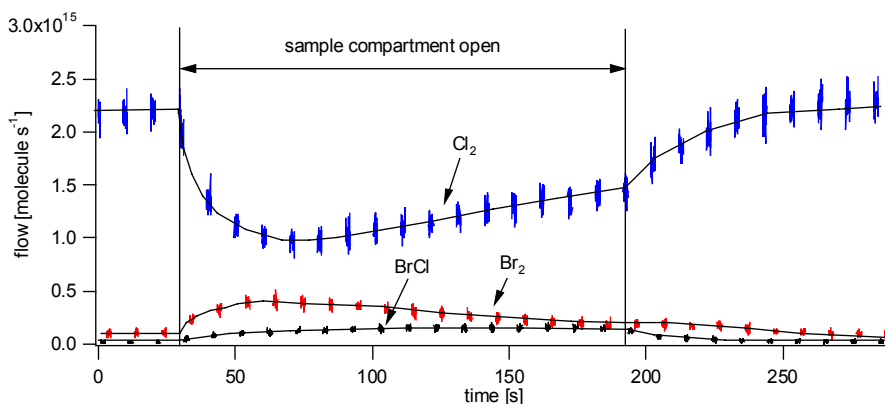


Figure 4.3.10: Cl_2 uptake experiment carried out on KBr grains in the 1mm-orifice reactor. Cl_2 , Br_2 and BrCl are monitored at $m/e = 70$, $m/e = 160$ and $m/e = 116$.

exposure of KBr to Cl_2 and consequently a slower conversion of BrCl to Br_2 (Reaction 4.3.7). BrCl may also desorb into the gas-phase according to reaction 4.3.10.



After an exposure time of 10 minutes, or so, saturation sets in in the 1mm-orifice reactor and the rate of production of Br_2 as well as BrCl tend to zero (Table 4.3.1, Experiment 4). Saturation means that only a fraction of the entire KBr sample is available to undergo a reaction with Cl_2 . This may be explained with a limited number of active surface-sites S .

In order to investigate the influence of adsorbed $\text{H}_2\text{O(a)}$ the KBr sample has been heated for 20h at $T = 473\text{K}$ (Table 4.3.1, Experiment 5). The initial uptake coefficient γ_0 remains unchanged but the Cl_2 uptake saturates faster than on a standard grain sample.

Figure 4.3.11 displays the temporal dependence of the uptake coefficient γ of a sample, which has not been heated (standard sample) and a sample which had been heated ex situ prior to its introduction into the reactor. The number of reactive sites able to take up Cl_2 decreases by heating the sample, which may be explained by a transition towards a better-ordered surface. This crystallographic effect has been demonstrated for thin KBr films sprayed on a gold-coated substrate (Section 4.1). Examination of the surface by Scanning Electron Microscopy SEM has shown a change in the surface-structure by heating the

Chapter 4

sample (Figure 4.1.3). This change of the surface-structure is irreversible on the time-scale of days, even if the sample had been exposed to ambient conditions. This is consistent with the assumption that surfaces with a high number of defect sites are more reactive than well-ordered surfaces (9).

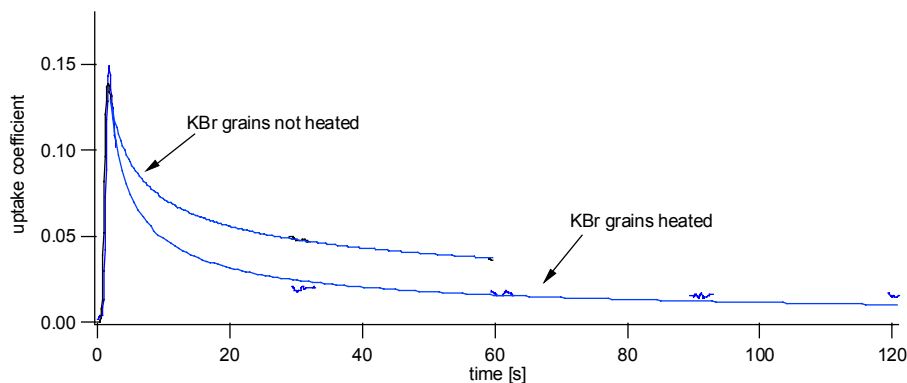


Figure 4.3.11: Uptake experiment of Cl_2 on KBr grains carried out in the 14mm orifice reactor. The uptake coefficient of Cl_2 on a heated and a standard sample is displayed as a function of time. One sample has been heated ex situ in an oven for 20h at temperature $T = 473\text{K}$.

The fact that the initial uptake coefficient γ_0 remains unchanged suggests that the reaction kinetics on a virgin sample is determined rather by adsorption of Cl_2 and by the amount of adsorbed $\text{H}_2\text{O}(\text{a})$ necessary to build the proposed reservoir (interfacial zone in Figure 4.3.9) than by the number of reactive surface sites located at the solid-interface zone (zone 2, Figure 4.3.9). In other words, the initial uptake is determined by interaction with the interface-gas-phase zone (zone 1 in Figure 4.3.9), whose “thickness” is influenced by the pumping time t_p (Figure 4.3.8). In agreement with this heating the sample changes the thickness of the interfacial-solid zone (zone 2, Figure 4.3.9) which manifests itself in a more rapid decrease of the uptake coefficient γ on a heated sample than on a standard sample (Figure 4.3.11) owing to a smaller reservoir of $\text{H}_2\text{O}(\text{a})$.

These observations may be a further indication for the two-zone character of the salt surface as displayed in figure 4.3.9.

Furthermore, experiments have been performed on thin films of KBr sprayed on a gold-coated copper support (Table 4.3.1, Experiment 6). The steady-state uptake coefficients

Chapter 4

$\gamma_{ss} = f(\text{concentration})$ and reaction-flows have been measured as a function of the Cl_2 concentration in the reactor (Figure 4.3.12). A plot of the steady state reaction flow versus the concentration of Cl_2 is presented in figure 4.3.13.

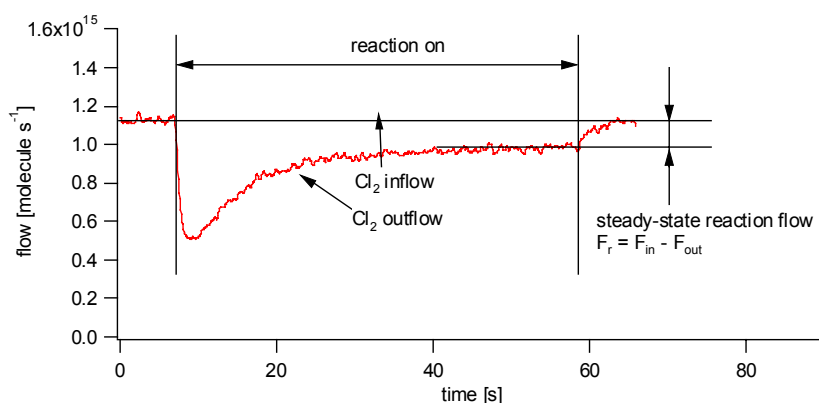


Figure 4.3.12: Steady-state uptake experiment of Cl_2 on a thin KBr film sprayed on a gold-coated copper substrate carried out in the 4mm-orifice reactor. Cl_2 has been monitored at $m/e = 70$.

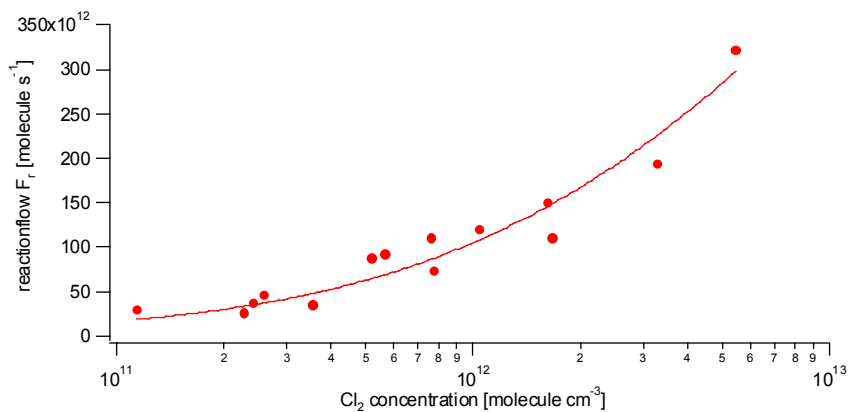


Figure 4.3.13: Steady-state reaction-flow $F_r = F_{in} - F_{out}$ versus Cl_2 concentration in the reactor. The full line represents a fit based on a Langmuir-Hinshelwood model with dissociation: $F_r = p \cdot c \cdot \left(\frac{1}{1 + \sqrt{k \cdot c}}\right)^2$, where p , k are constants and c the concentration of Cl_2 .

The reaction flow has been fitted using the following Langmuir-Hinshelwood based model including dissociation (Figure 4.3.14).

Chapter 4

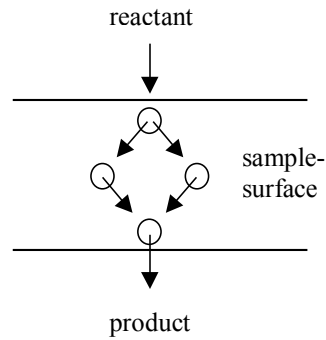


Figure 4.3.14: Schematic illustration of the reaction model. The reactant adsorbs on two adjacent reactive surface sites and dissociates. The two intermediate species react and form the reaction product.

The change in surface coverage due to adsorption with dissociation may be expressed as (equation 4.3.2) (18)

$$\dot{\theta}_a = k_1 c (1-\theta)^2 \quad (\text{equation 4.3.2})$$

and the change in surface coverage due to product desorption may be written as (equation 4.3.3):

$$\dot{\theta}_d = k_2 \theta^2 \quad (\text{equation 4.3.3})$$

where c means the concentration expressed in molecule cm^{-3} and $c \in [8 \cdot 10^{10}, 6 \cdot 10^{12}]$.

k_1 and k_2 are the reaction constants and are expressed in $[k_1] = \text{cm}^3 (\text{molecule s})^{-1}$ and $[k_2] = \text{s}^{-1}$, θ represents the surface coverage defined in equation 4.3.6, $0 \leq \theta \leq 1$.

Chapter 4

At steady-state there is no net change in surface coverage θ and we may apply the steady state condition:

$$\dot{\theta} = \dot{\theta}_a - \dot{\theta}_d = 0 \quad (\text{equation 4.3.4})$$

Equating and solving equations 4.3.2 and 4.3.3 for θ leads to:

$$\theta = \frac{\sqrt{kc}}{1+\sqrt{kc}}, \quad \text{with } k := \frac{k_1}{k_2} \quad (\text{equation 4.3.5})$$

furthermore,

$$\theta = \frac{S}{S_t} \quad (\text{equation 4.3.6})$$

where S and S_t means the number of occupied surface sites and the total number of reactive surface sites, respectively.

The derivation of equation 4.3.6 with respect to adsorption leads to:

$$\dot{S}_a = S_t \dot{\theta}_a \quad (\text{equation 4.3.7})$$

\dot{S}_a corresponds to the reaction flow F_r and we may write:

$$F_r = S_t \dot{\theta} \quad (\text{equation 4.3.8})$$

Introducing equations 4.3.5 and 4.3.8 into equation 4.3.2 results in:

$$F_r = qc \left(\frac{1}{1+\sqrt{kc}} \right)^2, \quad \text{with } q = k_1 S_t \quad (\text{equation 4.3.9})$$

Chapter 4

Introducing equation 4.3.8 into equation 2.1.10 for the steady-state uptake coefficient we get:

$$\gamma = \left(\frac{F_{\text{in}}}{F_{\text{out}}} - 1 \right) \frac{k_{\text{esc}}}{\omega} \quad (\text{equation 2.1.10})$$

$$\gamma_{\text{ss}} = \frac{4q}{\bar{v}(1+\sqrt{kc})^2 A_s} = \tilde{q} \frac{1}{(1+\sqrt{kc})^2}, \text{ with } \tilde{q} = \frac{4q}{\bar{v}A_s} \quad (\text{equation 4.3.10})$$

where \bar{v} is the mean velocity of the molecule and A_s the surface of the sample.

We have compared the model described above with a linear model without dissociation using a least-squares criterion χ^2 , which is defined by equation 4.1.1. The model we described above is clearly favoured using the χ^2 criterion.

A sample pumped for $t_p = 1.5\text{h}$ and $t_p = 11.5\text{h}$ contains $4.5 \cdot 10^{16}$ and $2.9 \cdot 10^{16}$ molecule cm^{-2} of $\text{H}_2\text{O}(\text{a})$, respectively according to the calibration curve for a thin KBr spray on a gold-coated copper substrate (Figure 4.1.6).

For a sample with $\text{H}_2\text{O}(\text{a}) = 4.5 \cdot 10^{16}$ molecule cm^{-2} we obtain:

$$k = 1.7 \cdot 10^{-13} \text{ cm}^3 \text{ molecule}^{-1}$$

$$q = 234 \text{ cm}^3 \text{ s}^{-1}$$

$$\tilde{q} = 0.16$$

and for the sample with $\text{H}_2\text{O}(\text{a}) = 2.9 \cdot 10^{16}$ molecule cm^{-2} leads to:

$$k = 2.0 \cdot 10^{-13} \text{ cm}^3 \text{ molecule}^{-1}$$

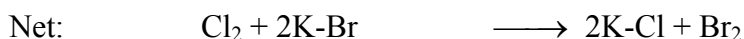
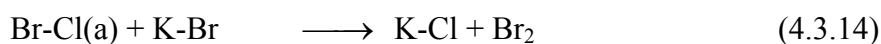
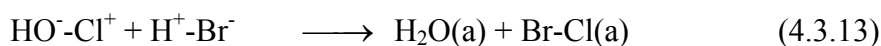
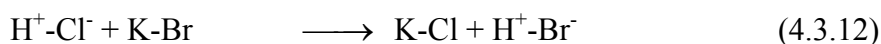
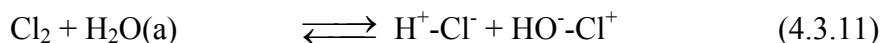
$$q = 207 \text{ cm}^3 \text{ s}^{-1}$$

$$\tilde{q} = 0.14.$$

Chapter 4

Introducing the obtained constants in equation 4.3.10 leads to a steady-state uptake γ_{ss} which is 40% higher for the sample containing more $H_2O(a)$.

According to the model described above we suggest that Cl_2 dissociates on two adjacent reactive sites on the substrate. The following mechanism describes the mechanism we found in terms of chemical equations:



The hyphens indicate a hydrated molecule. The reaction mechanism 4.3.11-14 includes dissociation of Cl_2 compared to the simpler mechanism displayed in 4.3.3-4.3.8. The dissociation leads to independent intermediate species which are justified by the mechanism we have introduced above whose characteristic feature is the dependence of the rate on the square of the surface coverage and the free adsorption sites, respectively.

4.3.3. Conclusion

Uptake experiments of Cl_2 on different KBr substrates have been carried out in a low-pressure flow reactor. The main reaction product is Br_2 but small amounts of $BrCl$ have also been observed. Furthermore, a partial regeneration of the sample even under low-pressure conditions has been observed. We suggest that the regeneration of the surface may be due to conversion of adsorbed chlorine to adsorbed polyhalide or bromine

Chapter 4

species. Thermodynamic consideration also allows a crystallisation of formed KCl which leads to a liberation of occupied sites.

Furthermore, we have shown that chlorine and bromine may be retained on the surface and play a crucial role in terms of product yield and reaction kinetics. Exposure of a contaminated sample to ambient conditions almost does not affect the initial reaction kinetics whereas the yield is significantly changed by water exposure. We conclude that an exposure of a contaminated sample enhances the conversion of adsorbed chlorine to surface adsorbed bromine or polyhalide species. Moreover, we propose that gaseous chlorine displaces surface-adsorbed bromine.

In order to investigate the nature of the reactive sites KBr has been dried in an oven before carrying out a Cl_2 uptake experiment. We noticed that heating the sample does not effect the initial uptake whereas the sample saturates faster than a standard sample. In contrast, pumping the sample causes a considerable decrease in the initial uptake coefficient γ_0 . Pumping mostly acts on weakly bound $\text{H}_2\text{O}(\text{a})$, which inspired us to introduce an interfacial reservoir of active surface sites S which may hydrolyse adsorbed Cl_2 on the surface according to reaction 4.3.11.

In order to confirm the hypothesis of dissociation we have measured the steady-state reaction-flow (equal to the reaction rate) as a function of the Cl_2 concentration. The good fit obtained by an adsorption-dissociation model involving the pair-wise involvement of reactive surface sites strengthens the assumption of the existence of a reservoir on the sample surface.

4.3.4. TablesTable 4.3.1: Experimental conditions and main results for continuous flow Cl₂ uptake experiments.

No	Orifice diameter [mm]	Type of surface	[Cl ₂] [molecule cm ⁻³]	Experimental conditions	Main products	Minor products	Uptake kinetics	Remarks
1a	14	g	3.7*10 ¹¹	First uptake on fresh sample	Br ₂	HOCl	γ ₀ = 0.13	Br ₂ production rate decreases with time, slow formation of HOCl
1b	14	g	3.4*10 ¹¹	Uptake on contaminated sample	Br ₂	BrCl	γ ₀ = 6*10 ⁻²	Br ₂ production decreases, BrCl production delayed
1c	1	g	4.6*10 ¹³	Uptake on contaminated sample	Br ₂	BrCl	γ = 5*10 ⁻⁴	Br ₂ production decreases, BrCl production delayed and increases
2	14	g	2*10 ¹⁰	Flow stopped with lifted plunger	Br ₂		γ ₀ = 0.25	Desorption of Cl ₂ (ads)
3	4	fg	6*10 ¹¹	Saturated sample	Br ₂			Regeneration as a function of time
4a	1	Au	7*10 ¹²	Cl ₂ exposure time t _c = 10min	Br ₂	BrCl		Saturation of the sample: Br ₂ saturates first than BrCl
4b	4	Au	3*10 ¹¹	Uptake on saturated sample, waiting time t _w = 10h	Br ₂	BrCl	γ ₀ = 1.5*10 ⁻²	Regeneration of the sample
5	14	g	2*10 ¹¹	Heated at T=473K for 20h	Br ₂	BrCl	γ ₀ = 0.13	Saturates faster than a only pumped substrate
6	4, 8, 14	fg	8*10 ¹⁰ – 6*10 ¹²				γ _{ss} = 13*10 ⁻³ $\gamma_{ss} = q \frac{1}{(1+\sqrt{kc})^2}$	

g : KBr grains Au : thin KBr film sprayed on gold coated copper substrate

Table 4.3.2: Experimental conditions and main results for Cl₂ pulsed valve experiments on thin KBr film sprayed on a Pyrex substrate.

No	Orifice diameter [mm]	Cl ₂ [molecule/pulse]	Experimental conditions	Main products	Minor products	Uptake kinetics	Remarks
1a	14	1.8*10 ¹³	Pumping time t _p = 40h	Br ₂		γ ₁ = 4*10 ⁻²	production Br ₂ / loss Cl ₂ is increasing with the number of pulses
1b	14	1.7*10 ¹³	Exposure to 20mbar H ₂ O, t _{exp} = 5min	Br ₂		γ ₁ = 3.5*10 ⁻²	production Br ₂ / loss Cl ₂ is decreasing with the number of pulses
2a	14	1.6*10 ¹³	Pumping time t _p = 0.25h	Br ₂		γ ₁ = 0.11	Reaction is faster than at long pumping time

γ_x : x = number of pulse, e.g. 1 = first pulse

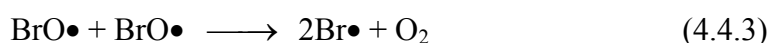
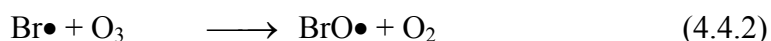
4.4. The Role of Adsorbed Molecular Bromine Br₂ on KBr and KCl Surfaces

4.4.1. Introduction

Br₂ plays an important role in tropospheric photochemistry (29). During daytimes Br₂ is easily photo-dissociated to atomic bromine (25).



Atomic bromine is most probably be involved in the arctic O₃ depletion (40, 41):



Our interest in Br₂ lies in the interaction with KBr surfaces in terms of adsorption and catalytic reaction cycles. While performing uptake experiments in a low-pressure flow reactor we have noticed that adsorbed bromine plays an important role in surface reactions involving KBr substrates. It has been observed that the reaction kinetics of Cl₂ and HOCl on KBr are enhanced by the presence of adsorbed bromine species. They are formed by the adsorption of Br₂, which is a reaction product and thus present in the flow reactor. The effect of Br₂ has been demonstrated by injecting an additional Br₂ flow into the reactor while an uptake experiment was being performed. These experiments are described in detail in section 4.7 of this chapter. Furthermore, changing the orifice affects the residence time of Br₂ in the reactor, which significantly influences the reaction kinetics. This is a further hint for an interaction of gaseous Br₂ with KBr surfaces. It has to be noticed, however, that a net Br₂ uptake on solid KBr samples has never been observed within the conditions of our Knudsen reactor steady-state experiments. Nevertheless, diffusion tube experiments of Br₂ on solid KBr films performed in our laboratory have revealed a significant interaction expressed as a surface residence time of Br₂ (42). Furthermore, pulsed valve Knudsen reactor experiments performed by Aguzzi et al. (43) obtained $\gamma_0 = 3 \cdot 10^{-3}$ for Br₂ on solid thin films of KBr sprayed onto a Pyrex support.

Finally, a substantial amount of HOBr and traces of HBr are outgassing from spray and ground grain substrates at $T = 620\text{K}$, which may be an indication for adsorbed molecular bromine on samples with high amounts of defect sites. A detailed description may be found in section 4.1.

4.4.2. Results and Discussion

In order to demonstrate a significant interaction of Br_2 with KBr a thin film of KBr sprayed on a Pyrex support has been exposed to 50mbar of Br_2 in a static reactor. Before the KBr sample has been exposed to Br_2 it had been pumped for 1h at ambient temperature in a standard vacuum line at a total pressure lower than 1mbar.

After 2 days of exposure Scanning Electron Microscope (SEM) images of a sample exposed to ambient conditions and one exposed to 50mbar of Br_2 have been taken in order to compare them. Figure 4.4.1 and 4.4.2 show a sample exposed to ambient conditions and exposed to

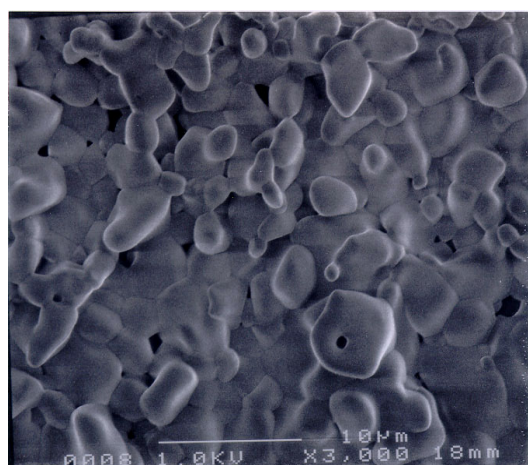


Figure 4.4.1: Thin KBr film sprayed on Pyrex substrate exposed 2 days to ambient conditions

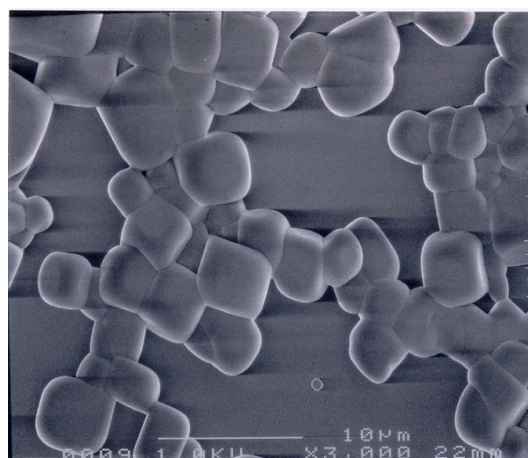


Figure 4.4.2: Thin KBr film sprayed on Pyrex substrate exposed for 2 days to 50 mbar of Br_2 .

Br_2 , respectively. The interaction of Br_2 with thin films manifests itself in a crystallisation of the KBr sample exposed to Br_2 , whereas the sample exposed to ambient condition did not show any change towards a more ordered surface. This crystallisation confirms an interaction of Br_2 with the KBr sample. The interaction of Br_2 with KBr has been further studied by uptake experiments of HOCl in a Knudsen flow reactor. The heterogeneous interaction of KBr with HOCl is discussed below in section 4.7.

The observed crystallisation of the thin KBr films we have seen in excess of surface-adsorbed bromine may be explained by the assumption of the existence of a quasi-liquid layer (QLL) (6) in the presence of adsorbed H₂O(a). We propose the following reaction mechanism (the hyphen means a hydrated ion-pair):



This means that few KBr units probably constituting defect sites may react with H₂O(a) (5) and form a KOH or possibly a weak K-OH ion pair bond (4). We have shown the existence of basic KOH sites on solid KBr samples by observing a reaction of CO₂ with KBr grains (Reactions 4.1.4 and 4.1.5). Furthermore, the excess of adsorbed bromine may lead to the proposed dehydration (Reaction 4.3.5) of KBr which may enhance the crystallisation of KBr.

In a further experiment a thin film of KCl sprayed on a Pyrex substrate has been exposed in a static reactor to 10 Torr of Br₂ during 2 days. Similar to the KBr substrate a recrystallisation of the thin KCl film in the presence of excess Br₂ has taken place. Figure 4.4.3 and 4.4.4 show SEM-images of a sample exposed to ambient conditions and a sample exposed to Br₂, respectively.

KBr and KCl ($\Delta H_f^0 = -393.8 \frac{\text{kJ}}{\text{mol}}$, $\Delta H_f^0 = -436.7 \frac{\text{kJ}}{\text{mol}}$, respectively (34)) in a hydrated

form are thermodynamically less stable than crystalline KBr and KCl ($\Delta H_f^0 = -373.9 \frac{\text{kJ}}{\text{mol}}$,

$\Delta H_f^0 = -419.5 \frac{\text{kJ}}{\text{mol}}$, respectively (34)). We have shown that the recrystallisation does not

occur or occurs very slowly at ambient condition. The presence of adsorbed Br₂ seems to lower the energy-barrier between the less and the more ordered state. Model calculations have revealed KBr (and KCl) does not completely dissociate on the surface and rather tends to form ion pairs like it is expected for concentrated aqueous solutions (44, 36, 45).

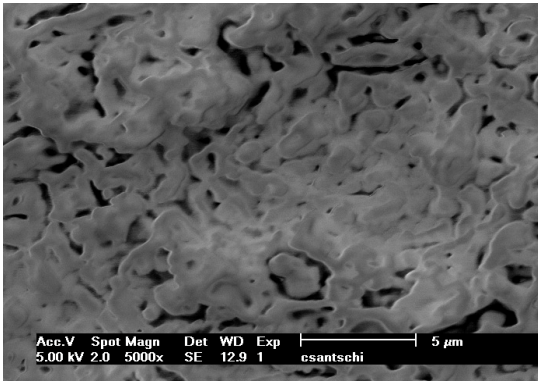


Figure 4.4.3: Thin KCl film sprayed on Pyrex substrate exposed for 2 days to atmospheric conditions.

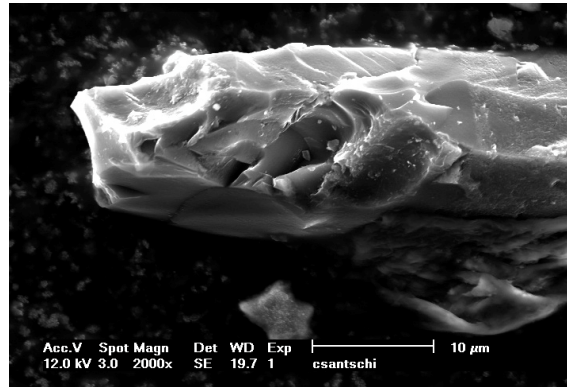


Figure 4.4.4: Thin KCl film sprayed on Pyrex substrate exposed for 2 days to 10 Torr of Br₂.

Br₂ has a solubility of 35,8g in 1l of H₂O(l) at T = 293K (33). Small amounts of Br₂ may be accommodated by the amount of H₂O(a) on the KBr sample leading to the equilibrium (4.4.5). In order to estimate the adsorption of Br₂ on KBr grains the grain sample has been exposed in the 4mm-orifice reactor to a concentration c of $1.2 \cdot 10^{13}$ molecule cm⁻³ of Br₂. After the exposure the flow of Br₂ had been halted while the plunger was left in the upper position in order to perform a stopped-flow experiment.

A comparison of the MS-signals of the bare sample holder and the sample holder filled with 1g of KBr grains has shown a slight difference in the decay of the MS-signal:

$k_{\text{esc}} = 0.279\text{s}^{-1}$ and $\tilde{k}_{\text{esc}} = 0.256\text{s}^{-1}$ for the filled and the bare sample holder, respectively (Figure 4.4.5).

Approximating the decay of the MS-signal by an exponential function we may determine the amount of adsorbed Br₂ in the following way:

In the absence of the sample we may express the number of molecules N in the reactor as

$$N(t) = N_0 e^{-k_{\text{esc}} t} \quad (\text{equation 4.4.1})$$

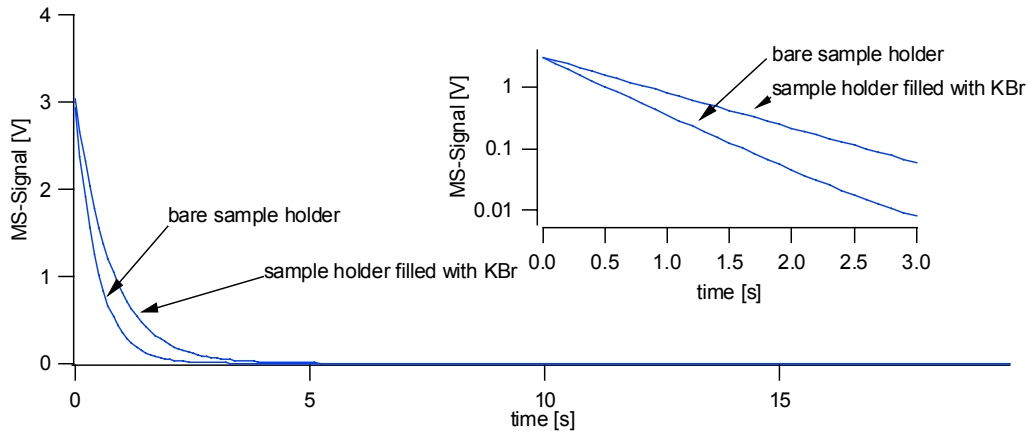


Figure 4.4.5: Stopped-flow experiment carried out in the 4mm-orifice reactor. The inflow of Br_2 has been halted leaving the plunger in the upper position. The decay of the MS-Signal of the sample holder filled with 1g of KBr is slightly slower than the decay of the signal of the bare sample holder. This indicates that small amounts of Br_2 may adsorb on KBr grains.

In the presence of the sample we have

$$N(t) = N_0 e^{-\tilde{k}_{\text{esc}} t} \quad (\text{equation 4.4.2})$$

where N_0 is the number of molecule in the reactor at $t = 0$

$$N_0 = c_0 V \quad (\text{equation 4.4.3})$$

where c_0 and V are the concentration of Br_2 at $t = 0$ and the reactor volume, respectively.

The amount of the adsorbed molecules is given by the difference of the number of molecule in the reactor in the absence and the presence of the sample.

$$S_{\text{Br}_2} = \int_0^{\infty} \tilde{F}_{\text{out}} dt - N_0 \quad (\text{equation 4.4.4})$$

\tilde{F}_{out} means the outflow in the presence of the sample.

Chapter 4

Using equation 2.1.7, 4.4.2 and 4.4.4 leads to

$$F_{\text{out}} = k_{\text{esc}}N \quad (\text{equation 2.1.7})$$

$$S_{\text{Br}_2} = \frac{Vc_0}{A_s} \left(k_{\text{esc}} \int_0^{\infty} e^{-\tilde{k}_{\text{esc}} t} dt - 1 \right) = \frac{Vc_0}{A_s} \frac{k_{\text{esc}} - \tilde{k}_{\text{esc}}}{\tilde{k}_{\text{esc}}} \quad (\text{equation 4.4.5})$$

The division by the surface area A_s of the sample results in the surface density of the number of adsorbed molecule S_{Br_2} where S_{Br_2} is given in molecule cm^{-2} . Introducing $c_0 = 1.2 \cdot 10^{13}$ molecule cm^{-3} , $V = 1830 \text{cm}^3$ and $A_s = 145 \text{cm}^2$ in equation 4.4.5 results in $S_{\text{Br}_2} = 1.3 \cdot 10^{13}$ molecule cm^{-2} . The determination of A_s is described in section 3.2.1. The surface number density of KBr is $5.8 \cdot 10^{14}$ molecule cm^{-2} (see Section 3.2.1). This means that the surface coverage of Br_2 is approximately 1.5% at concentration c_0 .

The desorption rate constants k_d and k_a may be determined using equation 4.4.2:

$$\dot{N} = -k_{\text{esc}}N + k_dS = -\tilde{k}_{\text{esc}}N \Rightarrow k_d S_{\text{Br}_2} A_s = (k_{\text{esc}} - \tilde{k}_{\text{esc}})cV \quad (\text{equation 4.4.6})$$

Using the constants obtained from the 4 and 14mm-orifice reactor results in the equation system:

$$\begin{pmatrix} N_0(14) & -S_{\text{Br}_2}(14) \\ N_0(4) & -S_{\text{Br}_2}(4) \end{pmatrix} \begin{pmatrix} k_a \\ k_d \end{pmatrix} = \begin{pmatrix} (\tilde{k}_{\text{esc}}(14) - k_{\text{esc}}(14))N_0(14) \\ (\tilde{k}_{\text{esc}}(4) - k_{\text{esc}}(4))N_0(4) \end{pmatrix} \quad (\text{equation 4.4.7})$$

Solving equation system 4.4.7 for k_a and k_d leads to:

$$\left. \begin{array}{l} \tilde{k}_{\text{esc}}(14) = 1.3 \text{s}^{-1}, k_{\text{esc}}(14) = 2.1 \text{s}^{-1} \\ \tilde{k}_{\text{esc}}(4) = 0.25 \text{s}^{-1}, k_{\text{esc}}(4) = 0.28 \text{s}^{-1} \\ N_0(14) = 2 \cdot 10^{12} \frac{\#}{\text{cm}^3}, S_{\text{Br}_2}(14) = 1.2 \cdot 10^{13} \frac{\#}{\text{cm}^2} \\ N_0(4) = 1.2 \cdot 10^{13} \frac{\#}{\text{cm}^3}, S_{\text{Br}_2}(4) = 1.4 \cdot 10^{13} \frac{\#}{\text{cm}^2} \end{array} \right\} \Rightarrow \begin{cases} k_a = 0.14 \frac{\text{cm}}{\text{s}} \\ k_d = 1.8 \frac{1}{\text{s cm}} \end{cases}$$

The existence of adsorbed Br_2 implies a surface residence time τ_s of Br_2 on solid KBr as measured by (42).

4.4.3. Conclusions

The presence of an excess of mobile halogen ions on the surface leads to recrystallisation of the KBr sample. The presence of adsorbed $\text{Br}_2(\text{a})$ seems to lower the energy-barrier for the transition of a less- to a better-ordered state. The QLL present on the surface of KBr substrates has a capacity to accommodate additional halogens from the gas-phase in order to establish equilibrium (4.4.5). This additional quantity of adsorbed Br_2 is highly mobile and may play together with adsorbed $\text{H}_2\text{O}(\text{a})$ an important role as intermediate reaction products between gas-phase and bulk.

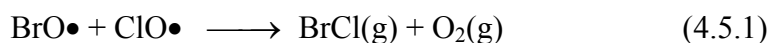
Furthermore, we estimated the number of adsorbed Br_2 at a given concentration c_0 . We have found that the surface coverage is about 1.5% under our experimental conditions ($T = 300 \text{ K}$, $[\text{Br}_2] = 1.2 \cdot 10^{13} \text{ molecule cm}^{-3}$).

4.5. Uptake Experiments of BrCl on KBr

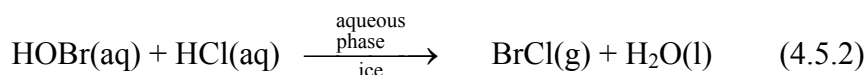
4.5.1. Introduction

Bromine chloride BrCl is anticipated as a possible precursor to atomic bromine in the troposphere, which plays an important role in ozone destruction (Reactions 4.4.2 and 4.4.3). Furthermore, BrCl is also expected to be a dominant source of atomic chlorine during polar sunrise. At Alert, Canada, BrCl levels as high as ~35ppt have been measured (29).

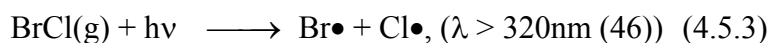
BrCl may be produced in the gas-phase by the following reaction:



A heterogeneous source is reaction 4.5.2:



In photochemistry BrCl plays an important role because it can be easily photodissociated.



BrCl has been observed in the laboratory as a reaction product in the reaction of Cl₂, Cl₂O and HOCl with KBr substrates (Sections 4.2, 4.6 and 4.7). In order to investigate those reactions a few uptake experiments of BrCl on KBr substrates have been performed.

4.5.2. Results

A mass spectrometric scan of BrCl has been carried out in the 4-mm orifice reactor in the absence and the presence of KBr grains. As expected the only detected reaction product is Br₂.

An uptake experiment has been performed in the 4mm-orifice reactor on KBr grains. An initial uptake coefficient of $\gamma_0 = 0.3$ has been measured. Immediately after lifting the plunger the rate of BrCl uptake goes to steady-state. On a fresh sample a delay in the formation of the reaction product Br₂ in the gas-phase is recorded. Figure 4.5.1 shows the loss rate of BrCl and the production rate of Br₂ as a function of time. Towards the end of the experiment the production rate of Br₂ tends towards the loss rate of BrCl.

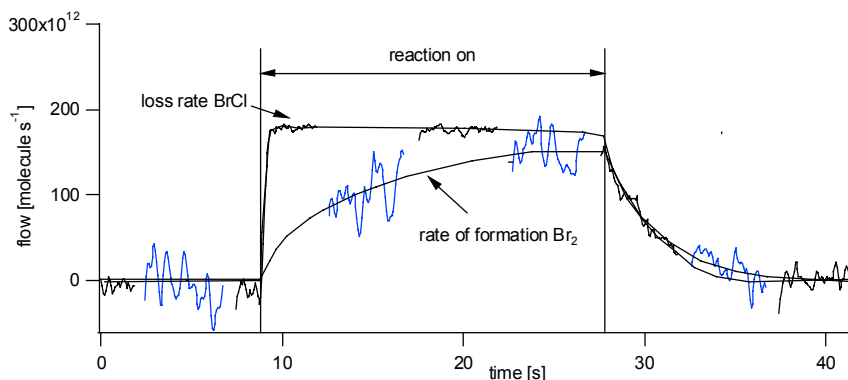
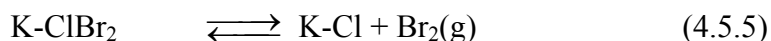
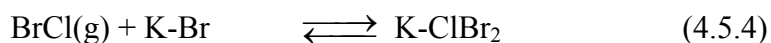


Figure 4.5.1: Uptake experiment of BrCl on KBr grains. The experiment has been carried out in the 4mm-orifice reactor. The graphs show the rate of loss of BrCl and the rate of formation of Br₂. BrCl and Br₂ are monitored at $m/e = 116$ and $m/e = 160$, respectively.

Bromine chloride is highly soluble in H₂O(l). The solubility of BrCl is 108g in 1l of H₂O(l) at T = 298K (47). The order of gas solubility of the studied halogens in H₂O(l) at T = 298K is:



The fact, that Br₂ appears delayed in the gas-phase and the high solubility of BrCl may confirm a proposed two step mechanism (29).



In order to investigate the role of the high solubility of BrCl in H₂O(l) additional uptake experiments as a function of adsorbed H₂O(a) should be performed.

4.6. Uptake Experiments of Cl₂O on KBr

4.6.1. Introduction

Dichloromonoxid or hypochlorous anhydride Cl₂O has not been detected in the atmosphere, but Cl₂O is an inevitable contamination of HOCl. In order to complete the studies on HOCl interaction with KBr the reaction of Cl₂O with KBr has been studied.

4.6.2. Results and Discussion

Steady-state and pulsed valve experiments on commercially available KBr grains have been carried out in both the 4 and 14mm-orifice reactor. Experimental conditions and main results are summarised in tables 4.6.2 and 4.6.3 attached at the end of this section.

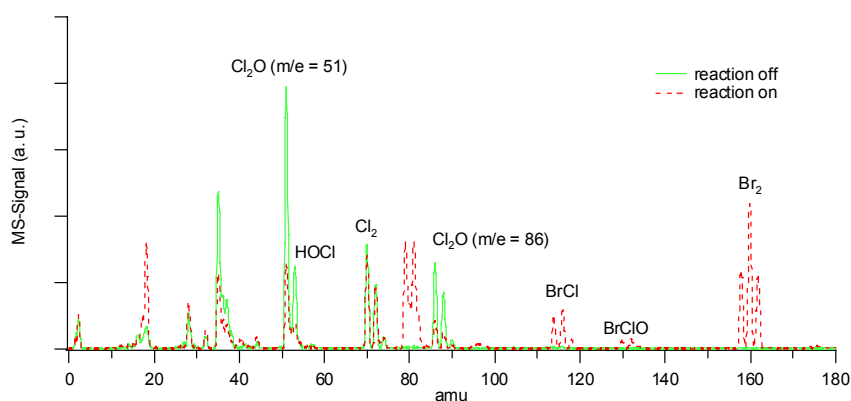


Figure 4.6.1: Mass spectrometric scan of the reaction Cl₂O on KBr grains carried out in the 4mm-orifice reactor. The base peak of Cl₂O is at m/e = 51. Br₂ and BrCl are the main products observed at m/e = 160 and m/e = 116/114, respectively. Furthermore, a slow production of BrOCl at m/e = 132 is observed.

Figure 4.6.1 shows a comparison of a mass-spectrometric scan in the presence and the absence of KBr grains. The detected main products are Br₂ and BrCl. In addition, a slow production of BrOCl has also been observed. Figure 4.6.2 shows a typical uptake experiment carried out in the 14mm-orifice reactor on a fresh thin KBr film sprayed onto a Pyrex substrate. The experimental data are listed in table 4.6.2, experiment 2. The rate of formation

of Br_2 decreases with time, whereas the formation of BrCl is delayed. Figure 4.6.3 shows MS-data on the loss of Cl_2O and the formation of Br_2 and BrCl as a function of time. It may be seen in figure 4.6.3 that after lifting the plunger the loss rate of Cl_2O corresponds to the rate of Br_2 formation, however, the agreement between the loss rate of Cl_2O and the rate of formation of Br_2 decreases and the rate of formation of BrCl increases with time.

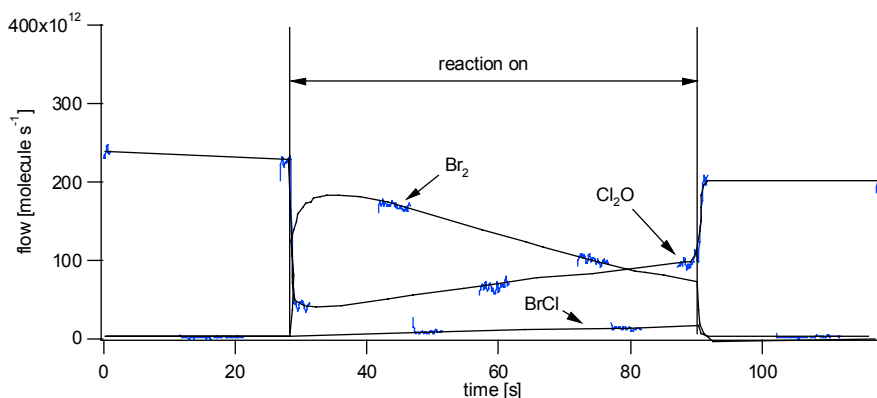


Figure 4.6.2: Typical steady-state uptake experiment of Cl_2O on a thin film of KBr sprayed onto a Pyrex substrate performed in the 14mm-orifice reactor. Cl_2O , BrCl and Br_2 are monitored at $m/e = 51$, $m/e = 114$ and $m/e = 160$, respectively.

On a fresh KBr film sprayed onto a Pyrex substrate a steady-state experiment has been carried out in the 4mm-orifice reactor (Table 4.6.2, Experiment 3). After the start of the experiment a Br_2 production rate of $5 \cdot 10^{14}$ molecule s^{-1} has been observed. As shown in figures 4.6.2 and 4.6.3 the production rate of Br_2 is slowly decreasing whereas the production rate of BrCl is increasing with time. The uptake of Cl_2O decreases towards a steady-state

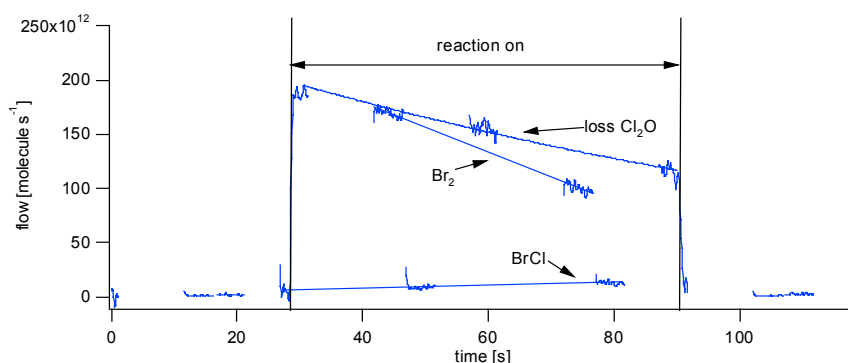
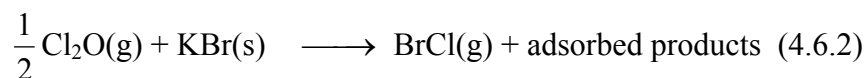
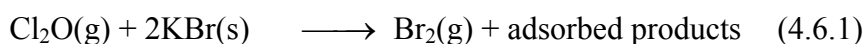


Figure 4.6.3: Loss rate of Cl_2O , rate of formation of Br_2 and BrCl . The uptake experiment has been carried out in the 14mm-orifice reactor on a thin KBr film sprayed onto a Pyrex substrate. The Cl_2O inflow is $F_{\text{in}} = 2.4 \cdot 10^{14}$ molecule s^{-1} .

uptake. In order to carry out a mass balance the amount of Br_2 produced in the reaction of the impurity Cl_2 corresponding to the net reaction of reactions 4.3.11-14 has been subtracted from the total amount of the formed Br_2 . The mass balance following the overall reaction-scheme 4.6.1 and 4.6.2 results in a deficiency of reaction products, which leads us to the suggestion of surface contamination as we have already seen in the previous sections. As proposed in section 4.3 the surface-contamination may be due to retained polyhalide intermediate species (38).



In order to check the sample for adsorbed Cl_2O the inflow of Cl_2O has been stopped after carrying out the experiment leaving the plunger in the upper position. The decay of the MS-signal with the plunger in the upper position has been identical with the decay leaving the plunger in the closed position. This means that, in contrast to Cl_2 and Br_2 , Cl_2O does not stick to the surface of the sample.

In order to investigate surface contamination subsequent uptake experiments have been carried out on the same substrate (Table 6.1.2, Experiment 3b). Figure 4.6.4 shows the production rate of Br_2 of subsequent uptake experiments performed on the same KBr grain sample. With the number of Cl_2O uptake experiments Br_2 shows a more pronounced peak after lifting the plunger, but saturates faster. A similar behaviour, however, less pronounced, has been observed for the BrCl production rate. Figure 4.6.5 shows the rate of formation of BrCl of a virgin and of a contaminated KBr substrate.

These observations confirm our suggestion of surface poisoning by chlorine and bromine species that we have already shown for Cl_2 and Br_2 in the previous sections. Furthermore, it suggests that, similar to the case of Cl_2 (Figures 4.3.7 and 4.3.9), surface reactions between adsorbed species occur even in the absence of gaseous Cl_2O .

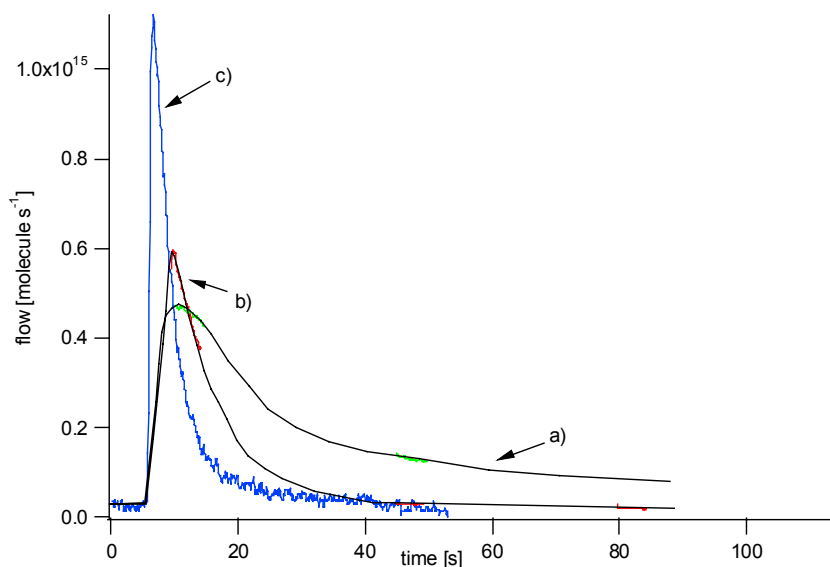


Figure 4.6.4: Steady-state Cl_2O uptake experiment on KBr grains carried out in the 4mm-orifice reactor. The graphs display the production rate of Br_2 of subsequent uptake experiments: a) 1. uptake, b) 2. uptake, and c) 6. uptake experiment.

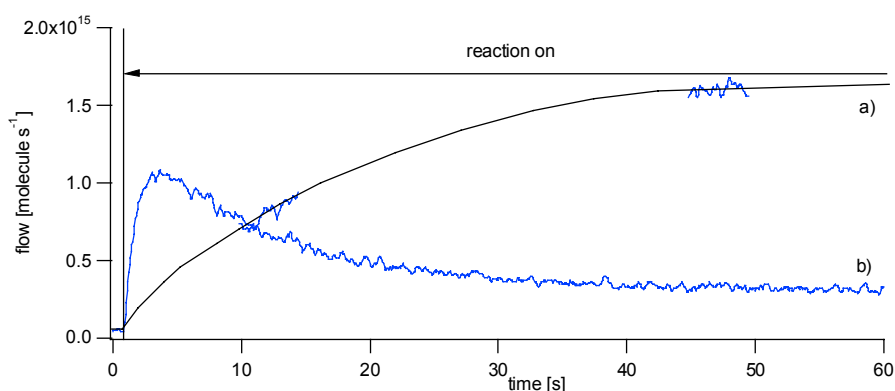
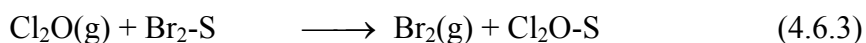


Figure 4.6.5: Steady-state Cl_2O uptake experiment on KBr grains carried out in the 4mm-orifice reactor. The graphs display the production rate of BrCl of subsequent uptake experiments: a) 1. uptake, and b) 7. uptake.

After several uptake experiments on contaminated KBr grains a slow production of HOCl and Cl_2 has been observed. The burst of Br_2 on a contaminated sample such as displayed in figure 4.6.4 may be explained by the displacement of surface adsorbed bromine species by chlorine species as we have seen in the uptake experiments with Cl_2 in section 4.3, Reaction 4.3.9. The overall reaction may be expressed in reaction 4.6.3.



The formation of HOCl stems from the reaction with adsorbed $\text{H}_2\text{O}(\text{a})$:

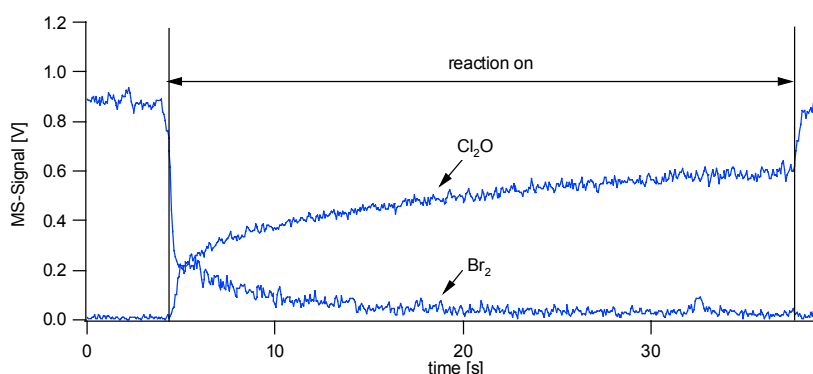


Figure 4.6.6: mass-spectrometric signal of an uptake experiment carried out on a thin KBr film sprayed on a gold-coated copper substrate in the 14mm-orifice reactor. Cl_2O and Br_2 have been monitored at $m/e = 51$ and $m/e = 160$, respectively.

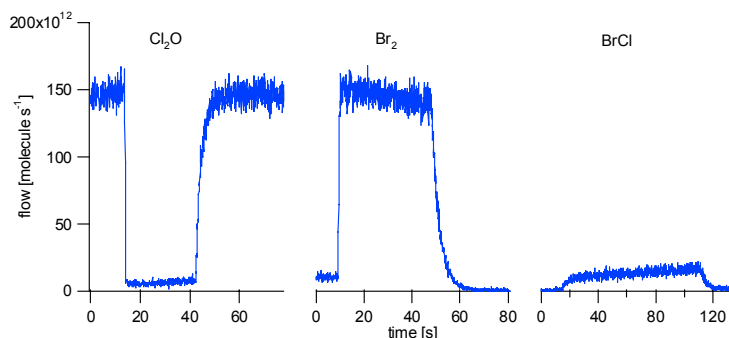


Figure 4.6.7: Uptake experiment of Cl_2O on a thin KBr film sprayed on a gold-coated copper substrate carried out in the 4mm-orifice reactor. The MS-data show the flows of Cl_2O , Br_2 and BrCl of three subsequent uptake experiments.

In order to study the influence of adsorbed $\text{H}_2\text{O}(\text{a})$ uptake experiments of Cl_2O on a thin film of KBr sprayed on a gold-coated copper substrate have been performed. The experiments have been carried out in the 14mm-orifice reactor. The experimental conditions are listed in table 4.6.2, experiment 4a. Figure 4.6.6 displays the mass-spectrometric signals of Cl_2O and Br_2 leading to an initial uptake coefficient of $\gamma_0 = 0.18$. In contrast to the uptake experiment

on a thin KBr film sprayed on a Pyrex substrate (Figure 4.6.2) the rate of Br₂ formation tends to zero after an exposure-time of 20s, or so. Because smaller amounts of H₂O(a) are adsorbed on a KBr sample sprayed on a gold-coated substrate than on a sample sprayed on a Pyrex substrate may suggest that the reaction of Cl₂O on KBr may depend on the amount of adsorbed H₂O(a). In order to check this suggestion the sample has been exposed for several minutes to ambient conditions (~6Torr of H₂O(g)) after carrying out the experiment and subsequently pumped for 1 minute after introducing it into the reactor. Figure 4.6.7 shows the calibrated MS-data of the flows of Cl₂O, Br₂ and BrCl of such an experiment.

In contrast to the uptake of Cl₂ the exposure to H₂O(g) does not only influence the release of Br₂ but also changes the kinetics of the reaction dramatically. As the solubility of Cl₂O is extremely high (1477g per l H₂O(l) (22)) we conclude that the hydrolysis reaction 4.6.4 plays a key role in the reaction kinetics of Cl₂O with KBr. Nevertheless, the immediate release of Br₂ after lifting the plunger may be another indication of the displacement of surface adsorbed bromine by chlorine as indicated in reaction 4.6.3.

Furthermore, the reaction of Cl₂O on thin KBr films sprayed on a gold-plated copper substrate brings to light the formation of HOBr and BrOCl.

This may be explained by adsorbed molecular bromine on this type of surface postulated in section 4.6.1.



Reaction 4.6.5 explains the formation of BrOCl and



the reaction sequence 4.4.6 and 4.6.7 is responsible for the formation of HOBr.

In order to study virgin KBr surfaces pulsed valve experiments on thin KBr films have been carried out. Small amounts of Cl₂O (with its impurities) have been injected into the reactor in order to contaminate the substrate as little as possible (Table 4.6.3, Experiment 1). Figure 4.6.8 shows the mass-spectrometric signals of a typical pulsed valve experiment. The loss of

Cl_2O has been determined by integration of the difference of the reaction and reference pulses over time and is of the order of $4.8 \cdot 10^{14}$ molecule pulse⁻¹. The total loss of Cl_2 and Cl_2O is of the order of $5.6 \cdot 10^{14}$ molecule pulse⁻¹ which corresponds to 5% of a monolayer of KBr assuming that one monolayer corresponds to $1.1 \cdot 10^{16}$ molecule for the total sample surface (calculated using equation 3.2.5). The small perturbation of the surface allows us to measure the uptake coefficient of an almost unmodified KBr substrate. The resulting uptake coefficient is $\gamma = 7 \cdot 10^{-2}$. The mass balance according to reactions 4.6.1 and 4.6.2 is not satisfied (Table 4.6.1) similar to the case for steady-state experiments carried out on a thin KBr film sprayed on a Pyrex substrate presented in figure 4.6.6.

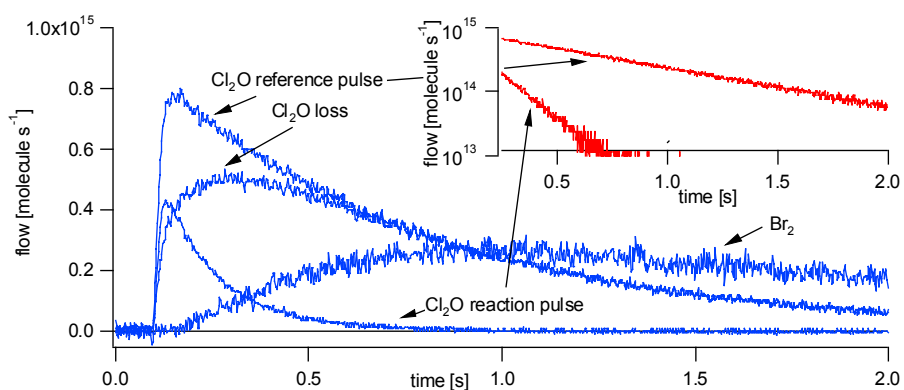


Figure 4.6.8: Pulsed valve experiment on a thin KBr film sprayed on a Pyrex substrate carried out in the 8mm-orifice reactor. The loss of Cl_2O is the difference between the reference and the reaction pulses. Cl_2O and Br_2 are monitored at $m/e = 51$ and $m/e = 160$, respectively.

Table 4.6.1: Mass balance of a pulsed valve experiment carried out in the 8mm-orifice reactor on a thin KBr film sprayed on a gold-coated copper substrate. k_{esc} and k_{dec} corresponds to the decay constant of the MS-signal of the reference and the reaction pulse, respectively.

	dose [10^{14} molecule]	loss [10^{14} molecule]	yield [10^{14} molecule]	yield – loss [10^{14} molecule]	$k_{\text{esc}}/k_{\text{dec}}$ [s^{-1}]
Cl_2O	5.5	4.8			1.4/6.5
Cl_2	1.3	0.7			1.5/3.7
Br_2			5.0		
total	6.8	5.5	5.0	-0.5	

Chapter 4

During this experiment very small amounts of BrCl but neither BrOCl nor HOBr have been observed. So reactions which are not leading to Br₂ may be neglected and the exponential character of the signals (Figure 4.6.8) corresponds to a first order rate loss for the reaction.

$$\dot{N}_1 = -k_{\text{esc}}(\text{Cl}_2\text{O})N_1 - \underbrace{k_r N_1}_{F_r} \quad (\text{equation 4.6.1})$$

$$\Rightarrow F_r = k_r N_1(t=0) e^{-(k_{\text{esc}}+k_r)t} \quad (\text{equation 4.6.2})$$

$$F_r(t=0) := k_r N_1(t=0)$$

$$k_r = k_{\text{dec}} - k_{\text{esc}} \quad (\text{equation 4.6.3})$$

where N_1 is the number of Cl₂O molecules in the reactor, k_r the rate constant and F_r the reactive flow of Cl₂O.

Assuming that Br₂ has no residence time on the surface the Br₂ flow may be calculated:

$$\dot{N}_2 = \underbrace{-k_{\text{esc}}(\text{Br}_2)N_2}_{F_{\text{out}}} + F_f \quad (\text{equation 4.6.4})$$

with

$$F_f = F_r \quad (\text{equation 4.6.5})$$

Where N_2 is the number of Br₂ molecules in the cell and F_f the Br₂ formation flow. Solving equation 4.6.4 with the initial condition $N_2(t=0) = 0$ leads to

$$N_2 = \frac{F_f}{k_{\text{esc}}(\text{Br}_2) - k_{\text{esc}}(\text{Cl}_2\text{O}) - k_r} \left(e^{-(k_{\text{esc}}(\text{Cl}_2\text{O}) + k_r)t} - e^{-k_{\text{esc}}(\text{Br}_2)t} \right) \quad (\text{equation 4.6.6})$$

introducing equation 4.6.6 into 4.6.4:

$$F_{\text{out}} = k_{\text{esc}}(\text{Br}_2) N_2 \quad (\text{equation 4.6.7})$$

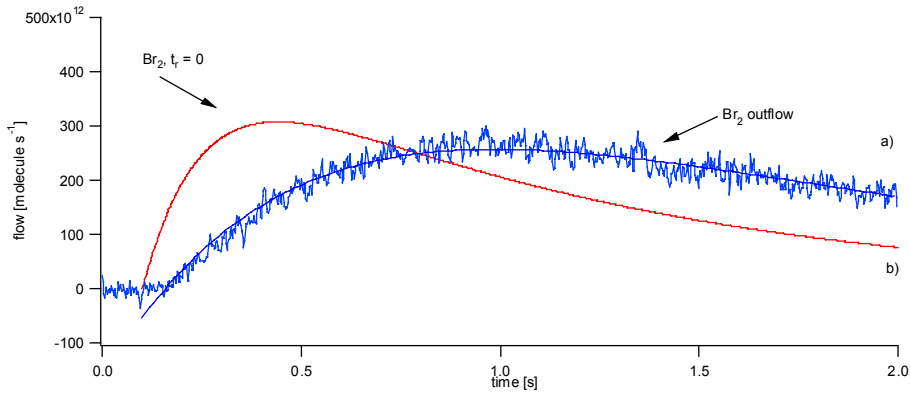


Figure 4.6.9: Br₂ rate of formation of an uptake experiment of Cl₂O on a thin KBr film sprayed on a gold-coated substrate. a) displays the calculated Br₂ outflow F_{out} assuming that the surface residence time t_r of bromine is zero.

$$F_{out} = \frac{k_{esc}(Br_2)F_f}{k_{esc}(Br_2) - k_{esc}(Cl_2O) - k_r} \left(e^{-(k_{esc}(Cl_2O) + k_r)t} - e^{-k_{esc}(Br_2)t} \right)$$

b) shows the measured outflow of Br₂.

Figure 4.6.9 shows the calculated and the measured Br₂ outflow. The Br₂ outflow has been calculated assuming that the surface residence time t_r of Br₂ is zero. The initial condition and constants are:

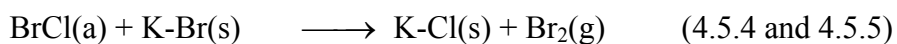
$$N_1(t = 0) = 5.5 \cdot 10^{14} \text{ molecule (Table 4.6.1 and equation 4.6.3)}$$

$$k_r = 5.1 \text{ s}^{-1} \quad (\text{Table 4.6.1})$$

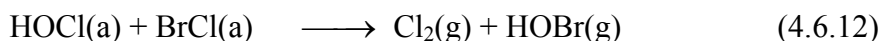
$$k_{esc}(Br_2) = 0.1 \text{ (determined by experiment)}$$

As expected, the comparison of the calculated with the measured Br₂ outflow shows a delay in the formation of Br₂. This means that the surface reactions are the limiting factor of the reaction rates for the formation of Br₂. As we have discussed in section 6.5 Br₂ possesses a surface residence time τ_s . The delay of the formation of Br₂ may be due partly to the surface residence time τ_s and partly due to the formation of Br₂ on the surface.

Similar to our discussion above the reaction of Cl_2O with $\text{H}_2\text{O}(\text{a})$ (Reaction 4.6.6) plays a crucial role and we propose the following overall mechanism:



The formation of Cl_2 and HOCl on a contaminated sample may be explained by an accumulation of KOCl on the surface.



4.6.3. Conclusions

The reaction of Cl_2O on different KBr substrates has been studied in a low-pressure flow reactor. The observed main reaction products are Br_2 and BrCl . Furthermore, slow production of HOCl , BrOCl and Cl_2 have also been detected. The mass balance has resulted in a deficiency for Br_2 compared to the loss of Cl_2O and Cl_2 . This led us to the conclusion of surface-contamination by polyhalogen species.

Subsequent uptake experiments on the same sample has shown that Br_2 effuses faster on a contaminated sample. We postulated a displacement of surface adsorbed bromine by chlorine species. The fact that Cl_2O is highly soluble in $\text{H}_2\text{O}(\text{l})$ and the strong influence of adsorbed $\text{H}_2\text{O}(\text{a})$ on the reaction kinetics suggests that the hydrolysis of Cl_2O plays a key role in this reaction. This has been confirmed by the fact that adsorbed Cl_2O does not - in contrast to Br_2 and Cl_2 - return to the gas-phase because the reaction rate is much larger than the desorption rate.

Chapter 4

The formation of BrOCl has been explained by the reaction of Cl₂O with adsorbed molecular bromine, which has been postulated in section 4.6.1.

Pulsed valve experiments have shown a delay of Br₂ formation. A comparison with the calculated formation of Br₂ assuming no residence time has shown a fairly high delay of bromine formation. This implies that the rate of formation of Br₂ is controlled by surface reactions.

4.6.4. TablesTable 4.6.2: Typical experimental conditions for Cl₂O uptake experiments on KBr grains and thin films of KBr sprayed on a Pyrex substrate and main results

No	Orifice diameter [mm]	[Cl ₂ O] [molecule cm ³]	Experimental conditions	Substrate	Main products	Minor products	Uptake kinetics	Remarks
1	4		Mass scan	g	Br ₂ , BrCl	BrOCl		
2	14	3*10 ¹⁰	First uptake	p	Br ₂	BrCl	0.27	Br ₂ production decreases, BrCl production delayed
3a	4	8*10 ¹²	First uptake on sample after carrying out a mass spectrometric scan	g	Br ₂ , BrCl		$\gamma_0 = 2*10^{-2}$ $\gamma_{ss} = 7*10^{-3}$	Br ₂ production decreases, BrCl production delayed Br ₂ production rate: 4.5*10 ¹⁵ molecule s ⁻¹
3b	4	8*10 ¹²	Subsequent uptake on contaminated substrate	g	Br ₂ , BrCl	HOCl Cl ₂	$\gamma_0 = 2*10^{-2}$ $\gamma_{ss} = 6*10^{-3}$	Burst of Br ₂ , no delay in BrCl production, slow production of Cl ₂
4a	14	6*10 ¹⁰	Subsequent uptake experiment	Au	Br ₂	BrCl, BrOCl HOBr	$\gamma_0 = 0.2$	Br ₂ production decreases, BrCl production decreases, slow production of BrCl and HOBr.
4b	4	2*10 ¹²	Subsequent uptake experiments on sample exposed to H ₂ O	Au	Br ₂	BrCl	$\gamma_0 = 8*10^{-2}$	Production of Br ₂ immediately after lifting the plunger. BrCl production delayed.

g : KBr grains, p : thin KBr film sprayed on a Pyrex substrate, Au : thin KBr film sprayed on a gold-coated copper substrate

Table 4.6.3: Typical experimental conditions for Cl₂O pulsed-valve experiments on thin KBr film sprayed on a Pyrex substrate

No	Orifice diameter [mm]	Cl ₂ O dose [molecule]	Experimental conditions	Main products	Minor products	Uptake kinetics	Remarks
1a	8	$5.5 \cdot 10^{14}$	Pulsed valve experiment on fresh sample, $t_0 = 10\text{ms}$	Br ₂	BrCl	$\gamma_0 = 7 \cdot 10^{-2}$	Mass balance satisfied, Br ₂ production delayed, loss Cl ₂ O = $4.8 \cdot 10^{14}$ molecule/pulse

4.7. Uptake Experiments of HOCl on KBr

4.7.1. Introduction

Hypochlorous acid HOCl is a photochemically active compound. In the presence of light HOCl decays into active Cl and OH radicals. Both of them contribute to the oxidation capacity of the atmosphere (Section 1.2 and 1.3) (48, 49).



Model studies of the troposphere predict a HOCl concentration of up to 35ppt (28). However, until now the tropospheric concentration of HOCl has not been confirmed by field measurements.

HOCl may be formed via the reaction of peroxy radicals with ClO (50):



or by the heterogeneous reaction



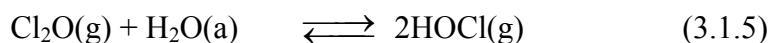
Potential sinks of HOCl in addition to reaction 4.7.1 may be heterogeneous reactions on aerosols, e.g. reactions on salt particles.

Especially the reaction of HOCl with bromine-containing sea salt aerosols may be a possible source of photochemically active bromine-containing compounds such as Br₂ and HOBr. Those compounds play an important role in the destruction of tropospheric ozone O₃. The catalytic destruction cycles of O₃ are described in section 1.3.

In this chapter a laboratory study of the reaction of HOCl on solid KBr salt is presented. Knudsen flow reactor experiments of the HOCl interaction with different KBr salt substrates such as grains, ground grains, thin films deposited on Pyrex and gold-plated metal substrates have been performed at ambient temperature. As we already pointed out in section 4.6.1 it has been established in numerous studies that surface adsorbed water plays an important role

in ion-exchange reactions at the surface (7). Strongly bound surface-adsorbed water is persistent even after heating the surface under vacuum. Surface-adsorbed $\text{H}_2\text{O}(\text{a})$ may lead to the regeneration of reactive sites on the substrate and induces a crystallisation of the non-volatile reaction products on the solid NaCl for the reaction of HNO_3 and NaCl (6, 31). In order to vary the amount of $\text{H}_2\text{O}(\text{a})$ adsorbed on the salt samples they have either been pumped for different time periods t_p at ambient temperature or heated under vacuum. In addition, different sample supports for solid KBr such as Pyrex or gold-plated supports have been used. Pyrex supports contain large amounts of adsorbed $\text{H}_2\text{O}(\text{a})$. In order to minimise its amount gold-coated supports have been used.

HOCl and Cl_2O are inextricably related to each other in equilibrium according to reaction 3.1.5.



The reaction of Cl_2O on KBr therefore may lead to the same reaction products as HOCl on KBr. This fact makes the distinction of the two reactions experimentally more difficult. Before carrying out an experiment using HOCl it has always been distilled at low temperature until the highest ratio $[\text{HOCl}]/[\text{Cl}_2\text{O}]$ measured at $m/e = 52$ and $m/e = 51$, respectively, has been obtained at a given temperature of typically $203\text{K} < T < 213\text{K}$. The desired flow rate of HOCl has been obtained by changing the corresponding temperature of the HOCl reservoir.

In order to avoid HOCl decomposition a 6mm-diameter Teflon tube and differential pumping have been applied instead of the capillary inlet. However, the differential pumping has prevented the use of pulsed valve experiments owing to too small stagnant pressure in the fore-line. Even a small increase of the pressure at the reactor inlet by decreasing the differential pumping resulted in enhanced decomposition of HOCl toward Cl_2O . The 6mm-diameter Teflon tubes have been kept as short as possible in order to obtain the best $[\text{HOCl}]/[\text{Cl}_2\text{O}]$ ratio. In spite of the differential pumping and the Teflon coat of the Pyrex vessel decomposition of HOCl within the 6mm-diameter inlet tube to the Knudsen flow reactor could not be completely avoided. A change of temperature of the HOCl reservoir not only modifies the inlet flow rate but also affects the ratio $[\text{HOCl}]/[\text{Cl}_2\text{O}]$ as expected from the chemical equilibrium 3.1.5.

4.7.2. Results and Discussion

For the uptake experiments the HOCl concentrations in the flow-reactor have been in the range 10^{10} to $5 \cdot 10^{12}$ and $2 \cdot 10^{11}$ to $1 \cdot 10^{14}$ molecule cm^{-3} in the 14 and 4mm-orifice reactor, respectively. Tables 4.7.1, 4.7.2, 4.7.3 and 4.7.4 show the experimental conditions and the summarised main results of the uptake experiment on grains, ground grains, thin sprayed films on Pyrex and thin films sprayed on a gold-plated substrate, respectively. The tables are attached at the end of this section.

In order to investigate the decomposition of HOCl on polar salt surfaces reference experiments on unreactive NaNO_3 salt grains have been performed. However, no decomposition of HOCl on NaNO_3 samples has been observed under our experimental conditions.

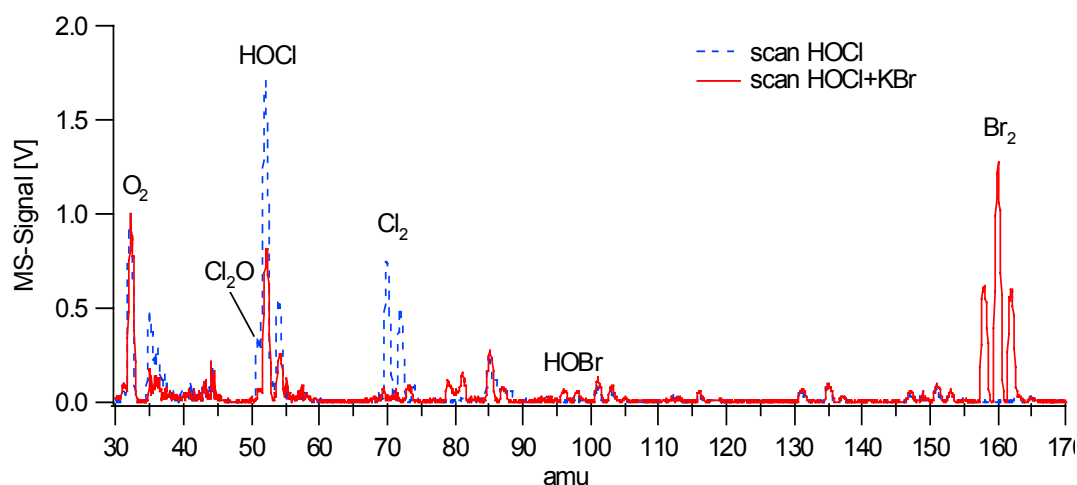


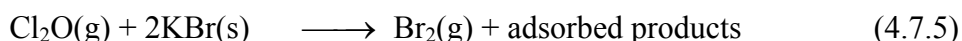
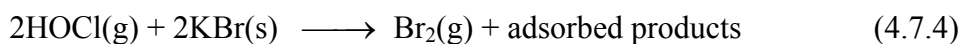
Figure 4.7.1: MS-scan of the reaction of HOCl on KBr grains. The signal is normalised with respect to the O_2 signal. HOCl is attributed to $m/e = 52$ and the contaminants Cl_2 and Cl_2O may be seen at $m/e = 70$ and $m/e = 51$ and 86 , respectively. Br_2 is the main product observed at $m/e = 160$. A slow production of HOBr is also observed at $m/e = 96/98$.

Figure 4.7.1 shows a typical mass spectrum of the HOCl flow out of the 4mm-orifice reactor in the absence and presence of KBr grains. The comparison of the two mass spectra reveals the main observed reaction products, namely Br_2 and small quantities of HOBr. Furthermore,

uptake of Cl_2O and Cl_2 has also been observed as indicated by the decrease of the corresponding MS-signals upon exposure of the KBr sample to the reactive gases.

A) Surface Activation

HOCl uptake experiments on fresh KBr grains and ground grains carried out in the 14mm-orifice reactor show a decrease of the uptake coefficient with reaction time displayed in table 4.7.1, experiment 1 and table 4.7.2, experiment 1. The mass balance according to reaction 4.7.4 and 4.7.5 is satisfied under those experimental conditions.



Subsequent uptake experiments in the 14mm-orifice reactor on the same sample lead to a smaller initial uptake coefficient γ_0 . However, HOCl uptake experiments carried out in the 14mm-orifice reactor under the same conditions on a sample previously exposed to HOCl in the 4mm-orifice reactor (Table 4.7.2, Experiment 1b) show a higher initial rate of uptake owing to surface poisoning of the substrate (Table 4.7.2, Experiments 1a and 1c). Figure 4.7.2 shows the MS-signal of a typical HOCl uptake experiment on a poisoned substrate taking place in the 14mm-orifice reactor.

On a sample of 1g of KBr grains pumped over one day having initially an estimated amount of $1 \cdot 10^{18}$ molecules of adsorbed $\text{H}_2\text{O}(\text{a})$ (Figure 4.1.7) no measurable uptake of HOCl has been observed on a virgin KBr substrate. Uptake experiments on fresh thin KBr films sprayed on a Pyrex support did not lead to uptake, either (Table 4.7.3, Experiment 1a).

Nevertheless, the mass balance between the loss of Cl_2O and the yield of Br_2 according to reaction 4.7.5 is satisfied under those conditions. The HOCl uptake experiment carried out in the 14mm-orifice reactor on a thin KBr film sprayed on a gold-plated copper substrate led to saturation of the surface within several seconds. The reaction results in a burst of Br_2 and some HOBr has been observed (Table 4.7.4, Experiment 1a). Figure 4.7.3 shows the loss rates of HOCl and Cl_2O and the rates of formation of Br_2 and HOBr of a typical uptake experiment performed under those conditions.

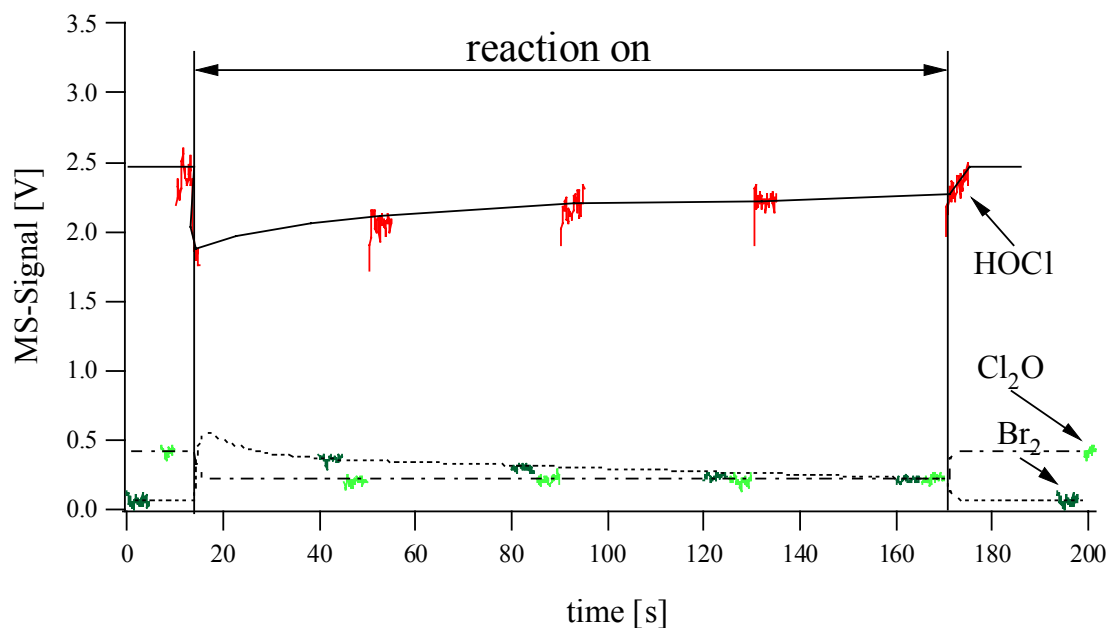


Figure 4.7.2: Typical MS-signals of the reaction HOCl on KBr grains with Cl_2O being present as an impurity. The experiment has been carried out in the 14mm reactor on an already exposed KBr sample. Br_2 has been observed as a reaction product. Cl_2O has been monitored at $m/e = 51$, HOCl at $m/e = 52$ and Br_2 at $m/e = 160$.

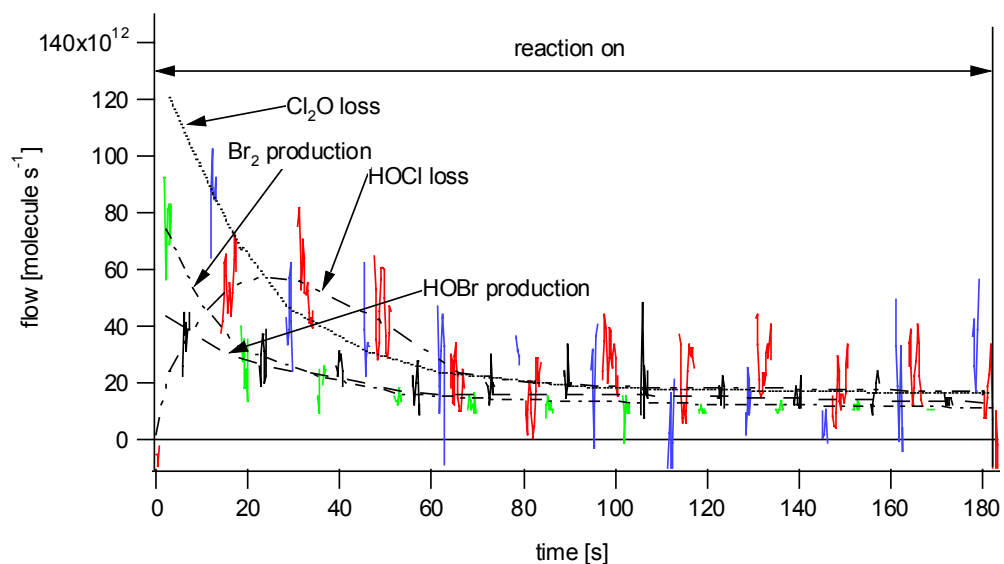


Figure 4.7.3: Uptake experiment on a thin salt film sprayed on a gold-plated support carried out in the 14mm-orifice reactor. Cl_2O has been monitored at $m/e = 51$, HOCl at $m/e = 52$, HOBr at $m/e = 96$ and Br_2 at $m/e = 160$.

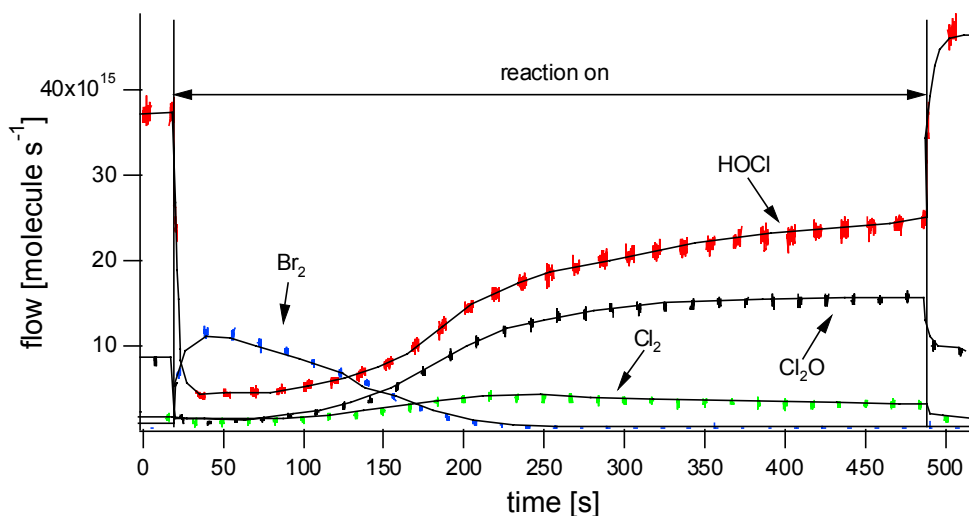


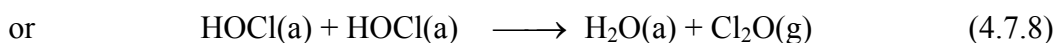
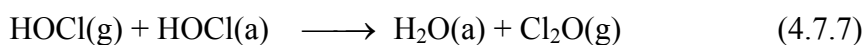
Figure 4.7.4: Uptake experiment in the 4mm-orifice reactor on KBr grains. Cl_2O has been monitored at $m/e = 51$, HOCl at $m/e = 52$, Cl_2 at $m/e = 70$ and Br_2 at $m/e = 160$.

In order to study the observed saturation and surface contamination effects, further uptake experiments on KBr grains and ground grains at higher HOCl concentrations have been performed in the 4mm-orifice reactor (Tables 4.7.1 and 4.7.2, Experiment 2). Figure 4.7.4 shows the MS-signal of a typical HOCl uptake experiment at the experimental conditions described in table 4.7.1, experiment 2. The Br_2 production is delayed and vanishes after an exposure time t_e on the order of 5 minutes. The rate of formation of HOBr and BrCl is slow and tends to the background level after an exposure time t_e on the order of 6 minutes (not shown in figure 4.7.4). The Cl_2O rate of uptake decreases with time at first, but subsequently exceeds the initial level after 180s resulting in net formation towards the end of the uptake experiment.

The formation of Cl_2O may be explained by the net reaction 4.7.6:



Since gas-phase reactions between two closed shell molecules are unlikely to occur in a Knudsen reactor, reaction 4.7.6 is thought to proceed in a heterogeneous manner as follows, where (g) and (a) correspond to the gas or adsorbed phase of HOCl:



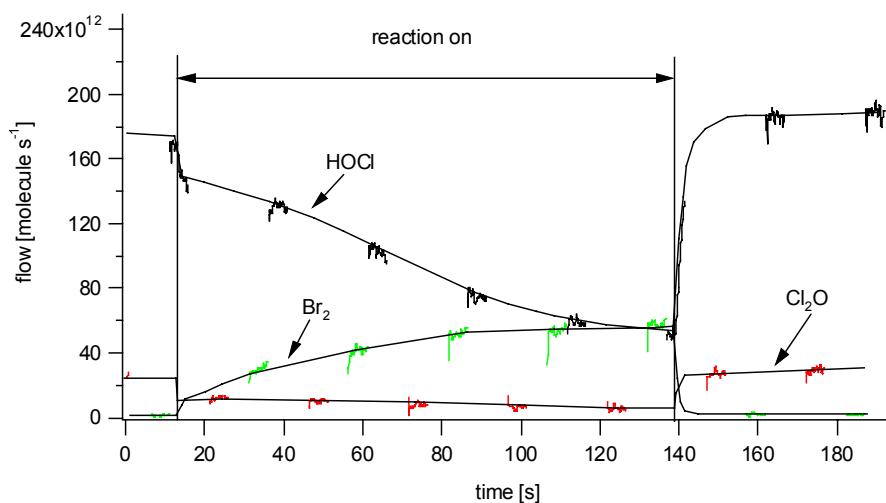


Figure 4.7.5: Steady-state uptake experiment on ground KBr grains carried out in the 4mm reactor. HOCl has been monitored at $m/e = 52$, Cl_2O at $m/e = 51$ and Br_2 at $m/e = 160$ (Br_2). The inflow of HOCl is $F_{\text{in}} = 1.8 \cdot 10^{14}$ molecule s^{-1} .

Surface contamination may occur owing to adsorbed HOCl(a). Uptake experiments in the 4mm-orifice reactor on virgin KBr samples such as ground grains and sprayed thin films show an increase of the HOCl rate of uptake after lifting the plunger (Figures 4.7.5 and 4.7.6). This is very unusual behaviour for molecular uptake on a solid surface and appears like an autocatalytic process which will be discussed in the following.

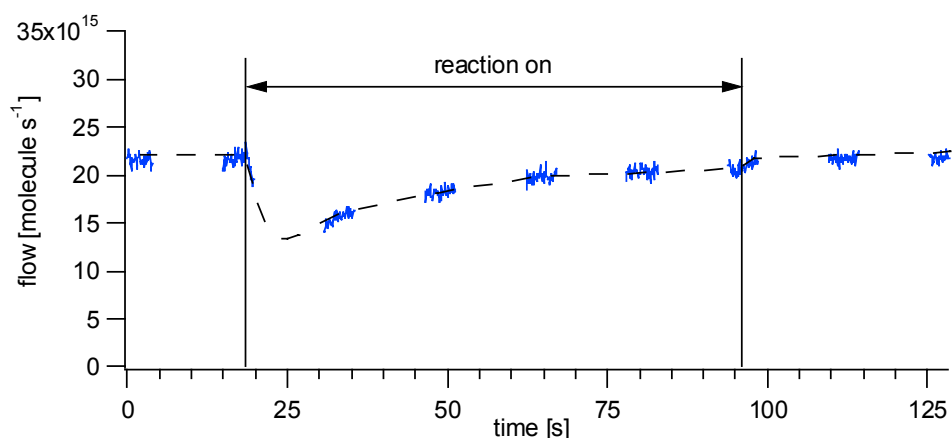


Figure 4.7.6: Typical steady-state uptake experiment of HOCl on a thin KBr film sprayed on a Pyrex substrate carried out in the 4mm reactor. HOCl has been monitored at $m = 52$. The dashed line indicates that the reaction is starting slowly after lifting the plunger.

In order to study the surface contamination which is probably due to adsorbed bromine species HOCl uptake experiments with an additional Br₂ flow have been performed on grains and ground grains (Tables 4.7.1 and 4.7.2, Experiment 3).

In the molecular flow regime no gas-phase reaction between Br₂ and HOCl is expected. This has been confirmed in a reference experiment where no gas-phase reaction has been observed in the absence of a KBr substrate. In order to distinguish between added and net produced Br₂ the KBr substrate had been exposed to HOCl until the reaction pathways resulting in bromine species were saturated before carrying out the experiment. To remove residual bromine species from the substrate surface it has been subsequently pumped for 30 minutes before carrying out the experiment with the added Br₂ flow.

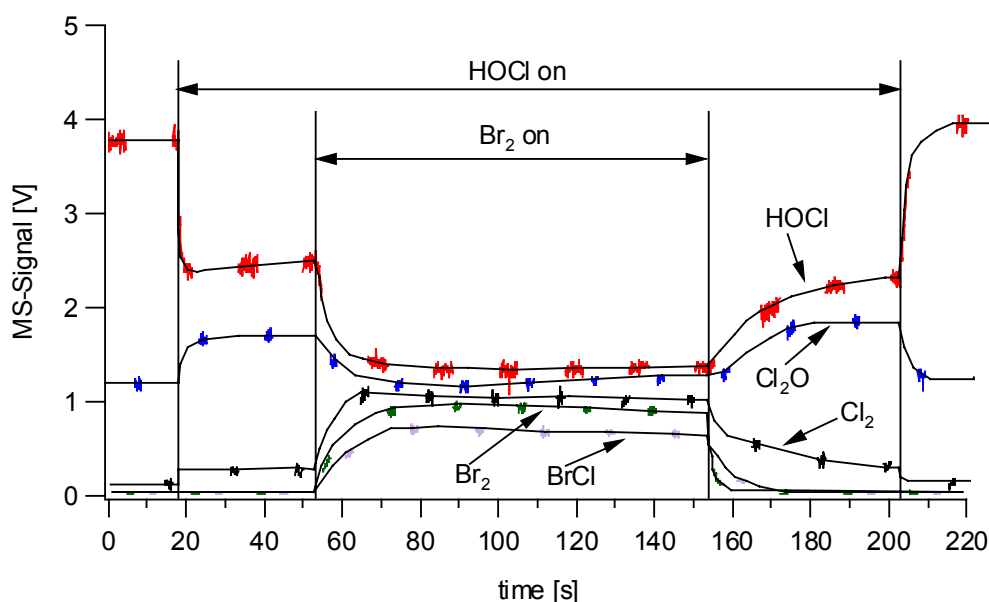


Figure 4.7.7: HOCl uptake experiment on KBr grains in the 4mm-orifice reactor. An additional Br₂ flow causes an increase of the HOCl uptake and leads to additional production of Cl₂. Cl₂O has been monitored at $m/e = 51$, HOCl at $m/e = 52$, Cl₂ at $m/e = 70$, BrCl at $m/e = 116$ and Br₂ at $m/e = 160$. The HOCl inflow is $F_{in} = 3 \cdot 10^{16}$ molecule s⁻¹.

The injection of Br₂ causes a further drop of the HOCl MS-Signal corresponding to an increase in the rate of HOCl uptake (Figure 4.7.7). Simultaneously, the concentration of Cl₂ increases and BrCl and small amounts of HOBr and Br₂O (the latter two are not shown in figure 4.7.7) have been detected. After halting the additional Br₂ flow the HOCl and Cl₂ MS-signals slowly revert to the previous levels and the HOBr and BrCl signals decrease to their background level. At higher [HOCl] and [Br₂] a correspondingly higher increase of γ_{ss} has

been observed (Tables 4.7.1 and 4.7.2, Experiment 3). Uptake coefficients in the absence and the presence of additional Br_2 are listed in tables 4.7.5 and 4.7.6.

Subsequently, the contaminated sample has only been exposed to a flow of Br_2 . An uptake of Br_2 has been observed on a contaminated KBr substrate that has previously been exposed to HOCl . On a contaminated KBr substrate γ_0 of Br_2 is on the order of $\gamma_0 = 6 \cdot 10^{-3}$ and does not depend on the amount of adsorbed $\text{H}_2\text{O}(\text{a})$. The reaction products are BrCl , Cl_2 and Cl_2O . Figure 4.7.8 shows the mass spectrometric row signals of such an experiment carried out in the 4mm-orifice reactor on KBr grains. The experimental conditions are listed in table 4.7.1, experiment 4a.

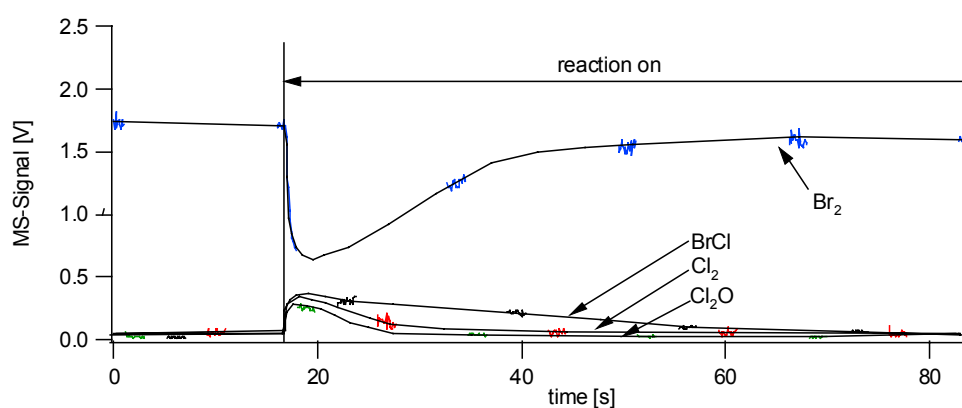


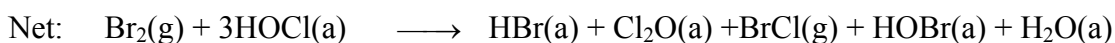
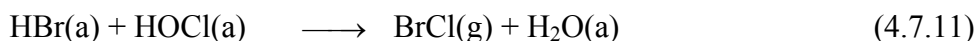
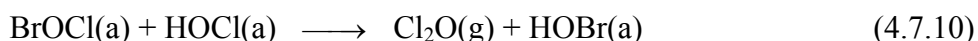
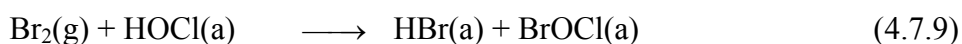
Figure 4.7.8: Steady-state uptake experiment of Br_2 on contaminated KBr grains. The experiment has been carried out in the 4mm-orifice reactor. Br_2 , BrCl , Cl_2O and Cl_2 have been monitored at $m/e = 160$, $m/e = 116$, $m/e = 51$ and $m/e = 70$, respectively.

In contrast, on fresh KBr grains no net Br_2 uptake has been observed within the sensitivity of our experiment. However, diffusion tube experiments of Br_2 on solid KBr films performed in our laboratory have revealed a significant interaction expressed as a surface residence time of Br_2 (42). Furthermore, pulsed valve Knudsen reactor experiments performed by Aguzzi et. al. (43) obtained $\gamma_0 = 3 \cdot 10^{-3}$ for Br_2 on solid thin films of KBr. However, the uptake of Br_2 on solid KBr saturated so that no major amounts of Br_2 are taken up over extended periods of time. Proof of the interaction of Br_2 with solid KBr in the presence of gaseous Br_2 has been obtained by observing substrate recrystallisation of KBr (Section 4.4).

The release of chlorine species, namely Cl_2 and Cl_2O , shows that Br_2 displaces surface adsorbed chlorine. In section 4.3 we have shown that surface adsorbed bromine species may be displaced by chlorine species on solid KBr. This suggests that both molecular chlorine and

bromine possess a potential for displacing surface adsorbed halogen species on solid KBr. The fact that the uptake of Br₂ on a contaminated KBr sample saturates after a short time may be a further hint for surface adsorbed polyhalide intermediates which may be displaced by molecular bromine.

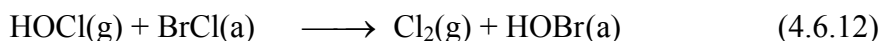
The production of Cl₂O, BrCl and the small rate of formation of HOBr may be explained by the following reaction scheme:



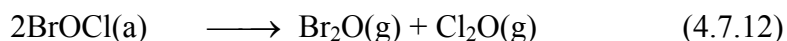
Including equilibrium 4.4.5 from section 4.5



leads to a catalytic cycle in Br₂ for the formation of Cl₂O in figure 4.7.4. Adding reaction 4.6.12 explains the formation of Cl₂ (Figure 4.7.4).



The uptake experiments of Br₂ on a contaminated sample lead to slow formation of Br₂O which may originate from the self-reaction of BrOCl:



Furthermore, a slow formation of BrOCl has been observed on KBr samples which have been heated to T = 400 K prior to carrying out the HOCl uptake experiment. Those experiments are discussed in the next section.

Those uptake experiments of Br₂ on contaminated KBr samples suggest that HOCl must be adsorbed on the substrate to a significant extent.

Finally, HOCl uptake experiments performed in the 14mm-orifice reactor on KBr substrates have not revealed any formation of HOBr and BrCl in contrast to the experiments carried out in the 4mm-orifice reactor. This may be related to the fact that the gas-phase residence time τ of Br₂ (a reaction product), hence the surface coverage, must be a factor of 10 or so higher in the 4mm-orifice reactor compared to the 14mm-orifice reactor. As we have seen above (Figure 4.7.7) the rate of uptake of HOCl as well the rate of production of Cl₂ and BrCl are strongly related to the presence of surface adsorbed Br₂.

In summary we have found:

- evidence for adsorbed HOCl(a), resulting from uptake experiments with concurrent Br₂ flow.
- evidence for adsorbed bromine species such as HOBr and HBr (with increasing and decreasing rate of uptake with time in the 4 and 14mm-orifice reactor, respectively)
- that the reaction of KBr with HOCl is strongly influenced by surface adsorbed species which act as catalysts (Figures 4.7.4 and 4.7.7).
- Autocatalytic behaviour due to adsorbed bromine and chlorine species (Reactions 4.7.9 – 4.7.11 and 4.4.5)
- Displacement of surface adsorbed chlorine by bromine at excess of Br₂ (Figure 4.7.8)
- HOCl uptake occurs through surface contaminants such as BrCl (Reaction 4.6.12) and HOCl(a) (Reaction 4.7.7)

B) Role of Adsorbed Water

In order to investigate the role of adsorbed H₂O(a) a comparison between HOCl uptake experiments on fresh KBr grains containing different amounts of adsorbed H₂O(a) have been performed in the 4mm-orifice reactor at the same concentration of HOCl. In order to determine the amount of adsorbed H₂O(a) the calibration curve of figure 4.1.7 has been used. 5g of KBr grains have been pumped for 2h, which corresponds to $2 \cdot 10^{19}$ H₂O(a) molecules

remaining on the sample before the uptake experiments have been performed. The sample pumped for 17h contained $5 \cdot 10^{18}$ $\text{H}_2\text{O}(\text{a})$ molecules. In the following we call them standard and dry grains, respectively.

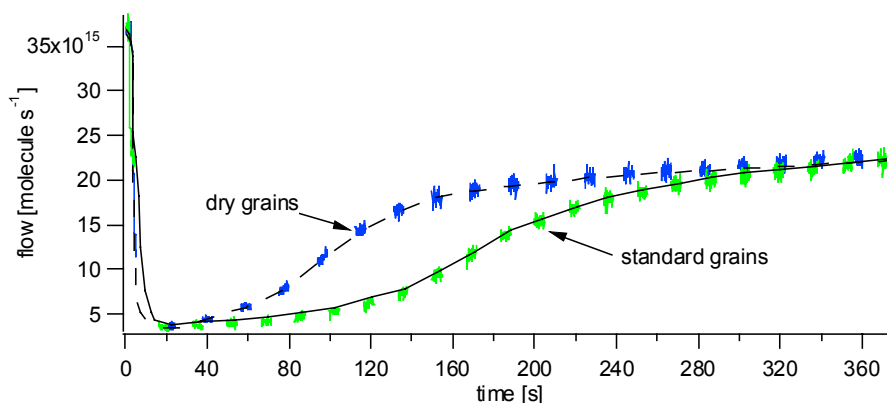


Figure 4.7.9: HOCl uptake experiment on KBr grains in the 4mm-orifice reactor at different amounts of adsorbed $\text{H}_2\text{O}(\text{a})$. The amounts of adsorbed $\text{H}_2\text{O}(\text{a})$ are $4 \cdot 10^{18}$ and $1 \cdot 10^{18}$ molecule g^{-1} on standard and dry grains, respectively.

The HOCl uptake experiments have shown no difference in γ_0 and γ_{ss} values, which means that the rate of HOCl uptake does not depend on the amount of surface adsorbed water, $\text{H}_2\text{O}(\text{a})$. Figure 4.7.9 shows the HOCl signal of the experiments carried out under the conditions described above.

However, the dryer sample saturates faster than the one with a higher amount of adsorbed $\text{H}_2\text{O}(\text{a})$. The total amount of Br_2 generated on the dry grain sample decreases by 20% compared to the standard grain sample. On the dry sample the total amount of produced HOBr and BrCl decreases by 33% or so compared to the standard grain. The total amount of released bromine, namely the sum of $2 \cdot \text{Br}_2 + \text{HOBr} + \text{BrCl}$ decreases by 25%. The measured yields and production rates are summarised in table 4.7.7. The maximum production rates of HOBr and BrCl are only weakly affected by the amount of $\text{H}_2\text{O}(\text{a})$. Figure 4.7.10 displays the rate of HOBr and BrCl formation as a function of time on a standard and dry grain sample.

We conclude that the number of reactive sites which leads to bromine release is linked to the amount of adsorbed $\text{H}_2\text{O}(\text{a})$ whereas the initial kinetics of the HOCl uptake is only weakly affected.

These results are in agreement with our surface model we have introduced in section 4.3 (Figure 4.3.9) and the suggested quasi-liquid layer (QLL) proposed by Allen et al. (6) on NaCl substrates. The QLL model means that molecules located at the surface of the sample

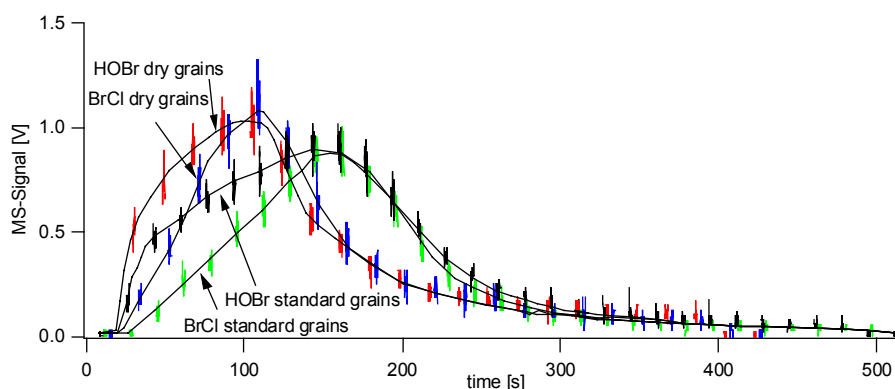


Figure 4.7.10: Rate of formation of BrCl and HOBr for HOCl uptake experiments carried out in the 4mm-orifice reactor. The experiments have been performed on standard and dried grains of KBr. The amount of $\text{H}_2\text{O}(\text{a})$ was $2 \cdot 10^{19}$ and $5 \cdot 10^{18}$ molecules, respectively.

have a higher mobility than molecules located within the bulk of the sample. Equally Beichert and Finlayson-Pitts (7) suggested that surface-adsorbed water (SAW) contained dissolved chloride- and sodium-ions from the underlying layers of the salt sample.

In the case of KBr salt samples we assume in analogy to NaCl that the surface of the substrate contains mobile K^+ - and Br^- -ions or as we have suggested in section 4.3 hydrated K-Br. Removing adsorbed $\text{H}_2\text{O}(\text{a})$ leads to dehydration of the K-Br and therefore to a change towards a better ordered surface (Figures 4.1.1 and 4.1.2). Assuming that only mobile K^+ , Br^- and hydrated K-Br may undergo an ion-exchange reaction explains that only a few molecules of the KBr bulk substrate lead to a release of gaseous bromine species such as Br_2 , BrCl and HOBr. The influence of adsorbed water, $\text{H}_2\text{O}(\text{a})$, on the number of reactive sites and the fact that only a limited number of sites undergoes a reaction be explained by reaction 4.1.1:



The existence of basic sites on KBr samples such as KOH is discussed in section 4.1. The recrystallisation of the surface upon pumping (Figure 4.1.1 and 4.1.2) may be consequence of the dehydration of the K-Br ion-pairs which is irreversible as we have seen in section 4.1. The assumption that only hydrated K-Br is available to undergo a reaction with HOCl explains the dependence of the reaction yields on the number of reactive sites or adsorbed

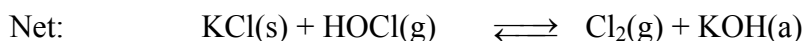
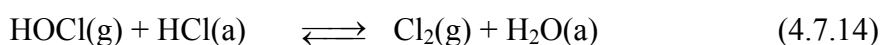
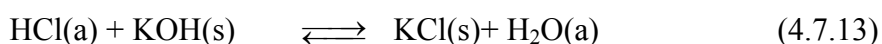
H₂O(a). Moreover, Dai (4) has shown using atomic force microscopy that hydration of surface ions weakens the ionic bond strength to the point where they become mobile, hence on a dry KBr sample the ion mobility is presumably smaller than on a standard KBr sample. Furthermore, in our experiments the amount of reactive bromine on the thin KBr film sprayed on a gold-plated substrate has been smaller compared to a KBr film on a Pyrex substrate. The yields of the corresponding formation of gaseous bromine products are listed in table 4.7.7. Measurements of adsorbed H₂O(a) on KBr films sprayed on gold-coated and Pyrex substrates have shown that films supported on a Pyrex substrate contains more adsorbed H₂O(a) than films on gold-coated substrate. This and the different yields suggests a direct link between H₂O(a) and ion mobility.

After saturation of the reaction pathway leading to the formation of Br₂, generation of Cl₂ and Cl₂O sets in (Figure 4.7.4) on the substrates we have used. Towards the end of the uptake experiment no gaseous bromine-containing species including Br₂, BrCl and HOBr have been observed. The formation of Cl₂ after saturation of all reaction pathways towards gaseous bromine species may be explained by surface adsorbed molecular bromine according to reaction 4.6.12. The formation of Cl₂O may be explained by reactions 4.7.9-4.7.11 and 4.4.5.

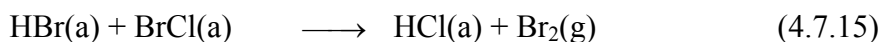
In contrast to uptake experiments of Cl₂ onto KBr (Section 4.3) no regeneration of surface sites which lead to production of bromine species were observed between two subsequent uptake experiments of HOCl on KBr. Once the reaction pathways towards formation of bromine species saturate subsequent HOCl uptake experiments on the same sample do not lead to the formation of gaseous bromine-containing compounds. In analogy to the dissociation of KBr in the presence of adsorbed H₂O(a) (Reaction 4.1.1) we suggest the following mechanism leading to gaseous Cl₂:



and in analogy



HCl(a) may be formed by the following reaction with HBr(a) generated in reaction 4.1.1 or in reactions 4.7.9 – 4.7.11:



which leads to formation of KCl at the beginning of the experiment according to reaction 4.3.1.



After the reactive KBr reservoir is used up HCl(a) accumulates at the surface by equilibrium 4.7.13 and 4.7.14 which leads to the depletion of chlorine species such as K-Cl and HCl(a) on the surface.

On sprayed thin KBr and KCl films we observed a recrystallisation after exposing the sample to an excess of molecular bromine and chlorine, respectively (Section 4.4). In order to explain that the KBr does not regenerate after an exposure to HOCl we postulate that adsorbed bromine and chlorine may be present at the surface in insufficient quantity for efficient crystallisation. We have discussed above that interfacial bromine is displaced by interfacial chlorine. The key reaction is 4.3.1. Furthermore, we proposed a depletion of chlorine at the surface of the substrate by reactions 4.7.13 and 4.7.14 which leads to a coverage of the surface by KOH.

Thermodynamically the remaining KOH does not tend to crystallise in the presence of H₂O(a), whereas a crystalline structure of KCl and KBr is thermodynamically favourable (34). The thermodynamic values are listed in table 4.7.8. We propose that a layer of KOH may be formed at the surface of the KBr substrate which isolates the underlying bromine towards a reaction with HOCl. This hypothesis is supported by the fact that we observed a regeneration of the surface for the Cl₂/KBr system (Section 4.3) owing to a crystallisation of the surface in the presence of excess of bromine and chlorine.

The initial reaction kinetics of HOCl on KBr only weakly depends on the amount of adsorbed $\text{H}_2\text{O}(\text{a})$ (Figure 4.7.9) in contrast to the reaction of Cl_2 with KBr whose rate of Cl_2 uptake is controlled by surface adsorbed $\text{H}_2\text{O}(\text{a})$ (Figure 4.3.8 and Reaction 4.3.11). Based on a fit of Cl_2 steady-state experiments on KBr substrates (Section 4.3) we suggested dissociation of Cl_2 on the surface according to reaction 4.3.11.

In order to explain that the reaction kinetics of HOCl with solid KBr only weakly depends on the amount of $\text{H}_2\text{O}(\text{a})$ we postulate that only a small concentration of Br^- may be found at the QLL/air interface (Figure 4.3.9, zone 1). This means therefore that the interactions between gas and condensed phase are controlled by the interaction of the gaseous reactant with adsorbed water, $\text{H}_2\text{O}(\text{a})$. This is in contrast to simulations and experiments with liquid salt solutions and aqueous aerosols (51, 52). Those studies suggest that for chloride-ions dissolved in water an enhanced concentration of the anion near the surface may be found.

In order to confirm this hypothesis we heated up the thin KBr film in the reactor cell to $T = 620 \text{ K}$. Harrison (10) showed that bulk diffusion of ions occurs by heating up a NaCl crystal even at temperatures much below its melting point of $T_m(\text{KBr}) = 1074\text{K}$ (33). True bulk diffusion appears to take place above $T_T = 537\text{K}$, the Tammann temperature, which is defined as half the bulk melting point in Kelvin. We therefore expect that by heating up the KBr ($T_m = 1007$ (33), $T_T = 504$) sample beyond T_T $\text{H}_2\text{O}(\text{a})$ should desorb and due to bulk diffusion Br^- ions should migrate to the sample surface and make them accessible for reactions with gas phase species. Thus we expect that a saturated sample becomes more reactive due to heating up the sample to $T > T_T$.

HOCl uptake experiments have been carried out in both the 14mm-orifice reactor (Table 4.7.4, Experiment 3) and 4mm-orifice reactor in order to saturate the reaction pathway towards bromine formation before heating up the thin KBr film sprayed on a gold-plated copper substrate (Table 4.7.4, Experiment 3).

As expected heating of the KBr film to $T = 620\text{K}$ made it highly reactive as displayed in figure 4.7.11. Under the assumption that 1 mole of Cl_2O is converted to 1 mole of Br_2 (Reaction 4.7.5) and 2 moles of HOCl are converted to 1 mole of Br_2 (Reaction 4.7.4) the mass balance requires a yield of Br_2 higher than the one measured.

For NaCl hydrated according to reaction 4.7.17 Lad (2) proposed that the hydrogen atoms of adsorbed $\text{H}_2\text{O}(\text{a})$ on solid NaOH were pointing away from the surface. We suggest the same situation for KBr in analogy to NaCl as far as H_2O adsorption is concerned.

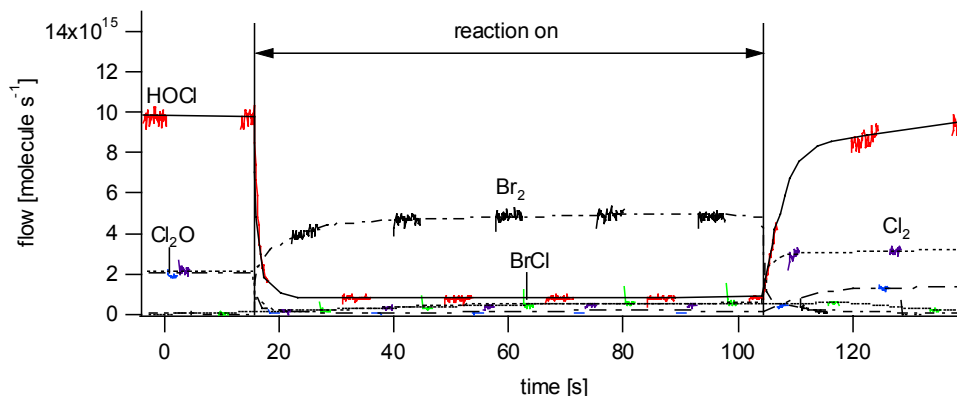


Figure 4.7.11: Steady-state HOCl uptake experiment on a thin KBr film sprayed on a gold-plated support carried out in the 4mm-orifice reactor. Before carrying out the experiment the substrate has been heated up to $T = 620\text{K}$. The observed reaction products are Br_2 and BrCl . HOCl has been monitored at $m/e = 52$, Cl_2O at $m/e = 51$, Cl_2 at $m/e = 70$, BrCl at $m/e = 116$ and Br_2 at $m/e = 160$.

The adsorption of H_2O on KBr, in figure 4.7.12 schematically illustrated, leads to KBr that is hydrated according to reaction 4.1.1. Furthermore, in figure 4.7.12 the difference between reaction of Cl_2O and HOCl on such a surface is illustrated. Figure 4.7.12a, process 1 shows the reaction of Cl_2O with surface adsorbed $\text{H}_2\text{O}(\text{a})$. The chlorine atom Cl of Cl_2O exchanges with the hydrogen H of $\text{H}_2\text{O}(\text{a})$ as displayed in figure 4.7.12a.

This exchange explains the existence of adsorbed HOCl (Reaction 4.7.16):



Theoretical calculations predict that HOCl acts as a proton donor to H_2O (53) and Geiger, Zhou and Dibble (54-56) found in theoretical calculations that HOCl binds to the oxygen-atom of the water through its proton. If the hydrogen atoms are pointing away from the surface as it is shown in figure 4.7.12 it is unlikely that HOCl reacts with or adsorbs on H_2O . This means that a surface represented schematically in figure 4.7.12 may not react very fast with HOCl as it is illustrated in figure 4.7.12b, process 3. Hence the absence of any direct reaction between KBr and HOCl may also be explained by $\text{H}_2\text{O}(\text{a})$ adsorbed on KBr much like the situation displayed in figure 4.7.12. This consideration is in agreement with our measurements.

Process 2 in figure 4.7.12b shows a possible reaction of HOCl on a contaminated sample. An adsorbed halogen X (Figure 4.7.12) is located at the surface and may exchange with the proton of HOCl.

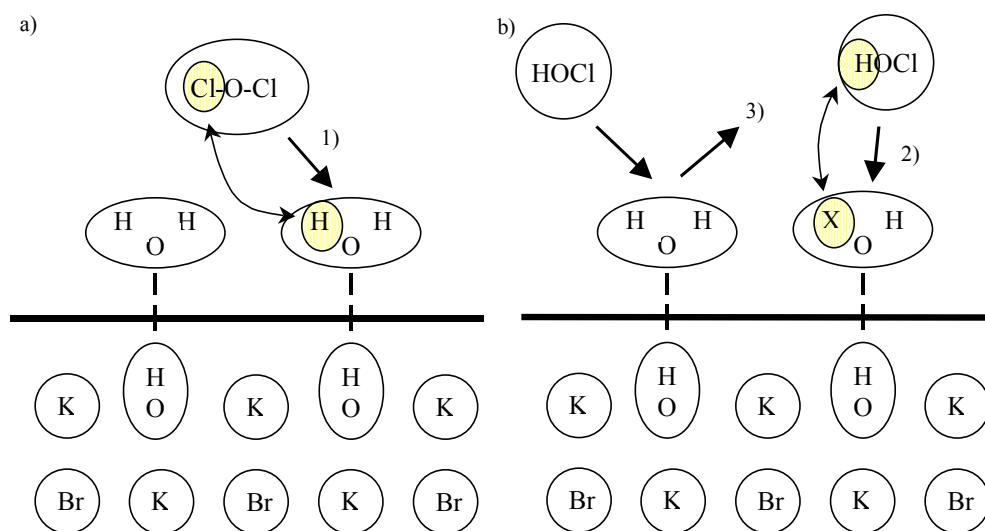


Figure 4.7.12: Schematic presentation of the structure for adsorbed water on hydrated KBr.

a) shows a schematic illustration of the reaction of Cl₂O on surface adsorbed H₂O:



b) displays a possible reaction of HOCl on a contaminated substrate (process 2)) and shows that HOCl does not react on this type of surface (process 3)).

By heating the KBr sample to $T = 620 \text{ K}$, in analogy to NaCl (10), we suggest that bromine atoms migrate to the surface which then becomes highly reactive for HOCl because the bromide is no longer screened by adsorbed H₂O(a).

In order to investigate the role of weakly adsorbed H₂O(a) a sample was heated up to $T = 400 \text{ K}$ which is below the Tammann T_T temperature. The calibrated MS-signals are displayed in figure 4.7.13 and the experimental details are listed in table 4.7.4, experiment 4d. H₂O that desorbs below $T = 400 \text{ K}$ is considered as weakly bound as already defined in section 4.1. In the 14mm-orifice reactor uptake of Cl₂O and production of HOCl and Br₂ have been measured at the start of the experiment. The fact that at the beginning of the experiment formation of HOCl has been observed may lead to the conclusion that a surface heated up to

$T = 400\text{K}$ may be of the type displayed in figure 4.7.12 justified by process 1) of figure 4.7.12.

In the 4mm-orifice reactor uptake of HOCl and Cl_2O have been measured as well as formation of Br_2 and slow formation of Cl_2 and BrOCl (Table 4.7.4, Experiment 3e). The observation of small amounts of BrOCl confirms its existence we proposed in the reaction scheme 4.7.9 – 4.7.11.

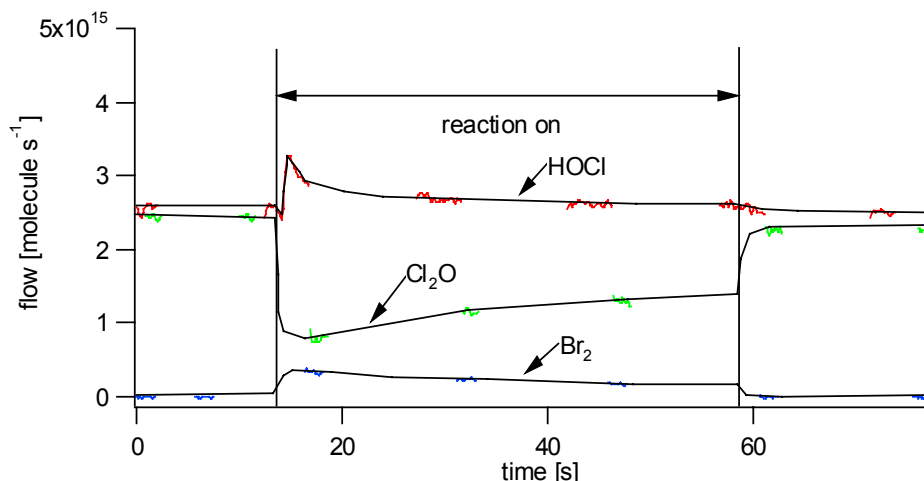


Figure 4.7.13: Uptake experiment of HOCl on a thin KBr film sprayed on a gold-coated copper substrate performed in the 14mm-orifice reactor. The sample has been heated at $T = 400\text{ K}$ before carrying out the uptake experiment. HOCl, Cl_2O and Br_2 are monitored at $m/e = 52$, $m/e = 51$ and $m/e = 160$, respectively.

Further experiments on dried KBr grains have been performed (Table 4.7.1, Experiment 5). The sample has been dried in situ using an industrial hot air gun by heating it until the H_2O MS-signal at $m/e = 18$ had returned to the initial background level characteristic of the empty flow reactor. Figure 4.7.14 shows a typical uptake experiment in the 4mm-orifice reactor on such a sample described above. The uptake experiment performed in the 14mm-orifice reactor on the fresh KBr sample did not show any uptake of HOCl. The measured Cl_2O uptake coefficient γ has been of the order of $1.2 \cdot 10^{-2}$ and the mass balance according to reaction 4.7.5 is satisfied. In contrast to the 14mm-orifice reactor γ of HOCl increased with time in the 4mm-orifice reactor as shown in figure 4.7.13. The increase of the rate of uptake on this type of sample is a further sign for the autocatalytic behaviour of the reaction of HOCl on solid KBr as we have seen in the previous section (Figures 4.7.5 and 4.7.6). The autocatalytic behaviour will be discussed in part D) of this section.

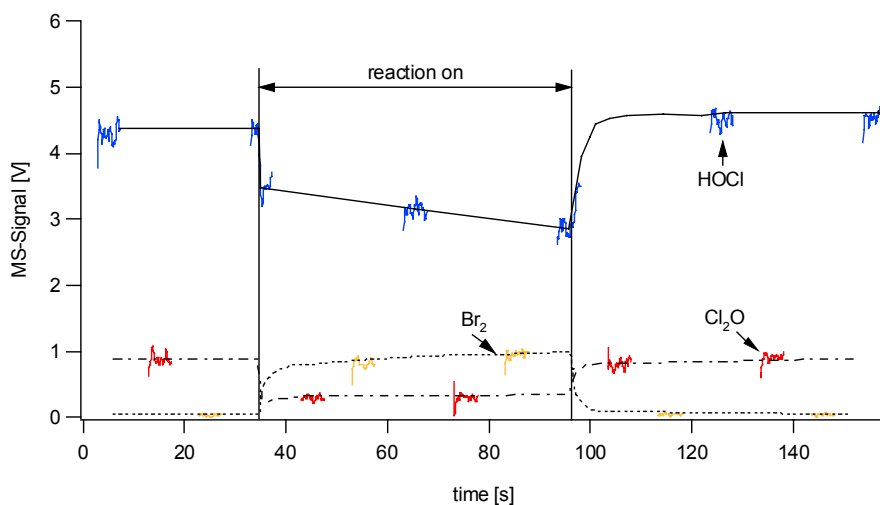


Figure 4.7.14: Typical uptake-experiment of HOCl on heated KBr grains carried out in the 4mm-orifice reactor. Cl₂O has been monitored at m/e = 51, HOCl at m/e = 52 and Br₂ at m/e = 160.

Using reactions 4.7.4 and 4.7.5 a correspondence at any given reaction time between the loss of HOCl and the formation of Br₂ has been observed.

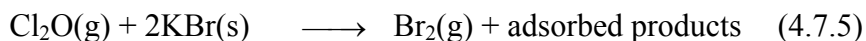
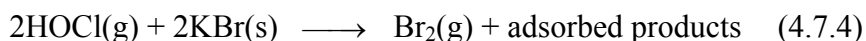


Figure 4.7.15 shows the rate of formation of Br₂ and the loss rate of HOCl divided by 2 (corresponding to Reaction 4.7.4) of an experiment carried out on heated KBr grains.

We have proposed above, that H₂O(a) screens the bromine against a reaction with HOCl by the hydrogen pointing away from the surface. This explanation is not sufficient to explain the interaction of HOCl on dried grains. Theoretical calculations have revealed that H₂O molecules are grouping around Na-Cl ion-pairs (12, 45, 57, 58). The fact that no HOCl uptake in the 14mm-orifice reactor, that is at low concentration, has been observed in contrast to an increasing rate of HOCl in the 4mm-reactor may lead to the suggestion that such a shell may also be formed for K-Br ion pairs present on the surface. At higher concentration of HOCl and Cl₂O this screening shell may be weakened or partially cracked and bromide becomes available to enable an uptake of HOCl.

Chapter 4

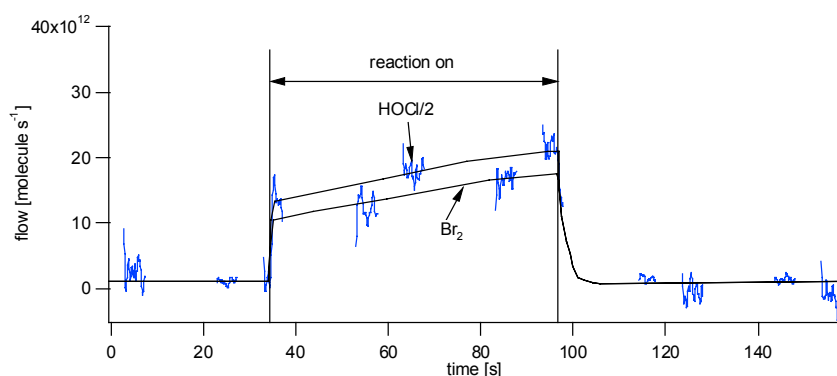


Figure 4.7.15: Steady-state uptake experiment of HOCl on heated KBr grains. The HOCl loss-rate has been corrected following reaction 4.7.4 and the Br₂ flow resulting from Cl₂O (Reaction 4.7.5) has been subtracted. HOCl and Br₂ have been monitored at $m/e = 52$ and $m/e = 160$, respectively.

In the performed experiments we have removed H₂O(a) from the substrate by pumping and heating. In subsequent experiments we have added water to the sample. In order to carry out such experiments KBr salt-methanol solutions containing up to 10%_v H₂O have been sprayed onto the Pyrex support. The HOCl uptake experiments in the 14mm-orifice reactor have shown formation rather than loss of HOCl in this case (Table 4.7.3, Experiment 3, Figure 4.7.16). The mass balance is satisfied in agreement with reactions 4.6.4 and 4.7.5.

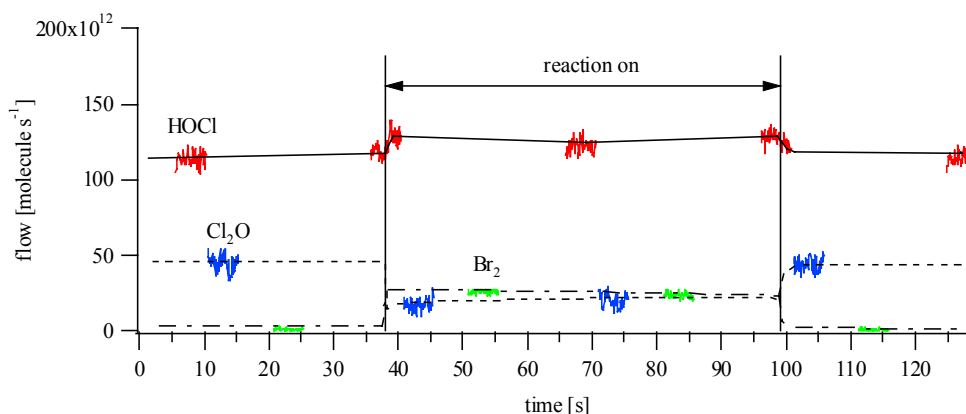
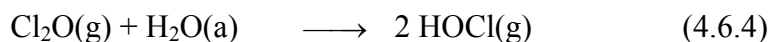


Figure 4.7.16: Typical HOCl uptake experiment on a thin KBr film sprayed on a Pyrex substrate using a methanol-H₂O salt solution. Cl₂O has been monitored at $m = 51$, HOCl at $m = 52$ and Br₂ at $m = 160$ (Br₂).

As we have seen in section 4.6 Cl_2O may undergo hydrolysis on the KBr surface (Reaction 4.6.4). The $\text{H}_2\text{O}(\text{a})$ apparently stems from the generation of the thin KBr film.



Finally, a comparison of production rates of Br_2 between dry grains and standard grains (Table 4.7.7 and Figure 4.7.17) shows the more adsorbed $\text{H}_2\text{O}(\text{a})$ remains on the surface the more the Br_2 release is delayed. The delay of formation of Br_2 on a sample containing more $\text{H}_2\text{O}(\text{a})$ may be explained by reaction 4.4.5 in the sense that the equilibrium 4.4.5 is shifted to the left-hand side and smaller amounts of adsorbed bromine may be retained on the substrate.

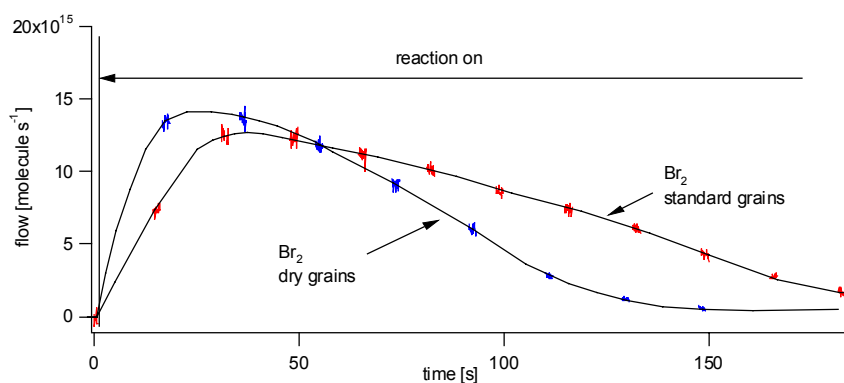


Figure 4.7.17: Uptake experiment of HOCl on KBr grains. The experiment has been carried out in the 4mm-orifice reactor. The figure shows the rate of formation of Br_2 on dry and standard grains. The meaning of dry and standard grains is defined at the beginning of this section.

In summary, the following conclusions may be given:

- The reaction pathway towards bromine species (Br_2 , BrCl , HOBr) saturates in the course of HOCl uptake.
- Only a limited number of surface sites undergo ion-exchange reactions. The number of reactive sites depends on the quantity of adsorbed $\text{H}_2\text{O}(\text{a})$ (Figure 4.7.9).
- $\text{H}_2\text{O}(\text{a})$ may retain reaction products (Reaction 4.4.5).

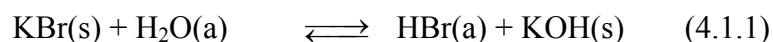
- Two different reaction sequences lead to a formation of Cl_2 (Reactions 4.6.12 and 4.7.13-14). Br^- is progressively replaced by Cl^- and subsequently removed from the surface by reaction 4.7.15.
- No regeneration of the KBr surface is observed. The reaction product KOH apparently does not tend to crystallise in the presence of $\text{H}_2\text{O}(\text{a})$.
- $\text{H}_2\text{O}(\text{a})$ may screen the ion-pairs against reaction with HOCl and consequently HOCl may not be taken up directly by a hydrated KBr sample.
- Heating the KBr sample to $T = 620 \text{ K}$ turns the sample highly reactive. Bromide migrates to the surface and becomes accessible to undergo a reaction.

C) Surface Defects

The reaction of solid NaCl with water leading to NaOH and HCl (Reaction 4.7.17) is strongly endothermic ($135 \frac{\text{kJ}}{\text{mol}}$ (9)).



Nevertheless, a reaction of H_2O with NaCl has been observed (59). The reaction presumably occurs at defect sites of the NaCl substrate located at the surface (9). By analogy we assume a similar behaviour of KBr.



In order to study the influence of surface defects steady state experiments of HOCl uptake have been performed on mechanically ground KBr grains (Table 4.7.2). A comparison of a mass spectrometric scan of HOCl in the absence and the presence of the KBr sample in the 4mm-orifice reactor has shown Br_2 as the main reaction product as well as a slight production of HOBr similar to HOCl uptake experiments on KBr grains.

Figure 4.7.18 shows an uptake experiment carried out in the 4mm-orifice reactor under conditions described in table 4.7.2, experiment 4. On grains the autocatalytic behaviour has also been observable albeit on a time scale of a few seconds as pointed out in figure 4.7.19.

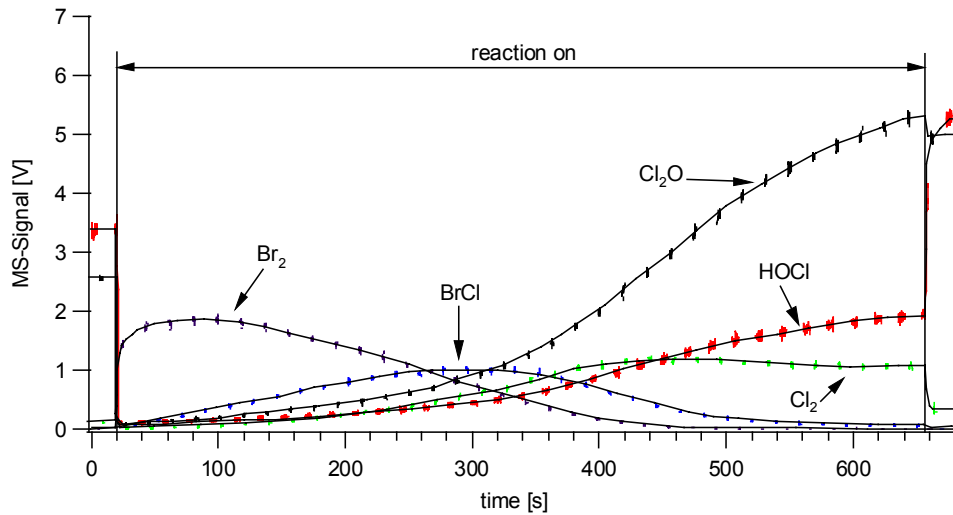


Figure 4.7.18: HOCl uptake experiment on ground KBr grains carried out in the 4mm-orifice reactor. The observed reaction products are Br_2 , BrCl , Cl_2 , HOBr , Br_2O and Cl_2O . Cl_2O has been monitored at $m/e = 51$, HOCl at $m/e = 52$, Cl_2 at $m/e = 70$, BrCl at $m/e = 116$ and Br_2 at $m/e = 160$.

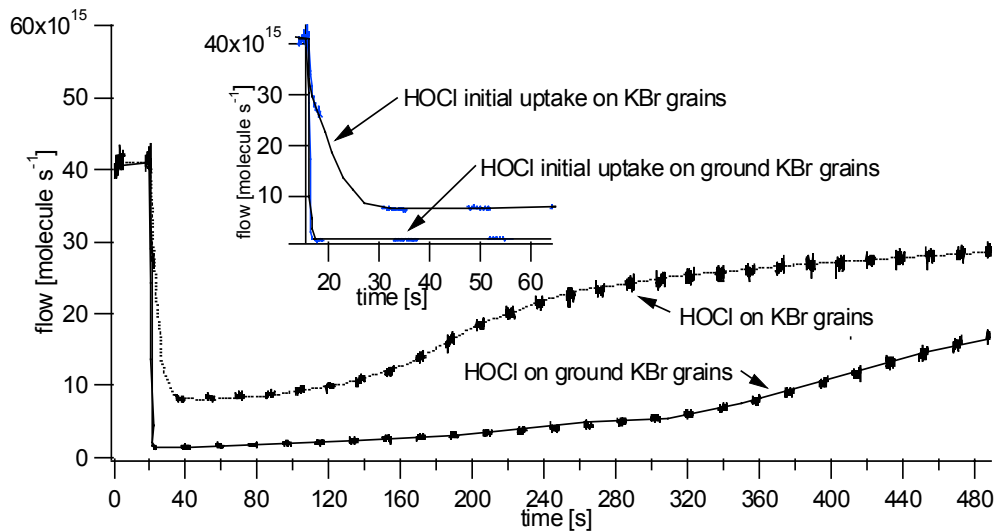


Figure 4.7.19: HOCl uptake experiments on standard and ground KBr grains carried out in the 4mm-orifice reactor at the same conditions. On KBr standard grains the autocatalytic behaviour of the reaction is apparent at the start of the experiment.

On ground grains the total amount of produced BrCl rises by a factor of 18, HOBr by a factor of 2 and the observed Br₂ increases by a factor of 3 or so compared to HOCl uptake experiments performed under the same conditions on standard grains. Yields and production rates are summarised in table 4.7.7. An estimate of the amount of adsorbed H₂O(a) between grains and ground grains resulted in no significant difference between the two types of sample. The amount of H₂O(a) on 5g standard and 5g ground grains is estimated as $1.9 \cdot 10^{19}$ and $2.2 \cdot 10^{19}$ molecule. The estimate has been performed using the graphs of figures 4.1.7 and 4.1.8 for standard and ground grains, respectively.

The reaction kinetics between an uptake experiment of HOCl on standard and ground KBr grains carried out under the same conditions have been compared in the experiments 2a and 4a displayed in tables 4.7.1 and 4.7.2, respectively. The HOCl uptake reaction on ground KBr grains is faster than on KBr standard grains where the autocatalytic behaviour of the reaction manifests itself by the increasing uptake at early time as seen in figure 4.7.19. In contrast no induction time has been observed immediately after lifting the plunger on ground KBr grains. The initial uptake coefficient of Cl₂O rises from $\gamma_0 = 2.8 \cdot 10^{-2}$ to $\gamma_0 = 0.14$ on standard and ground grains, respectively. The maximum rate of HOBr formation remains almost unchanged although the maximum rate of BrCl production is almost a factor of 5 higher on ground than on standard grains as displayed in figure 4.7.20.

The enhanced yield of the total amount of released bromine may be explained in analogy to NaCl by the more likely dissociation of H₂O related to surface defects (Reaction 4.7.18)

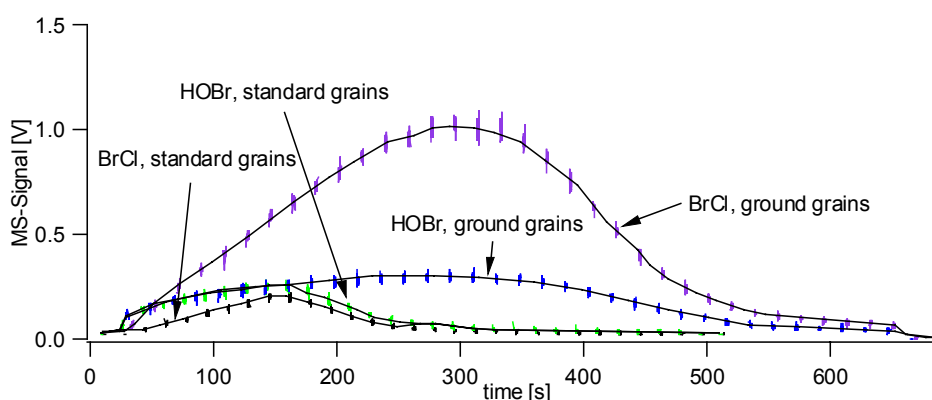


Figure 4.7.20: Rate of formation of HOBr and BrCl of HOCl uptake experiments performed on standard and ground grains. The experiments have been carried out in the 4mm-orifice reactor. BrCl and HOBr are monitored at $m/e = 116$ and $m/e = 96$.

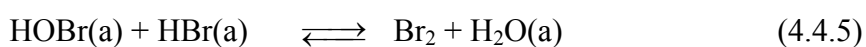
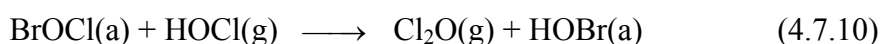
created by grinding action that has been documented for NaCl (6, 9). An analogy to NaCl substrates may be stated for KBr substrates as we already discussed above.



The higher number of reactive sites and the absence of an induction time for the reaction of HOCl on ground grains may not only have do to with enhanced water adsorption. In section 4.6 we have suggested the formation of BrCl with the presence of adsorbed molecular bromine. This suggestion results from desorption experiments carried out in section 4.1.

On fresh standard grains adsorbed molecular bromine has to be formed (reaction 4.7.15) before HOCl may react (reaction 4.7.9), which explains the induction time of the HOCl experiments on standard grains. The fact that no induction time for HOCl uptake may be observed on ground grains is a further indication that formation of molecular bromine may be enhanced by grinding the grains and we suggest that it plays an important role for reaction kinetics and product ratios (Figures 4.7.19 and 4.7.20) for the reaction of HOCl on KBr.

The fact that the rate of formation of HOBr does not change as the rate of formation of BrCl does (Figure 4.7.10) may also be explained by the presence of molecular bromine at the surface.



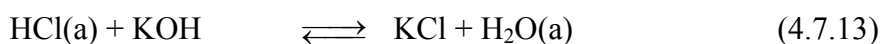
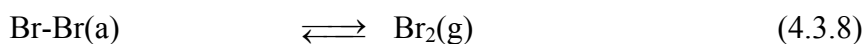
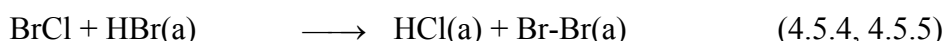
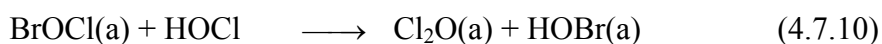
In summary we have found:

- An increase of the yield of gaseous bromine-containing products on ground grains due to surface defects.
- Further indication for the presence of adsorbed molecular bromine which may induce the reaction of HOCl with KBr.

D) Mechanism and Autocatalytic Behaviour

The present experiments have shown that the value of γ_0 for HOCl interacting with fresh KBr grains and thin KBr films sprayed on a Pyrex substrate always starts from zero and increases with time as shown in Figures 4.7.6 and 4.7.19. We have shown that surface-contamination is crucial for the reactivity and kinetics of the reaction of HOCl with KBr as we have not seen any direct reaction of HOCl. It is difficult to devise a starting mechanism for this reaction because many concurrent reactions are occurring in this system and it is difficult to distinguish between them because of many common reaction products.

We propose the following reaction scheme for the reaction with HOCl on solid KBr. The initiation of the reaction is enabled by the presence of molecular bromine on the surface. We assume that molecular bromine stems from the reaction with Cl_2O and KBr according to reactions 4.6.6-4.6.9, 4.5.4 and 4.5.5 or that it is already present on ground grains and thin KBr films sprayed on a gold-coated copper substrate as discussed in section 4.1. Furthermore, the presence of HBr(a) is explained by the dissociation of H_2O on KBr defect sites (Reaction 4.7.18).



Br-Br(a) means adsorbed hydrated Br_2 . The autocatalytic behaviour is explained by the equilibrium 4.3.8 which leads to an adsorption of Br_2 on the KBr surface due to its residence time τ_s and consequently to an accumulation of molecular bromine on the surface. This

manifests itself in the difference of the reaction kinetics in the 4mm- and 14mm-orifice reactor because changing the orifice leads to a change of the residence time τ_s of Br_2 in the reactor. It has been shown that the uptake of HOCl increases with time in the 4mm-reactor whereas in the 14mm it decreases (Figures 4.7.2 and 4.7.19).

4.7.3. Conclusions

The reaction of HOCl on KBr has been presented in this section. Impurities such as Cl_2O , secondary reactions and adsorbed products make the study of this reaction very difficult. This reaction has been studied on different substrates such as grains, ground grains and thin films sprayed on Pyrex and gold-coated copper substrates in order to elucidate the underlying reaction mechanism.

Br_2 has been the main observed reaction product on fresh KBr samples. Formation of BrCl, HOBr and a very slow formation of BrOCl and Br_2O with time has been observed as well.

The reaction of HOCl on KBr has been studied under the point of view of surface activation, adsorbed $\text{H}_2\text{O}(\text{a})$, and surface defects. It has been shown that an irreversible saturation of the reaction pathway towards gaseous bromine species such as Br_2 , BrCl and HOBr sets in with time. Simultaneously to the saturation of the formed bromine-containing products formation of Cl_2 and Cl_2O sets in. Under the present experimental conditions no regeneration of the surface towards bromine-containing products has been observed. These observations lead to the conclusion that both HOCl as well as bromine species such as Br_2 , BrCl and HOBr may be retained on the surface of the solid KBr substrate.

The reaction kinetics as well as the formation of products are controlled by the presence of surface-contaminants such as $\text{Br}_2(\text{a})$ and $\text{HOCl}(\text{a})$ and possibly other species such as $\text{HBr}(\text{a})$, $\text{BrCl}(\text{a})$ and $\text{HOBr}(\text{a})$. Furthermore, we have shown in uptake experiments of Br_2 on contaminated solid KBr substrates that bromine may displace chlorine on the surface when present in excess in the gas-phase.

From the fact that the surface does not regenerate in contrast to the reaction of Cl_2 on KBr and that only chlorine products have been observed as reaction products in the long term experiments we have concluded that interfacial bromine $\text{Br}_2(\text{a})$ and $\text{HBr}(\text{a})$ are displaced by

chloride and potassium hydroxide. Moreover, the formed chloride may react with HOCl and form a protective layer of KOH.

As a result of HOCl uptake experiments with a concurrent Br₂ flow, we have concluded that two different reaction mechanisms may lead to release of Cl₂O and Cl₂ namely one in the presence of adsorbed Br₂ (Reactions 4.7.9-4.7.12) and the other in the absence of adsorbed Br₂ (Reactions 4.7.13 and 4.7.14).

On a fresh sample no uptake of HOCl has been observed in the 14mm-orifice reactor, whereas in the 4mm-orifice reactor an increasing rate of uptake with time has been measured. In order to explain this we propose that adsorbed H₂O(a) screens the interfacial bromine species such as hydrated KBr and HBr(a) against reaction with HOCl. Such a situation is schematically indicated in figure 4.7.12. The hypothesis of the screening effect of H₂O(a) is also supported by uptake experiments of HOCl on heated KBr samples. A KBr sample heated to T = 620 K becomes highly reactive, whereas a sample heated to T = 400 K does not change its behaviour significantly. The high temperature leads to a migration of bromine ions towards the surface and expose it directly to the gas in order to facilitate reactions. On the other hand, molecular bromine adsorbs on the surface and enables the reaction of HOCl with adsorbed species which leads to an autocatalytic reaction mechanism with increasing uptake of HOCl with time. This situation is explained in part D) of the previous section.

Furthermore, it has been observed that mechanical treatment of KBr grains enhances the number of reactive sites leading to the formation of gaseous bromine-containing species such as Br₂, BrCl and HOBr. The fact that on ground grains no induction time for the uptake of HOCl is needed provides further indication of adsorbed molecular bromine which has been proposed in section 4.1. Moreover, the reaction kinetics is strongly influenced by adsorbed molecular bromine in the initial phase of the heterogeneous reaction.

4.7.4. Tables**Table 4.7.1:** Typical experimental conditions for HOCl uptake experiments on KBr grains and main results

No	Orifice diameter [mm]	[HOCl] [molecule cm ³]	Experimental conditions	Main products	Minor products	Uptake kinetics	Remarks
1a	14	$3.3 \cdot 10^{10}$	First uptake on fresh sample $t_p = 24h$	Br ₂		$\gamma_0 = 0.04$ γ decreases with time	Cl ₂ O uptake with $\gamma_0 = 0.01$ 2Mol HOCl react to 1Mol Br ₂ Br ₂ production decreases with time
1b	14	$3.3 \cdot 10^{10}$	Subsequent uptake experiments on poisoned sample	Br ₂		$\gamma_0 = 0.1$ $\gamma_{ss} = 6 \cdot 10^{-3}$	γ_0 decreases with number of uptake experiment
2a	4	$4 \cdot 10^{13}$	First uptake on fresh sample $t_p = 2h$	Br ₂	HOBr, BrCl, Cl ₂	$\gamma_0 = 0.04$ $\gamma_{ss} = 4 \cdot 10^{-3}$	Reaction pathway towards bromine species saturates. Total Br ₂ production on the order of 10^{18} molecules Cl ₂ production
2b	4	$4 \cdot 10^{13}$	Subsequent uptake experiments on poisoned sample	Cl ₂ , Cl ₂ O			Reaction pathway towards bromine species saturated.
3a	4	$3.5 \cdot 10^{13}$	Additional Br ₂ flow [Br ₂] = $7 \cdot 10^{12}$ molecule cm ⁻³	Cl ₂	HOBr, BrCl Br ₂ O	$\gamma_{ss} = 5 \cdot 10^{-3}$	Br ₂ injection causes an increase of γ_{ss} from $1.6 \cdot 10^{-3}$ to $5 \cdot 10^{-3}$.

3b	4	$4.5 \cdot 10^{13}$	Additional Br ₂ flow [Br ₂] = $4 \cdot 10^{13}$ molecule cm ⁻³	Cl ₂	HOBr, BrCl Br ₂ O	$\gamma_{ss} = 0.01$	Increase of γ_{ss} from $2.8 \cdot 10^{-3}$ to $10 \cdot 10^{-3}$. ³ γ_{ss} depends on [Br ₂]
4a	4		Uptake of Br ₂ on contaminated sample, [Br ₂] = $6 \cdot 10^{12}$ molecule cm ⁻³	BrCl, Cl ₂ , Cl ₂ O		$\gamma_0(\text{Br}_2) = 6 \cdot 10^{-3}$	Decreasing rate of uptake of Br ₂ , saturation within 40s, or so.
5a	14	$2 \cdot 10^{10}$	Dried sample	Br ₂			No uptake of HOCl despite uptake of Cl ₂ O
5b	4	$1.3 \cdot 10^{11}$	Dried sample	Br ₂		$\gamma_0 = 1.5 \cdot 10^{-3}$	HOCl uptake increases with time

Table 4.7.2: Typical experimental conditions for HOCl uptake experiments on KBr ground grains and main results

No	Orifice diameter [mm]	[HOCl] [molecule cm ³]	Experimental conditions	Main products	Minor products	Uptake kinetics	Remarks
1a	14	$1 \cdot 10^{10}$	First uptake on fresh sample, $t_p = 24\text{h}$	B ₂		n. u.	Uptake of Cl ₂ O, $\gamma(\text{Cl}_2\text{O}) = 2 \cdot 10^{-2}$, Br ₂ formation from reaction of Cl ₂ O
1b	4	$2 \cdot 10^{11}$	Subsequent uptake on poisoned sample	Br ₂	BrCl	$\gamma_0 = 8 \cdot 10^{-4}$ $\gamma_{ss} = 1.5 \cdot 10^{-2}$	γ increases with time, BrCl observed after several uptake experiments Br ₂ production rate = $2.1 \cdot 10^{14}$ molecule s ⁻¹
1c	14	$1 \cdot 10^{10}$	Uptake on poisoned sample	Br ₂		$\gamma_0 = 5 \cdot 10^{-2}$ $\gamma_{ss} = 5 \cdot 10^{-3}$	γ decreases with time, no BrCl measured

Chapter 4

2a	4	$4 \cdot 10^{13}$	First uptake on fresh sample, $t_p = 2h$	Br_2	HOBr, BrCl, Cl_2, Cl_2O	γ_0 n. m. $\gamma_{max} = 0.18$ $\gamma_{ss} = 1.2 \cdot 10^{-2}$	γ decreases from zero to γ_{max} and increases to γ_{ss} . Production of Cl_2 sets in.
2b	4	$4 \cdot 10^{13}$	Uptake on poisoned sample	Cl_2	Cl_2O	$\gamma_0 = 7.4 \cdot 10^{-3}$ $\gamma_{ss} = 4 \cdot 10^{-3}$	No bromine containing species such as Br_2 , HOBr and BrCl observed
3a	4	$3 \cdot 10^{13}$	Additional Br_2 flow $[Br_2] = 4 \cdot 10^{12}$ molecule cm^{-3} $t_p = 2h$	Cl_2	HOBr, BrCl	$\gamma_{ss} = 5 \cdot 10^{-3}$	Increase of γ_{ss} from $5 \cdot 10^{-3}$ to $7 \cdot 10^{-3}$. γ_{ss} depends on $[Br_2]$
3b	4	$3 \cdot 10^{13}$	Additional Br_2 flow $[Br_2] = 5 \cdot 10^{13}$ molecule cm^{-3} $t_p = 2h$	Cl_2	HOBr, BrCl	$\gamma_{ss} = 12 \cdot 10^{-3}$	Increase of γ_{ss} from $5 \cdot 10^{-3}$ to $12 \cdot 10^{-3}$. γ_{ss} depends on $[Br_2]$
3c	4	$2 \cdot 10^{12}$	Additional Br_2 flow $[Br_2] = 2 \cdot 10^{12}$ molecule cm^{-3} $t_p = 2h$	HOBr, BrCl	Cl_2	$\gamma_{ss} = 3 \cdot 10^{-3}$	Increase of γ_{ss} from $1 \cdot 10^{-3}$ to $3 \cdot 10^{-3}$. γ_{ss} depends on $[Br_2]$
4a	4	$4 \cdot 10^{12}$	First uptake on fresh sample, $t_p = 2h$	Br_2	HOBr	n. u. $\gamma_{ss} = 0.15$	γ increases from zero to γ_{ss} within 20s
4b	4	$4 \cdot 10^{12}$	uptake on poisoned sample, $t_p = 2h$	Br_2	HOBr, Cl_2	$\gamma_0 = 2 \cdot 10^{-2}$ $\gamma_{ss} = 3.3 \cdot 10^{-3}$	γ decreases
5	4	$2 \cdot 10^{11}$	First uptake on fresh sample, $t_p = 4h$	Br_2	Br_2	$\gamma_0 = 2.8 \cdot 10^{-3}$ $\gamma_{ss} = 0.1$	γ and Br_2 formation increase with time, $\gamma_{ss}(t_p=4h)/\gamma_{ss}(t_p=4h) \sim 7$
6a	14	$2 \cdot 10^{11}$	Dried substrate	Br_2	HOBr	$\gamma_0 \sim 0$ $\gamma_{max} = 1 \cdot 10^{-2}$	Br_2 production rate = $2.6 \cdot 10^{14}$ molecule s^{-1} HOBr but no BrCl observed

n. u. : not measurable at the conditions of our experiment.

Table 4.7.3: Typical experimental conditions for HOCl uptake experiments on thin sprayed KBr films on Pyrex and main results

No	Orifice diameter [mm]	[HOCl] [molecule cm ³]	Experimental conditions	Main products	Minor products	Uptake kinetics	Remarks
1a	14	$6 \cdot 10^{10}$	First uptake on fresh sample $t_p = 20h$	Br ₂	BrCl	n. u.	Cl ₂ O uptake
2a	4	$3 \cdot 10^{13}$	First uptake on fresh sample $t_p = 4h$	Br ₂ HOBr	Cl ₂	$\gamma_0 \sim 0$ $\gamma_{max} = 3 \cdot 10^{-3}$	Reaction pathways towards Br ₂ and HOBr saturate completely
2b	4	$4 \cdot 10^{13}$	Uptake on poisoned sample	Cl ₂		$\gamma_0 = 1.3 \cdot 10^{-3}$	No bromine products, no regeneration
3a	14	$1 \cdot 10^{12}$	First uptake on fresh H ₂ O-methanol thin film $t_p = 5h$	HOCl Br ₂			Additional formation of HOCl
4a	4	$2 \cdot 10^{11}$	Exposed to 50Torr of Br ₂ , $t_{exp} = 14h, t_p = 1h$	Br ₂	HOBr	$1.5 \cdot 10^{-3}$	Br ₂ persists in reactor

n. u. : not measurable at the conditions of our experiment

Table 4.7.4: Typical experimental conditions for HOCl uptake experiments on thin KBr films sprayed on gold plated copper substrate and main results

No	Orifice diameter [mm]	[HOCl] [molecule cm ⁻³]	Experimental conditions	Main products	Minor products	Uptake kinetics	Remarks
1a	14	$5 \cdot 10^{10}$	First uptake on fresh sample $t_p = 22\text{h}$	Br ₂	HOBr	Burst of Br ₂ , Saturation after several seconds	
1b	4	$5 \cdot 10^{11}$	Uptake on poisoned sample	Cl ₂	Cl ₂ O	$\gamma_0 = 1.7 \cdot 10^{-3}$ No bromine products, no regeneration	
1c	14	$1 \cdot 10^{10}$	Exposed to H ₂ O, [H ₂ O] = $1 \cdot 10^{13}$	Cl ₂		$\gamma_0 = 3 \cdot 10^{-3}$ No regeneration	
1d	4	$1 \cdot 10^{11}$	Exposed to H ₂ O, [H ₂ O] = $1 \cdot 10^{13}$	Cl ₂		$\gamma_0 = 0.6 \cdot 10^{-3}$ No regeneration	
2a	14	$5 \cdot 10^{10}$	First uptake on fresh sample $t_p = 3\text{h}$	Br ₂	HOBr	$\gamma_{\max} = 2 \cdot 10^{-2}$ Burst of Br ₂ and HOBr γ_{\max} has been reached after 20s or so	
2b	4	$1 \cdot 10^{11}$	Uptake on poisoned sample	Cl ₂	Cl ₂ O	$\gamma_{\max} = 3 \cdot 10^{-3}$ Saturation after several seconds	
3a	14	$1 \cdot 10^{12}$	First uptake on fresh sample $t_p = 0.5\text{h}$	Br ₂	HOCl	Formation of HOCl	
3b	4	$2 \cdot 10^{13}$	Uptake on poisoned sample	Br ₂		$\gamma_0 = 1.6 \cdot 10^{-3}$ HOCl uptake and formation of Br ₂ tends to zero	
3c	4	$6 \cdot 10^{12}$	Heated up to T = 620K	Br ₂	BrCl	$\gamma = 6 \cdot 10^{-2}$ No saturation	
3d	14	$1 \cdot 10^{12}$	Heated up to T = 400K	Br ₂	Cl ₂	$\gamma_{\max} = 3 \cdot 10^{-2}$ At t = 0 formation and towards the end an uptake of HOCl	
3e	4	$6 \cdot 10^{12}$	Heated up to T = 400K	Br ₂	Cl ₂ BrOCl	$\gamma_0 = 4 \cdot 10^{-3}$	

Table 4.7.5: uptake coefficient γ of HOCl on KBr grains in presence of an additional Br₂ flow in the 4mm-orifice reactor.

HOCl [molecule cm ⁻³]	Br ₂ [molecule cm ⁻³]	γ_{mi} [%]	γ_{ss}^* [%]	Pumping time [h]
4.0*10 ¹³	no Br ₂	4.5	0.4	2
4.0*10 ¹³	no Br ₂	4.5	0.4	17.5
4.3*10 ¹³	3.0*10 ¹²		0.12/0.21	17.5
7.9*10 ¹³	3.0*10 ¹²		0.2/0.25	17.5
2.6*10 ¹³	2.6*10 ¹³		0.23/1.1	17.5
3.5*10 ¹³	3.4*10 ¹³		/0.53	17.5
3.8*10 ¹³	7.6*10 ¹³		0.16/0.54	2
5.2*10 ¹³	7.6*10 ¹³		/0.43	2
4.5*10 ¹³	7.6*10 ¹³		0.22/0.47	2
4.9*10 ¹³	3.6*10 ¹³		0.28/1.1	2
5.5*10 ¹³	3.9*10 ¹³		/0.29	2

 γ_{mi} : initial uptake coefficient γ : steady state coefficient* : without injection of Br₂/with injection of Br₂

Table 4.7.6: uptake coefficient γ of HOCl on ground KBr grains in the presence of an additional Br₂ flow in the 4mm-orifice reactor.

HOCl [molecule cm ⁻³]	Br ₂ [molecule cm ⁻³]	γ_{mi} [%]	γ_{ss}^* [%]	Pumping time [h]	γ_{mi} :	initial uptake coefficient
					γ :	steady state coefficient
					*	without injection of Br ₂ /with injection of Br ₂
2*10 ¹¹	No Br ₂	0.08	2	24		
2*10 ¹¹	No Br ₂	0.28	11	4		
4*10 ¹²	No Br ₂	0	15	2		
4.10 ¹³	No Br ₂	18	10	2		
3*10 ¹³	4*10 ¹²		0.6/0.7	2		
3*10 ¹³	5*10 ¹²		0.6/1.2	2		

Table 4.7.7: Production and maximal production rate of BrCl, HOBr and Br₂ of HOCl on KBr grains and ground grains with different amount of adsorbed H₂O(a). m(KBr) = 5g for standard and ground grains samples.

t _p	H ₂ O(a)	Br ₂		BrCl		HOBr		Br		g :	ggs :	P :
		yield	production rate	yield	production rate	Yield	production rate	sum of Br ⁻	yield			
g	2	2*10 ¹⁹	1.4*10 ¹⁸	1.2*10 ¹⁶	2.4*10 ¹⁷	2.2*10 ¹⁵	1.5*10 ¹⁸	8*10 ¹⁵	4.5*10 ¹⁸	[t _p]	grains	ground grain
g	17	5*10 ¹⁸	1.1*10 ¹⁸	1.4*10 ¹⁶	1.8*10 ¹⁷	1.8*10 ¹⁵	1*10 ¹⁸	8*10 ¹⁵	3.4*10 ¹⁸	[yield]	sprayed thin film on Pyrex	= h
gg	2	2.2*10 ¹⁹	5*10 ¹⁸	7*10 ¹⁵	4.2*10 ¹⁸	10*10 ¹⁵	3.3*10 ¹⁸	10*10 ¹⁶	17.5*10 ¹⁸	[production rate]	= molecule s ⁻¹	
P	4		2.4*10 ¹⁷				2.3*10 ¹⁷		7*10 ¹⁷			
Au	4	3*10 ¹⁷	4.5*10 ¹⁵				2*10 ¹⁵		1.1*10 ¹⁶			

Table 4.7.8: Enthalpies ΔH crystalline and hydrated KBr, KCl and KOH at $T = 298.15 \text{ K}$ (34)

	$\Delta H (\text{cr}) [\text{kJ mol}^{-1}]$	$\Delta H (\text{in } \infty \text{ H}_2\text{O}) [\text{kJ mol}^{-1}]$
KBr	-393.8	-373.9
KCl	-436.7	-419.9
KOH	-424.8	-482.3

cr : crystalline solid

in $\infty \text{ H}_2\text{O}$: infinitely diluted in H_2O

4.8. Uptake Experiments of Cl₂O on NaCl

4.8.1. Introduction

Dichloromonoxid or hypochlorous anhydride Cl₂O has not been detected in the atmosphere, but Cl₂O is an inevitable contamination of HOCl by virtue of its equilibrium (Reaction 3.1.5). In order to study the reaction of HOCl on NaCl a few uptake experiments of Cl₂O on NaCl have been carried out in a low-pressure flow reactor on NaCl grains and thin NaCl films sprayed on a Pyrex substrate. Cl₂O has been detected at its parent peak $m/e = 51$. The parent peak of Cl₂O is at $m/e = 86$.

4.8.2. Results and Discussion

Steady-state uptake experiments on commercially available NaCl have been carried out in the 4mm- and 14mm-orifice reactor. The experimental conditions and main results are summarised in table 4.8.1. Before carrying out Cl₂O uptake experiments on NaCl substrates a reference uptake experiment of Cl₂O carried out in the 4mm-orifice reactor on the bare Pyrex sample-holder has been performed but has not led to an uptake of Cl₂O.

A mass-spectrometric scan of Cl₂O in the absence and the presence of NaCl grains has shown formation of Cl₂ and a small production rate of HOCl as seen in figure 4.8.1.

Similar to uptake experiments of Cl₂O on KBr samples steady-state experiments on NaCl grains have shown different behaviour between a fresh and an already exposed sample. The observed differences are in terms of the uptake kinetics as well as the formation of products, namely HOCl and Cl₂. Figure 4.8.2 shows a typical Cl₂O uptake experiment on NaCl grains carried out in the 4mm-orifice reactor (Table 4.8.1, Experiment 2b).

Chapter 4

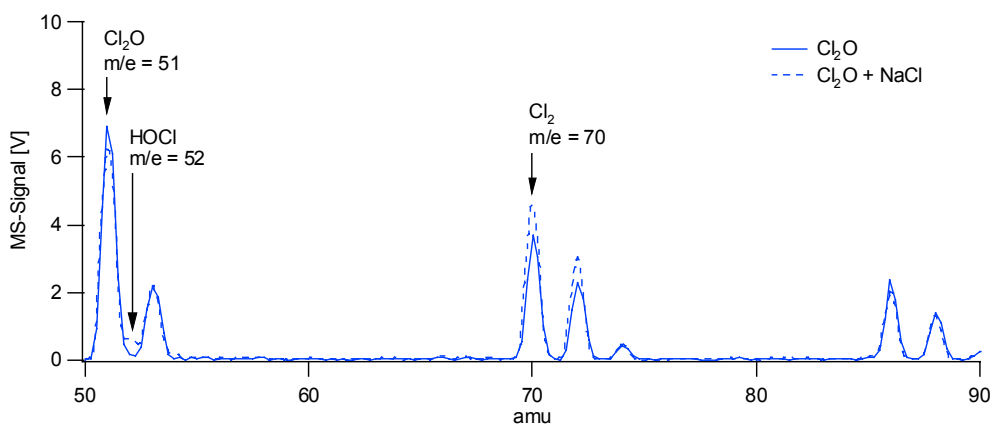


Figure 4.8.1: Mass-spectrometric scan of Cl_2O in the absence and the presence of NaCl performed in the 4mm-orifice reactor.

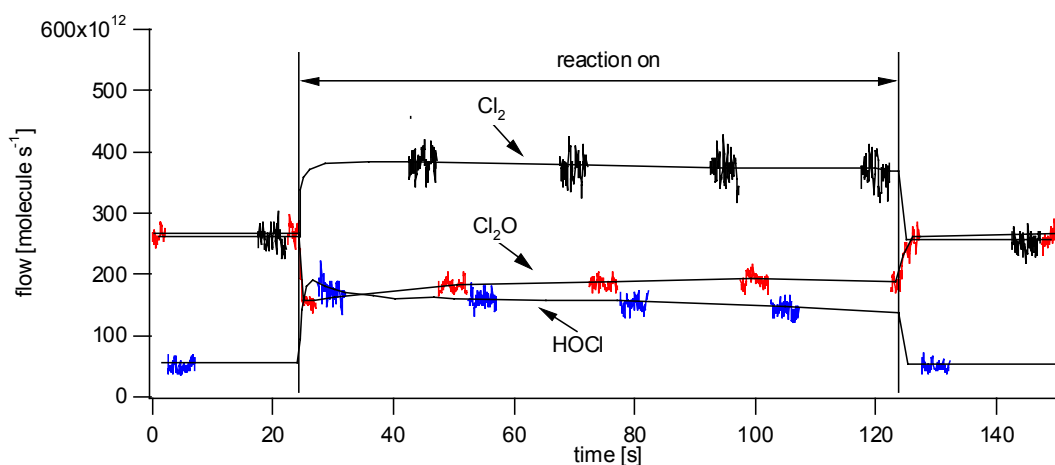


Figure 4.8.2: Typical steady-state uptake experiment of Cl_2O on a contaminated NaCl surface. The experiment has been performed in the 4mm-orifice reactor.

Uptake experiments on a fresh sample of NaCl grains carried out in the 14mm-orifice reactor have not shown any production of Cl_2 (Table 4.8.1, Experiment 2a). In contrast, the formation of one mole of gaseous HOCl has been observed per mole of lost Cl_2O . The formation of gaseous HOCl stems from the reaction of Cl_2O with adsorbed $\text{H}_2\text{O}(\text{a})$ as we have already seen with Cl_2O experiments on KBr samples discussed in section 4.6.



Chapter 4

Furthermore, subsequent Cl_2O uptake experiments on the poisoned sample carried out in the 4mm-orifice reactor leads to formation of Cl_2 (Table 4.8.1, Experiment 2).

Additional experiments have been carried out on thin films of NaCl sprayed onto a Pyrex substrate. These uptake experiments have not led to an uptake of Cl_2O .

In relation to surface activation subsequent uptake experiments of Cl_2O have been performed in the 4mm-orifice reactor on the same NaCl grains. Figure 4.8.3 shows the formation of Cl_2 resulting from Cl_2O uptake experiments performed sequentially on NaCl grains. The first uptake experiment shows an increase of the rate formation of Cl_2 after lifting the plunger, whereas further uptake experiments lead to formation of Cl_2 immediately after lifting the plunger.

Uptake experiments of HOCl on solid KBr presented in section 4.7 have shown that HOCl may adsorb on the KBr substrate. Similarly, we suggest that HOCl may reside on the surface of a solid NaCl substrate and play an important role for the reaction with Cl_2O .

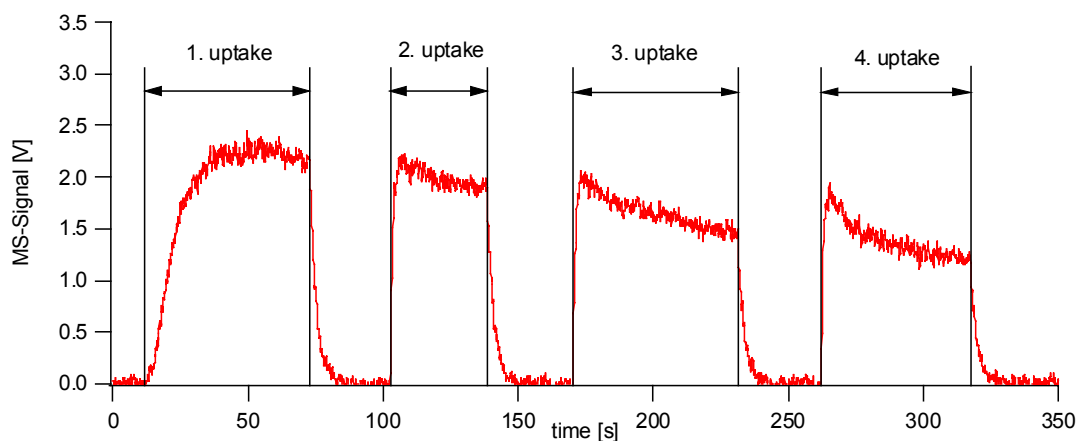


Figure 4.8.3: MS-Signal of the formation of Cl_2 in the reaction of Cl_2O on NaCl grains. The consecutive experiments have been carried out in the 4mm-orifice reactor.

Chapter 4

In order to study the role of surface-adsorbed HOCl subsequent Cl₂O uptake experiments have been carried out. The formation of HOCl and Cl₂ has been monitored and the total amount of lost and formed molecule, respectively, has been determined. Figure 4.8.4 shows the ratio R between the yield of Cl₂ and the lost Cl₂O, $R_1 = \frac{N_{Cl_2}}{N_{Cl_2O}}$, as well

between the yield of HOCl and the lost Cl₂O, $R_2 = \frac{N_{HOCl}}{N_{Cl_2O}}$, as a function of the number of uptake experiments. The experimental conditions are listed in table 4.8.1, Experiment 3.

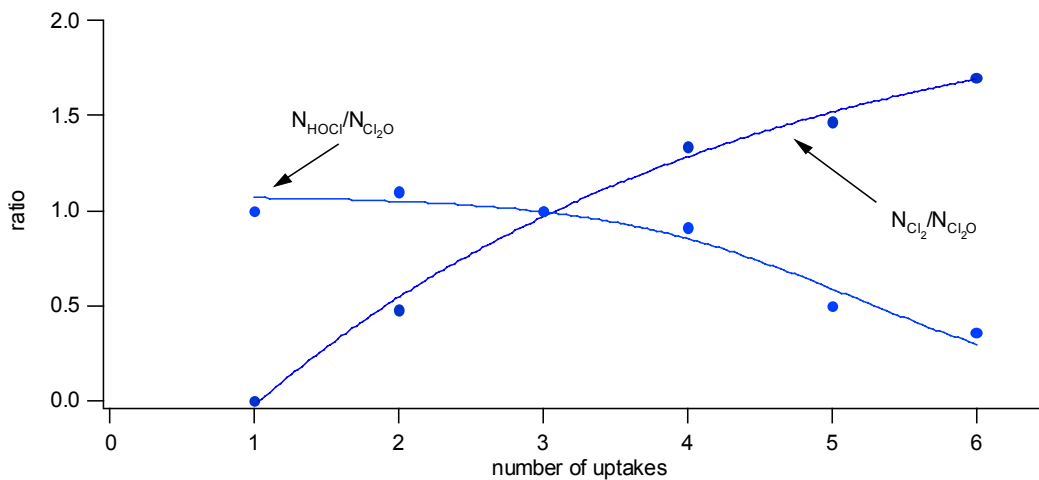


Figure 4.8.4: Ratio between production of Cl₂ and HOCl and loss of Cl₂O as a function of the number of sequential uptake experiments performed on the same NaCl grain sample. The experiment has been carried out in the 14mm-orifice reactor.

With the number of the uptake experiments performed on the same NaCl sample the amount of formed HOCl decreases whereas the amount of Cl₂ increases due to surface poisoning. The ratio of the number of produced Cl₂, N_{Cl_2} , and the number of lost Cl₂O, N_{Cl_2O} , tends towards 2 with increasing number of uptake experiments (equation 4.8.1).

Chapter 4

$$\frac{N_{\text{Cl}_2}}{N_{\text{Cl}_2\text{O}}} \rightarrow 2 \quad (\text{equation 4.8.1})$$

The fact that on a fresh NaCl sample the yield of HOCl corresponds to the loss of Cl₂O as it is indicated by the first point in figure 4.8.4 leads us to the conclusion that Cl₂O reacts with adsorbed H₂O(a) in the following way:



Reaction 4.6.4 is a further indication for adsorption of HOCl on salt surfaces. Furthermore, adsorbed HOCl leads to the contamination of the NaCl substrate. As it is shown in figure 4.8.4 the yield of Cl₂ goes from zero for the uptake on a virgin sample to twice the amount of Cl₂O lost with increasing number of uptake experiments. Also, the Cl₂O uptake experiment performed in the 4mm-orifice reactor has shown that the formation of Cl₂ sets in slowly as shown in figure 4.8.3. This may suggest that Cl₂O does not interact directly with the NaCl ion-pair but rather with surface-adsorbed H₂O(a). For the interaction of HOCl with solid KBr we have proposed the screening of the KBr ion-pairs by adsorbed H₂O(a) molecules in section 4.7, part B). Using this concept we may also explain that formation of HOCl sets in immediately after the beginning of the reaction, whereas the formation of Cl₂ is delayed and the rate of formation rises only slowly.

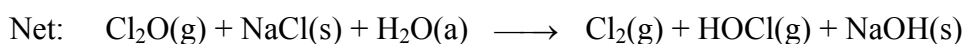
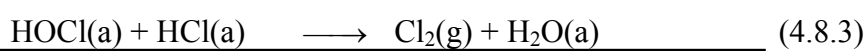
The fact that HOCl has been observed immediately after lifting the plunger according to reaction 4.6.4 and the formation of gaseous Cl₂ occurs delayed leads us to the suggestion that the chloride-ion of the solid sample is not readily accessible by gaseous species and that the reaction starts with a collision with surface adsorbed H₂O(a). Based on the fact that further uptake experiments of Cl₂O on a contaminated NaCl substrate lead to an immediate formation of Cl₂ we furthermore suggest that on a contaminated surface Cl⁻ ions become directly available for gaseous species (Reaction 4.8.1).



Chapter 4

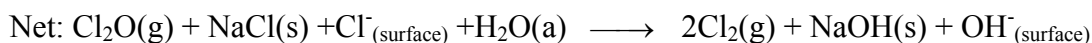
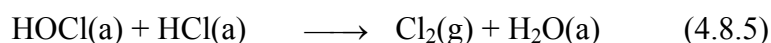
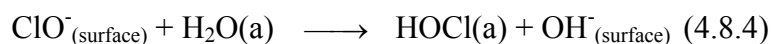
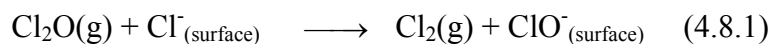
We suggest a similar mechanism for the reaction of Cl₂O with solid NaCl as we have done for solid KBr based on adsorbed H₂O(a) as it is shown in figure 4.7.12a, process 1) namely one chlorine atom of Cl₂O may exchange with the proton of the adsorbed H₂O(a) leading to HOCl(a) and HOCl(g) according to reaction 4.6.4 This exchange leads to the presence of readily accessible adsorbed chlorine on the substrate.

For the reaction of Cl₂O on a fresh NaCl sample we propose the following reaction scheme which starts with reaction 4.6.4 and the equilibrium of H₂O(a) with NaCl (9) in analogy to the mechanistic scheme discussed for the HOCl/KBr interaction:



This explains the immediate release of HOCl and the delay of Cl₂ after lifting the plunger as well as the surface contamination by adsorbed HOCl.

In order to explain the reaction on a contaminated NaCl substrate the following mechanism has been constructed:



Chapter 4

This mechanism explains the conversion of one mole of lost Cl_2O to two moles of Cl_2 . It also includes the surface contamination, which is represented by Cl^- coming from reaction 4.6.4. Adsorbed $\text{H}_2\text{O}(\text{a})$ is not consumed. It acts only in a catalytic way.

As already mentioned in section 4.7, part B) Knipping (51) and Wilson (52) have found evidence that in aqueous solutions of NaCl the Cl^- ions occupy a significant part of the surface of the sample. They showed that experimental and model predictions can only be reconciled if reactions of gases with ions at the interface control the chemistry. In contrast to this we suggest that no Cl^- ions are located at the solid-gas interface on a fresh solid NaCl sample. This suggestion is based on the fact that HOCl release occurs immediately after lifting the plunger whereas the formation of Cl_2 occurs in a delayed manner as shown in figure 4.8.3 or is totally absent at low concentration (Table 4.8.1, Experiment 2a). We conclude that Cl_2O only interacts with adsorbed $\text{H}_2\text{O}(\text{a})$ on a virgin surface. Nevertheless, surface-contaminating species may weaken the proposed screening of the NaCl-pairs and Cl^- becomes accessible for the reaction leading to Cl_2 (Reaction 4.8.1). This hypothesis is based on the observation of immediate release of Cl_2 on a contaminated substrate and the fact that the yield of Cl_2 tends to the double amount of the loss of Cl_2O after several experimental sequences.

Finally, uptake experiments of Cl_2O have been performed on a NaCl sprayed on gold-coated copper substrate. The NaCl sample has been heated to $T = 620 \text{ K}$ before carrying out the experiment (Table 4.9.2, Experiment 1). The Cl_2O uptake has led to a formation of Cl_2 . In contrast to a standard sample the mass balance between loss of Cl_2O and yield of Cl_2 has shown a one to one correspondence. As we already mentioned in section 4.7 heating the sample may lead to bulk diffusion (10) and chlorine ions may segregate to the surface of the sample, where they are accessible for reaction with Cl_2O (Reaction 4.8.1).

4.8.3. Conclusions

Uptake experiments of Cl_2O on NaCl substrates have been performed in a low-pressure flow reactor. The observed reaction products are Cl_2 and HOCl. The formation of HOCl is related to adsorbed $\text{H}_2\text{O}(\text{a})$ following reaction 4.6.4. On a fresh NaCl sample the mass balance has shown a one to one correspondence of the loss of Cl_2O with the formation of HOCl. This leads to an accumulation of chlorine species such as HOCl(a) on the NaCl surface. Experiments carried out at low concentration have not led to formation of Cl_2 . Subsequent uptake experiments on a contaminated NaCl surface have shown a ratio between lost Cl_2O and the formation of Cl_2 tending towards two with the number of uptake experiments. The release of gaseous Cl_2 is delayed when an experiment on a fresh substrate is carried out whereas on a contaminated NaCl sample the uptake of Cl_2O leads to a formation of Cl_2 immediately after lifting the plunger.

Similar to the HOCl/KBr system we propose the screening of the surface-ions due to adsorbed $\text{H}_2\text{O}(\text{a})$. The delayed release of Cl_2 and the increasing yield of Cl_2 has been explained by weakening of the protective screen of hydrated NaCl.

Furthermore, on heated samples Cl_2O may undergo direct ion-exchange reaction on the surface. Chloride-ions may segregate to the surface.

Uptake experiments of Cl_2O on thin films of NaCl sprayed on a Pyrex substrate have not led to an uptake of Cl_2O .

4.8.4. TablesTable 4.8.1: Typical experimental conditions for Cl₂O uptake experiments on NaCl grains and main results

No	Orifice diameter [mm]	[Cl ₂ O] [molecule cm ⁻³]	Experimental conditions	Main products	Minor products	Uptake kinetics	Remarks
1	4		Scan	Cl ₂			Mass-spectrometric scan of Cl ₂ O in the absence and the presence of NaCl grains
2a	14	1.3*10 ¹⁰	Steady-state uptake experiment on fresh sample	HOCl		$\gamma_0 = 8*10^{-2}$ $\gamma_{ss} = 3*10^{-2}$	No production of Cl ₂ , steady-state after 50s
2b	14	2*10 ¹⁰	Steady-state uptake experiment on contaminated sample	HOCl	Cl ₂	$\gamma_0 = 3*10^{-2}$	Slow formation of Cl ₂ sets in
2c	4	4*10 ¹¹	Steady-state uptake experiment on contaminated sample	Cl ₂		$\gamma_0 = 4*10^{-3}$	Formation of HOCl and Cl ₂
3	4	0.1-1*10 ¹²	Subsequent uptake experiments	HOCl			$\frac{N_{Cl_2}}{N_{Cl_2O}} \rightarrow 2, \frac{N_{HOCl}}{N_{Cl_2O}} \rightarrow 0$

Table 4.8.2: Typical experimental conditions for Cl₂O uptake experiments on thin NaCl films sprayed on a gold-coated copper substrate and main results

No	Orifice diameter [mm]	[Cl ₂ O] [molecule cm ³]	Experimental conditions	Main products	Minor products	Uptake kinetics	Remarks
1a	14	$3 \cdot 10^{11}$	Heated to T = 620 K	Cl ₂		$\gamma_0 = 6 \cdot 10^{-3}$	One to one correspondence of loss of Cl ₂ O and yield of Cl ₂
1b	4	$2 \cdot 10^{12}$	Heated to T = 620 K	Cl ₂		$\gamma_0 = 9 \cdot 10^{-4}$	One to one correspondence of loss of Cl ₂ O and yield of Cl ₂

4.9. Uptake Experiments of HOCl on NaCl

4.9.1. Introduction

Hypochlorous acid HOCl is a photochemically active compound. In the presence of light HOCl decays into active Cl and OH radicals. Both of them contribute to the oxidation capacity of the atmosphere (Sections 1.2 and 1.3) (48, 49).



Model studies of the troposphere predict a HOCl concentration up to 35ppt (28). However the tropospheric concentration of HOCl has not been confirmed by field measurements until now. Sources and sinks of HOCl are already described in section 4.7.1.

4.9.2. Results

Uptake experiments of HOCl on NaCl substrates have been performed in a low-pressure flow reactor. The experimental conditions and main results are listed in table 4.9.1.

HOCl uptake experiments on a thin NaCl film sprayed on a gold-coated substrate carried out in the 4mm- and 14-orifice reactor have not shown any uptake of HOCl where the sample has been pumped over night (Table 4.9.1, Experiment 1).

In order to investigate the role of adsorbed H₂O(a) an HOCl uptake experiment has been performed on a NaCl film sprayed on a gold-coated copper substrate pumped only for a short time. No uptake of HOCl has been observed in the 14mm-orifice reactor, on the contrary, a slow formation of HOCl has even been observed. A further HOCl uptake on

Chapter 4

the same NaCl sample carried out in the 4mm-orifice has led to formation of HOCl and Cl₂ (Table 4.9.1, Experiment 2). As discussed in section 4.8 the uptake of Cl₂O on NaCl leads to the mentioned reaction products so that we attribute these reaction products to the reaction of the Cl₂O impurity on NaCl.

Further experiments have been performed on thin NaCl films sprayed on a gold-coated copper substrate (Table 4.9.1, Experiment 3). Before carrying out the experiment the substrate has been heated to $T = 620$ K. Even under these conditions no uptake of HOCl on the NaCl substrate has been observed, neither in the 14mm- nor in the 4mm-orifice reactor. Nevertheless, uptake experiments performed in the 1mm-orifice reactor have shown a small uptake of HOCl without formation of a reaction product.

We conclude that the reaction of HOCl with interfacial Cl⁻ is very slow. This is in contrast to experiments of HOCl interacting with adsorbed HCl on ice surfaces (60).

4.9.3 Tables

Table 4.9.1: Typical experimental conditions for HOCl uptake experiments on NaCl substrates and main results

No	Orifice diameter [mm]	[HOCl] [molecule cm ⁻³]	Experimental conditions	Main products	Minor products	Uptake kinetics	Remarks
1a	14	$5 \cdot 10^{10}$	Thin film on gold coated copper substrate, pumped over night			n.u.	
1b	4	$5 \cdot 10^{11}$	Thin film on gold coated copper substrate, pumped over night			n.u.	
2a	14	$7 \cdot 10^{10}$	Thin film on gold coated copper substrate	HOCl		n.u.	Formation of HOCl, by reaction with Cl ₂ O and H ₂ O(a)
2b	4	$8 \cdot 10^{11}$	Thin film on gold coated copper substrate	HOCl		n.u.	Formation of HOCl and Cl ₂ , by reaction with Cl ₂ O and H ₂ O(a)
3a	14	$6 \cdot 10^{10}$	Thin film on gold coated copper substrate heated to T = 620K	Cl ₂		n.u.	Formation of Cl ₂ , by reaction with Cl ₂ O and H ₂ O(a)
3b	4	$6 \cdot 10^{11}$	Thin film on gold coated copper substrate heated to T = 620K	Cl ₂		n.u.	Formation of Cl ₂ , by reaction with Cl ₂ O and H ₂ O(a)
3c	1	$8 \cdot 10^{12}$	Thin film on gold coated copper substrate heated to T = 620K	Cl ₂		$\gamma = 2 \cdot 10^{-5}$	Formation of Cl ₂ , by reaction with Cl ₂ O and H ₂ O(a)

n.u. : no measurable uptake within the conditions of our experiment

4.10. General Discussion

Mechanistic and kinetic studies of chlorine- and bromine-containing compounds such as Cl_2 , Br_2 , BrCl , HCl , HOCl on KBr and NaCl substrates have been carried out in a low-pressure flow reactor in order to study release of halogen compounds and moreover, the conversion of gaseous chlorine- to gaseous bromine-containing compounds. This conversion may be a potential source for photochemically active bromine related to the bromine explosion mentioned in section 1.6. For a better understanding of this type of reaction, in particular the role of adsorbed water $\text{H}_2\text{O}(\text{a})$, the influence of surface defect sites, and the aspect of surface-contamination have been investigated.

The reactions of chlorine compounds with KBr lead to a substantial release of bromine compounds where the observed main product has been Br_2 . Furthermore, BrCl , HOBr and small amounts of BrOCl and Br_2O have been observed as well. In general, the formation of the gaseous reaction products occurs stepwise on the salt surface. This leads to the formation of various surface adsorbed intermediates which control the kinetics of the reactions. As the gaseous reaction products are in equilibrium with its adsorbed counterpart the kinetics of a reaction is thus strongly related with its gaseous environment. We have shown this influence by introducing additional Br_2 into the reactor while carrying out HOCl uptake experiments on solid KBr (see Section 4.7, Part A)).

In the case of HOCl we have suggested that no direct reaction with solid KBr occurs. We proposed a screening of the surface due to adsorbed $\text{H}_2\text{O}(\text{a})$. With this protective H_2O layer we may also explain the release of HOCl and the absence of Cl_2 at the beginning of an uptake experiment of Cl_2O on NaCl . Furthermore, we have shown that a sample heated up to $T = 620 \text{ K}$ becomes highly reactive which we also explained with the screening character of adsorbed $\text{H}_2\text{O}(\text{a})$. The protective H_2O layer may be weakened by adsorption of contaminating species and the reaction kinetics may change dramatically. In our case the contaminants have been chlorine- and bromine-containing species such as Br_2 , Cl_2 , HOCl and BrCl . It is conceivable that other contaminants such as nitrogen

Chapter 4

oxides or nitric acid also may influence the kinetics of reactions on salt substrates thereby weakening the screening effect of the H₂O layer.

Screening of the substrate is one role of adsorbed H₂O(a). We also noticed that samples containing more adsorbed H₂O(a) lead to larger yields of gaseous bromine-containing compounds. The adsorption of H₂O leads to hydration of the surface and may weaken the bond-strength of KBr or even dissolve it. The ions at the surface become mobile and surface migration is enabled.

Our detection technique only enables the observation of gas-phase species. Thus we do not know if the surface species are totally dissolved or present in form of ion-pairs. We have estimated that per molecule of KBr about 15 molecules of H₂O remain on the substrate. This led us to the suggestion that probably both dissolved KBr and ion-pairs may be present at the surface.

Furthermore, the yield of bromide on ground grains increases considerably whereas the amount of adsorbed H₂O(a) does not change significantly. Desorption experiments have shown a release of HOBr when the sample is heated to T = 620 K. We have suggested that a mechanical treatment of the substrate leads to the formation of molecular bromine on the surface, perhaps centered on lattice defects. The fact that no induction time in the reaction of HOCl on ground grains of KBr has been observed has led us to the conclusion that adsorbed molecular bromine is readily available in order to undergo a reaction with HOCl.

Figure 4.10.1 shows a schematic illustration of the KBr surface. A core of KBr is covered with an interfacial layer due to adsorbed H₂O(a). The interfacial layer hydrates the surface of the solid core but also may take up species from the gas-phase and retain them. We suggest that a reaction of the halogen species such as Cl₂, Cl₂O, BrCl and Br₂ only occurs through hydrated species which are located in the interfacial zone. Thus, the surface of KBr may also act in a catalytic way as we have shown with HOCl uptake experiments using an additional Br₂ flow.

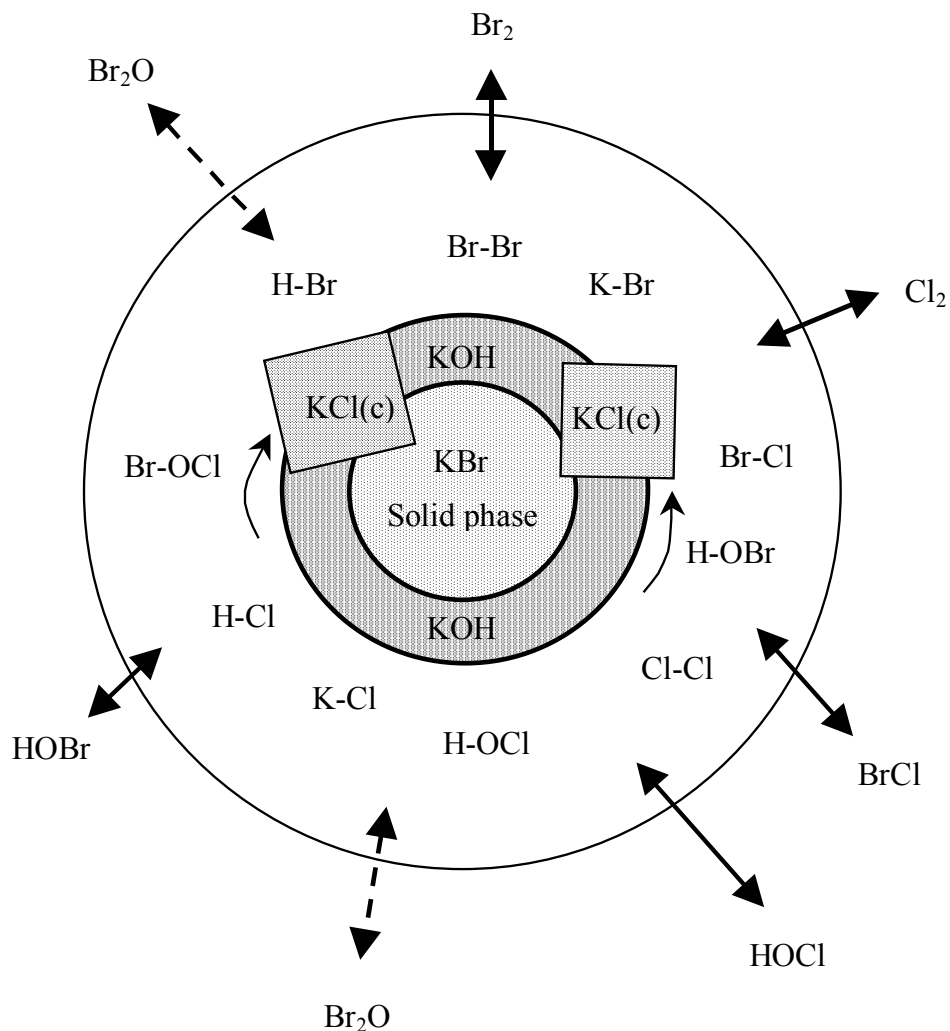


Figure 4.10.1: Schematic illustration of a KBr surface. The solid core of the particle is covered by an interfacial layer. The arrows represent the interaction between gas-phase and interfacial layer whereas minor products are represented by dashed arrows. The cubic forms on the core indicate crystallisation of KCl. The hyphen stands for hydration of the molecule.

The inner core of the KBr sample itself is screened by a protective layer of adsorbed H₂O(a) as indicated in figure 4.7.12. The protective layer may be destroyed by heating up the sample to $T = 620\text{K}$ as we have done. The sample has become highly reactive as a consequence.

4.11. References

- (1) Seinfeld J. H. and S. N. Pandis: *Atmospheric Chemistry and Physics*. (John Wiley & Sons, 1998).
- (2) Lad R. A.: *Adsorption of Water on Sodium Chloride - Effect of Prior Exposure to Hydrogen Chloride Carbon Dioxide and Water Vapor*. *Surface Science*, (1968), vol. 12, pp. 37-45.
- (3) Otterson D. A.: *Influence of Room-Temperature Atmospheric Reaction Products on Ductility of Sodium Chloride Single Crystals*. *Journal of Chemical Physics*, (1963), vol. 38, pp. 1481-1486.
- (4) Dai Q., J. Hu and M. Salmeron: *Adsorption of water on NaCl(100) surfaces: Role of atomic steps*. *Journal of Physical Chemistry B*, (1997), vol. 101, pp. 1994-1998.
- (5) Wassermann B., S. Mirbt, J. Reif, J. C. Zink and E. Matthias: *Clustered Water-Adsorption on the NaCl(100) Surface*. *Journal of Chemical Physics*, (1993), vol. 98, pp. 10049-10060.
- (6) Allen H. C., J. M. Laux, R. Vogt, B. J. Finlayson-Pitts and J. C. Hemminger: *Water-induced reorganization of ultrathin nitrate films on NaCl: Implications for the tropospheric chemistry of sea salt particles*. *Journal of Physical Chemistry*, (1996), vol. 100, pp. 6371-6375.
- (7) Beichert P. and B. J. Finlayson-Pitts: *Knudsen cell studies of the uptake of gaseous HNO₃ and other oxides of nitrogen on solid NaCl: The role of surface-adsorbed water*. *Journal of Physical Chemistry*, (1996), vol. 100, pp. 15218-15228.

Chapter 4

- (8) Davies J. A. and R. A. Cox: *Kinetics of the heterogeneous reaction of HNO₃ with NaCl: Effect of water vapor*. Journal of Physical Chemistry A, (1998), vol. 102, pp. 7631-7642.
- (9) Dai D. J., S. J. Peters and G. E. Ewing: *Water-Adsorption and Dissociation on NaCl Surfaces*. Journal of Physical Chemistry, (1995), vol. 99, pp. 10299-10304.
- (10) Harrison L. G., J. A. Morrison and G. S. Rose: *An Investigation of Chloride Ion Diffusion in Subsurface Layers of Sodium Chloride by an Isotopic Exchange Technique*. Journal of Physical Chemistry, (1957), vol. 61, pp. 1314-1318.
- (11) Harrison L. G., J. A. Morrison and R. Rudham: *Chloride Ion Diffusion in Sodium Chloride - Interactions between Point Imperfections at Low Temperatures*. Transactions of the Faraday Society, (1958), vol. 54, pp. 106-115.
- (12) Asada T. and K. Nishimoto: *Monte-Carlo Simulations of M(+)*Cl*(-)(H₂O)_n (M=Li, Na) Clusters and the Dissolving Mechanism of Ion-Pairs in Water*. Chemical Physics Letters, (1995), vol. 232, pp. 518-523.
- (13) Baranenko V. I., L. N. Falkovskii, V. S. Kirov, L. N. Kurnyk, A. N. Musienko and A. I. Piontkovskii: *Solubility of Oxygen and Carbon-Dioxide in Water*. Soviet Atomic Energy, (1990), vol. 68, pp. 342-346.
- (14) Gutzwiller L.: *Heterogeneous kinetics of some atmospherically relevant reactions. Experiments and modeling*. Thesis N^o 1527, (Ecole Polytechnique Fédérale de Lausanne (EPFL), 1996) pp. 167.
- (15) Jungwirth P.: *How many waters are necessary to dissolve a rock salt molecule?* Journal of Physical Chemistry A, (2000), vol. 104, pp. 145-148.

Chapter 4

- (16) Butman M. F., A. A. Smirnov, L. S. Kudin and Z. A. Munir: *Mass spectrometric study of the vaporization kinetics of potassium bromide single crystals*. Journal of Materials Synthesis and Processing, (2000), vol. 8, pp. 55-63.
- (17) Kittel C.: *Einführung in die Festkörperphysik*. (R. Oldenbourg Verlag, 1993) pp. 733.
- (18) Atkins P. W.: *Physical Chemistry*. (Oxford University Press, 1998) pp. 1014.
- (19) Engkvist O. and A. J. Stone: *Adsorption of water on the NaCl(001) surface. III. Monte Carlo simulations at ambient temperatures*. Journal of Chemical Physics, (2000), vol. 112, pp. 6827-6833.
- (20) Foster M. and G. E. Ewing: *An infrared spectroscopic study of water thin films on NaCl (100)*. Surface Science, (1999), vol. 428, pp. 102-106.
- (21) Vodopyanov K. L.: *Saturation Studies of H₂O and HDO near 3400 cm⁻¹ Using Intense Picosecond Laser-Pulses*. Journal of Chemical Physics, (1991), vol. 94, pp. 5389-5393.
- (22) NIST-Chemistry-WEBBook: *NIST Chemistry WEBBook*.
- (23) Graedel T. E. and W. C. Keene: *Tropospheric Budget of Reactive Chlorine*. Global Biogeochemical Cycles, (1995), vol. 9, pp. 47-77.
- (24) Fenter F. F., F. Caloz and M. J. Rossi: *Kinetics of Nitric-Acid Uptake by Salt*. Journal of Physical Chemistry, (1994), vol. 98, pp. 9801-9810.
- (25) Finlayson-Pitts B. J.: *Chemistry of the Upper and Lower Atmosphere*. (Academic Press, 2000) pp. 969.

Chapter 4

- (26) Spicer C. W., E. G. Chapman, B. J. Finlayson-Pitts, R. A. Plastridge, J. M. Hubbe, J. D. Fast and C. M. Berkowitz: *Unexpectedly high concentrations of molecular chlorine in coastal air*. *Nature*, (1998), vol. 394, pp. 353-356.
- (27) Finlayson-Pitts B. J.: *Chlorine Atoms as a Potential Tropospheric Oxidant in the Marine Boundary-Layer*. *Research on Chemical Intermediates*, (1993), vol. 19, pp. 235-249.
- (28) Vogt R., P. J. Crutzen and R. Sander: *A mechanism for halogen release from sea-salt aerosol in the remote marine boundary layer*. *Nature*, (1996), vol. 383, pp. 327-330.
- (29) Foster K. L., R. A. Plastridge, J. W. Bottenheim, P. B. Shepson, B. J. Finlayson-Pitts and C. W. Spicer: *The role of Br₂ and BrCl in surface ozone destruction at polar sunrise*. *Science*, (2001), vol. 291, pp. 471-474.
- (30) Wennberg P.: *Atmospheric chemistry - Bromine explosion*. *Nature*, (1999), vol. 397, pp. 299-301.
- (31) Finlayson-Pitts B. J. and J. C. Hemminger: *Physical chemistry of airborne sea salt particles and their components*. *Journal of Physical Chemistry A*, (2000), vol. 104, pp. 11463-11477.
- (32) Ghosal S. and J. C. Hemminger: *Effect of water on the HNO₃ pressure dependence of the reaction between gas-phase HNO₃ and NaCl surfaces*. *Journal of Physical Chemistry A*, (1999), vol. 103, pp. 4777-4781.
- (33) Weast R. C.: *Handbook of Chemistry and Physics*. (CRC Press, 1986).

Chapter 4

- (34) Wagman D. D., W. H. Evans, V. B. Parker, R. H. Schumm, I. Halow, S. M. Bailey, K. L. Churney and R. L. Nuttal: *The NBS tables of chemical thermodynamic properties*. (American Chemical Society, 1982), vol. 11.
- (35) Laux J. M., T. F. Fister, B. J. FinlaysonPitts and J. C. Hemminger: *X-ray photoelectron spectroscopy studies of the effects of water vapor on ultrathin nitrate layers on NaCl*. *Journal of Physical Chemistry*, (1996), vol. 100, pp. 19891-19897.
- (36) Degreve L. and F. L. B. da Silva: *Large ionic clusters in concentrated aqueous NaCl solution*. *Journal of Chemical Physics*, (1999), vol. 111, pp. 5150-5156.
- (37) Mochida M., J. Hirokawa, Y. Kajii and H. Akimoto: *Heterogeneous reactions of Cl₂ with sea salts at ambient temperature: Implications for halogen exchange in the atmosphere*. *Geophysical Research Letters*, (1998), vol. 25, pp. 3927-3930.
- (38) Galwey A. K. and L. Poppl: *The Role of Liquid Halogen in the Reaction of Crystalline KBr with Gaseous Cl₂*. *Nature*, (1981), vol. 294, pp. 434-436.
- (39) Berko H. N., P. C. McCaslin and B. J. Finlayson-Pitts: *Formation of Gas-Phase Bromine Compounds by Reaction of Solid NaBr with Gaseous ClONO₂, Cl₂, and BrCl at 298 K*. *Journal of Physical Chemistry*, (1991), vol. 95, pp. 6951-6958.
- (40) Boule P.: *Environmental Photochemistry*. (Springer-Verlag, 1999) pp. 359.
- (41) Hausmann M. and U. Platt: *Spectroscopic Measurement of Bromine Oxide and Ozone in the High Arctic During Polar Sunrise Experiment 1992*. *Journal of Geophysical Research-Atmospheres*, (1994), vol. 99, pp. 25399-25413.

Chapter 4

- (42) Koch T. G., F. F. Fenter and M. J. Rossi: *Real-time measurement of residence times of gas molecules on solid surfaces*. Chemical Physics Letters, (1997), vol. 275, pp. 253-260.
- (43) Aguzzi A. and M. J. Rossi: *The kinetics of the heterogeneous reaction of BrONO₂ with solid alkali halides at ambient temperature. A comparison with the interaction of ClONO₂ on NaCl and KBr*. Physical Chemistry Chemical Physics, (1999), vol. 1, pp. 4337-4346.
- (44) Ciccotti G., M. Ferrario, J. T. Hynes and R. Kapral: *Constrained Molecular-Dynamics and the Mean Potential for an Ion-Pair in a Polar-Solvent*. Chemical Physics, (1989), vol. 129, pp. 241-251.
- (45) Degreve L. and F. L. B. da Silva: *Structure of concentrated aqueous NaCl solution: A Monte Carlo study*. Journal of Chemical Physics, (1999), vol. 110, pp. 3070-3078.
- (46) Cooper M. J., P. J. Jackson, L. J. Rogers, A. J. Orr-Ewing and B. J. Whitaker: *Ion imaging studies of the ²Cl(P_j) and ²Br(P_j) atomic products resulting from BrCl photodissociation in the wavelength range 235-540 nm*. Journal of Chemical Physics, (1998), vol. 109, pp. 4367-4377.
- (47) Bartlett W. P. and D. W. Margerum: *Temperature dependencies of the Henry's Law constant and the aqueous phase dissociation constant of bromine chloride*. Environmental Science & Technology, (1999), vol. 33, pp. 3410-3414.
- (48) Burkholder J. B.: *Ultraviolet-Absorption Spectrum of HOCl*. Journal of Geophysical Research-Atmospheres, (1993), vol. 98, pp. 2963-2974.
- (49) Molina L. T. and M. J. Molina: *Ultraviolet-Spectrum of HOCl*. Journal of Physical Chemistry, (1978), vol. 82, pp. 2410-2414.

Chapter 4

- (50) Knight G. P., T. Beiderhase, F. Helleis, G. K. Moortgat and J. N. Crowley: *Reaction of HO₂ with ClO: Flow tube studies of kinetics and product formation between 215 and 298 K*. Journal of Physical Chemistry A, (2000), vol. 104, pp. 1674-1685.
- (51) Knipping E. M., M. J. Lakin, K. L. Foster, P. Jungwirth, D. J. Tobias, R. B. Gerber, D. Dabdub and B. J. Finlayson-Pitts: *Experiments and simulations of ion-enhanced interfacial chemistry on aqueous NaCl aerosols*. Science, (2000), vol. 288, pp. 301-306.
- (52) Wilson M. A. and A. Pohorille: *Interaction of Monovalent Ions with the Water Liquid Vapor Interface - a Molecular-Dynamics Study*. Journal of Chemical Physics, (1991), vol. 95, pp. 6005-6013.
- (53) Brown A. R. and D. J. Doren: *HOCl adsorption on ice surfaces*. Journal of Physical Chemistry B, (1997), vol. 101, pp. 6308-6312.
- (54) Dibble T. S. and J. S. Francisco: *Ab-Initio Study of the Structure, Binding-Energy, and Vibrations of the HOCl-H₂O Complex*. Journal of Physical Chemistry, (1995), vol. 99, pp. 1919-1922.
- (55) Geiger F. M., J. M. Hicks and A. C. de Dios: *Ab initio study of HOCl, HCl, H₂O, and Cl₂ interacting with four water molecules*. Journal of Physical Chemistry A, (1998), vol. 102, pp. 1514-1522.
- (56) Zhou Y. F. and C. B. Liu: *Theoretical study of HOCl adsorption on ice surface*. Journal of Physics and Chemistry of Solids, (1999), vol. 60, pp. 2001-2004.

Chapter 4

- (57) Perera L. and M. L. Berkowitz: *Many-Body Effects in Molecular-Dynamics Simulations of $\text{Na}^+(\text{H}_2\text{O})_n$ and $\text{Cl}^-(\text{H}_2\text{O})_n$ Clusters*. Journal of Chemical Physics, (1991), vol. 95, pp. 1954-1963.
- (58) Petersen C. P. and M. S. Gordon: *Solvation of sodium chloride: An effective fragment study of $\text{NaCl}(\text{H}_2\text{O})_n$* . Journal of Physical Chemistry A, (1999), vol. 103, pp. 4162-4166.
- (59) Estel J., H. Hoinkes, H. Kaarmann, H. Nahr and H. Wilsch: *Problem of Water Adsorption on Alkali-Halide Cleavage Planes, Investigated by Secondary Ion Mass-Spectroscopy*. Surface Science, (1976), vol. 54, pp. 393-418.
- (60) Oppliger R.: *Kinetics Studies of heterogeneous Reactions of chlorine and bromine Reservoirs relevant to the lower Stratosphere*. Thesis N° 1779, (1998) pp. 161.

Chapter 5

5. Preparation of Mineral Dust and Acidic Samples

In this section we describe the sample preparation of the samples used for the experiments of acidic compounds on mineral dust.

5.1. Gaseous Samples

CO₂ and SO₂ are stored in gas-bottles and we used it without any special purification procedures. A mass spectrometric scan has not shown any traces of impurities at the detection limit of the mass spectrometer.

The preparation of HCl has already been described in chapter 3 section 3.1.1.

5.1.1. Preparation of HNO₃

HNO₃ has been prepared by mixing liquid HNO₃ (Fluka) with liquid H₂SO₄ (Fluka) in a volume ratio of 1:3. Liquid H₂SO₄ has been used as stabiliser because of its low vapour pressure at ambient temperature. The purity of HNO₃ and H₂SO₄ is at least 99.5% and 95%, respectively (data sheet of the supplier).

Before carrying out the first experiment of the day the stabilised HNO₃ has been purged bubbling through gaseous nitrogen N₂ for ten minutes or so.

The mass spectrometric parent peak of HNO₃ is at m/e = 46 (100). Fragment peaks are at m/e = 30 (60) and m/e = 63 (1). The values in the brackets mean the percentage of the signal relative to the main peak.

5.2. Solid Samples

5.2.1. Precipitated CaCO₃

The uptake experiments described in section 6 have been carried out on two types of precipitated calcium carbonate CaCO₃.

The CaCO₃, named in the following “high-ordered CaCO₃”, was supplied by Merck and has been stocked for 5 or 6 years in the laboratory under ambient conditions. Figure 6.1.1 shows a SEM-image of high-ordered CaCO₃. The purity is better than 99.5%.

The BET surface we have measured is 3.7 m²g⁻¹. The BET measurements are performed under conditions described in Appendix A, Table A.1.

The density of the CaCO₃ powder ρ_p has been calculated by measuring the weight of a known volume of CaCO₃ results in ρ_p = 1.3 g cm⁻³. The true density of CaCO₃ is ρ = 2.9 g cm⁻³ (1). When we calculate the diameter of a CaCO₃ using the BET surface and the density of CaCO₃ in equation 3.2.4 we obtain a particle diameter d of 0.5 μm.

$$A_S = \frac{A_V}{\rho_g} = 6 \frac{1}{\rho_c d} \quad (\text{equation 3.2.4})$$

A comparison with the SEM-image of Figure 6.1.1 suggests that the particle diameter d is underestimated in this approximation. This may be attributed to the roughness of the sample surface (Figure 5.1.1). A spherical particle has a smaller surface than a non spherical particle with the same diameter. This fact leads to an underestimation of the diameter d using equation 3.2.4.

On high-ordered CaCO₃ the amount of adsorbed H₂O(a) has been measured to be 4 mg g⁻¹ at ambient conditions (rh = 33% and ϑ = 21°C). The experimental conditions are described in

Appendix B, Table B.1. The number surface density n_s of CaCO_3 is $n_s = 6.7 \cdot 10^{14} \text{ molecule cm}^{-2}$ which has been calculated using equation 3.2.5 and $M_A = 100 \text{ gmol}^{-1}$ (2).

$$n_s = \frac{2}{3} \sqrt{\frac{\rho_V}{M_A} N_A} \quad (\text{equation 3.2.5})$$

Using the BET surface the total number of interfacial molecules N results in $N = 2.5 \cdot 10^{19}$ molecule. 4 mg of H_2O correspond to $1.3 \cdot 10^{20}$ molecule, therefore under ambient conditions about 5 monolayers (with respect to CaCO_3) of $\text{H}_2\text{O(a)}$ are adsorbed on CaCO_3 .

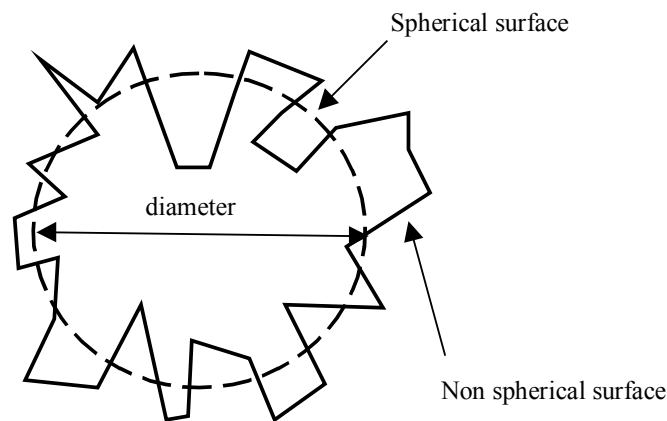


Figure 5.1.1: Two-dimensional schematic illustration of the surface of a spherical and a non-spherical particle.

The precipitated CaCO_3 is called in the following “low-ordered CaCO_3 ” and was supplied by Fluka. Figure 6.3.7 shows a SEM-image a of low-ordered precipitated CaCO_3 sample. The measured BET surface is $5.1 \text{ m}^2\text{g}^{-1}$ (Appendix A, Table A.1).

5.2.2. Roughened and Polished Marble

Cylindrical marble bars were sawed up into disks of a thickness of approximately 5mm. The used marble comes from Carrara which is noted for the purity of its marble. The obtained marble disks are in the following named roughened marble plates referring to the rough

surface of the plates. In order to dry the plates they have been heated in an oven at $T = 330 \text{ K}$ for 24 h.

Some of the plates have been polished using grinding paper. In order to obtain a flat surface the grinding paper has been fixed on a polished steel plate and the marble plates have been moved across the grinding paper by carrying out a circular movement. The used grinding paper has been changed subsequently from a coarse grained to a finer grained paper. The final roughness has been $6 \mu\text{m}$.

The diameter of the plates is 5cm. This results in a geometrical surface of $A_s = 47 \text{ cm}^2$ taking into account also the lateral area of the plate as well as both fores.

5.2.3. Various Mineral Dusts

Kaolinite and Arizona Road Dust (ARD) are commercially available mineral dusts. The Kaolinite dust was obtained from the Source Clays Repository of the University of Missouri. The ARD was supplied by Ken Ellis & Son LTd T/A, Ellis Components. The Saharan Dust comes originally from a deposit located on the Cap Verde Islands and is not commercially available. It has been given to us by J. Crowley from the Max Planck Institute for Chemistry in Mainz.

The chemical composition of the dust components are listed in Table 5.2.1.

Table 5.2.1: Chemical composition of Kaolinite and Arizona Road Dust The data are given by the supplier.

Chemical	Kaolinite low- / high-defect [% of weight]	Arizona Road Dust [% of weight]
SiO ₂	44.2 / 43.9	68-76
Al ₂ O ₃	39.7 / 38.5	10-15
Fe ₂ O ₃	0.13 / 0.98	2-5
Na ₂ O	0.013 / < 0.005	2-4
CaO		2-5
MgO	0.03 / 0.03	1-2
TiO ₂	1.39 / 2.08	0.5-1
K ₂ O	0.05 / 0.065	2-5
FeO	0.08 / 0.15	
P ₂ O ₅	0.034 / 0.045	

The BET surfaces are listed in Appendix A, Table A1. The amount of adsorbed H₂O at ambient conditions is listed in Appendix B, Table B1.

ARD with two different size distributions has been used. The mean particle size of coarse and medium grade is 25 μm and 12 μm, respectively.

5.3. References

- (1) Weast R. C.: *Handbook of Chemistry and Physics*. (CRC Press, 1986).
- (2) NIST-Chemistry-WEBBook: *NIST Chemistry WEBBook*.

Chapter 6

6. Reactions of Acidic Compounds on Mineral Dust

In this chapter uptake experiments of acidic compounds on a variety of mineral dust samples have been performed using a low-pressure flow reactor. The experiments have been focused on CaCO_3 samples such as precipitated CaCO_3 and Carrara marble plates. As well a few uptake experiments have been carried out on Saharan dust, Kaolinite and Arizona Road Dust.

6.1. H_2O on CaCO_3

6.1.1. Introduction

On earth water is present in the solid, liquid and gaseous phase. Consequently, it is an ubiquitous atmospheric constituent. H_2O is a potent greenhouse gas whose

concentration is highly variable in the troposphere owing to its short life-time (Table 1.1.2). The total mass of atmospheric H₂O has been estimated to be on the order of 1.3×10^{16} kg (2).

Water is necessary not only for many biological processes but plays also an important role in the atmosphere amongst which also in heterogeneous chemical reactions as we have already seen in Chapter 4. Together with O₃ and photons H₂O is involved in the formation of hydroxyl radicals OH (reactions 1.2.5 and 1.2.6) which is the main oxidant in the troposphere.

Calcium is a metallic element and the fifth element in abundance in the earth's crust (3) to which it contributes approximately 3.5% by weight. Calcium does not occur as a pure element in the earth's crust but rather as a compound whose most important representative is calcium carbonate, CaCO₃. A particular modification of calcium carbonate is limestone which is a common building material since classical antiquity. The pyramids were built with limestone by the Egyptians. Limestone is formed by sedimentation of CaCO₃ in the ocean.

The most stable form of calcium carbonate is calcite. It is formed in caves where lime-containing water flows. Aragonite is similar to calcite but is less durable.

Another common mineral of calcium carbonate is marble. Marble is formed from limestone under high pressure. The most famous occurrence of marble is found in Italy near Carrara. Already the Romans used Carrara marble as a building material.

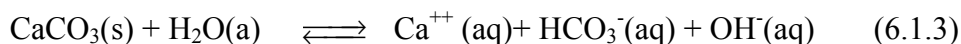
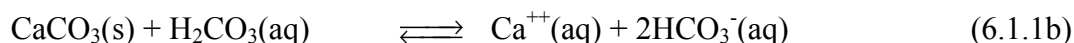
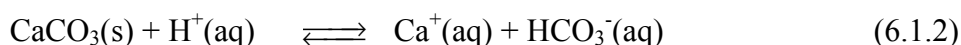
Carbonates tend to be highly porous. Porosity is defined as the amount of water held per volume of aquifer material; this is expressed as a percentage. For example 25% porosity means that one cubic centimetre of aquifer holds 0.25 cubic centimetre of water. If all the porosity volume is filled with water, the rock is termed water-saturated. For marble the porosity attains approximately 0.5-1% whereas limestone may reach values of as much as 45% (4). This implies that calcium carbonates may contain large amounts of liquid water.

Calcium carbonate is very little soluble in H₂O. For example, the solubility for calcite is 1.4*10⁻³ g l⁻¹ but CaCO₃ in contact with H₂O and CO₂ is in equilibrium with Calcium and bicarbonate ions:



Equilibrium 6.1.1a is involved in karst dissolution and plays an important role in global carbon cycles (5). The CO₂ may originate from gaseous CO₂ present in ambient air.

In general, CaCO₃ dissolves more easily in contact with an acidified water solution (4, 6). The overall reaction leading to the dissolution of calcium carbonate is described by the following reactions (7):



Reactions 6.1.1-6.1.3 indicate that H₂O plays an important role for the reactions of CaCO₃ with acids like HCl and HNO₃ which we are going to present in this chapter.

6.1.2. Results

Surface adsorbed H₂O plays a crucial role for the heterogeneous reactions of acidic components on CaCO₃ surfaces. Desorption experiments have been carried out in order to estimate the adsorbed H₂O on the CaCO₃ sample. Furthermore, images using Scanning Electron Microscopy (SEM) have been taken in order to characterise the substrate. Figure 6.1.1 shows a SEM-image of precipitated CaCO₃.

In order to minimise additional H₂O desorbing from the sample holder a gold-coated sample-holder has been used. Its description is given in Section 2.3. Before the experiments had been performed a reference experiment was carried out on a bare

sample-holder. The bare gold-coated sample-holder was pumped for 30 minutes before it had been heated to $T = 600$ K. An amount of $2 \cdot 10^{16}$ molecule of adsorbed H_2O has been measured in the desorption experiment which corresponds to less than 1% of the amount of $\text{H}_2\text{O}(\text{a})$ on CaCO_3 (see below).

For the desorption experiments the following protocol has been applied:

- 1) Pumping of a fresh sample of 1g of precipitated CaCO_3 for a given time t_p at ambient temperature T in the 14mm-orifice reactor.
- 2) Heating of the sample to $T = 470$ K and recording the MS-signal of H_2O at $m/e = 18$ until it reached the background level.
- 3) Integration and calibration of the MS-signal.

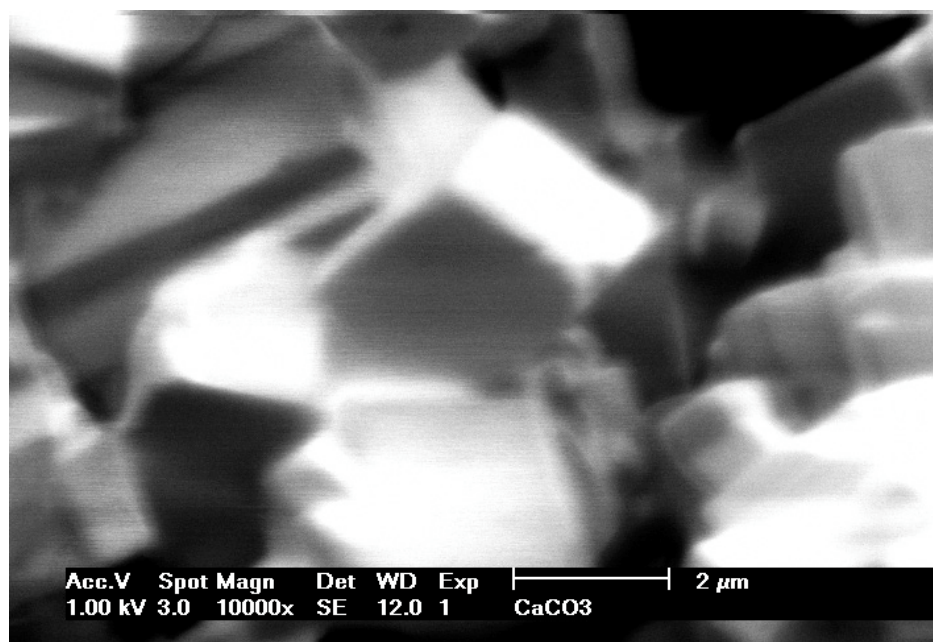


Figure 6.1.1: SEM-image of precipitated CaCO_3 . The sample has been stocked for 5 to 6 years in our laboratory at ambient conditions.

Figures 6.1.2 and 6.1.3 show the MS-signals of such an experiment and the quantity of adsorbed H_2O as a function of pumping time t_p , respectively. Using the BET surface area (Appendix A, Table A.1) of $3.7 \text{ m}^2 \text{ g}^{-1}$ a number on the order of $3 \cdot 10^{13} \text{ molecule cm}^{-2}$ has been calculated for the surface density of adsorbed $\text{H}_2\text{O}(\text{a})$.

In order to measure the amount of H_2O adsorbed on CaCO_3 at ambient condition a known amount of CaCO_3 has been introduced into a metallic tube. The tube including CaCO_3 had been weighed before it was connected to the 14mm-reactor. Subsequently, the tube was heated using a hot air gun and the desorbing H_2O monitored by MS. After the MS-signal of H_2O had reached the background level the tube had been kept under vacuum, removed from the reactor and weighed again.

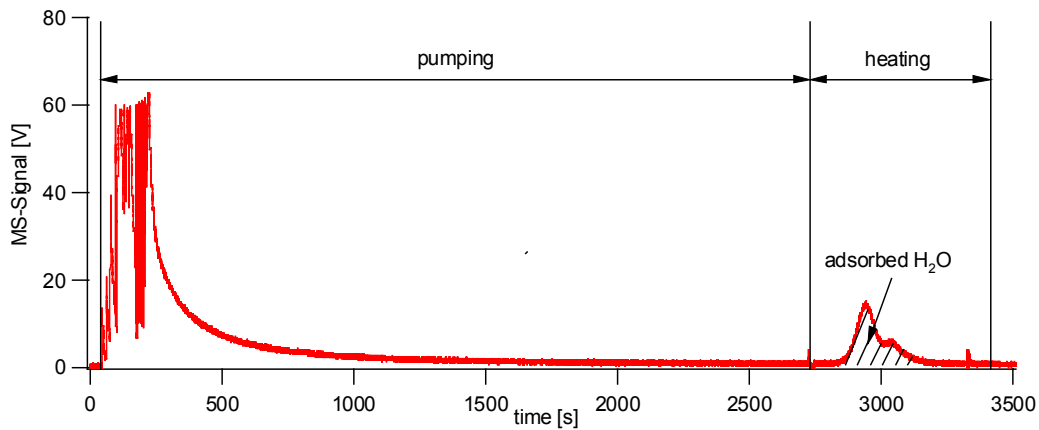


Figure 6.1.2: MS-signal of a pump and heating experiment. A sample of precipitated CaCO_3 has been pumped at ambient temperature prior to heating to $T = 470 \text{ K}$.

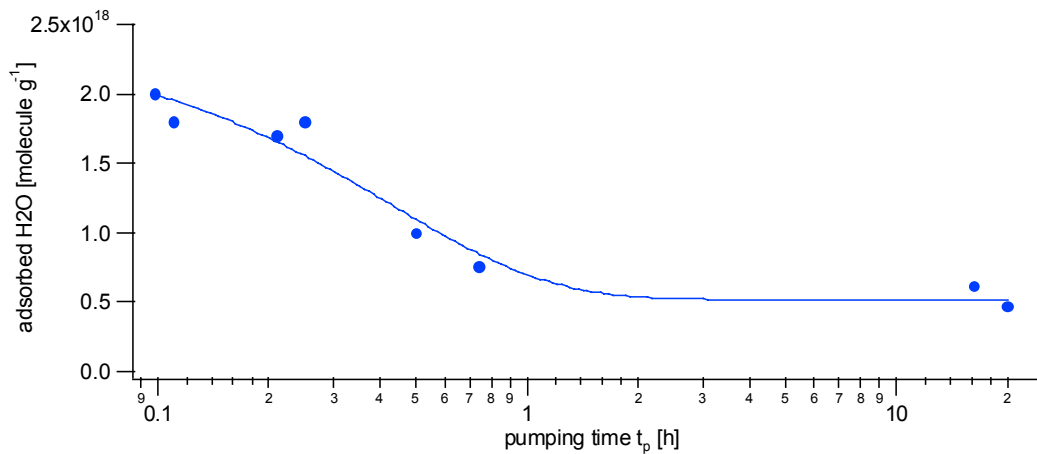


Figure 6.1.3: Adsorbed H_2O on precipitated CaCO_3 as a function of pumping time t_p using the 14mm-orifice reactor.

The difference in weight indicates the amount of adsorbed H_2O that could be removed by the combined action of pumping and heating. For precipitated CaCO_3 an amount of 4 mg of $\text{H}_2\text{O} \text{ g}^{-1}$ of CaCO_3 has been measured for a temperature $\vartheta = 21^\circ\text{C}$ and a

relative humidity of 33%. Using the BET area from Appendix A, Table A.1 leads to a surface density of $4 \cdot 10^{15}$ molecule cm^{-2} . As we may see from Figure 6.1.3 only $2 \cdot 10^{18}$ molecule corresponding to $5 \cdot 10^{13}$ molecule cm^{-2} remain on the surface after 5 minutes of pumping time which corresponds to about 1 or 2% of the adsorbed water at ambient temperature. This suggests that most of the adsorbed H_2O is weakly bound and may be removed by pumping the surface. The nominal surface density of CaCO_3 has been calculated to be $6.7 \cdot 10^{14}$ molecule cm^{-2} (Section 5.2.1). This means that the surface coverage of adsorbed H_2O compared to the surface density of CaCO_3 corresponds to less than 10% after 5 minutes of pumping time.

6.2. Uptake Experiments of CO_2 on CaCO_3

6.2.1. Introduction

Carbon dioxide CO_2 is an important greenhouse gas. Concentration and lifetime in the atmosphere are given in Table 1.1.1.

In liquid systems CO_2 plays an important role in the dissolution of carbonate minerals (reaction 6.1.1a) (8, 6) which again plays an important role in the global carbon cycle (5).

Furthermore, CO_2 is a reaction product of reactions of acidic compounds with calcium carbonate mineral dust. In order to investigate the influence of CO_2 on reactions with gaseous compounds leading to acids upon contact with H_2O a few uptake experiments of CO_2 with CaCO_3 have been performed in the low-pressure flow reactor.

In order to investigate the surface of calcium carbonate substrates we used CO_2 as a probe molecule for basic sites on the solid CaCO_3 .

6.2.2. Results and Discussion

Uptake experiments of CO_2 on precipitated CaCO_3 have been performed. Figure 6.2.1 shows a typical uptake experiment carried out in the 1mm-orifice reactor. The detailed

experimental conditions are listed in Table 6.2.1, Experiment 1. After halting the CO_2 -inflow and reopening the sample compartment partial desorption of CO_2 has been observed at a ratio $\frac{\text{loss}}{\text{recovery}} = \frac{4}{1}$. The fact that only 25% of the integral amount of the adsorbed CO_2 molecules are recovered may suggest a fast adsorption and a slower secondary reaction of CO_2 on the surface via an intermediate species.

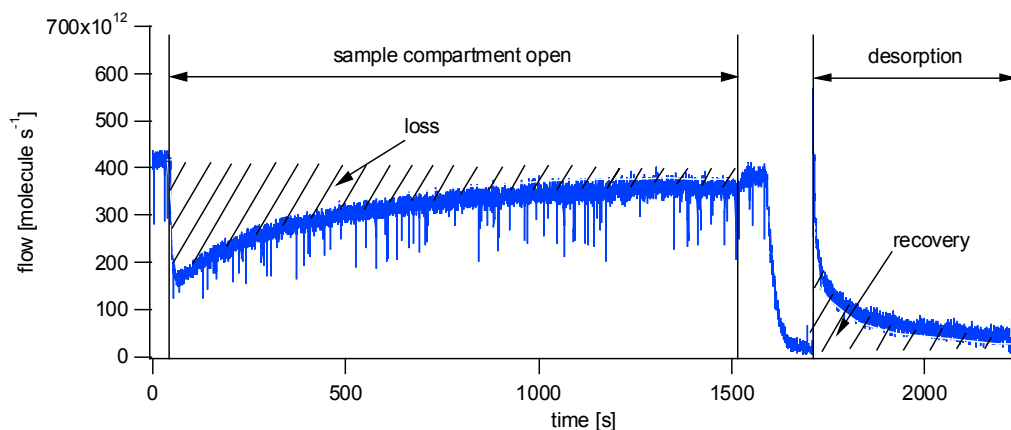


Figure 6.2.1: Typical mass-spectrometric signal of an uptake experiment of CO_2 on 30g of precipitated CaCO_3 carried out in the 1mm-orifice reactor. For desorption of CO_2 the 14mm-orifice has been used. The amount of adsorbed H_2O is approximately $3 \cdot 10^{19}$ molecule estimated using the curve in Figure 6.1.3. CO_2 has been monitored at $m/e = 44$.

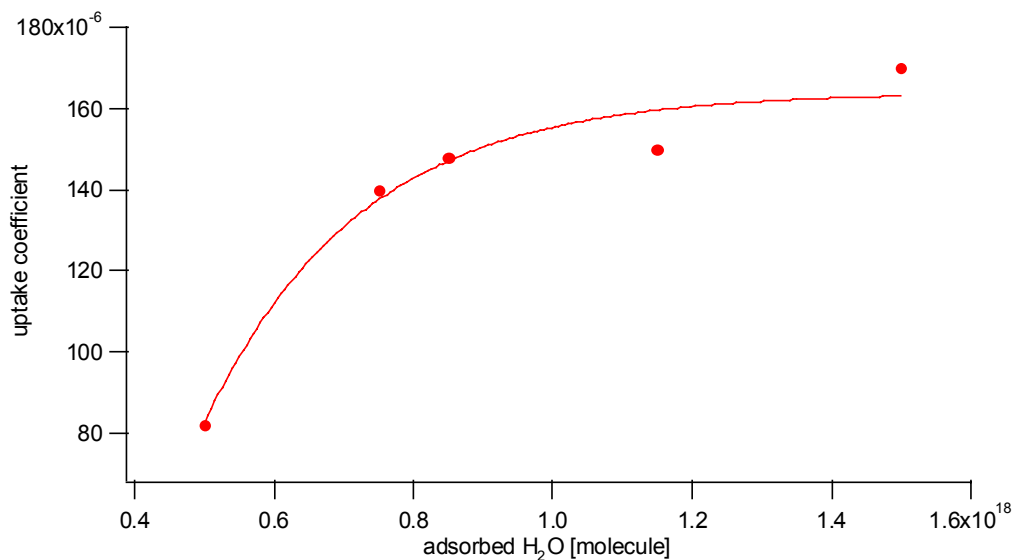
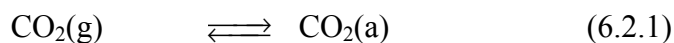


Figure 6.2.2: Initial uptake coefficient γ_0 of the reaction of CO_2 with 1g precipitated CaCO_3 as a function of the amount of adsorbed H_2O . Experimental details are listed in Table 6.2.1, Experiment 2.



In order to investigate the influence of adsorbed H_2O on the reaction kinetics uptake experiments of CO_2 on precipitated CaCO_3 at different pumping times have been performed. The amount of adsorbed H_2O has been calibrated with the help of Figure 6.1.3. Figures 6.2.2 and 6.2.3 show a graph of the initial uptake coefficient and the total loss of CO_2 , respectively. The experiments have been carried out in the 1mm-orifice reactor for adsorption and for desorption the 14mm-orifice reactor has been used. The experimental conditions are listed in Table 6.2.1, Experiment 2. The initial uptake and the total loss of CO_2 increase with the amount of adsorbed H_2O . This means that the number of reactive sites is related to the amount of adsorbed H_2O . Furthermore, both the partial recovery of adsorbed CO_2 as well as the total amount of adsorbed CO_2 as displayed in Figure 6.2.1 also increases with the amount of adsorbed

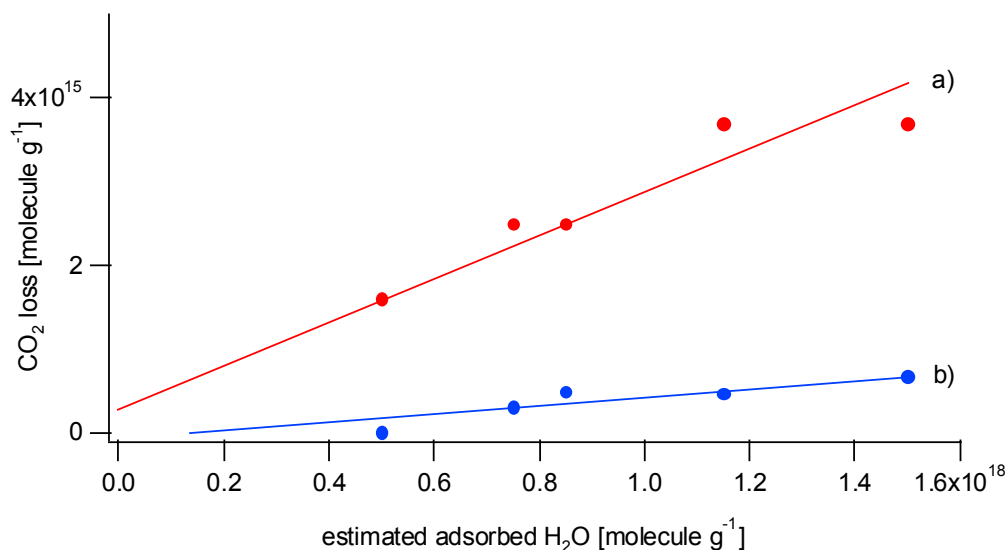
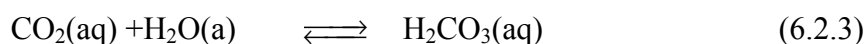


Figure 6.2.3: The total amount of CO_2 taken up a) and the recovered amount b) of CO_2 interacting with 1 g of precipitated CaCO_3 in the 1mm-orifice reactor at $[\text{CO}_2] = 7 \cdot 10^{12} \text{ molecule cm}^{-3}$. The experimental details are listed in Table 6.2.1, experiment 2. The difference between a) minus b) indicates the amount of CO_2 permanently adsorbed on the sample.

H₂O. Figure 6.2.3 shows the partial recovery and the total amount of adsorbed CO₂ as a function of the quantity of adsorbed H₂O. Before the partial recovery of adsorbed CO₂ the sample chamber had been closed for $t_w = 90$ s. The data shown in Figure 6.2.3 suggest that the net loss of CO₂ (trace a)- trace b)) is linearly related to the amount of adsorbed H₂O. The fact that the amount of recovered CO₂ is linearly dependent on the amount of H₂O(a) suggests that the number of surface sites which lead to an adsorption of CO₂ are strongly related to the amount of adsorbed H₂O.

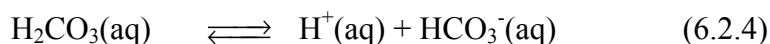
It is known that CO₂ dissolves in aqueous solution of H₂O according to equilibrium 6.2.3. Most of the dissolved CO₂ remains in the form of dissolved gas CO₂(aq) (9, 10) rather than as rearranged carbonic acid according to equilibrium 6.2.3. Less than 1% occurs as truly hydrated H₂CO₃(aq) (11).



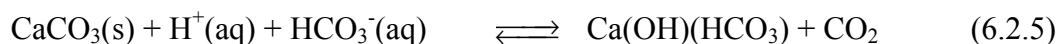
Reaction 6.2.3 follows a true first order rate law with the rate constant $k = 3 \cdot 10^{-3} \text{ sec}^{-1}$ at 25°C (12) which means that it is rather a sluggish reaction.

The fact that the amount of recoverable CO₂ linearly depends on the amount of adsorbed water suggests that equilibrium 6.2.3 may be a potential surface buffer for adsorbed CO₂.

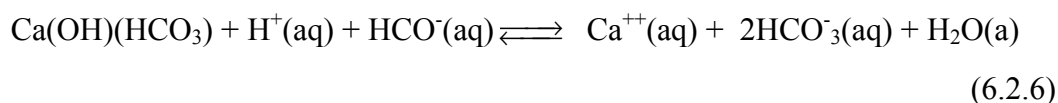
Furthermore, H₂CO₃ may very quickly dissociate according to equilibrium 6.2.4 (12)



whose bicarbonate ion HCO₃⁻ may finally react with CaCO₃ to yield a surface intermediate that is proposed to be the surface reactant for the heterogeneous reactions discussed below.

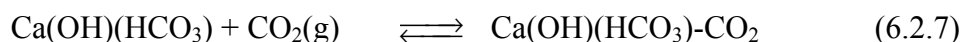


The product of reaction 6.2.5 may undergo a further reaction which leads to calcium bicarbonate $\text{Ca}(\text{HCO}_3)_2$ which is only stable in solution.

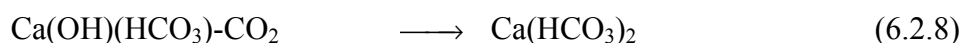


For water solutions the Henry's law constant for CO_2 is $K_H = 0.035 \text{ mol l}^{-1} \text{ bar}^{-1}$ (13). At a CO_2 concentration of $7 \cdot 10^{12} \text{ molecule cm}^{-3}$, which corresponds to a pressure of 30 mPa, $6.3 \cdot 10^{15}$ molecule of CO_2 per litre of H_2O are expected to dissolve based on Henry's law. At the CO_2 concentration in the flow reactor the measured amount of adsorbed CO_2 on CaCO_3 is on the order of $7 \cdot 10^{14}$ molecule (Figure 6.2.3), which would, based on Henry's law, correspond to 0.1 litre or $3.3 \cdot 10^{24}$ molecules of H_2O adsorbed on 1g of CaCO_3 . Compared to the measured amount of $1.6 \cdot 10^{18} \text{ molecule g}^{-1}$ of H_2O , adsorbed on CaCO_3 as presented before (Figure 6.2.3) the amount of H_2O necessary to dissolve the measured quantity of CO_2 according to Henry's law is more than six orders of magnitudes too large. Therefore, the quantity of H_2O adsorbed can not explain the amount of CO_2 adsorbed on the surface. In other words, there must be an additional process other than dissolution of CO_2 in liquid H_2O that binds CO_2 to the CaCO_3 sample.

The fact of the linear dependence of the amount of $\text{CO}_2(\text{a})$ on $\text{H}_2\text{O}(\text{a})$ (Figure 6.2.3) may lead to the proposal of a hydrated CaCO_3 as an intermediate species, which may be attacked by CO_2 . The intermediate species may be formed by reaction 6.2.5 where CO_2 and H_2O originate from ambient air. This is supported by the fact that we observe desorbing CO_2 from the sample while pumping on it. CO_2 may adsorb in the following way:



The fact that only about 25% of the adsorbed CO_2 may be recovered means that the major part of the consumed CO_2 leads to a stable reaction product:



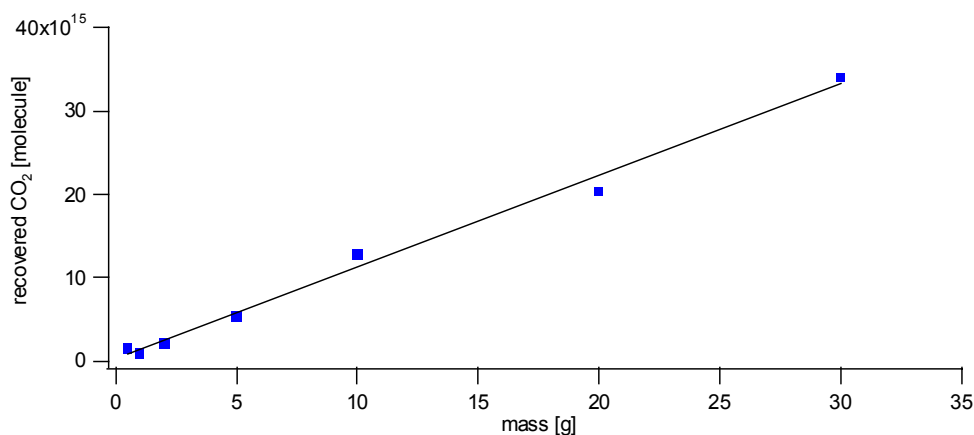


Figure 6.2.4: Recovered CO₂ as a function of the mass m of precipitated CaCO₃. The sample has been pumped for $t_p = 30$ min, which corresponds to an estimated amount of remaining adsorbed H₂O of $1.1 \cdot 10^{18}$ molecule g⁻¹.

Powder diffusion may be a problem for the interpretation of desorption experiments we have carried out. We compare the amount of adsorbed H₂O of the whole internal sample surface with desorption of CO₂ (Figure 6.2.3). In order to assure that not only desorption of the topmost-layers but desorption of the whole surface area contributes to the MS-signal in our experiment a few experiments have been carried out with different sample masses corresponding to different sample thicknesses h . We have found that the amount of desorbing CO₂ is linear with the thickness of the sample, which means that the desorbing CO₂ is provided by the whole internal sample surface. Figure 6.2.4 shows the recovered quantity of adsorbed CO₂ as a function of the sample mass. The experimental conditions are listed in Table 6.1.1, Experiment 3.

In addition, the dependence of the amount of CO₂ adsorbed as a function of the CO₂ concentration has been investigated and is displayed in Figure 6.2.5. The experimental details are listed in Table 6.2.1, Experiment 4. Each uptake experiment has been performed on a fresh CaCO₃ sample which was prepared under the same conditions. The amount of adsorbed CO₂ increases linearly with the pressure under the condition of a constant amount of H₂O(a) on the CaCO₃ sample according to the results displayed in Figure 6.1.3 and discussed above.

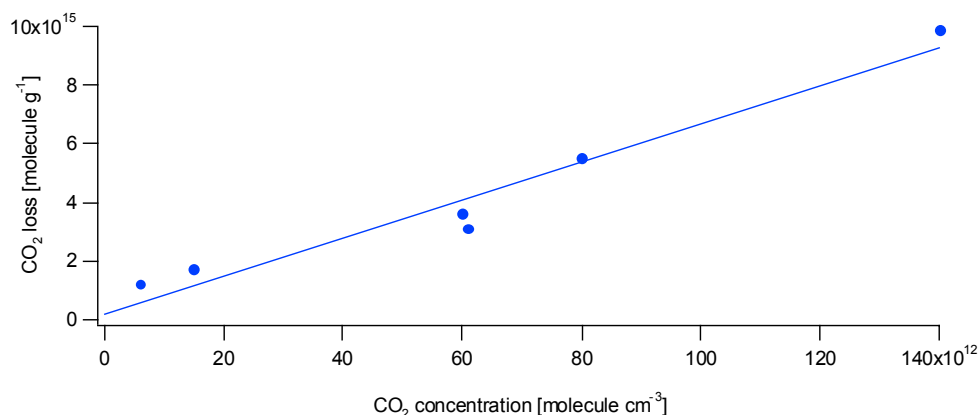


Figure 6.2.5: Uptake experiment in the 1mm-orifice reactor carried out on 1g of precipitated CaCO₃. The total amount of adsorbed CO₂ is displayed as a function of the concentration of CO₂. The amount of adsorbed H₂O has been evaluated as 1.1*10¹⁸ molecule g⁻¹.

The result may be expressed as follows:

$$\text{CO}_2(a) = \tilde{K} [\text{CO}_2] \quad (\text{equation 6.2.1})$$

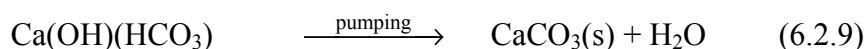
with $\text{H}_2\text{O}(a) = 1.1 \cdot 10^{18} \text{ molecule g}^{-1}$

The constant \tilde{K} was determined as $\tilde{K} = 65 \frac{\text{cm}^3}{\text{g}}$. When we convert to units of the

Henry's law constant we obtain $K_H = 8 \cdot 10^4 \frac{\text{mol}}{\text{bar kg}}$. When we compare this to the

Henry's law constant of CO₂ in water $K_H = 0.034 \frac{\text{mol}}{\text{bar kg}}$, we conclude that adsorbed

H₂O can not act as a solvent for CO₂ akin to a standard aqueous solution. Instead, we propose that the intermediate reacting with CO₂ may be the reaction product in reaction 6.2.7. The dependence of the quantity of adsorbed CO₂ on the amount of H₂O(a) as presented in Figure 6.2.3 may be explained by slow destruction of the intermediate by evaporation of H₂O according to reaction 6.2.9



and the adsorption of CO₂ on the intermediate (Reaction 6.2.7).

6.2.3. Conclusions

We have shown that the amount of CO_2 adsorbed depends on the amount of adsorbed $\text{H}_2\text{O}(\text{a})$ and is linearly dependent on $[\text{CO}_2]$. In neutral aqueous solution the dissociation of calcium carbonate is governed by dissolved CO_2 in water. We propose that adsorbed water leads to the intermediate species $\text{Ca}(\text{OH})(\text{HCO}_3)$ in equilibrium with CaCO_3 , a proposal we carry over to the situation under vacuum. Using Henry's law constant for CO_2 dissolution in aqueous solution it becomes obvious that CO_2 undergoes a chemical change at the solid-gas interface. We have shown, based on the comparison with the Henry's law constant for CO_2 in water that physical dissolution of gaseous CO_2 in $\text{H}_2\text{O}(\text{a})$ that is adsorbed on precipitated CaCO_3 is not likely. We propose an intermediate species in order to explain the dependence of the amount of adsorbed CO_2 on the amount of $\text{H}_2\text{O}(\text{a})$ and $[\text{CO}_2]$ having an effective Henry's law constant many orders of magnitude larger than physical dissolution of CO_2 in $\text{H}_2\text{O}(\text{a})$.

6.2.4. TablesTable 6.2.1: Typical experimental conditions for CO₂ uptake experiments on precipitated CaCO₃ and main results

No	Orifice diameter [mm]	[CO ₂] [molecule cm ³]	Experimental conditions	Uptake kinetics	Remarks
1	1	$7 \cdot 10^{12}$	Estimated amount of H ₂ O : $3 \cdot 10^{19}$ molecules	$\gamma_0 = 4 \cdot 10^{-4}$	Adsorption and desorption of CO ₂ observed, loss/recovery = 0.25
2	1	$7 \cdot 10^{12}$	$1 \cdot 10^{17} < \text{H}_2\text{O(a)} < 2 \cdot 10^{18}$, m = 1g, t _w before recovering = 90s		$\gamma_0 = f(\text{H}_2\text{O(a)})$, loss = f(H ₂ O(a)) and recovered CO ₂ molecules = f(H ₂ O(a))
3	1	$7 \cdot 10^{12}$	$0.5\text{g} \leq m(\text{CaCO}_3) \leq 30\text{g}$		The amount of recovered CO ₂ is linear to the sample mass.
4	1	$2 \cdot 10^{12} < c < 2 \cdot 10^{14}$	m = 1g, estimated amount of adsorbed H ₂ O: $1.1 \cdot 10^{18}$ molecule	$3 \cdot 10^{-5} < \gamma_0 < 8 \cdot 10^{-5}$	CO ₂ (a) linear dependence of concentration. γ_0 decreases with increasing concentration.

6.3. Uptake Experiments of SO₂ on CaCO₃

6.3.1. Introduction

The most important atmospheric sulphur-containing gases are H₂S, DMS, COS, and CS₂. Natural sources are biogenic reactions in soils, marshland and plants. In the oxygen-rich terrestrial atmosphere they are oxidised to SO₂. The main anthropogenic source of SO₂ is fossil fuel burning. The anthropogenic flux of sulphur into the atmosphere is on the order of 78 Tg (S) year⁻¹ (14).

SO₂ is a precursor to H₂SO₄ which together with HNO₃ is the most important acidic compound in the atmosphere (see section 1.5).

It has been claimed that the heterogeneous oxidation of SO₂ on aerosol may account for nearly 60% of the oxidation of SO₂ to SO₄²⁻ in the marine troposphere (reactions 1.5.1-1.5.6) (15, 14). This underlines the importance of heterogeneous chemistry in the sulphur cycle. In this work we look more closely at the role of mineral dust, particularly the uptake of SO₂ on calcium carbonate CaCO₃.

6.3.2. Results and Discussion

Uptake experiments of SO₂ on precipitated CaCO₃ have been performed in a low-pressure flow reactor. The only observed reaction product has been CO₂. Figure 6.3.1 displays a typical uptake experiment carried out in the 14mm-orifice reactor. Immediately after lifting the plunger CO₂ has been observed in the gas-phase. Saturation of SO₂ sets in after 15 minutes, or so, and CO₂ decreases to the background level at the same time. After a given time t_w the lid has been lifted again and desorption of SO₂ has been observed. The mass balance has shown a conversion of one mole of SO₂ taken up to one mole of CO₂ evolved. The experimental details are listed in Table 6.3.1, Experiment 1a.

In order to investigate the surface regeneration of the CaCO_3 substrate the saturated sample has been pumped over night and a further uptake experiment has been performed in the 14mm-orifice reactor.

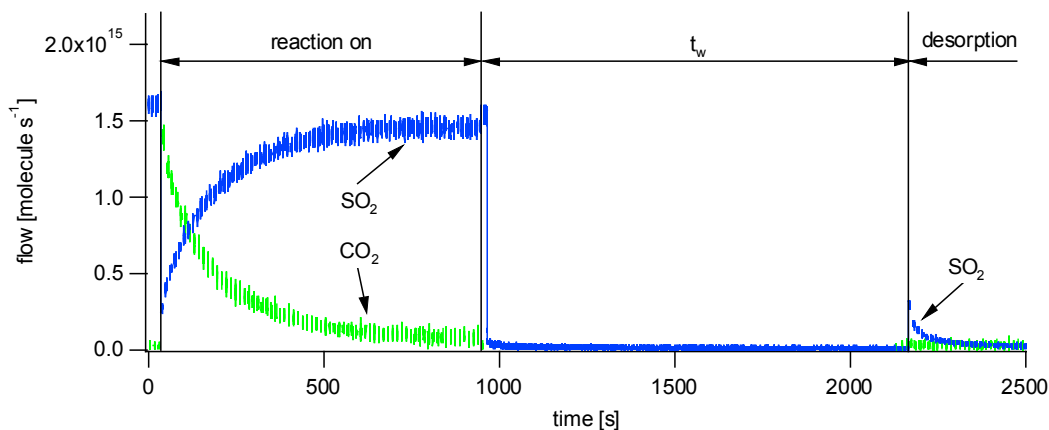


Figure 6.3.1: Uptake experiment of SO_2 on 1 g of precipitated CaCO_3 . The experiment has been performed in the 14mm-orifice reactor. CO_2 has been observed as reaction product. SO_2 and CO_2 have been monitored at $m/e = 64$ and $m/e = 44$, respectively. The sample has been exposed for 15 minutes. After 20 minutes the plunger has been lifted again and desorption of SO_2 has been observed.

A further uptake of SO_2 but no formation of CO_2 has been observed. Several minutes after closing the sample chamber the plunger had been lifted for a second time. Out-gassing of SO_2 has been observed. A comparison of the amount of adsorbed and the recovered amount of SO_2 has shown a net uptake of SO_2 . Figure 6.3.2 shows an uptake experiment on a saturated sample from a previous uptake. The experimental conditions are summarised in Table 6.3.1, Experiment 1b.

45% of the total amount of adsorbed SO_2 has been recovered on a saturated sample of CaCO_3 . The result is that surface sites leading to loss of SO_2 may regenerate whereas surface sites leading to formation of CO_2 remain saturated under vacuum conditions on a long-term basis.

Furthermore, a two step experiment has been performed. A sample had been saturated in the 14mm-orifice reactor under the same conditions as described in Table 6.3.1, Experiment 1a. Afterwards, the sample has been stocked for 5 days at ambient conditions

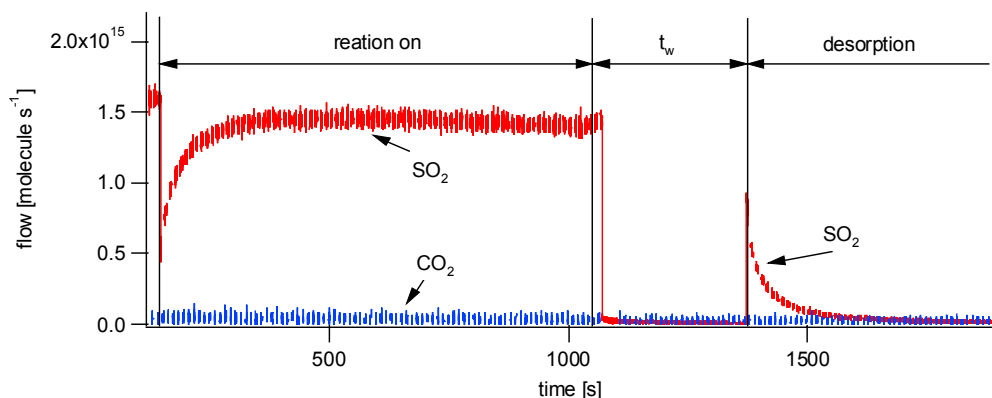


Figure 6.3.2: Uptake experiment of SO_2 on 1 g of precipitated CaCO_3 . The experiment has been performed in the 14mm-orifice reactor. Before performing the uptake experiment the sample had been totally saturated and pumped overnight. The sample has been exposed for 15 minutes to SO_2 . 5 minutes after isolation of the sample the plunger has been lifted again and desorption of SO_2 has been observed. SO_2 and CO_2 have been monitored at $m/e = 64$ and $m/e = 44$, respectively.

before a second SO_2 uptake experiment has been carried out under the same conditions as the first SO_2 uptake experiment. The experimental details are listed in Table 6.3.1, Experiment 1c. Again, the mass balance has shown a one to one correspondence between the loss of SO_2 and yield of CO_2 on a virgin as well on a spent CaCO_3 substrate. Also the initial uptake coefficient γ_0 remains unchanged. In contrast to the first uptake experiment the sample saturates earlier and the total yield of CO_2 and therefore the loss of SO_2 have been a factor of 4, or so, smaller. Figure 6.3.3 displays an uptake experiment performed on a virgin and contaminated sample whereas the contaminated sample has been exposed to ambient conditions for 5 days.

Those experiments have shown that under vacuum sites leading to CO_2 may not regenerate, whereas under ambient conditions a part of those sites will. Stable species of sulfite have to be formed on the surface. Sites leading to loss of SO_2 may regenerate even under vacuum conditions which implies different surface sites for SO_2 adsorption and CO_2 release. One leads to CO_2 and the other to loss of SO_2 . Furthermore, we have observed a measurable net loss of SO_2 only after saturation where net loss means SO_2

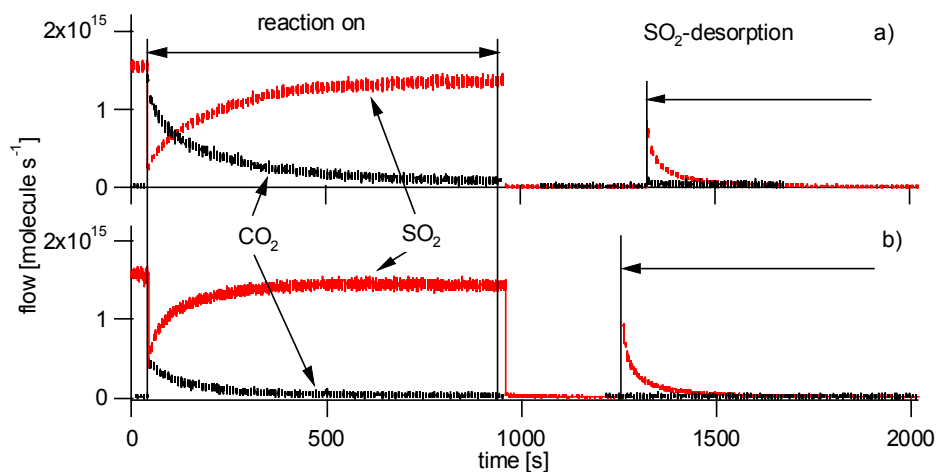


Figure 6.3.3: Uptake experiment of SO_2 on a fresh and a contaminated CaCO_3 sample. The uptake experiment has been carried out in the 14mm-orifice reactor on 1g of precipitated CaCO_3 . a) shows the flow of an uptake experiment performed on a virgin sample and b) on the same sample stocked for 5 days at ambient conditions before carrying out the experiment.

that does not lead to the formation of CO_2 . This observation suggests that the reaction leading to the net loss of SO_2 is slow compared to the reaction leading to CO_2 .

In order to investigate the reaction leading to a loss of SO_2 experiments in the 14mm-orifice reactor have been carried applying the following protocol:

1. Exposure of the precipitated CaCO_3 to SO_2 until saturation is reached.
2. Covering the sample compartment for a given time t_w
3. Measurement of the desorption of SO_2

Figure 6.3.4 shows the calibrated MS-signal of SO_2 in such an experiment carried out following the above protocol. The experimental details may be found in Table 6.3.1, Experiment 2. It has been observed that the amount of recoverable SO_2 decreases with time t_w while the sample chamber was closed. Figure 6.3.5 displays the amount of desorbed SO_2 as a function of t_w . The experiments carried out did not lead to desorption

of CO_2 as may be seen in Figure 6.3.4. Therefore, we conclude that adsorbed SO_2 undergoes a slow reaction towards loss of SO_2 that cannot desorb.

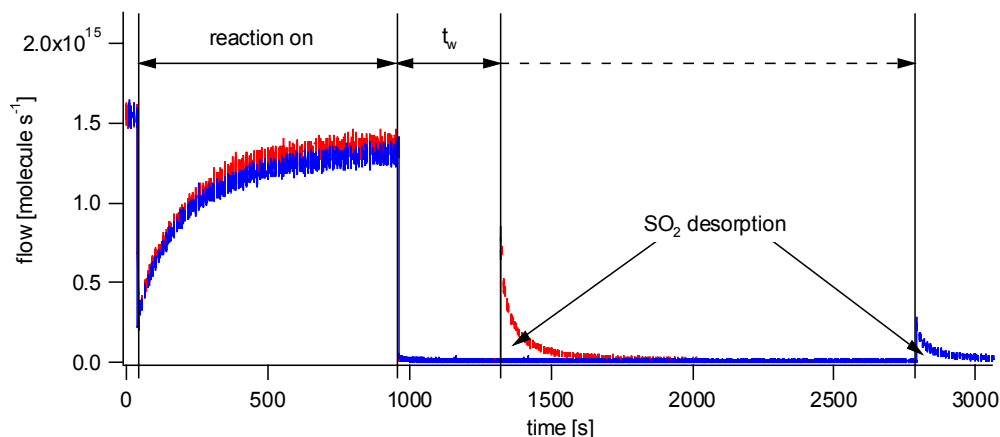


Figure 6.3.4: Uptake experiment of SO_2 on 1g of precipitated CaCO_3 carried out in the 14mm-orifice reactor. The sample has been saturated and the desorption of SO_2 has been measured as a function of the waiting time t_w during which the sample compartment has been closed. The evaluated amount of adsorbed H_2O has been $1.1 \cdot 10^{18}$ molecule.

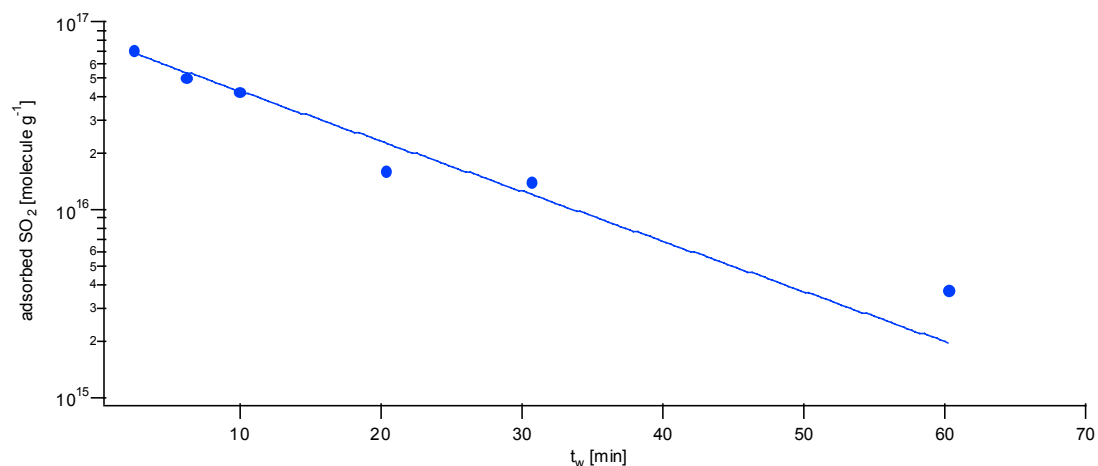


Figure 6.3.5: The amount of recovered SO_2 as a function of time t_w during which the sample compartment has been covered. The amount of $\text{H}_2\text{O}(a)$ has been estimated as $1.1 \cdot 10^{18}$ molecule. The data lead to the measurement of k_s displayed in equation 6.3.1.

Chapter 6

The exponential decay of surface adsorbed SO₂ may be expressed using a first order reaction:

$$\dot{S} = -k_s S \quad (\text{equation 6.3.1})$$

Where S denotes the amount of adsorbed SO₂.

For the decay constant and SO₂(a)(t = 0) the following values have been calculated:

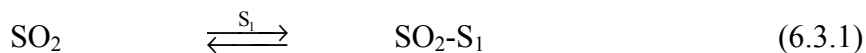
$$k_s = 1.2 \cdot 10^{-3} \text{ s}^{-1}$$

$$S(t = 0) = 8 \cdot 10^{16} \text{ molecule g}^{-1}$$

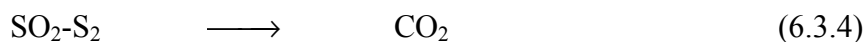
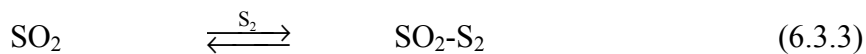
An SO₂ uptake experiment under conditions listed in Table 6.3.1, experiment 1, leads to a yield of CO₂ and a loss of SO₂ of approximately 3 · 10¹⁷ molecule g⁻¹.

We assume that we have two parallel pathways, one leading to CO₂ and the other to loss of SO₂ through different intermediate surface sites:

Pathway 1:



Pathway 2:



S₁ and S₂ represent two different types of active surface sites leading to adsorbed SO₂.

In order to estimate the amount of lost SO₂ by pathway 1 we assume that adsorption expressed by reaction 6.3.1 is not the rate-limiting step leading towards the loss of SO₂.

Chapter 6

Therefore, we assume that $S_1(t) = S_1(0) = 8 \cdot 10^{16}$ molecule. Using the reaction constant k_s determined above according to reaction 6.3.1 we obtain an amount of $8 \cdot 10^{16}$ molecule of SO_2 that would be lost during the 15 minutes of reaction.

In the experiment presented in figure 6.3.1, table 6.3.1, experiment 1a, we have seen that during an SO_2 experiment $2.7 \cdot 10^{17}$ molecules of SO_2 are converted to $2.7 \cdot 10^{17}$ molecule of CO_2 . Thus, the conversion of 1 mole of SO_2 to 1 mole of CO_2 would not be satisfied by a mechanism with two different sites for adsorption S_1 and S_2 . Therefore, the proposed mechanism can not longer be maintained and we conclude that such a mechanism is not appropriate for the description of the system at hand and we must have only one type of sites for adsorption of SO_2 .

In order to investigate the substrate for the potential presence of $\text{Ca}(\text{OH})_2$ a SO_2 uptake experiment on solid $\text{Ca}(\text{OH})_2$ has been carried out. $\text{Ca}(\text{OH})_2$ may be present on the sample because of its formation in the following reaction:



Where $\text{Ca}(\text{OH})(\text{HCO}_3)$ may be formed according to reaction 6.2.5 which describes the conditioning of CaCO_3 in the presence of water vapour and atmospheric CO_2 .

The experimental details are given in Table 6.3.1, Experiment 3. We measured an uptake coefficient of $\gamma = 0.4$. No products, no saturation and no desorption of SO_2 have been observed.

Because of the fast reaction of SO_2 on $\text{Ca}(\text{OH})_2$ and the one to one conversion of SO_2 to CO_2 in the course of the SO_2 uptake experiments on CaCO_3 we conclude that there may only be small amounts of $\text{Ca}(\text{OH})_2$ present on the CaCO_3 sample.

The corresponding reaction of SO_2 on $\text{Ca}(\text{OH})_2$ is given by reaction 6.3.6.



For the following SO₂ uptake experiments we have halted the SO₂ uptake before total saturation of the CaCO₃ sample. After lowering the plunger thus halting the uptake we lifted it again in order to observe the desorption of residual species from the surface. In such a case only a small amount of SO₂ desorbing from the substrate has been observed whereas formation of CO₂ occurred while the sample chamber was isolated. Figure 6.3.6 shows the calibrated MS-signals of such a SO₂ uptake experiment carried out in the 14mm-orifice reactor. The experimental details are given in Table 6.3.1, Experiment 4.

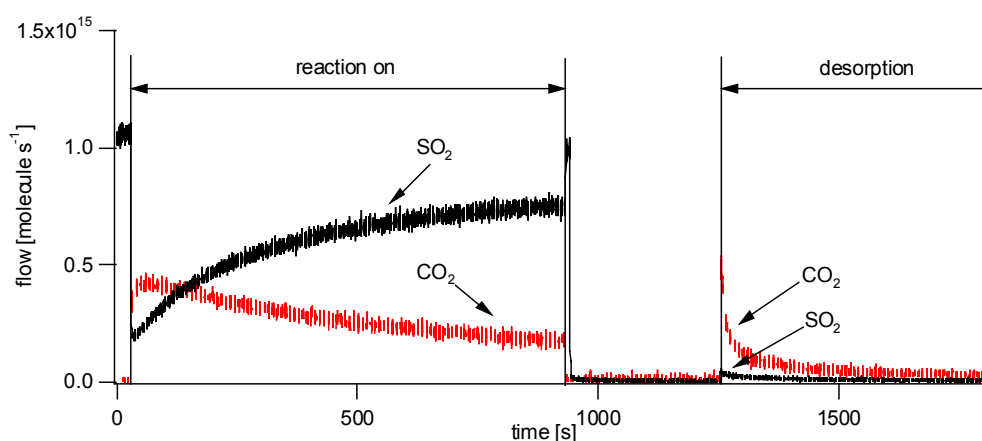


Figure 6.3.6: SO₂ uptake experiment on precipitated CaCO₃ carried out in the 14mm-orifice reactor. The experiment has been carried out on a low ordered sample (SEM-image Figure 6.3.7) and was halted before saturation of the uptake occurred.

In contrast to the CaCO₃ sample used to carry out the previous SO₂ uptake experiments the CaCO₃ sample used for this SO₂ uptake experiment contains more defect sites and is called “low-ordered” CaCO₃. SEM-images low- and high-defect CaCO₃ samples are shown in Figures 6.1.1 and 6.3.7, respectively.

The mass balance between loss of SO₂ and formation of CO₂ has not been satisfied on a low-ordered CaCO₃ sample. For SO₂ uptake during 15 minutes 3 moles of SO₂ taken up corresponds to formation of 2 moles of CO₂. This is in contrast to the SO₂ uptake experiments performed on a high-ordered CaCO₃ sample discussed above.

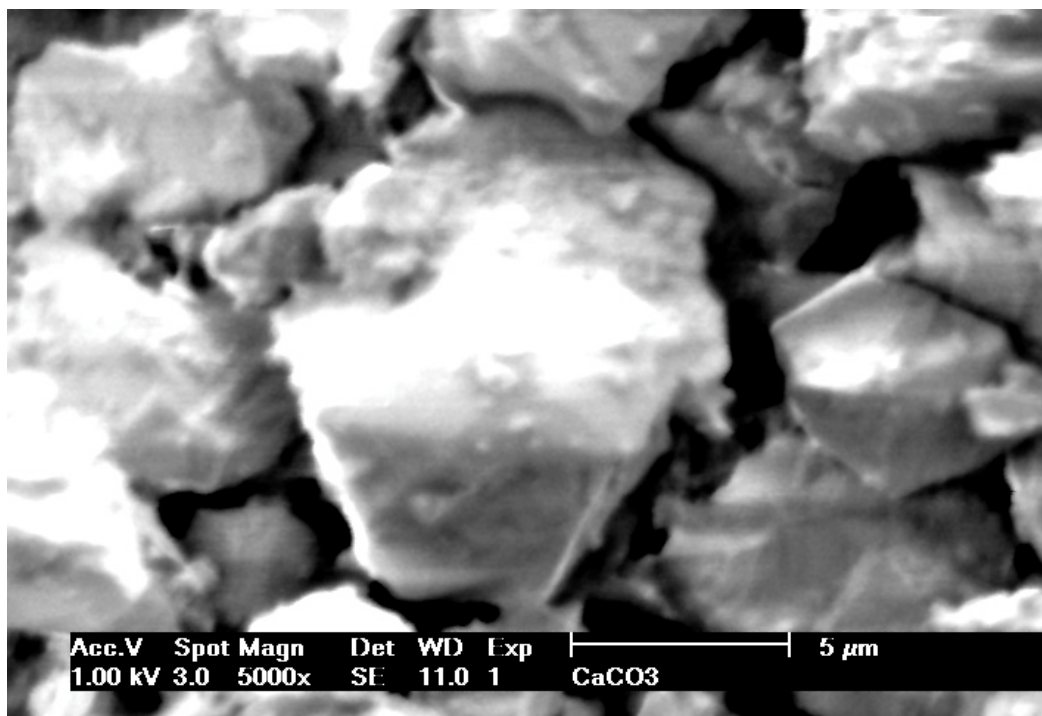


Figure 6.3.7: SEM-image of a precipitated low-order CaCO_3 sample.

The fact that a low-ordered sample does not saturate under the same conditions clearly shows that the reaction of SO_2 on CaCO_3 strongly depends on the morphology of the sample. Moreover, the fact that the ratio of the loss of SO_2 to the yield of CO_2 changes from 1 to 1.5 on a high- and low-ordered CaCO_3 sample, respectively, and the fact that the yield of CO_2 does not change significantly may suggest the existence of a parallel reaction mechanism. The existence of a parallel mechanism will be discussed below. Figure 6.3.8 illustrates a possible parallel and a sequential reaction mechanism.

For kinetic reasons discussed above we have excluded two different adsorption sites. Therefore, we propose a mechanism with common sites S for adsorption. If we assume the sequential reaction of Figure 6.3.8 for a moment we find that one CO_2 may be formed per reaction site leading to loss of SO_2 (Figure 6.3.8) which would fit the observations above for the high-ordered CaCO_3 sample. However, for the low-ordered CaCO_3 sample

we observed a ratio of 1.5 for the loss of SO₂ to the yield of CO₂ which means that we must have additional sites leading to loss of SO₂ without concomitant formation of CO₂. Only the parallel mechanism as indicated in Figure 6.3.8 may explain the increase of the ratio between the loss of SO₂ and the yield of CO₂. Therefore, we favour the parallel over the serial mechanism at this point.

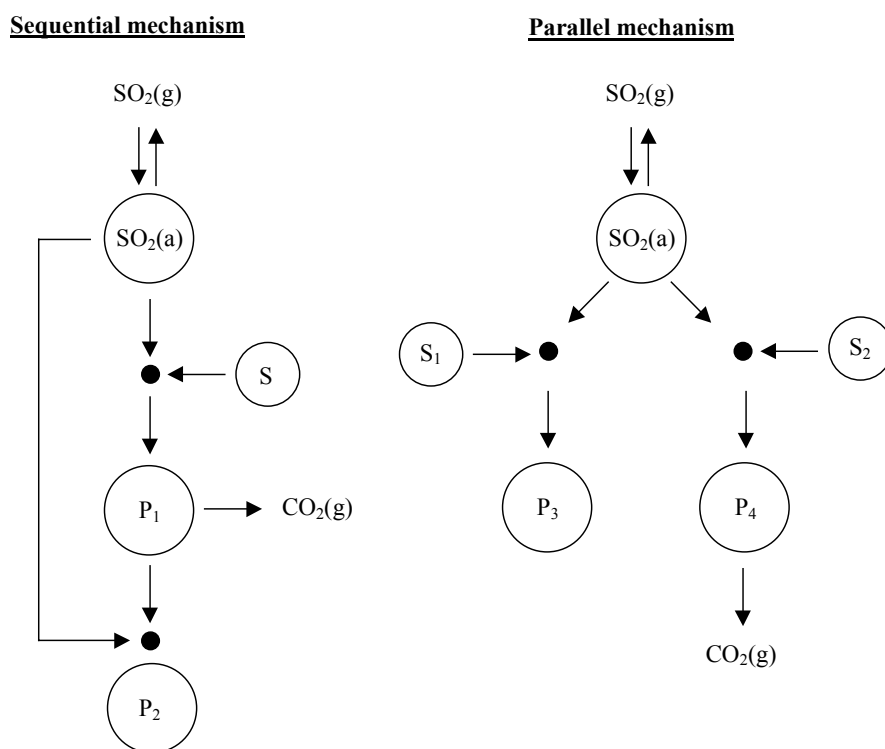
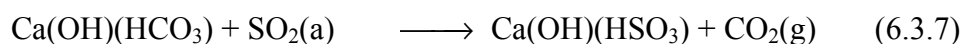


Figure 6.3.8: Schematic illustration of a possible sequential and parallel mechanism for the reaction of SO₂ on precipitated CaCO₃. S, S₁ and S₂ are labels for different types of reactive surface sites. P₁, P₂, P₃ and P₄ represent the adsorbed reaction products.

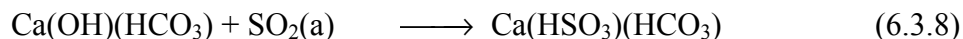
Finally, this leads us to the following mechanism where the reaction intermediate reacting with SO₂ is identified with the species Ca(OH)(HCO₃) discussed in Section 6.2.

For the reaction leading to CO₂ we propose reaction 6.3.7 as follows:



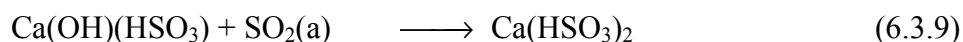
Chapter 6

For the reaction leading to loss of SO₂ we propose the following reaction:



We propose that the reaction of SO₂ with the intermediate species Ca(OH)(HCO₃) may lead to two different reaction products. Based on the fact that CO₂ is formed immediately after lifting the plunger and the mass balance between loss of SO₂ and formation of CO₂ is satisfied we suggest that reaction 6.3.8 is rather slow such that reaction 6.3.7 is preferred at the beginning.

Furthermore, we can not exclude that the reaction product of reaction 6.3.7 undergoes a further reaction with SO₂ according to reaction 6.3.9 which also leads to loss of SO₂.



Also reaction 6.3.6 would be a reaction leading to loss of SO₂. However, as we have seen reaction 6.3.6 is a very fast reaction and may therefore be excluded because the reaction leading to loss of SO₂ turns out to be slow.

As we have seen above we have not observed a regeneration of the surface sites under vacuum leading to a formation of CO₂ but an uptake of SO₂ not leading to formation of CO₂ has been observed as shown in Figure 6.3.2 and Table 6.3.1, Experiment 1b. The loss of SO₂ has been measured to be 6*10¹⁶ molecule g⁻¹ which approximately corresponds to the loss we calculated using the reaction constant k_s and equation 6.3.1. Based on this calculation and the parallel reaction mechanism we suggest that after saturation of the reaction pathway leading to CO₂ the parallel loss pathway of SO₂ has not saturated. In addition, the sites leading to adsorption of SO₂ may regenerate with time even under vacuum.

Additional SO₂ uptake experiments on precipitated CaCO₃ at different amounts of adsorbed H₂O(a) have been performed. The samples have been pumped for 30 minutes and 21h, which corresponds to 1.1*10¹⁸ and 5*10¹⁷ molecule g⁻¹ of H₂O(a), respectively.

The uptake experiments carried out in the 14mm-orifice reactor have not shown any significant difference in the loss of SO₂ and the yield of CO₂. The initial uptake coefficient γ_0 has been a factor of two higher for the sample containing more H₂O(a). The experimental conditions and main results are listed in Table 6.3.1, Experiment 5. Figure 6.3.9 displays the calibrated MS-signals of SO₂ uptake experiments performed on precipitated CaCO₃ with different amounts of adsorbed H₂O.

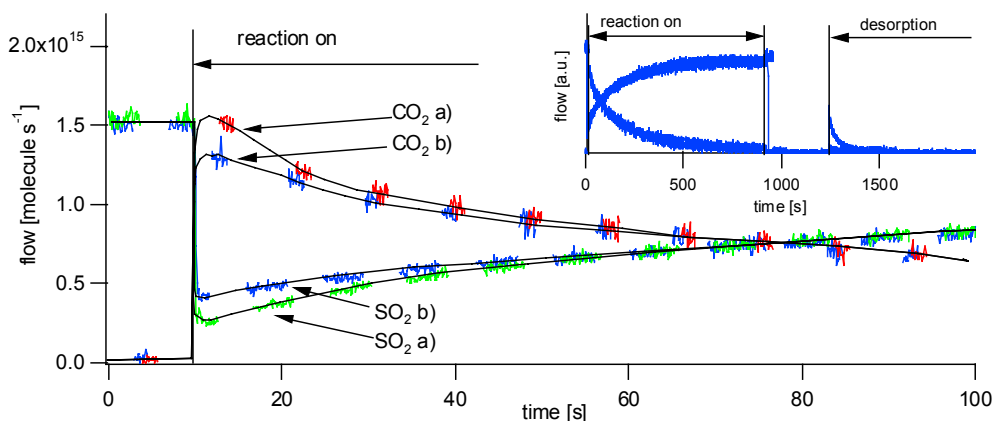


Figure 6.3.9: The formation of CO₂ and uptake of SO₂. The experiments have been carried out in the 14mm-orifice reactor on precipitated CaCO₃. Signals a) and b) correspond to a SO₂ uptake on a sample containing $1.1 \cdot 10^{18}$ and $5 \cdot 10^{17}$ molecule of H₂O(a), respectively. SO₂ has been monitored at $m/e = 64$ and CO₂ at $m/e = 44$.

The lower initial uptake may be explained by the decrease of the number of intermediate Ca(OH)(HCO₃) upon pumping of the sample which is also consistent with the experiments of CO₂ on precipitated CaCO₃ we have described in section 6.2. The influence of pumping time is not very important, probably due to the slow dehydration of the proposed intermediate species according to reaction 6.3.10.



The slow dehydration of the intermediate species may be the reason for the slow desorption of adsorbed H₂O by pumping (a factor 2 in 20h) as shown in Figure 6.1.3.

The existence of the intermediate species is also supported by the fact that the surface of a poisoned sample regenerates and leads to additional CO₂ when left under ambient

conditions in the presence of H₂O and CO₂ (Figure 6.3.3). This is a strong indication for the presence of the proposed reactive surface species.

6.3.3. Conclusions

In this section we have shown the existence of different surface sites that react with SO₂. One reactive surface species leads to formation of CO₂ whereas the other surface species leads to loss of SO₂. A regeneration of the surface sites leading to loss of SO₂ under vacuum and of the sites leading to CO₂ under ambient conditions has been observed. The regeneration of surface sites leading to CO₂ supports the existence of the surface intermediate species we introduced in Section 2, namely Ca(OH)(HCO₃).

Desorption experiments of SO₂ lead to the conclusion that the reaction leading to loss of SO₂ is a slow reaction. A reaction constant $k_S = 1.2 \cdot 10^{-3} \text{ s}^{-1}$ according to reaction 6.3.8 has been determined for the high-ordered CaCO₃ sample.

The quantitative comparison of uptake experiments on low- and high-ordered precipitated CaCO₃ leads to the suggestion of a parallel mechanism (Figure 6.3.8).

Furthermore, we have shown that the morphology of CaCO₃ plays a crucial role for the reaction of SO₂ with CaCO₃. A low-ordered sample contains more reactive sites than a high-ordered sample.

Finally, we have shown that the influence of adsorbed H₂O on the reaction of SO₂ on precipitated CaCO₃ is not very important, probably due to the slow dehydration of the proposed intermediate species to crystalline CaCO₃.

6.3.4. TablesTable 6.3.1: Typical experimental conditions and main results of SO₂ uptake experiments on precipitated CaCO₃

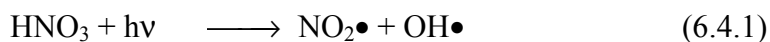
No	Orifice diameter [mm]	[SO ₂] [molecule cm ³]	Experimental conditions	Uptake kinetics	Remarks
1a	14	2.2*10 ¹¹	Estimated amount of H ₂ O : 1.1*10 ¹⁸ molecule	$\gamma_0 = 0.13$	mass balance: 1 mole SO ₂ -> 1 mole CO ₂ , desorption of SO ₂ , yield of CO ₂ : 2.7*10 ¹⁷ molecule
1b	14	2.2*10 ¹¹	Saturated sample pumped overnight	$\gamma_0 = 0.12$	No CO ₂ , mass balance: loss of 65% of the total amount of adsorbed SO ₂ which is 1.1*10 ¹⁷ molecule
1c	14	2.2*10 ¹¹	Stocked at ambient conditions for 5 days after saturation, same conditions as 1a	$\gamma_0 = 0.13$	mass balance: 1 mole SO ₂ -> 1 mole CO ₂ , desorption of SO ₂ , yield of CO ₂ : 7*10 ¹⁶ molecule
2	14	2.2*10 ¹¹	Estimated amount of H ₂ O : 1.1*10 ¹⁸ molecule		The amount of recoverable SO ₂ decreases exponentially with t _w .
3	14	2.2*10 ¹¹	Experiment on Ca(OH) ₂	$\gamma = 0.4$	No products and no desorption of SO ₂ observed, no saturation within 15 minutes, 1.5 mole SO ₂ -> 1 mole of CO ₂ , yield of CO ₂ : 2.7*10 ¹⁷ molecule.
4	14	1.5e10 ¹¹	Not saturated, low ordered sample	$\gamma_0 = 0.2$	
5	14	2.2*10 ¹¹	Estimated amount of H ₂ O : 1.1*10 ¹⁸ and 5*10 ¹⁷ molecule	$\gamma_0 = 0.2$ $\gamma_0 = 0.1$	The initial uptake coefficient is higher for the sample containing more H ₂ O(a). formation of CO ₂ 3*10 ¹⁷ and 2.5*10 ¹⁷ molecule for high and low water level, respectively.

6.4. Uptake Experiments of HNO₃ on CaCO₃

6.4.1. Introduction

Together with H₂SO₄ nitric acid, HNO₃, is the most important acidic compound in the troposphere and contributes to acid rain (Section 1.5). HNO₃ is formed by reaction pathways based on reactions with nitrogen oxides. Several pathways leading to HNO₃ are listed in Section 1.5.

Important sinks of HNO₃ are rainout and washout, but gaseous nitric acid also photodissociates during daytime to form NO₂• via



However, this process is slow even at noontime in the midtroposphere ($7.3 * 10^{-7} \text{ s}^{-1}$) (16). Furthermore, heterogeneous reactions of HNO₃ on mineral dust aerosols may also be an efficient sink of nitric acid (15, 1, 17) which corresponds to dry deposition of HNO₃.

In this section the uptake of HNO₃ on different CaCO₃ samples such as precipitated CaCO₃, polished and roughened marble has been studied.

6.4.2. Results and Discussion

HNO₃ reference experiments have been performed on the bare gold-coated sample holder. A small rate of uptake which however saturates after a short time on the order of seconds has been observed. The corresponding initial uptake coefficients are $\gamma_0 = 2.7 * 10^{-3}$ and $2.4 * 10^{-4}$ for the 14- and 4mm-orifice reactor, respectively. The experimental details are given in Table 6.4.1, Experiments 1a and 1b.

Uptake experiments of HNO_3 on a polished marble substrate have been carried out in the 14mm-orifice reactor. The marble plate has been prepared as described in more detail in Section 5.2.2. The uptake of HNO_3 is almost saturated after an exposure of 2 minutes, or so. No CO_2 has been observed as a reaction product. In order to determine whether formation of H_2O has taken place the amount of water coming from the marble sample has been subtracted. The amount of H_2O originating from the sample was determined by lifting the plunger with the sample present. Care was taken to measure the HNO_3 uptake on a sample that was always pumped for the same length of time compared to the measurement of $\text{H}_2\text{O}(\text{a})$ by desorption in order to have identical conditions for the H_2O reference and the HNO_3 uptake experiment. Figure 6.4.1 shows the calibrated MS-signal of such an experiment.

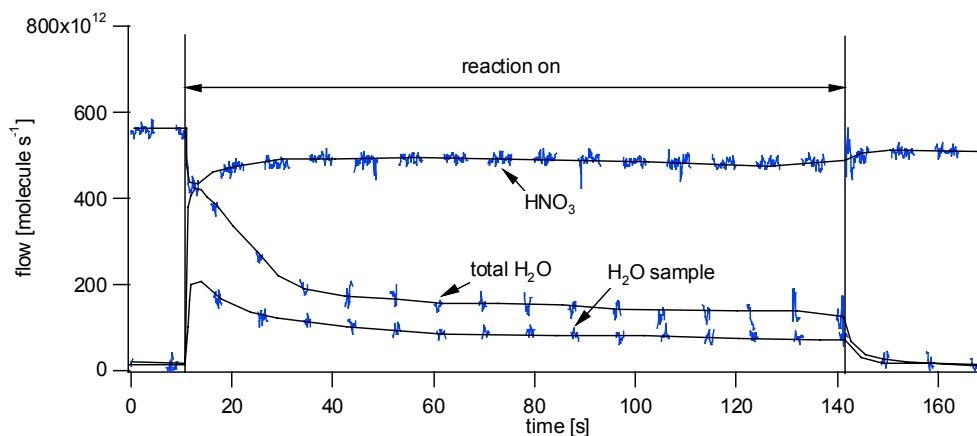


Figure 6.4.1: Uptake experiment of HNO_3 on a polished marble plate carried out in the 14mm-orifice reactor. The amount of H_2O contributed from the sample has been determined by lifting the plunger only when the sample was present. The total rate of H_2O means sum of the H_2O originating from the sample and that formed by the reaction with HNO_3 . HNO_3 and H_2O are monitored at $m/e = 46$ and $m/e = 18$, respectively.

When carrying out the above subtraction a formation of H_2O has been observed when the marble plate was exposed to HNO_3 . The total yield of H_2O and the loss of HNO_3 has been $2.2 \cdot 10^{14}$ and $2.9 \cdot 10^{14}$ molecule cm^{-2} , respectively, using the total geometrical area of 47 cm^2 (Section 5.2.2). When we compare the loss of HNO_3 with the yield of H_2O the

result suggests a one to one correspondence between the loss of HNO_3 and the yield of H_2O . The surface density of CaCO_3 has been calculated to be $6.4 \cdot 10^{14}$ molecule cm^{-2} using equation 3.2.5 which means that only about 50% of one monolayer of CaCO_3 contributes to the reaction of HNO_3 on polished marble within 2 minutes. An uptake coefficient $\gamma = 1 \cdot 10^{-2}$ has been determined which is a factor of 10 higher than Crowley and coworkers observed on polished CaCO_3 single crystals ($\gamma = 9.6 \cdot 10^{-4}$ (1)).

A HNO_3 uptake experiment carried out in the 4mm-orifice reactor on the same substrate has shown an uptake of HNO_3 but neither formation of H_2O nor of CO_2 within our detection limit. The experimental conditions and main results are listed in Table 6.4.1, Experiment 2c.

In order to investigate the sample for adsorbed species the polished marble sample was subsequently heated to $T = 470\text{K}$. A small amount of CO_2 but no HNO_3 has been observed desorbing from the substrate. The experimental details are listed in Table 6.4.1, Experiment 2d. This small amount of desorbing CO_2 indicates that a slow reaction involving a precursor and leading to CO_2 may take place on the surface of the substrate.

Further uptake experiments have been carried out on milled marble plates. Figure 6.4.2 shows the calibrated MS-signal of a HNO_3 uptake experiment on a milled CaCO_3 plate carried out in the 14mm-orifice reactor (Table 6.4.1, Experiment 3a). A strong HNO_3 uptake which turns into steady state is observed after lifting the plunger. As on the polished marble H_2O but no CO_2 has been observed as reaction product.

Figure 6.4.3 displays the calibrated MS-signals of the loss rate of HNO_3 and the rate of formation of H_2O . A close correlation between the loss rate of HNO_3 and the rate of formation of H_2O is apparent. This confirms the release of H_2O by the reaction of HNO_3 with surface sites other than CaCO_3 . As we have suggested in the preceding sections intermediate species may play an important role for the reaction of CaCO_3 with acids. In analogy to this concept we adopt the intermediate $\text{Ca}(\text{OH})(\text{HCO}_3)$ from the previous sections with which we may explain the release of H_2O and the fact that no CO_2 has been observed.

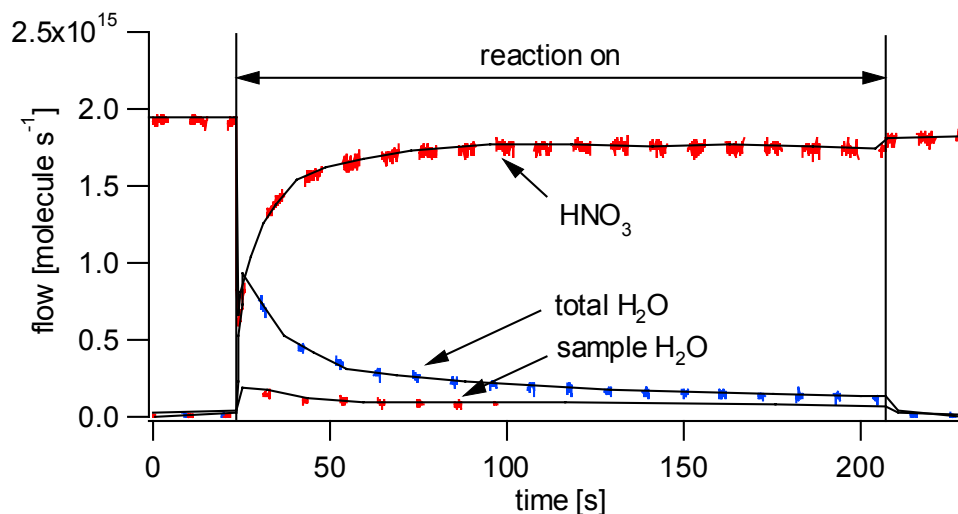


Figure 6.4.2: HNO_3 uptake experiments performed on a milled CaCO_3 marble plate in the 14mm-orifice reactor. The total H_2O flow and the flow of H_2O originating from the sample are shown. The total rate of H_2O means the H_2O originating from the sample and formed by the reaction with HNO_3 .

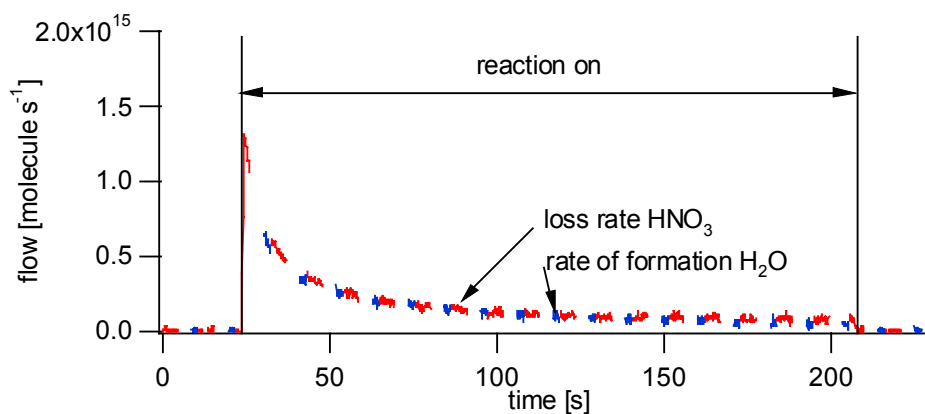


Figure 6.4.3: Correlation of loss the rate of HNO_3 and the rate of formation of H_2O pertaining to an experiment carried out on a milled marble plate in the 14mm-orifice reactor. The rate of formation of H_2O has been determined by subtracting the rate of H_2O desorption from the rate of H_2O formation we measured while HNO_3 is interacting with the sample.

Chapter 6

The intermediate species may be formed by reaction 6.2.5 in the presence of ambient H_2O and CO_2 as we discussed in Section 6.2.2.



We have seen from the results of uptake experiments of SO_2 on low- and high-ordered precipitated CaCO_3 that the morphology of the substrate plays an important role in terms of the amount of intermediate reactive species. When comparing an uptake experiment on polished and on milled CaCO_3 (Figures 6.4.1 and 6.4.2) we may see that a roughened substrate is more reactive than a polished substrate. The difference of the initial uptake coefficient $\gamma_0 = 1 \cdot 10^{-2}$ and $\gamma_0 = 4 \cdot 10^{-2}$ on the polished and the milled marble plate, respectively, corresponds to a factor 4 under the same experimental conditions. The total amount of lost HNO_3 rises by a factor 3, or so, on a milled substrate. This confirms the presence of additional reactive sites on a roughened compared to a polished substrate.

Furthermore, on a roughened substrate desorption of small amounts of HNO_3 has been observed after lifting the plunger once the HNO_3 inflow had been halted. Figure 6.4.4 illustrates this desorption by means of a HNO_3 uptake experiment carried out in the 4mm-orifice. The desorption of HNO_3 after halting the inflow suggests the presence of intermediate sites which may adsorb HNO_3 on the substrate according to reaction 6.4.3.



Furthermore, the uptake coefficient γ has been plotted as function of time and inflow of HNO_3 . Figure 6.4.5 shows the uptake coefficient $\gamma(t)$ of those HNO_3 uptake experiments on roughened marble plates carried out in the 14mm-orifice reactor with different HNO_3 inflows. The experimental details are listed in Table 6.4.1, Experiment 4. A sample exposed to a higher concentration of HNO_3 saturated faster than a sample exposed to lower concentration. The uptake coefficients tend to approximately the same value after about 6 minutes of exposure time t_e . The different behaviour of saturation of the uptake

Chapter 6

coefficient γ as a function of HNO_3 concentration illustrates the assumption of a limited reservoir of active surface sites.

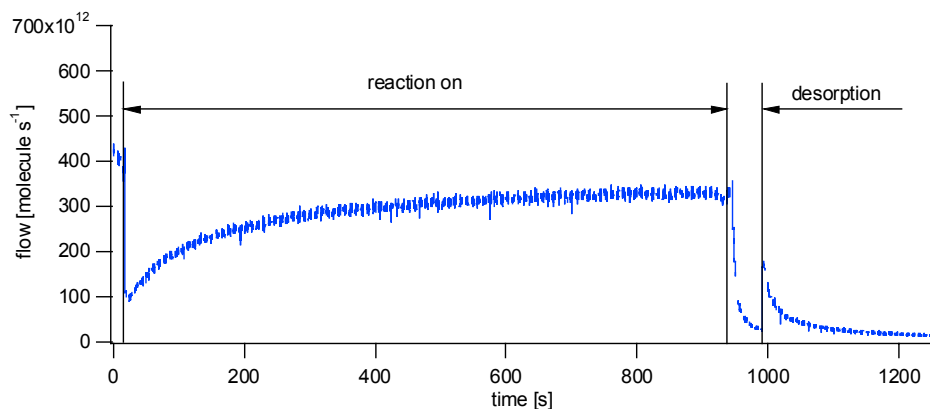


Figure 6.4.4: HNO_3 uptake experiment on a roughened marble plate carried out in the 4mm-orifice reactor. After halting the inflow of HNO_3 the plunger has been lifted again and approximately 20% of the total lost HNO_3 desorbs from the substrate.

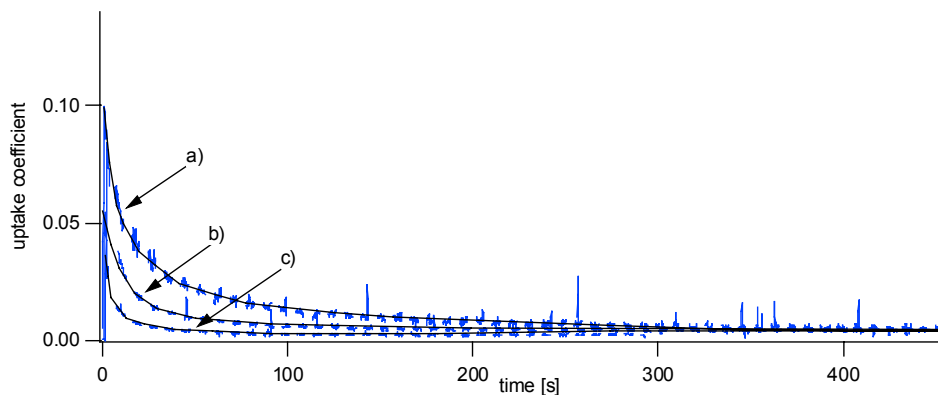


Figure 6.4.5: Uptake coefficient $\gamma(t)$ of HNO_3 uptake experiments as a function of time carried out in the 14mm-orifice reactor on roughened marble plates. a) shows an uptake experiment carried out at a concentration of $2.8 \cdot 10^{10}$ molecule cm^{-3} , b) at $8.5 \cdot 10^{10}$ molecule cm^{-3} and c) at $2.8 \cdot 10^{11}$ molecule cm^{-3} , respectively.

In order to investigate the substrate for regeneration of its adsorption capacity the milled marble plate had been exposed to HNO_3 . Afterwards the chamber had been closed and

after 15 minutes, or so reopened. No regeneration of the sample has been observed under those conditions.

On milled marble plates the total amount of lost HNO_3 molecule is on the order of $1.2 \cdot 10^{15}$ molecule cm^{-2} , which corresponds to approximately 4 times the lost amount of HNO_3 on polished marble plates.

In order to propose a reaction mechanism the following reactions have been tested. They are based on the reaction of a gas-phase species with a limited number of reactive sites on the surface of the solid substrate:



$$\dot{\text{S}}(t) = k_1 \underbrace{N(\text{S}_0 - \text{S}(t))}_X \quad (\text{equation 6.4.1})$$

$\text{S}(t)$ and S_0 are the number of reactive sites at time t and the total number of reactive sites, respectively, and N corresponds to the number of molecules in the reactor. $\dot{\text{S}}$ corresponds to the net flow towards the surface F_r

$$\dot{\text{S}} = F_{\text{in}} - F_{\text{out}} - \dot{\text{N}} = F_r \quad (\text{equation 6.4.2})$$

Equation 6.4.1 may not be solved analytically. In order to solve problem 6.4.1 we calculated X given in equation 6.4.1 in the following way:

$$\text{S}(t) = \int_0^t \dot{\text{S}}(\tau) d\tau \quad (\text{equation 6.4.3})$$

where τ is the integration variable.

$$S_0 = \int_0^{\infty} \dot{S}(t) dt \quad (\text{equation 6.4.4})$$

$\dot{S}(t)$ may be calculated using equation 6.4.2 and S_0 corresponds to the integration over the whole duration of the experiment.

$$N = \frac{F_{\text{out}}}{k_{\text{esc}}} \quad (\text{equation 2.1.7})$$

$$\dot{N} = \frac{\dot{F}_{\text{out}}}{k_{\text{esc}}} \quad (\text{equation 6.4.5})$$

\dot{N} has been estimated using equation 6.4.6:

$$\dot{N} \approx \frac{N(t) - N(t+\Delta t)}{\Delta t} \quad (\text{equation 6.4.6})$$

It has been found that \dot{N} contributes less than 3% to equation 6.4.2 and may therefore be neglected for calculation of F_r .

As we can measure F_{in} and F_{out} we calculate N using equation 2.1.7. Finally, we calculate $X(t)$ and obtain a linear equation in X for the reaction flow F_r using equations 6.4.1 and 6.4.2:

$$F_r(t) = k_1 X(t) \quad (\text{equation 6.4.7})$$

Figure 6.4.6 displays a plot of $F_r = f(X)$.

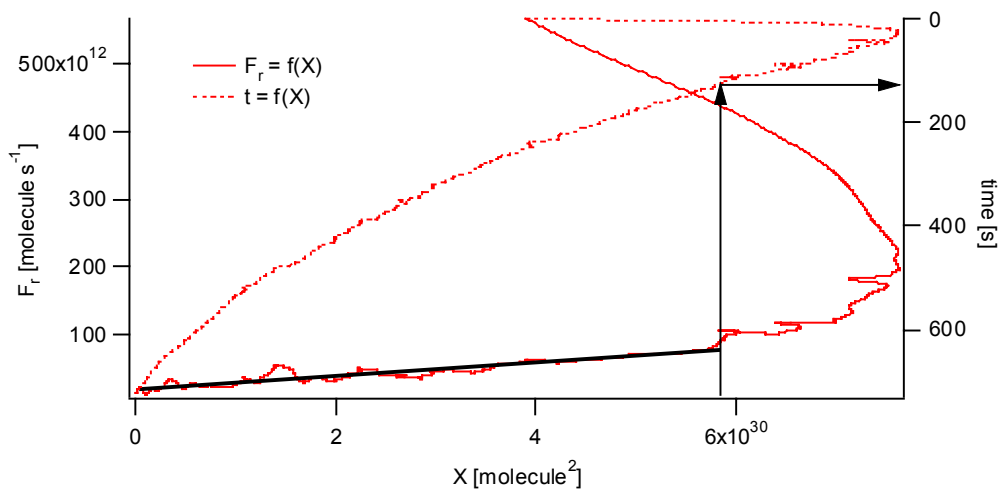


Figure 6.4.6: The graph shows a plot of $\dot{S} = k_1 \underbrace{N(S_0 - S)}_X$ and the time $t = f(X)$. The plot is fitted by a linear function $F_r = a X$ with $a = 9.4 \cdot 10^{-18} \text{ molecule}^{-1} \text{ s}^{-1}$ for $t > 120 \text{ s}$. The experiment from which the data are taken is shown in Figure 6.4.4.

Actually Figure 6.4.6 shows:

$$t \quad \longrightarrow \quad X(t) \quad \longrightarrow \quad F_r(X(t)) \quad (\text{equation 6.4.8})$$

where t , $X(t)$, and $F_r(X(t))$ are represented on the right, bottom and left axis, respectively. We may determine $F_r(t)$ in a graphic way by inverting equation 6.4.8.

In Figure 6.4.6 it may be seen that after 120s or so this model consideration agrees well with respect to the experiment (Figure 6.4.4) owing to the linear relationship between F_r and X . For $t < 120 \text{ s}$ the reaction flow F_r is too high in order to be described by such a mechanism. As we have observed desorption of HNO_3 from the surface we expect a reservoir on the surface and we suggest that the initial uptake γ_0 of HNO_3 on a milled marble plate is governed by filling up this reservoir.

For $t > 120$ s this model may be explained by equation 6.4.1 with a limited amount of intermediate species $\text{Ca}(\text{OH})(\text{HCO}_3)$ present on the substrate. However, at $t < 120$ s the uptake of HNO_3 may be governed by adsorption of HNO_3 on the substrate which leads to a larger loss rate as predicted by the model.

Finally, experiments of HNO_3 on precipitated CaCO_3 have been carried out. The following experiments have been performed on samples, which we called high-ordered precipitated CaCO_3 in Section 6.3. The corresponding SEM-image may be found in Figure 6.1.1 and the experimental details are given in Table 6.4.1, Experiment 5.

The reaction product we have observed on this type of sample is CO_2 . Because of the huge amount of H_2O desorbing from such a sample it has not been possible to distinguish between H_2O eventually generated by the reaction of HNO_3 on precipitated CaCO_3 and H_2O desorbing from the sample. Figure 6.4.7 displays a typical uptake experiment of HNO_3 on precipitated CaCO_3 carried out in the 14mm-orifice reactor.

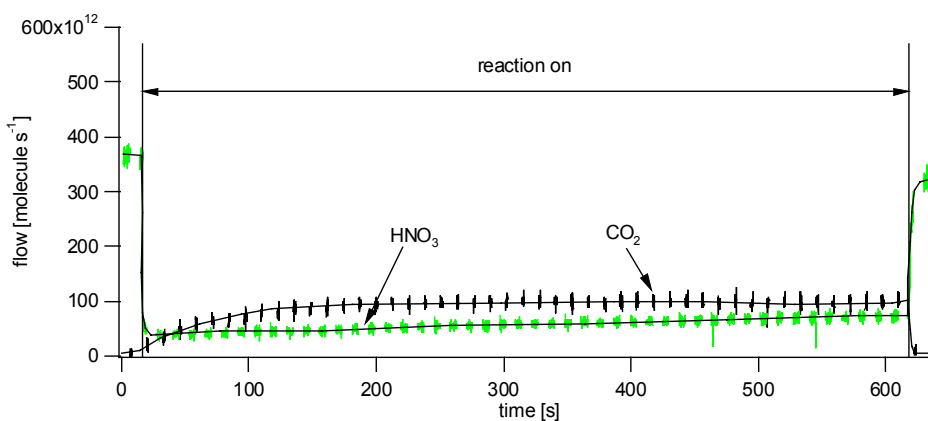


Figure 6.4.7: Uptake experiment of HNO_3 on high-ordered precipitated CaCO_3 carried out in the 14mm-orifice reactor. HNO_3 and CO_2 are monitored at $m/e = 46$ and 44 .

In Figure 6.4.7 it can clearly be seen that there is delayed formation of CO_2 compared to HNO_3 uptake. Figure 6.4.8 shows the loss rate of HNO_3 and the rate of formation of CO_2 in more detail. In order to estimate the total loss of HNO_3 we extrapolated its loss rate linearly until it reaches zero. For the total estimated loss of HNO_3 we thus obtained

$4.8 \cdot 10^{17}$ molecule g^{-1} . This is in good agreement with twice the yield of CO_2 ($2.7 \cdot 10^{17}$ molecule g^{-1}) resulting from uptake experiments of SO_2 on the same type of precipitated CaCO_3 performed under the same experimental conditions (Table 6.3.1, Experiment 1a). The total yield of CO_2 for the SO_2 uptake experiments was attributed to the amount of reactive sites, namely $\text{Ca}(\text{OH})(\text{HCO}_3)$ (reaction 6.3.7). This leads us to the suggestion that under conditions prevailing in the reactor HNO_3 may only react with the intermediates species we proposed and that one intermediate may react with two molecules of nitric acid which is the reason for the stoichiometric factor of two when relating the loss of HNO_3 with the yield of CO_2 :

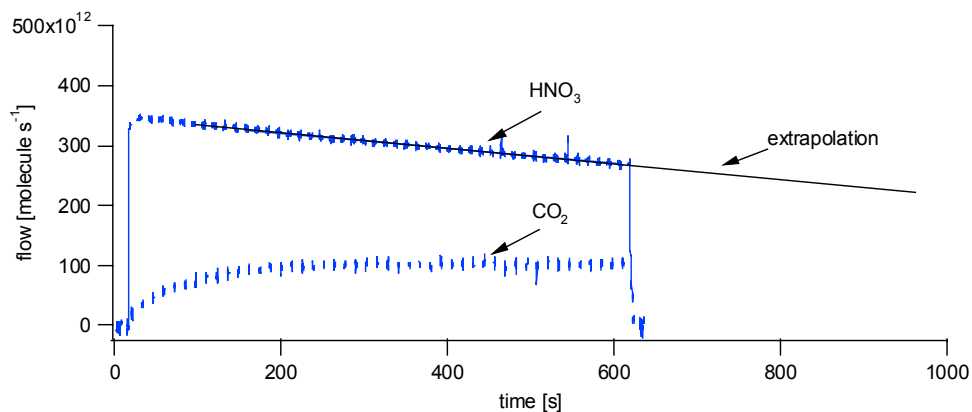
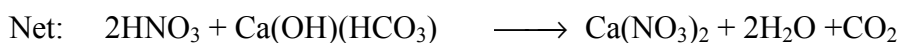
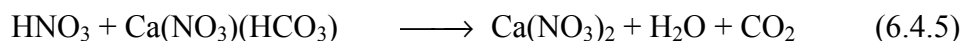
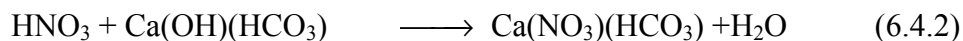
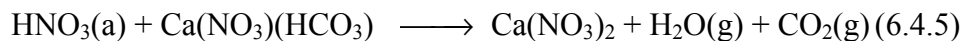
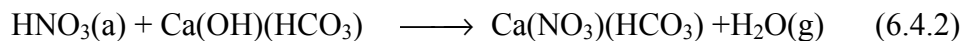


Figure 6.4.8: Loss rate of HNO_3 and rate of formation of CO_2 of a typical uptake experiment of HNO_3 on high-ordered precipitated CaCO_3 carried out in the 14mm-orific reactor.

This reaction scheme therefore explains the delay of the formation of CO_2 and the formation of H_2O we observed in HNO_3 uptake experiments on marble plates. The absence of CO_2 as a reaction product for this substrate may be due to the small number of reactive sites in this case.

The over all mechanism we propose is as follows:



The fact that no CO_2 has been observed performing HNO_3 uptake experiments on marble plates may be due to the fact that reaction 6.4.5 is a slow reaction. This suggestion is based on the fact that small amounts of CO_2 have been observed heating the sample after the exposure of the marble disk to HNO_3 and the delay of formation of CO_2 in the uptake experiments of HNO_3 on precipitated CaCO_3 .

6.4.3. Conclusions

Uptake experiments of nitric acid HNO_3 on different calcium carbonate samples have been carried out in this section. The uptake of HNO_3 on precipitated CaCO_3 leads to formation of H_2O and CO_2 whereas on the polished and roughened marble plates no formation of CO_2 has been observed.

Furthermore, saturation of the surface for a reaction with HNO_3 has been observed which points towards a limited number of reactive sites.

A comparison of the uptake experiments carried out on roughened and polished marble plates have shown that surface roughening leads to an enhanced uptake coefficient γ as well an increase of the total number of reactive sites by a factor of 3.

A model consideration of the HNO_3 uptake on roughened marble plates let us suggest that the uptake follows the rate law given by $\dot{S} = k_1 \underbrace{N(S_0 - S)}_x$ after 120s, or so in agreement with Langmuir-adsorption kinetics. At the beginning of the uptake experiment

Chapter 6

the reaction flow is too high to be consistent with such a mechanism. We explained this by surface adsorption which has been confirmed by the desorption of HNO_3 after halting the HNO_3 flow.

HNO_3 experiments performed on high-ordered precipitated CaCO_3 have led to delayed formation of CO_2 . The evaluation of the total amount of lost HNO_3 has been in good agreement with twice the amount of the yield of CO_2 from SO_2 uptake experiments. Based on this observation we have proposed the concept of intermediate species that explains the delayed formation of CO_2 on precipitated CaCO_3 and the formation of H_2O on the marble substrates.

Chapter 6

6.4.4. Tables

Table 6.4.1: Typical experimental conditions and main results of HNO₃ uptake experiments on CaCO₃ samples

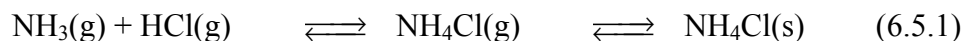
No	Orifice diameter [mm]	[HNO ₃] [molecule cm ³]	sample	Experimental conditions	Uptake kinetics	Remarks
1a	14	1.6*10 ¹¹	Au	Bare sample-holder	$\gamma_0 = 2.7*10^{-3}$	Saturation after a few seconds
1b	4	2.1*10 ¹²	Au	Bare sample-holder	$\gamma_0 = 2.4*10^{-4}$	Saturation after a few tens of seconds
2a	14	2.7*10 ¹¹	pm	$t_p = 21h$, first uptake, $t_e = 2$ min	$\gamma_0 = 1*10^{-2}$ $\gamma_{ss} = 2*10^{-3}$	Formation of H ₂ O, no formation of CO ₂ , loss of HNO ₃ : 1.4*10 ¹⁶ molecule
2b	14	2.7*10 ¹¹	pm	$t_p = 21h$, second uptake, $t_e = 2$ min	$\gamma_0 = 7*10^{-3}$ $\gamma_{ss} = 2*10^{-3}$	No formation of CO ₂ , no formation of H ₂ O, loss of HNO ₃ : 4.7*10 ¹⁵ molecule
2c	4	7*10 ¹¹	pm	$t_p = 21h$, third uptake, $t_e = 2$ min	$\gamma_0 = 7*10^{-3}$ $\gamma_{ss} = 7*10^{-4}$	No formation of CO ₂ , no formation of H ₂ O, loss of HNO ₃ : 1.3*10 ¹⁶ molecule
2d			pm	Heated at T = 470K		Small amounts of CO ₂ observed
3a	4	5*10 ¹¹	mm	$t_p = 21h$, $t_e = 3$ min	$\gamma_0 = 8*10^{-2}$ $\gamma_{ss} = 2*10^{-3}$	Formation of H ₂ O, no formation of CO ₂ , loss of HNO ₃ : 5.7*10 ¹⁶ molecule, desorption of HNO ₃ : 9*10 ¹⁵ molecule
4	14	0.2-3*10 ¹¹	mm	$t_p = 20$ min		γ_0 decreases and γ_{ss} does not change with concentration
5	14		p	High-ordered precipitated CaCO ₃	$\gamma_0 = 0.3$	Formation of CO ₂ sets in delayed

t_p : pumping time Au : gold-coated substrate p : high-ordered precipitated CaCO₃
 t_e : exposure time pm : polished marble mm : milled marble

6.5. Uptake Experiments of HCl on CaCO₃

6.5.1. Introduction

Hydrogen chloride HCl is an important compound contributing to acid rain (section 1.5). Concentrations of 100-300ppt HCl are commonly measured at the surface in remote marine areas. In or near urban areas the concentration may range up as high as 3000ppt (18). Important sources of HCl are coal combustion and volcanic activity (14) but it may also be formed by heterogeneous reaction of NO_y with salt particles for example by the reaction of nitric and sulfuric acid with sodium chloride according to reactions 1.4.1 and 1.4.2. Together with ammonia, NH₃, gaseous hydrogen chloride may lead to the formation of particles (2) according to reaction 6.5.1.



HCl does not contribute to tropospheric photochemistry because it does not photodissociate above 290 nm (19), however, HCl may react on mineral dust which may be an important sink for HCl.

In this section we present the study of the heterogeneous reaction of HCl on CaCO₃ substrates such as polished and roughened marble and precipitated CaCO₃. The experiments have been performed in a low-pressure flow reactor.

6.5.2. Results and Discussion

Uptake experiments of HCl on high-ordered precipitated CaCO₃ have been performed in the 14mm-orifice reactor where we associate high-order with low density of defect sites as we have seen in section 6.3. A SEM-image of high-ordered CaCO₃ is shown in Figure 6.1.1. Figure 6.5.1 shows the calibrated MS-signal signal of such an experiment.

Experimental details and main results are summarised in Table 6.5.1. The only observed reaction product was CO_2 . In contrast to HNO_3 uptake experiments on precipitated CaCO_3 no formation of gaseous H_2O has been observed. Similar to the HNO_3 experiments performed on the same substrate the formation of CO_2 sets in with delay and the uptake of HCl decreases with time.

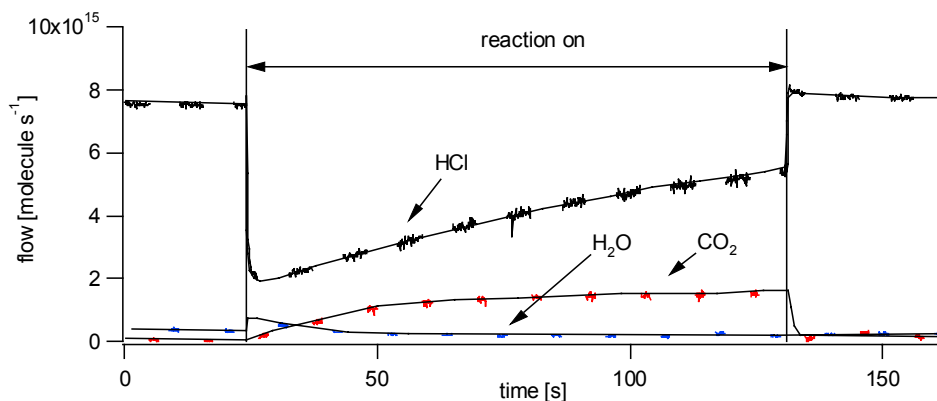


Figure 6.5.1: Typical HCl uptake experiment on high-ordered precipitated CaCO_3 carried out in the 14mm-orifice reactor. HCl , H_2O and CO_2 have been monitored at $m/e = 36$, $m/e = 18$ and $m/e = 44$, respectively.

Subsequent HCl uptake experiments performed on the same substrate led to steady-state uptake. The loss rate of HCl and the rate of formation of CO_2 led to a two to one conversion rate of HCl to CO_2 . Figure 6.5.2 displays the loss rate of HCl and the rate of formation of CO_2 resulting from a HCl uptake experiment on a substrate previously contaminated by HCl . In order to compare the loss of HCl with the yield of CO_2 the HCl loss rate and the rate of formation of CO_2 have been integrated over all HCl experiments carried out on this sample. On average a total loss of HCl of $8.8 \cdot 10^{17}$ molecule g^{-1} has been recorded in conjunction with a total yield of CO_2 of $4.1 \cdot 10^{17}$ molecule g^{-1} . This means that two moles of HCl are converted to one mole of CO_2 .

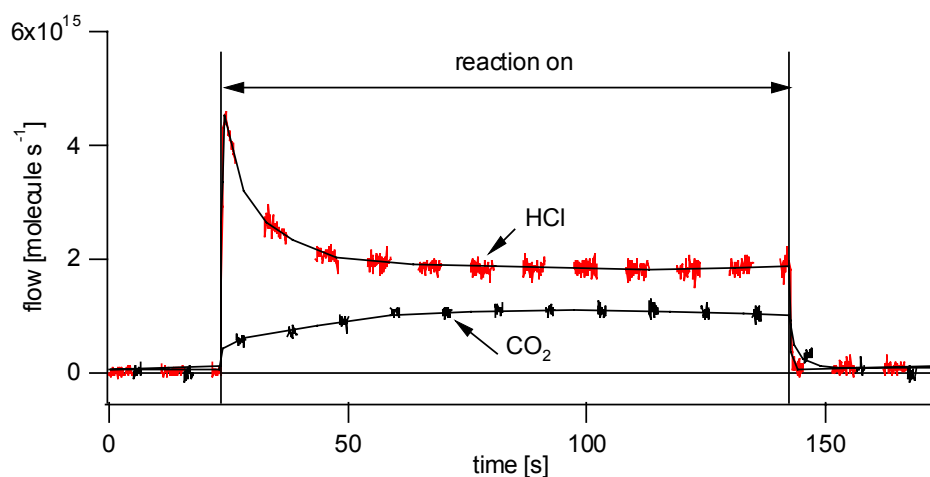


Figure 6.5.2: Loss rate of HCl and rate of formation of CO₂ on high-ordered precipitated CaCO₃ performed in the 14mm-orifice reactor. The sample had previously already been exposed to HCl before the presented uptake experiment had been carried out.

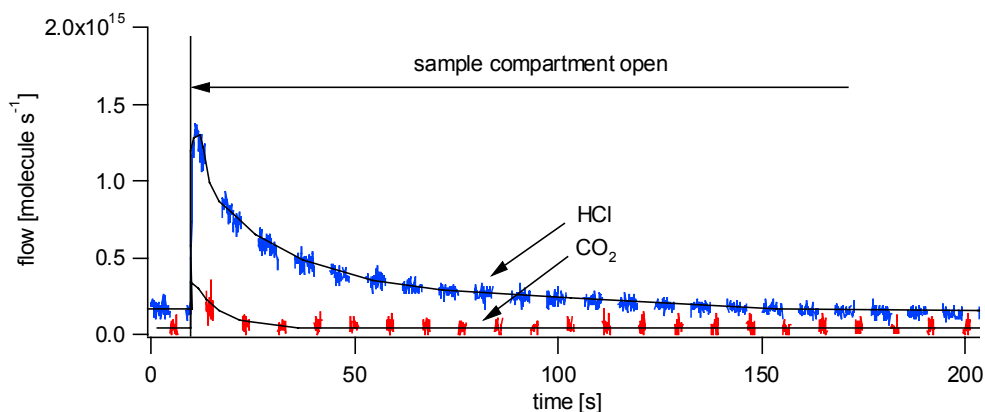


Figure 6.5.3: Desorption of HCl and CO₂ from a high-ordered precipitated CaCO₃ substrate. The sample has been exposed to HCl at [HCl] = 4·10¹¹ molecule cm⁻³ in the 4mm-orifice reactor. After HCl exposure the sample compartment has been closed for 1 minute before desorption.

After lowering the plunger and halting the HCl flow the plunger had been lifted once more in order to investigate the sample with respect to HCl desorption. Figure 6.5.3 shows the calibrated MS-signal of such a HCl desorption experiment. The experimental conditions are summarised in Table 6.5.1, Experiment 2.

As we have already seen in the previous section the desorption of HCl from the surface indicates the existence of a reservoir state on the substrate holding a weakly-bound HCl precursor.



In order to control the amount of adsorbed H_2O the high-ordered precipitated CaCO_3 samples have been pumped for different times t_p . The amount of adsorbed H_2O has been evaluated using the calibration curve of Figure 6.1.3. Figure 6.5.4 shows the MS-signals of HCl uptake experiments performed on samples containing different amounts of H_2O (a) using the 14mm-orifice reactor.

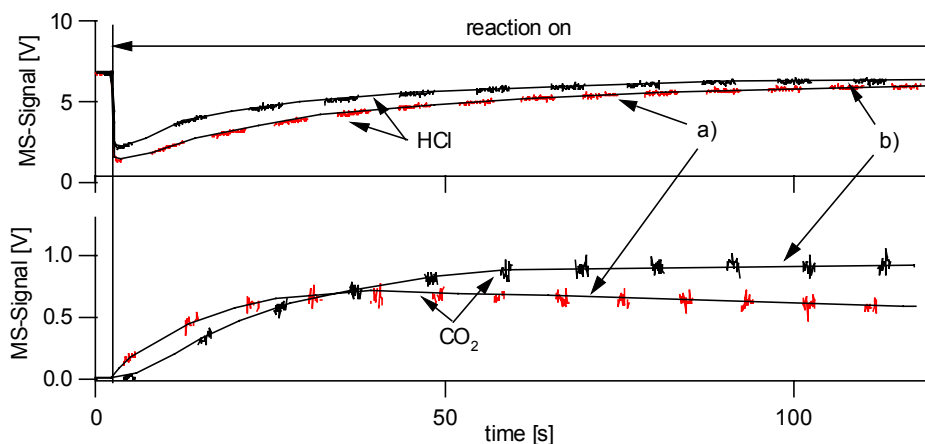
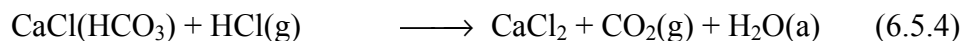
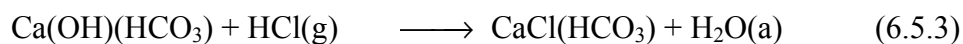


Figure 6.5.4: MS-Signals of HCl uptake experiments carried out in the 14mm-orifice reactor on high-ordered precipitated CaCO_3 with different amounts of H_2O (a) at $[\text{HCl}] = 6 \cdot 10^{11} \text{ molecule cm}^{-3}$. The sample of experiment a) and b) contains $1.6 \cdot 10^{18}$ and $5 \cdot 10^{17} \text{ molecule g}^{-1}$ of adsorbed H_2O , respectively. The higher and the lower part show the rate of uptake of HCl and the rate of formation of CO_2 , respectively.

The rate of uptake of HCl on CaCO_3 increases with the amount of H_2O (a). In addition, the presence of lower amounts of H_2O (a) delays the formation of gaseous CO_2 (Figure 6.5.4 a) and b)).

Chapter 6

This may suggest the following explanation using the proposed intermediate $\text{Ca(OH)(HCO}_3\text{)}$ which is the entity interacting with HCl :



With decreasing amounts of $\text{H}_2\text{O(a)}$ the equilibrium 6.3.10 is shifted to the right-hand side and with it the amount of the intermediate species $\text{Ca(OH)(HCO}_3\text{)}$ which leads to a smaller rate of uptake of HCl . With smaller amounts of intermediates the reaction sites leading to a loss of HCl (Reaction 6.5.3) are faster saturated and the formation of CO_2 (Reaction 6.5.4) may set in earlier.

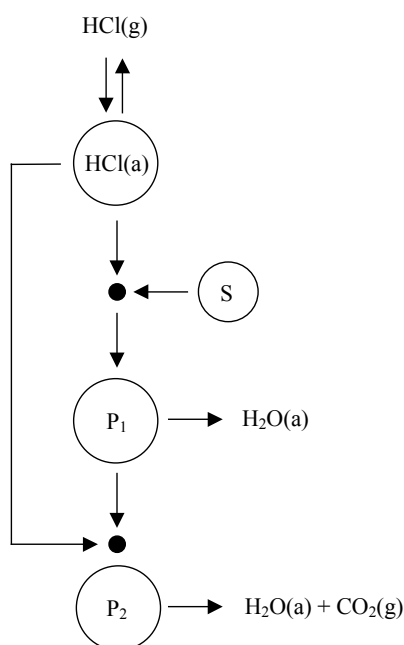


Figure 6.5.5: Illustration of the reaction mechanism of the reaction of HCl on CaCO_3 . S represents the reactive sites and P_1 and P_2 the non-gaseous reaction products.

In order to explain the fact that on the CaCO_3 sample containing more adsorbed $\text{H}_2\text{O(a)}$ and therefore more intermediate sites we observed the formation of CO_2 which is more

prompt (Figure 6.5.4) we suggest the reaction mechanism displayed in Figure 6.5.5. With the presence of more reactive sites P_1 the rate of formation leading to sites P_2 which enables the formation of CO_2 increases. Therefore, we suggest that formation of CO_2 sets in earlier. Furthermore, the presence of smaller amounts of S indicates a smaller loss rate of HCl towards P_1 which on the other hand enhances the loss rate of HCl toward formation of P_2 with its accompanied formation of CO_2 .

Figure 6.5.6 shows the initial uptake coefficient γ_0 as a function of the amount of $\text{H}_2\text{O}(\text{a})$. The experimental details are listed in Table 6.5.1, Experiment 3. The experiments have been carried out in the 14mm-orifice reactor. The initial uptake γ_0 increases from $\gamma_0 = 0.1$ to $\gamma_0 = 0.19$ with the amount of adsorbed $\text{H}_2\text{O}(\text{a})$ from $5 \cdot 10^{17}$ to $1.6 \cdot 10^{18}$ molecule g^{-1} which corresponds to the same values in the $\text{SO}_2/\text{CaCO}_3$ system (Section 6.3).

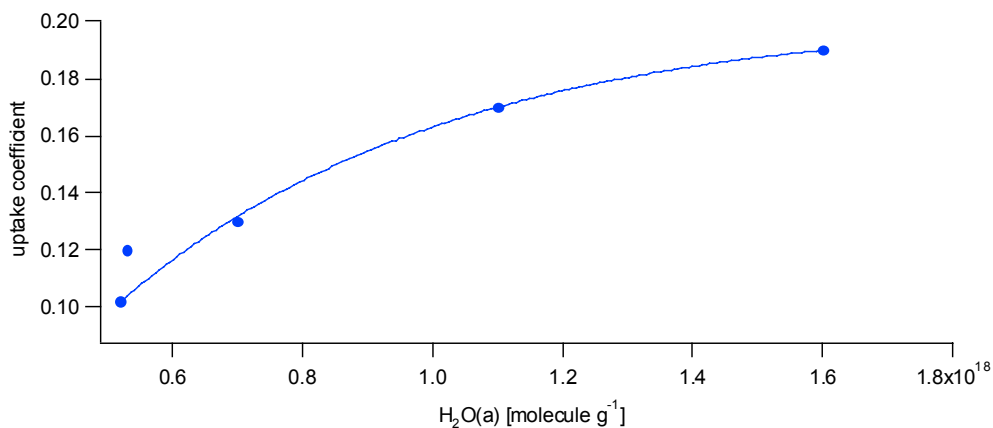


Figure 6.5.6: HCl uptake experiments on high-ordered precipitated CaCO_3 carried out in the 14mm-orifice reactor at $[\text{HCl}] = 6 \cdot 10^{11}$ molecule cm^{-3} . The graph shows the initial uptake coefficient as a function of the $\text{H}_2\text{O}(\text{a})$. $\text{H}_2\text{O}(\text{a})$ has been evaluated using the calibration curve of Figure 6.1.3. The uptake coefficient has been calculated based on the geometrical area of the sample.

With both reactions 6.5.3 and 6.5.4 formation of H_2O would be expected. However, the HCl uptake experiments did not reveal any formation of gaseous H_2O . This is in stark contrast to HNO_3 uptake experiments on high-ordered precipitated CaCO_3 described in section 6.4. The lifting of the plunger even causes a decrease of the H_2O background

level. Figure 6.5.7 shows an HCl uptake experiment on high-ordered CaCO_3 performed in the 14mm-orifice reactor. The experimental details are listed in Table 6.5.1, Experiment 4.

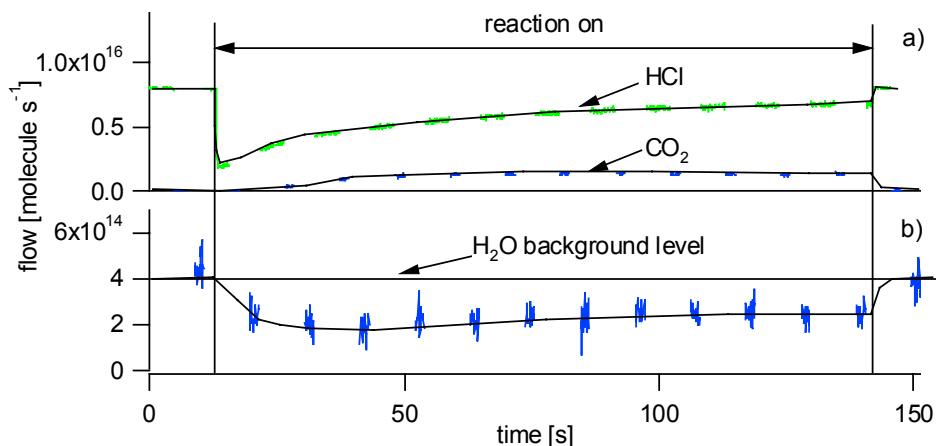
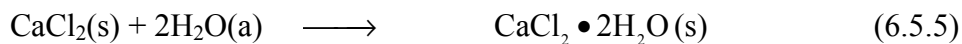


Figure 6.5.7: Uptake experiment of HCl on high-ordered precipitated CaCO_3 performed in the 14mm-orifice reactor: Graph a) shows the calibrated MS-signal of HCl and CO_2 , b) shows the uptake of the background H_2O . HCl, CO_2 and H_2O have been monitored at $m/e = 36$, $m/e = 44$ and $m/e = 18$, respectively.

The final reaction product of reaction 6.5.4 is calcium chloride CaCl_2 . It is known that CaCl_2 is a highly hygroscopic species. CaCl_2 with two H_2O molecule may even form a stable crystalline structure $\text{CaCl}_2 \cdot 2\text{H}_2\text{O}$ (20).



Finally, HCl uptake experiments carried out on polished marble plates have not led to an uptake of HCl. However, HCl uptake experiments on roughened marble plates led to a small uptake of HCl but no reaction products have been observed. Figure 6.5.8 shows the calibrated MS-signals of an HCl uptake experiment performed in the 1mm-orifice reactor. The experimental details are listed in Table 6.5.1, Experiment 5.

The fact that only loss of HCl and no reaction products are observed supports the thesis of a reaction whose mechanism involves the proposed intermediate species $\text{Ca(OH)(HCO}_3\text{)}$:

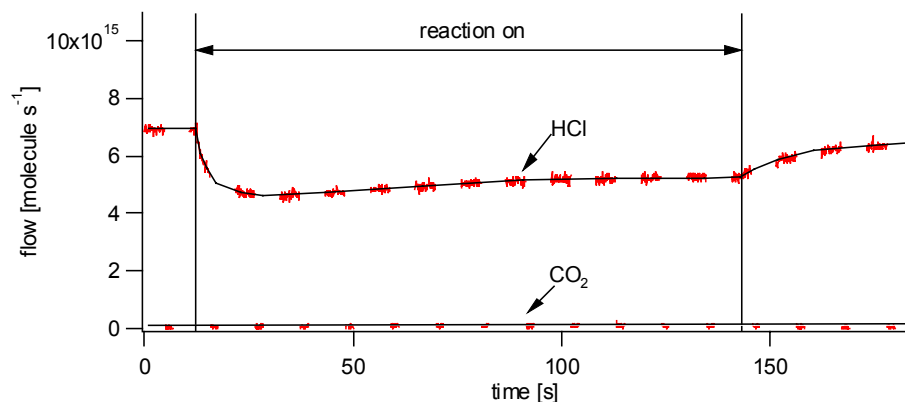
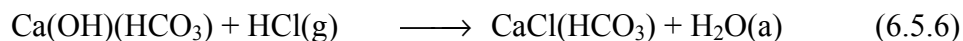


Figure 6.5.8: HCl uptake experiment on roughened marble plate carried out in the 1mm-orifice reactor.

Furthermore, the fact that on polished marble plates no uptake of HCl has been observed confirms the fact that the concentration of the intermediates depends on the surface structure. This means that more surface defects and the presence of H_2O may enhance the formation of the intermediate species (Reaction 6.3.10).

6.5.3. Conclusions

In this section uptake experiments of HCl on different CaCO_3 substrates such as high-ordered precipitated CaCO_3 , polished and roughened marble plates have been described. The observed reaction product is CO_2 , although the expected formation of H_2O has not been observed. The HCl uptake experiments on high-ordered precipitated CaCO_3 have shown a two to one conversion of HCl with respect to generated CO_2 .

Chapter 6

After carrying out HCl uptake experiments desorption of HCl has been observed which means that adsorption sites for HCl exists on the surface (reaction 6.5.2) which leads to a surface adsorbed intermediate.

Furthermore, we imported the concept of intermediate sites $\text{Ca(OH)(HCO}_3\text{)}$ in order to explain the delay of the formation of CO_2 and the dependence of the uptake coefficient on the amount of adsorbed $\text{H}_2\text{O(a)}$.

We explained the fact that no formation of gaseous H_2O has been observed with the hygroscopic reaction product CaCl_2 which may form a stable crystalline structure $\text{CaCl}\cdot 2\text{H}_2\text{O}$ in the presence of H_2O .

Finally, HCl uptake experiments on roughened marble plates have led to a small uptake of HCl but not to formation of gaseous reaction products. The uptake experiments on polished marble have not led to any uptake of HCl.

6.5.4. TablesTable 6.5.1: Typical experimental conditions and main results of HCl uptake experiments on CaCO₃ samples

No	Orifice diameter [mm]	[HCl ₃] [molecule cm ³]	sample	Experimental conditions	Uptake kinetics	Remarks
1a	14	6*10 ¹¹	p	Estimated H ₂ O(a): 5*10 ¹⁸ molecule g ⁻¹ , first uptake	γ ₀ = 0.13	Formation of CO ₂ is delayed, no formation of gaseous H ₂ O measured.
1b	14	6*10 ¹¹	p	Third uptake experiment	γ ₀ = 6*10 ⁻²	formation of CO ₂ , loss rate of HCl / rate of formation of CO ₂ tends towards 2
2	4	5*10 ¹²	p	Desorption from a sample previously exposed to HCl		Desorption of HCl and of small amounts CO ₂
3	14					
4	14	6*10 ¹²	p	Estimated H ₂ O(a): 5*10 ¹⁸ molecule g ⁻¹	γ ₀ = 0.13	Uptake of H ₂ O, γ(H ₂ O) = 7*10 ⁻²
5	1	1*10 ¹⁴	mm		γ = 3*10 ⁻⁴	No reaction products observed

mm : milled marble

p : high-ordered precipitated CaCO₃.

6.6. Uptake Experiments of HNO₃ on Various Mineral Dusts

In addition to the uptake experiments on calcium carbonate, CaCO₃, a few uptake experiments of HNO₃ on Kaolinite, Arizona Road Dust and Saharan Dust have been performed. On all of these substances a fast uptake of HNO₃ but no reaction products have been observed. Furthermore, these types of samples have not shown any saturation under our experimental conditions.

It has been observed that huge amounts of adsorbed H₂O(a) must be present on these substrates. The amounts of adsorbed H₂O(a) under ambient conditions are summarised in Appendix B, Table B.1. In Appendix B a short description of how the adsorbed H₂O(a) has been measured is given. In addition, the BET surface of all dust substrates has been measured. The values for the corresponding BET surfaces are listed in Appendix A, Table A.1.

Figure 6.6.1 shows a typical HNO₃ uptake experiment on 1g of Saharan Dust. An uptake of HNO₃ has been observed but no gaseous reaction product has been detected.

The corresponding uptake coefficient γ may be found in Table 6.6.1 together with the uptake coefficients of HNO₃ experiments on Kaolinite, Arizona Road Dust and CaCO₃

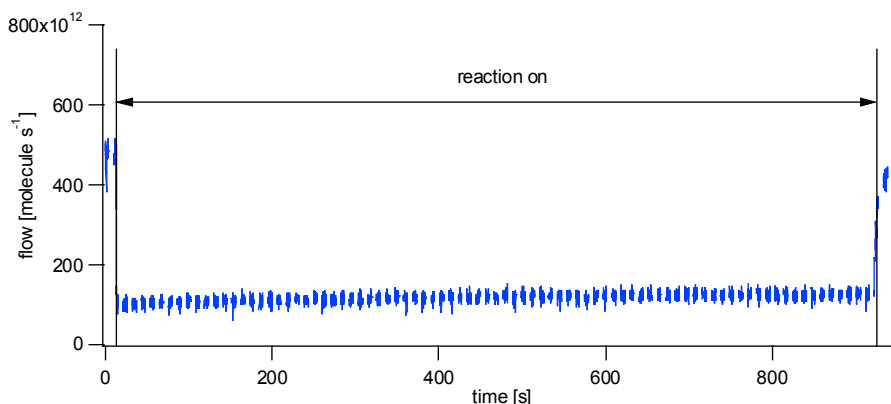


Figure 6.6.1: Typical HNO₃ uptake experiment on 1g of Saharan Dust performed in the 14mm-orifice reactor. HNO₃ has been monitored at $m/e = 46$.

Chapter 6

samples. The initial uptake coefficients γ_0 and the uptake coefficients at $t = 120\text{s}$ are given in Table 6.6.1.

Table 6.6.1: Uptake coefficients γ of HNO_3 onto various dust substrates compared to the value of Crowley and coworkers (1)

Substrate	γ_{ini}	$\gamma_{\text{ss}} (t = 120\text{s})$	γ
CaCO_3 (powder)	0.29	0.25	0.18
Polished marble	$2 \cdot 10^{-2}$	$< 1 \cdot 10^{-3}$	
Roughened marble	0.14	$4 \cdot 10^{-3}$	
Kaolinite well ordered	0.29	0.2	
Kaolinite poorly ordered	0.38	0.36	
Arizona Road Dust (medium grade)	0.2	0.16	0.06
Arizona Road Dust (coarse grade)	0.16	0.15	
Saharan Dust	0.26	0.2	0.11

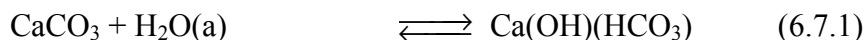
6.7. General Discussion

In this chapter the interactions of CO_2 , SO_2 , HNO_3 and HCl with calcium carbonate, CaCO_3 , have been investigated in detail. The influence of adsorbed H_2O has also been studied. In order to quantify the amount of adsorbed H_2O desorption experiments have been performed which resulted in a calibration curve.

We have seen that after 5 minutes pumping action more than 99% of adsorbed H_2O may be removed. Therefore, we conclude that most of the adsorbed H_2O is weakly-bound on CaCO_3 substrates. Nevertheless, pumping of the sample during $t_p = 20\text{h}$ lowers the amount of adsorbed H_2O only by a factor 4 as it may be seen in Figure 6.1.3. All uptake experiments have shown that only a limited number of sites are available to undergo a reaction on calcium carbonate.

Chapter 6

Thus, we have introduced as reactive site the intermediate species $\text{Ca(OH)(HCO}_3\text{)}$ which may be formed under ambient conditions in the overall reaction 6.7.1 where ambient conditions imply the presence of H_2O and CO_2 .

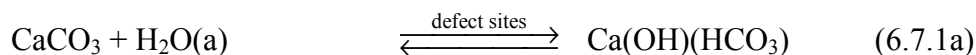


We have shown using SO_2 uptake experiments that under vacuum no intermediates may be formed. In contrast, the sample does regenerate on the time scale of days under ambient conditions.

Pumping of the substrate leads to a shift of the equilibrium 6.7.1 towards the left-hand side. Reaction 6.7.1 is a slow reaction which may explain that the uptake of the studied gases do not depend significantly on pumping time t_p .

In contrast to pumping time t_p we have shown that defect sites influence the number of intermediates enormously. This has been shown using low- and high-ordered precipitated CaCO_3 samples and polished and roughened marble plates.

Thus, we may rewrite reaction 6.7.1



Finally, we observed as expected that acidic compounds HCl and HNO_3 attack with preference the OH part of the intermediate which leads to loss of acidic molecules but not to formation of CO_2 and consequently to a delay of the formation of CO_2 . In contrast to acidic compounds, SO_2 attacks with preference the bicarbonate HCO_3 part of the intermediate whereas the reaction with the OH part is rather slow. The reaction of SO_2 with the bicarbonate shows up in the prompt formation of CO_2 immediately after lifting the plunger. The reaction of SO_2 with the OH results in a slow loss of SO_2 without any formation of CO_2 .

6.8. References

- (1) Hanisch F. and J. N. Crowley: *Heterogeneous reactivity of gaseous nitric acid on Al_2O_3 , $CaCO_3$, and atmospheric dust samples: A Knudsen cell study*. Journal of Physical Chemistry A, (2001), vol. 105, pp. 3096-3106.
- (2) Seinfeld J. H. and S. N. Pandis: *Atmospheric Chemistry and Physics*. (John Wiley & Sons, 1998).
- (3) Weast R. C.: *Handbook of Chemistry and Physics*. (CRC Press, 1986).
- (4) Graedel T. E.: *Mechanisms for the atmospheric corrosion of carbonate stone*. Journal of the Electrochemical Society, (2000), vol. 147, pp. 1006-1009.
- (5) Gombert P.: *Role of karstic dissolution in global carbon cycle*. Global and Planetary Change, (2002), vol. 33, pp. 177-184.
- (6) Plummer L. N., T. M. L. Wigley and D. L. Parkhurst: *Kinetics of Calcite Dissolution in CO_2 -Water Systems at 5- Degrees-C to 60-Degrees-C and 0.0 to 1.0 Atm CO_2* . American Journal of Science, (1978), vol. 278, pp. 179-216.
- (7) Compton R. G. and P. R. Unwin: *The Dissolution of Calcite in Aqueous-Solution at PH Less-Than- 4 - Kinetics and Mechanism*. Philosophical Transactions of the Royal Society of London Series a-Mathematical Physical and Engineering Sciences, (1990), vol. 330, pp. 1-45.
- (8) Gabrovsek F. and W. Dreybrodt: *Role of mixing corrosion in calcite-aggressive $H_2O-CO_2-CaCO_3$ solutions in the early evolution of karst aquifers in limestone*. Water Resources Research, (2000), vol. 36, pp. 1179-1188.

Chapter 6

- (9) Baedecker P. A. and M. M. Reddy: *The Erosion of Carbonate Stone by Acid-Rain - Laboratory and Field Investigations*. Journal of Chemical Education, (1993), vol. 70, pp. 104-108.
- (10) Krauskopf K. B. and B. K. Bird: *Introduction to geochemistry*. (Mac-Graw Hill, Inc., 1995) pp. 647.
- (11) Lasaga A. C.: *Kinetic theory in earth science*. (Princeton University Press, 1998) pp. 811.
- (12) Dreybrodt W., J. Lauckner, Z. H. Liu, U. Svensson and D. Buhmann: *The kinetics of the reaction $CO_2+H_2O \rightarrow H^+ + HCO_3^-$ as one of the rate limiting steps for the dissolution of calcite in the system $H_2O-CO_2-CaCO_3$* . Geochimica Et Cosmochimica Acta, (1996), vol. 60, pp. 3375-3381.
- (13) NIST-Chemistry-WEBBook: *NIST Chemistry WEBBook*.
- (14) Hobbs P. V.: *Introduction to Atmospheric Chemistry*. (Cambridge University Press, 2000) pp. 262.
- (15) Dentener F. J., G. R. Carmichael, Y. Zhang, J. Lelieveld and P. J. Crutzen: *Role of mineral aerosol as a reactive surface in the global troposphere*. Journal of Geophysical Research-Atmospheres, (1996), vol. 101, pp. 22869-22889.
- (16) Zhang Y., Y. Sunwoo, V. Kotamarthi and G. Carmichael: *Photochemical Oxidant Processes in the Presence of Dust: An Evaluation of the Impact of Dust on Particulate Nitrate and Ozone Formation*. Journal of Applied Meteorology, (1994), vol. 33, pp. 813-824.

Chapter 6

- (17) Underwood G. M., C. H. Song, M. Phadnis, G. R. Carmichael and V. H. Grassian: *Heterogeneous reactions of NO₂ and HNO₃ on oxides and mineral dust: A combined laboratory and modeling study*. Journal of Geophysical Research-Atmospheres, (2001), vol. 106, pp. 18055-18066.
- (18) Graedel T. E. and W. C. Keene: *Tropospheric Budget of Reactive Chlorine*. Global Biogeochemical Cycles, (1995), vol. 9, pp. 47-77.
- (19) Finlayson-Pitts B. J.: *Chemistry of the Upper and Lower Atmosphere*. (Academic Press, 2000) pp. 969.
- (20) Leclaire A. and M. M. Borel: *Study on Calcium Halides .I. Calcium Dichloride Dihydrate*. Acta Crystallographica Section B-Structural Science, (1977), vol. 33, pp. 1608-1610.

Chapter 7

7. Outlook

In this work we presented a study of heterogeneous reactions of atmospherically relevant chlorine- and bromine-containing compounds on alkali salt and acidic compounds on model mineral dust substrates. The experiments have been performed in a low-pressure flow reactor equipped with a quadrupole mass spectrometer. The quadrupole mass spectrometer allows the observation of the gaseous reactants as well the gaseous reaction products.

Adsorbed $\text{H}_2\text{O}(\text{a})$ plays a crucial role for the reactions on salt as well as on mineral dust substrates. In order to measure the amount of adsorbed $\text{H}_2\text{O}(\text{a})$ we carried out desorption experiments and obtained a calibration curve for the different substrates. Furthermore, we have found for salt substrates that adsorbed halogen species such as Br_2 , BrCl , HOCl and Cl_2 play a crucial role in the reaction kinetics.

In order to measure the amount and the evolution in time of adsorbed $\text{H}_2\text{O}(\text{a})$ and other adsorbed species it would be helpful to investigate the condensed phase during the experiment. This could be performed for example using an infrared technique such as Fourier transform infrared spectroscopy (FTIR).

The adsorption and desorption kinetics of gaseous species may be investigated by modulation of the inflow of the gas of interest.

Furthermore, we have shown in HOCl experiments with an additional Br₂ flow that the presence of additional gases may influence the reaction kinetics considerably. Furthermore, experiments of SO₂ on mineral dust have shown a regeneration of the sample under ambient conditions but not in the low-pressure reactor. Therefore, it would be interesting to study the interaction of different reaction systems which corresponds to the behaviour of a substrate in the presence of different gases. Moreover, experiments at atmospheric pressure should be developed in order to investigate the reactions under more realistic conditions such as elevated relative humidity and in the presence of different gases at the same time. This may improve the knowledge of the reactions for atmospheric modelling purposes.

A low-pressure reactor allows one to carry out mechanistic studies of the reaction. In order to render the prediction of a possible reaction mechanism more accurate it would be helpful to complete the measurements and check the proposed mechanisms by numerical calculations. Using numerical calculations the concurrent reactions may be separated and consequently investigated more accurately.

Experiments performed in a low-pressure flow reactor are suitable in order to study reaction mechanisms. Those experiments are a first step in order to understand surfaces of atmospheric particles. In fact surfaces of real particles are much more complicated in terms of adsorbed H₂O(a) and surface defects which may lead to a different behaviour of the gas-solid interaction of atmospheric gases with real aerosols. The surface of real aerosols should better be characterised in order to extrapolate the results obtained in a low-pressure flow reactor to ambient conditions.

Appendix A

BET-Measurements

The BET surfaces of various mineral dusts have been determined using the Sorptomatic 1990 supplied by Finsons Instruments. Nitrogen has been used as adsorbate.

The surface is calculated in the following way:

$$S_{\text{BET}} = \frac{A_{\text{N}}\alpha V_{\text{m}}}{W} \quad (\text{equation A.1})$$

where A_{N} Avogadro's number, V_{m} the volume of a monolayer and α the cross-sectional area of the adsorbate is. For N_2 the cross-sectional area α is 16.2 \AA^2 (1). The BET surfaces of various mineral dusts are listed in Table A.1.

Table A.1: BET surfaces of various Mineral Dusts

Substrate	Conditions		BET-Surface [$\text{m}^2 \text{ g}^{-1}$]
	Temperature	Pumping time	
CaCO_3 (powder)	50 °C	3.5 h	3.7
CaCO_3 low ordered	250°C	2.5h	5.1
Kaolinite well ordered	50 °C	3.5 h	15.3
Kaolinite poorly ordered	50 °C	3.5 h	22.5
Arizona Road Dust (medium grade)	50 °C	3.5 h	10.5
Arizona Road Dust (coarse grade)	50 °C	3.5 h	10.8
Saharan Dust	50 °C	3.5 h	51.4
Saharan Dust	250 °C	2.5h	67.7

- (1) Lowell: *Introduction to Powder Surface Area*. (John Wiley & Sons, New York, 1979) pp. 199.

Appendix B

Adsorbed H₂O

The amount of H₂O(a) adsorbed on various mineral dusts at ambient condition has been measured in the following way:

A known amount m of the substrate of interest has been introduced into a metallic tube. The tube including substrate was weighed, using a balance provided by Mettler Toledo model AE 240, before it has been connected to the 14mm-reactor. Subsequently, the tube was heated using a hot air gun and the desorbing H₂O has been monitored by MS. After the MS-signal of H₂O had reached the background level the tube had been kept under vacuum, removed from the reactor and weighed again.

The amount of adsorbed H₂O(a) is:

$$m_{\text{H}_2\text{O}} = \frac{m_1 - m_2}{m} \quad (\text{equation B.1})$$

where m_1 and m_2 are the masses of the tube including substrate before and after heating, respectively. m and $m_{\text{H}_2\text{O}}$ are the mass of the substrate and the mass of the adsorbed H₂O, respectively.

The obtained values for the amount of adsorbed H₂O(a) are listed in Table B.1.

Table B.1: Adsorbed H₂O(a) on different mineral dust substrates under ambient conditions. Relative humidity rh = 33% and temperature $\vartheta = 21^{\circ}\text{C}$.

Substrate	H ₂ O (a) [mg g ⁻¹]
CaCO ₃ high-ordered (powder)	4
Kaolinite well ordered	14
Kaolinite poorly ordered	23
Arizona Road Dust (medium grade)	22
Arizona Road Dust (coarse grade)	11
Saharan Dust	20

Curriculum Vitae

Christian SANTSCHI

Date of Birth : June 20, 1963
Place of Birth : Wigoltingen, Switzerland
Nationality : Swiss

EDUCATION

1998-2003 Ph. D. student in the Laboratoire de Pollution Atmosphérique directed by Prof. Hubert van den Bergh, at the Swiss Federal Institute of Technology in Lausanne (EPFL), Switzerland
1992-1997 Studies of physics at the Swiss Federal Institute of Technology in Zürich (ETHZ), Switzerland
1989-1992 Industrial experience as electronic engineer in hard- and software development.
1986-1989 Studies of electronic engineering at the Zürcher Fachhochschule Winterthur (ZFW), Switzerland.
1983-1986 Industrial experience as electronic technician
1979-1983 apprenticeship as electronic technician

LANGUAGES

German	Mother tongue
French	Very good knowledge
English	Very good knowledge
Spanish	Very good knowledge
Russian	Basic knowledge
Italian	Basic knowledge